Aspects of Nonlinearity and Dissipation in Magnetohydrodynamics

Thesis

Aspects of
Nonlinearity and Dissipation
in Magnetohydrodynamics

Erwin André Omer Verwichte
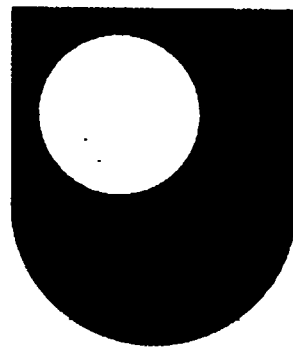
The Open
University

Thesis submitted for the degree of Doctor of Philosophy,
in the Department of Applied Mathematics of The Open University.

15th September 1999

Abstract

We investigate two projects: (i) the weakly nonlinear evolution of two oppositely travelling waves and (ii) the dissipative instability of a tangential discontinuity.

We show that the ponderomotive force is a basic nonlinear force, which is, to leading-order, proportional to the product of a wave quantity and a gradient of a wave quantity. The ponderomotive force of Alfvén waves corresponds to a magnetic wave pressure force.

The motion of beads on a string and the fluid motions in an oscillating tube are shown to be good mechanical analogues for the weakly nonlinear evolution of bounded Alfvén waves, especially in plasmas with a low plasma β.

We examine, analytically and numerically, the weakly nonlinear evolution of bounded fast magneto-acoustic waves in the cold-plasma limit and show that the ponderomotive force moves plasma along the equilibrium magnetic field. The maximum density enhancement is proportional to a^2/β, with a the wave amplitude and β of the order of the plasma β. We obtain the wave amplitude and frequency modulation and discuss the problems with the cold-plasma assumption.

The weakly nonlinear interaction of Alfvén pulses is investigated in the cold-plasma limit and for finite-β plasmas. We find excellent agreement between analytical and numerical results. We describe a density enhancement, maximally of order $a^2\beta^{1/2}$, at the position of Alfvén pulse excitation, which splits into two slow pulses. We describe the shock-formation of the Alfvén and slow pulses.

The dissipative instability of the tangential discontinuity is examined and applied to coronal hole boundaries. We derive a dispersion relation, which includes weak viscosity and thermal conduction, and is solved for a specific model, using perturbation theory. The effect of viscosity and thermal conduction on stability are discussed. It is shown that dissipation lowers the threshold flow speed for instability.

Contents

Acknowledgements

First and foremost I would like to thank my parents for always respecting my choices of study and supporting me throughout. Therefore I wish to dedicate this thesis to them. I also thank my two brothers Eric and Ronny.

I wish to give thanks and recognition to my official supervisor Dr Pat Edwin for her supervision, for all the constructive criticism which accompanied each draft I sent her and for her patient corrections of my persistent *mispelinks*. I thank my joint supervisor from St Andrews University, Prof Alan Hood, for his big support, advice and for the many fruitful discussions.

I thank the Open University for giving me financial and administrative support, which enabled me to pursue a PhD and I thank the School of Mathematical and Computational Sciences of the University of St Andrews, and Prof Alan Hood and Prof Bernard Roberts in particular, for providing the facilities so that I could pursue my postgraduate studies with the Solar Theory Group. I thank Prof Marcel Goossens for introducing me to the subject of solar magnetohydrodynamics and for his help in obtaining a postgraduate grant.

I should also like to express my gratitude to Dr Valery Nakariakov for the many inspiring discussions, which have greatly enhanced my interest in science. I am also gratefull to him for his personal advice. I thank Dr Aaron Longbottom for, after a couple of minutes of *"Why do you want to study waves for?"*, helping me with those small and big numerical problems and for always being prepared to modify his numerical codes for me. I also thank Dr Thomas Neukirch for the many helpful and encouraging comments on how to solve my mathematical problems. Dr Klaus Galsgaard deserves my thanks for helping me see things in more perspectives than imagined before. I am grateful to Dr Patricia Heggie for ensuring that all the computers, on which we rely so much, behave as they should.

I am greatly indebted to Claire Foullon for her continuing love, commitment and encouragements and for her patience and support during the stressing time of writing-up. Without her, none of this would be meaningful for me.

I thank Helena Bijnens and her family for the happy times we shared and for reviving my interest in art.

I owe many thanks to my close and dear friends Gaitee Hussain, Neil McDonald and Clodagh Finnegan, for all their good company and support. I shall always remember the

good times we had in St Andrews (of which many were in a pub, I am glad to say). Furthermore I thank Neil for being such a first-class flat-mate. I also wish to thank my friends Gordon Laing, Jack Ireland, Duncan Mackay, Cheryl Mundie, Mark Daniell and Jeremie Blaizot. Also thanks to my office mates Richard Ryan and Zaharenia Romeou.

I would also like to thank a number of people not in Scotland, which include family and friends who have always shown great interest in my progress. I especially thank my Godmother Els Wynants and my grandparents from Germany for their keen support. I also thank my grandparents on my mother's side, my grandmother on my father's side and especially my great-grandmother.

I wish to thank my close friends Frank Daerden, Paul Vanhoutte, Wim Cuppens, Bert Timmers and Patrick Vandeweert for the many years of friendship. I owe many thanks to the people of J.V.S. Descartes and the Europlanetarium for all the fun and astronomy. I am grateful to Guiseppe Canonaco for giving me the enthusiasm and enjoyment for astronomical observing. Finally I thank my friends Ilse Saenen, Esther Salk, Pieter Siebelink and the guys from 8/1.

Dankwoord

Eerst en vooral wil ik graag mijn ouders bedanken voor hun onvermoeizame steun en hun respect voor mijn studiekeuzes. Daarom wil ik deze thesis ook aan hun wijden. Ik dank ook mijn twee broers Eric en Ronny.

Ik dank en erken mijn officiele promotor Dr Pat Edwin voor haar toezicht, voor al de positieve kritiek die elk werk begeleidde en voor haar geduldig corrigeren van *spelinksfauten*. Ik dank mijn promotor van de universiteit van St Andrews, Prof Alan Hood, voor zijn grote steun, advies en vele vruchtbare discussies.

I dank the Open University voor me de financiele en administratieve steun te verlenen voor mijn doctoraatsstudies en ik dank the School of Mathematical and Computational Sciences van the University of St Andrews, Prof Alan Hood en Prof Bernard Roberts in het bijzonder, voor me de faciliteiten te verlenen zodat ik mijn doctoraatsstudies bij de Solar Theory Group kon doen. Dank aan Prof Marcel Goossens voor me in het onderwerp van magnetohydrodynamica van de zon in te leiden en me te helpen een doctoraatsbeurs te verkrijgen.

Ik wil ook graag mijn dank betonen aan Dr Valery Nakariakov voor de vele inspirerende discussies, die mijn wetenschappelijk interesse hebben aangewakkerd. Ik dank hem ook voor zijn persoonlijk adviezen. Ik bedank Dr Aaron Longbottom voor, na een paar minuten van "Why do you want to study waves for?", me te helpen met die kleine en grote numerieke problemen, en om steeds bereid te zijn zijn numerieke codes voor mij aan te passen. Ik dank ook Dr Thomas Neukirch voor de vele behulpzame en aanmoedigende opmerkingen over hoe mijn wiskundige problemen op te lossen. Dr Klaus Galsgaard verdient mijn dank door me de dingen in meer dimensies te laten zien dan verwacht. Ik dank Dr Patricia Heggie voor ervoor te zorgen dat de computers, waar we afhankelijk van zijn, doen wat ze moeten doen.

Ik ben enorm veel verschuldigd aan Claire Foullon voor haar liefde, verbintenis en aanmoedigingen en haar geduld en steun tijdens de stresserende tijd van het schrijven van mijn thesis. Zonder haar, zou dit voor mij niet betekenisvol zijn.

Ik dank Helena Bijnens en haar familie voor de gelukkige tijden die we deelden en voor mijn interesse voor kunst leven in te blazen.

Ik ben veel dank verschuldigd aan mijn hechte vrienden Gaitee Hussain, Neil MacDonald en Clodagh Finnegan, voor hun goed gezelschap en steun. Ik zal altijd de goede tijden (waarvan velen op café) in St Andrews blijven herinneren. Vervolgens dank ik Neil dat hij zo'n schitterend kotgenoot is. Ik dank ook mijn vrienden Gordon Laing, Jack Ireland, Duncan Mackay, Cheryl Mundie, Mark Daniell en Jeremy Blaizot. Dank ook aan mijn kantoorgenoten Richard Ryan en Zaharania Romeou.

Ik zou ook graag enkele personen buiten Schotland willen bedanken: familie en vrienden die steeds groot interesse in mijn vooruitgang hebben getoond. Ik dank vooral mijn meter Els Wynants en mijn grootouders van Duitsland voor hun grote steun. Ik dank ook mijn grootouders aan moeders zijde, mijn grootmoeder aan vaders zijde en in het bijzonder mijn overgrootmoeder.

Ik dank mijn hechte vrienden Frank Daerden, Paul Vanhoutte, Wim Cuppens, Bert Timmers en Patrick Vandeweert voor de vele jaren van vriendschap. Ik ben veel dank verschuldigd aan J.V.S. Descartes en het Europlanetarium voor al het plezier en sterrenkunde. Ik dank Guiseppe Canonaco voor mij het enthousiasme en plezier in het waarnemen te geven. Tot slot bedank ik mijn vrienden Ilse Saenen, Esther Salk, Pieter Sieblink en de mensen van 8/1.

List of Figures

List of Tables

Chapter 1

Introduction

1.1 Motivation

In this thesis we investigate magnetohydrodynamical (MHD) models, which include non-linearity or dissipation.

The universe consists for the most part of plasmas, with the important exception of planets (like the Earth). These astrophysical plasmas are threaded by magnetic fields. The theory of magnetohydrodyamics is succesfully applied to the large-scale dynamics of many astrophysical and laboratory plasmas (*e.g.* solar theory: Priest, 1982; MHD instabilities in confined plasmas: Manheimer & Lashmore-Davies, 1989; stellar and planetary magnetism: Soward, 1983; magnetic field in astrophysics: Zeldovich *et al.*, 1983).

Ideal and linear magnetohydrodynamics is a well-developed and succesful branch of magnetohydrodynamics. Because nature is not linear, there are many situations where linear theory is insufficient. The study of nonlinear MHD took off in the seventies (Syrovatskii, 1971; Rutherford, 1973; Rosenbluth *et al.*, 1973; Taylor, 1974; Kadomtsev & Pogutse, 1974; Cohen & Kulsrud, 1974; Kadomtsev, 1975; Mio *et al.*, 1976). A basic feature in nonlinear MHD (and plasma physics) is the ponderomotive force. My interest in the ponderomotive force started with the papers by Allan *et al.* (1990, 1991, 1992, 1996), which modelled the accumulation of plasma at the equatorial plane of the day-side magnetosphere, by the action of the ponderomotive force of magnetohydrodynamical waves. In this thesis, we wish to examine the action of the ponderomotive force of MHD waves in simple models.

The gained knowledge of the part of this thesis, which deals with nonlinearities, could

1

be applied to more realistic models of the solar atmosphere. In this decade, space telescopes such as Yokhoh, SoHO and TRACE have greatly improved the quality of solar observations and have produced a wealth of observations. Also, the improved computing power has made it possible to perform complicated full nonlinear, three-dimensional simulations. It is therefore a challenge to explain the observed features, in which nonlinearity may play an important role (*e.g.* Ofman *et al.*, 1999; Nakariakov *et al.*, 1999).

The work on the dissipative instability of a tangential discontinuity, which we present in this thesis, is a continuation of my undergraduate dissertation (Verwichte, 1995), where I derived a dispersion relation of this model. It has been investigated in two limits, but which did not take into account the effect of thermal conduction (Ruderman, Verwichte, Erdélyi & Goossens, 1996). We therefore wish to investigate the dispersion relation for cases where the effect of thermal conduction is included. We apply the results to a simple model of a solar coronal hole boundary. A coronal hole is known to be the source of the steady, fast solar wind. We therefore expect velocity shears to be present at the boundary between a coronal hole and an active region.

This introductory chapter is structured as follows. In the next section we introduce the set of non-ideal magnetohydrodynamical equations, which we shall use in this thesis. We discuss the ideal and the cold-plasma limit, and the boundary conditions, which we shall use. Furthermore, we discuss the Lorentz and ponderomotive force. In the second section we consider waves in an ideal and inhomogeneous plasma and present the MHD equations for perturbations from an equilibrium, for this model. We discuss the weakly nonlinear approach. The linear MHD waves in an infinite plasma are discussed. We give a brief overview of the quadratically nonlinear equations. Finally, we discuss the numerical code, which has been used to perform the simulations.

1.2 Magnetohydrodynamical equations

In the previous section, we used the terminologies 'plasma', 'magnetohydrodynamics' and 'ponderomotive force'. In this section we shall explain these terms and how we apply them in this thesis. A *plasma* is known as the fourth state of matter (solid, fluid and gas being the other three) in which, through heating, the thermal energy of the constituent particles of a gas becomes so great that the electrostatic forces, which bind electrons to atomic nuclei,

are overcome (Dendy, 1993). A plasma therefore consists of populations of neutral particles and oppositely charged particles: electrons and ions. A plasma is the most common state of matter in the universe, although on Earth it only occurs naturally in lightning and the aurora.

Charge separation produces electrostatic forces which restore electric neutrality, on a time scale proportional to ω_p^{-1}, where $\omega_p = ne^2/m\epsilon_0$ is the plasma frequency. ($e = 1.60 \times 10^{-19}$ C and $\epsilon_0 = 8.85 \times 10^{-12}$ F m^{-1} are the electron charge and permittivity of a vacuum). On this time scale, the plasma is on average electrically neutral. Yet, electric currents are still possible by the collective motions of electrons relative to the ions (Spitzer, 1962). These currents generate large-scale internal magnetic fields, which are described by Maxwell's equations.

We can apply a single-fluid description to a plasma if a plasma is dominated by collisions, so that the distribution of the particles is Maxwellian. Therefore the characteristic time-scale, τ, is required to be much longer than the typical time between particle collisions. We define (Braginskii, 1965):

$$\tau_e = 10^4 \, T_e^{3/2} \, n_e^{-1} \, \text{s} \quad , \quad \tau_i = 6 \times 10^5 \, T_i^{3/2} \, n_i^{-1} \, \text{s} \, , \tag{1.1}$$

as the collision time of electrons and ions respectively. We assumed that the Coulomb logarithm is equal to 20 (see *e.g.* Priest, 1982) for a solar coronal environment. In a single-fluid description, we assume that the temperatures and number densities of the different particle species are equal ($T_i = T_e$, $n_i = n_e$). We see from Expression (1.1) that we require $\tau \gg \tau_i$. Or, in terms of length-scales, we require that the characteristic length-scale, L, is much larger than the mean-free path of ions, ℓ. The length ℓ is defined as the average distance an ion travels at the thermal speed $(k_b T/m_i)^{1/2}$, in the time τ_i (k_b is the Boltzmann constant and is equal to 1.38×10^{-23} JK^{-1} and m_i is the ion mass).

In the presence of a strong magnetic field, we also require that in the direction perpendicular to the magnetic field L is much larger than the typical Larmor gyration radius of the particles (Woods, 1987). The Hall effect may be neglected if τ is much longer than the gyration period of ions. The requirement that each population of particle species has the same temperature is fulfilled if τ is much longer than the time needed to reach local thermal equilibrium (Dendy, 1993).

If all the previous requirements are met, it is possible to define at any time, t, at each

3

point in space, $\vec{r}$, a mass density, ρ, kinetic pressure, p, temperature, T and velocity, $\vec{v}$. We call the single-fluid description of a plasma, *magnetohydrodynamics (MHD)*. It is a macroscopic description of a electrically conducting fluid in the presence of external and internal magnetic fields (Dendy, 1993). The magnetic induction vector, $\vec{B}$, is loosely referred to as the magnetic field vector.

The magnetohydrodynamical description of a plasma is well-known and commonly applied to many laboratory and astrophysical plasmas (see *e.g.* Cowling, 1957; Lighthill, 1960; Spitzer, 1962; Goedbloed, 1979; Parker, 1979; Priest, 1982; Glassmeier & Scholer, 1991). We use the following set of magnetohydrodynamical equations (Goedbloed, 1979). The equation of mass conservation is

$$\frac{\partial \rho}{\partial t} + \vec{\nabla}.\left(\rho\vec{v}\right) = 0 .$$ (1.2)

The equation of motion is given by

$$\rho\frac{d\vec{v}}{dt} = -\vec{\nabla}p + \frac{1}{\mu_0}\left(\vec{\nabla}\times\vec{B}\right)\times\vec{B} + \vec{\nabla}.\hat{\Pi} ,$$ (1.3)

where

$$\frac{d}{dt} = \frac{\partial}{\partial t} + \left(\vec{v}.\vec{\nabla}\right) ,$$ (1.4)

is the time derivative following the motion. The forces per unit volume on the right-hand side of Equation (1.3) are the kinetic pressure, Lorentz and viscous forces. The tensor $\hat{\Pi}$ is the viscous stress tensor, which is a function of the velocity vector. The quantity μ_0 is the permeability of a vacuum and is equal to $4\pi\times 10^{-7}$ H m^{-1}. We do not consider gravitation. We consider an infinitely conducting plasma. In the MHD limit, this means that an electric field is only generated by induction: $\vec{E} = -\vec{v}\times\vec{B}$. There is no electric field in the frame of reference moving with the plasma. This has the consequence that the magnetic flux, through a surface which moves with the plasma, is conserved (Dendy, 1993), or in the words of Alfvén : *"The matter of the fluid is fastened to the lines of force."* In an infinitely conducting plasma, the magnetic field vector is advected by the motion of the plasma. Faraday's law, with an inductive electric field, is equal to:

$$\frac{\partial \vec{B}}{\partial t} = \vec{\nabla}\times\left(\vec{v}\times\vec{B}\right) .$$ (1.5)

We call Equation (1.5) the induction equation. The solenoidal condition

$$\vec{\nabla}.\vec{B} = 0 ,$$ (1.6)

4

says that there are no sources or sinks of magnetic field. There are many forms of the energy equation (see *e.g.* Priest, 1982), of which we adopt the following:

$$\frac{dp}{dt} + \gamma p \vec{\nabla}.\vec{v} = -(\gamma - 1)\left(\vec{\nabla}.\vec{q} + \left(\hat{\Pi}.\vec{\nabla}\right).\vec{n}\right) ,\qquad(1.7)$$

where the two terms on the right-hand side are the heat conduction and viscous heating terms respectively. The vector quantity $\vec{q}$ is the heat flux, which is a function of the plasma temperature. The quantity γ is equal to the ratio of the specific heats and is, for fully ionized plasmas, equal to 5/3. The thermodynamical quantities of a plasma are related to each other by the ideal gas law:

$$p = \frac{\Re \rho T}{\tilde{\mu}} ,\qquad(1.8)$$

where $\tilde{\mu}$ is the mean atomic weight, which for an ionized hydrogen plasma is equal to 0.5. The quantity $\Re$ is the gas constant and is equal to 8.3×10^3 J K^{-1}kg^{-1}. Equations (1.2)-(1.7) form a closed set of nine, nonlinear partial differential equations, which depend on eight variables. This set of equations is over-determined. This is reflected by the solenoidal condition (1.6), which restricts the magnetic field vector.

The current density, $\vec{j}$, is calculated, from the magnetic field vector, by Ampère's law:

$$\vec{j} = \frac{1}{\mu_0}\vec{\nabla} \times \vec{B} .\qquad(1.9)$$

The displacement current has been neglected in Ampère's law, because the time-scales applied in MHD are much longer than the time required for light to transverse the plasma.

With the present mathematical knowledge of systems of nonlinear, partial differential equations, it is not possible to solve the MHD equations in general. It is therefore necessary to make assumptions which simplify the mathematical task. A special class of solutions to the MHD equations are equilibria, for which the plasma quantities do not vary with time (*e.g.* Parker, 1979; Priest, 1982). In this thesis we consider plasmas where the equilibrium quantities are homogeneous. It can be seen easily that, for this case, Equations (1.2)-(1.7) are trivially satisfied.

1.2.1 Lorentz force

We consider the Lorentz force in Equation (1.3) and expand the triple vector product:

$$\frac{1}{\mu_0}\left(\vec{\nabla} \times \vec{B}\right) \times \vec{B} = \left(\vec{B}.\vec{\nabla}\right)\frac{\vec{B}}{\mu_0} - \vec{\nabla}\left(\frac{B^2}{2\mu_0}\right) .\qquad(1.10)$$

5

The first and second terms on the right-hand side of Equation (1.10) are the magnetic tension and pressure force, respectively.

The magnetic tension force acts parallel to the magnetic field-lines, and is of magnitude B^2/μ_0. This force resists bending of the field-lines. This can be seen by decomposing this term into components, locally, parallel and perpendicular to the magnetic field (Shercliff, 1965):

$$\left(\vec{B}.\vec{\nabla}\right)\frac{\vec{B}}{\mu_0} = \frac{d}{ds}\left(\frac{B^2}{2\mu_0}\right)\vec{1}_{\parallel} + \left(\frac{B^2}{\mu_0}\right)\frac{\vec{1}_{\perp}}{R} , \qquad (1.11)$$

where $\vec{1}_{\parallel}$ and $\vec{1}_{\perp}$ are the unit vectors in the directions parallel and perpendicular (principal normal) to the magnetic field respectively, with d/ds the gradient in the parallel direction. The quantity R is the radius of curvature of the magnetic field line. The first term of the right-hand side of Expression (1.11) is due to the non-uniformity of the tension along the magnetic field-line and acts to stretch a magnetic field-line. The second term is a tension acting along the lines of force (Woods, 1987). It acts to shorten curved magnetic field-lines. Therefore, if a magnetic field-line is perturbed transversely, it springs back like a stretched, elastic string.

The second term, namely $\vec{\nabla}(B^2/2\mu_0)$, is an isotropic magnetic pressure force, where the quantity $B^2/2\mu_0$ is the magnetic pressure. This force can also be decomposed into a parallel and perpendicular component. The parallel component acts to stretch a magnetic field-line and it cancels exactly with the parallel component of the tension force. Hence the Lorentz force is directed perpendicular to the magnetic field, which is of course what we expect from the vector cross product on the left-hand side of Expression (1.10).

The sum of the kinetic and magnetic pressure is called the *total pressure*. The ratio of the kinetic and magnetic pressure is called the *plasma β*:

$$\text{plasma } \beta = \frac{\text{kinetic pressure}}{\text{magnetic pressure}} = \frac{p}{B^2/2\mu_0} . \qquad (1.12)$$

The value of the plasma β is a measure of the importance of the magnetic field in a plasma. When the plasma β is much larger than unity, the magnetic effects are weak. This is satisfied in the solar interior. When the plasma β is much smaller than unity, the magnetic effects are strong and dominate the plasma dynamics. This is satisfied in the solar corona (Priest, 1982).

We see that for ideal plasmas three forces are competing with each other: the kinetic

6

pressure, magnetic pressure and magnetic tension force, which are capable of supporting wave motions.

1.2.2 Dissipative terms in strongly magnetised plasmas

In the presence of a magnetic field, charged particles spiral around the field-lines and are inhibited from diffusing across magnetic flux surfaces (Dendy, 1993). Diffusion mechanisms, for example viscosity and thermal conduction, become anisotropic (Braginskii, 1965). A plasma is *strongly magnetised* if the particles gyrate many cycles around the magnetic field-line between particle collisions. Therefore we require that the Larmor gyration frequencies, which are defined as

$$\omega_{ci} = \frac{ZeB}{m_i} \quad , \quad \omega_{ce} = \frac{eB}{m_e} \, , \tag{1.13}$$

are much larger than the collision frequencies τ_i^{-1} and τ_e^{-1} respectively. The quantities Z, m_i and m_e are the proton number, ion mass and electron mass ($m_e = 9 \times 10^{-31}$ kg) respectively. In strongly magnetised plasmas, the viscous stress tensor and heat flux are given by Braginskii (1965).

Viscous stress tensor

The viscous stress tensor is equal to (Braginskii, 1965):

$$\hat{\Pi} = -\eta_0 \hat{W}_0 - \eta_1 \hat{W}_1 - \eta_2 \hat{W}_2 - \eta_3 \hat{W}_3 - \eta_4 \hat{W}_4 \, , \tag{1.14}$$

with

$$W_{0,i,j} = \frac{3}{2} \left(b_i b_j - \frac{1}{3}\delta_{i,j} \right) \sum_{m,n=1}^{3} \left(b_n b_m - \frac{1}{3}\delta_{n,m} \right) W_{n,m} \, , \tag{1.15}$$

$$W_{1,i,j} = \sum_{m,n=1}^{3} \left(\delta_{i,n}^{\perp} \delta_{j,m}^{\perp} + \frac{1}{2}\delta_{i,j}^{\perp} b_n b_m \right) W_{n,m} \, , \tag{1.16}$$

$$W_{2,i,j} = \sum_{m,n=1}^{3} \left(\delta_{i,n}^{\perp} b_j b_m + \delta_{j,m}^{\perp} b_i b_n \right) W_{n,m} \, , \tag{1.17}$$

$$W_{3,i,j} = \sum_{m,n,k=1}^{3} \frac{1}{2} \left(\delta_{i,n}^{\perp} \epsilon_{j,k,m} + \delta_{j,m}^{\perp} \epsilon_{i,k,n} \right) b_k W_{n,m} \, , \tag{1.18}$$

$$W_{4,i,j} = \sum_{m,n,k=1}^{3} \left(b_i b_n \epsilon_{j,k,m} + b_j b_m \epsilon_{i,k,n} \right) b_k W_{n,m} \, , \tag{1.19}$$

where $\hat{W}$ is the rate-of-strain tensor

$$W_{i,j} = \frac{\partial v_i}{\partial x_j} + \frac{\partial v_j}{\partial x_i} - \frac{2}{3}\delta_{i,j}\vec{\nabla}.\vec{v} \; . \qquad (1.20)$$

The quantities $\vec{b}$, $\delta_{i,j}$ and $\epsilon_{i,j,k}$ are the unit vector in the direction of the magnetic field, the Kronecker delta and the anti-symmetric unit tensor, respectively, and $\delta_{i,j}^{\perp} = \delta_{i,j} - b_i b_j$. The five quantities, η, are the dynamical viscosity coefficients and are given as (Braginskii, 1965):

$$\eta_0 = 7.8 \times 10^{-18} T^{5/2} \; \mathrm{kgm^{-1}s^{-1}} \; ,$$

$$\eta_1 \sim (\omega_{ci}\tau_i)^{-2} \quad , \quad \eta_2 \sim (\omega_{ci}\tau_i)^{-2} \quad , \quad \eta_3 \sim (\omega_{ci}\tau_i)^{-1} \quad , \quad \eta_4 \sim (\omega_{ci}\tau_i)^{-1} \; , \quad (1.21)$$

where we have taken the Coulomb logarithm equal to 20. In strongly magnetised plasmas, the coefficient η_0, which is the compressive viscosity coefficient, is much larger than the other coefficients. We therefore only consider the contribution of the term $-\eta_0 \hat{W}_0$ to the viscous stress tensor. It can be shown, by transforming Expression (1.15), that the viscous stress tensor in strongly magnetised plasmas, is equal to:

$$\hat{\Pi} = -\eta_0 \left(\vec{b} \otimes \vec{b} - \frac{1}{3}\hat{I} \right) \left(3 \left(\vec{b}.\vec{\nabla} \right) \left(\vec{b}.\vec{v} \right) - \vec{\nabla}.\vec{v} \right) \; , \qquad (1.22)$$

where $\hat{I}$ is the second-order unit tensor and $\otimes$ is the tensorial product.

Heat flux

The heat flux is equal to (Braginskii, 1965):

$$\vec{q} = -\kappa_{\|}\vec{b} \left(\vec{b}.\vec{\nabla} \right) T - \kappa_{\perp} \vec{\nabla}_{\perp}T + \kappa_{\wedge} \vec{b} \times \vec{\nabla}T \; , \qquad (1.23)$$

where the operator $\vec{\nabla}_{\perp}$ is the gradient in the direction perpendicular to the magnetic field. The three coefficients, κ, are the thermal conduction coefficients and are given as (Braginskii, 1965):

$$\kappa_{\|} = 9 \times 10^{-12} \, T^{5/2} \; \mathrm{Wm^{-1}K^{-1}} \quad , \quad \kappa_{\perp} \sim (\omega_{ce}\tau_e)^{-2} \quad , \quad \kappa_{\wedge} \sim (\omega_{ce}\tau_e)^{-1} \; , \qquad (1.24)$$

where, again, we have taken the Coulomb logarithm equal to 20. In strongly magnetised plasmas, the parallel thermal conduction coefficient is much larger than the other coefficients. Therefore we only consider the first term of Expression (1.23). Thus, the heat flux in strongly magnetised plasmas is equal to:

$$\vec{q} = -\kappa_{\|}\vec{b} \left(\vec{b}.\vec{\nabla} \right) T \; . \qquad (1.25)$$

1.2.3 Ideal MHD equations

An *ideal* plasma is defined as a plasma which conserves momentum, magnetic flux and energy. This case is widely used (*e.g.* Goedbloed, 1979). In our case, this implies that the thermal conduction and viscous terms in Equations (1.2)-(1.7) are neglected. This is possible when the time-scale of the considered problem is much shorter than the typical diffusion time. Hence, the ideal MHD equations, are:

$$\frac{\partial \rho}{\partial t} + \vec{\nabla}.(\rho \vec{v}) = 0 . \tag{1.26}$$

$$\rho \frac{d\vec{v}}{dt} = -\vec{\nabla}p + \frac{1}{\mu_0}\left(\vec{\nabla} \times \vec{B}\right) \times \vec{B} , \tag{1.27}$$

$$\frac{\partial \vec{B}}{\partial t} = \vec{\nabla} \times \left(\vec{v} \times \vec{B}\right) , \tag{1.28}$$

$$\vec{\nabla}.\vec{B} = 0 , \tag{1.29}$$

$$\frac{dp}{dt} + \gamma p \vec{\nabla}.\vec{v} = 0 . \tag{1.30}$$

The ideal energy equation (1.30) is, using Expression (1.26), transformed into

$$\frac{d}{dt}\left(\frac{p}{\rho^\gamma}\right) = 0 , \tag{1.31}$$

which shows that disturbances in the plasma evolve adiabatically.

In Chapters 2, 3 and 4 we consider a model of an ideal plasma and apply the set of Equations (1.26)-(1.30), to which we add the ideal gas law (1.8). For the model in Chapter 3, it is more convenient to use the vector potential $\vec{B} = \vec{\nabla} \times \vec{A}$ and we eliminate the magnetic field vector in Equations (1.27) and (1.28) in favour of the vector potential. The induction equation (1.28) is consequently equal to

$$\frac{\partial \vec{A}}{\partial t} = \vec{v} \times \left(\vec{\nabla} \times \vec{A}\right) . \tag{1.32}$$

In Chapter 5, we shall consider a model with dissipation which is governed by the set of Equations (1.2)-(1.8).

1.2.4 Cold-plasma limit

A *cold plasma*, or low-β plasma, is defined as a plasma in the limit of the plasma β tending to zero, *i.e.* the kinetic pressure is neglected in comparison with the magnetic pressure. This definition is not to be confused with the definition used in plasma physics, where a

cold plasma is a plasma of zero temperature (Stix, 1962). For example, the cold-plasma limit is often applied to the solar corona (*e.g.* Yang & Hollweg, 1991; Ruderman, 1991), where the temperature is of order of a million Kelvin !

By neglecting the kinetic pressure force from the momentum Equation (1.3), the MHD equations are significantly simplified. The energy equation (1.7) is decoupled from the rest of the MHD equations and is therefore not necessary for determining the dynamics of the plasma. The plasma is described by the plasma density and the velocity and magnetic field vectors. At each moment in time, though, the kinetic pressure can be calculated from these quantities, using Equation (1.7) and it may then be checked, by calculating the kinetic pressure force, if the assumption of a cold plasma is still valid.

In a cold and ideal plasma, the component of the velocity in the direction of the magnetic field remains constant in time, because the only considered force, the Lorentz force, always acts perpendicular to the magnetic field. This can be interpreted as a direct consequence of the fact that the plasma is advected with the magnetic field.

In Chapters 2, 3 and 4 we encounter the situation that a plasma, which initially satisfies the assumption of a cold plasma, evolves nonlinearly to an unphysical situation. The failure to describe the whole evolution of the plasma, is that momentum balance in the direction of an equilibrium magnetic field is not achieved. This leads to a locally, infinite density. This means that at some point in time before this occurs, the cold-plasma assumption becomes invalid. We shall discuss this problem in the next chapters in more detail.

Another problem with a cold plasma is that the effect of thermal conduction cannot be taken into account in a consistent manner (Ruderman, 1991). This is because the thermal conduction term appears in the energy equation which does not contribute to the dynamics of the plasma. In Chapter 5, we show that this can lead to an incomplete picture in the application of a dissipative model to the solar corona, where the effects of viscosity and thermal conduction are of equal importance.

We conclude that the assumption of a cold-plasma limit is useful for considering the dynamics of a plasma which is dominated by magnetic fields. It is, though, important to also bear in mind the limitations which this assumption brings. This can be seen as one of the themes of this thesis.

1.2.5 Ponderomotive force

The word 'ponderomotive' is derived from the words 'ponderous', which means 'weighty', and 'motive', which means 'having power to cause motion' (Geddie, 1952). Dendy (1993) calls the ponderomotive force (PMF) the 'mass-moving'-force. The concept of the pondero-motive force was introduced by Einstein when he proposed the concept of photons as an explanation of the photo-electric phenomena (Arons & Peppard, 1965). The definition of the ponderomotive force has varied with time. In the beginning of this century, the whole Lorentz force was referred to as the ponderomotive force. Landshoff (1957), on the other hand, calls the MHD version of the Lorentz force in Equation (1.3) the ponderomotive force.

Presently, the *ponderomotive force* is defined as a basic nonlinear force, which consists of a spatial gradient of a wave-field intensity, which has a non-vanishing effect when averaged over the wave period (*e.g.* Bittencourt, 1986; Allan *et al.*, 1991):

$$\vec{F}_{PMF} \sim \vec{\nabla} < A^2_{\text{wave}} > \ . \tag{1.33}$$

Therefore the ponderomotive force acts on a slower time-scale than the wave period and is directed towards the maxima of the intensity wave-field. In this thesis we call the pondero-motive force the nonlinear terms of the momentum equation, which contain a combination of wave quantities. We shall show that the terms of this force, of leading order in a small wave amplitude, have the form of the product of a wave quantity and a gradient of a wave quantity. A travelling wave in a homogeneous plasma does not give rise to a non-vanishing contribution because at a fixed position, the ponderomotive force from the positive and negative slopes of the intensity wave fields cancel each other, over a wave period. This can easily be seen by substituting the form of a travelling wave, $A = \cos(x - t)$ into Expression (1.33). We are, though, interested in situations where the ponderomotive force does have a non-vanishing contribution when averaged over the wave period. This occurs in various ways. Firstly, the interaction of two oppositely travelling sinusoidal waves gives rise to fixed spatial gradients in the intensity wave-field, *i.e.* a 'standing' wave. We do not use the terminology of standing waves because the gradients of the wave may evolve nonlinearly. We shall therefore use the terminology *bounded* instead. We expect bounded waves to have a non-vanishing ponderomotive force (*e.g.* Allan *et al.*, 1991; Rankin *et al.*, 1993). We shall study this case in Chapters 2 and 3. Secondly, two oppositely travelling pulses give rise to a non-vanishing ponderomotive force when they cross each other (Verwichte *et al.*,

1999). We shall investigate this case in Chapter 4. Thirdly, a smooth inhomogeneity in the equilibrium quantities alters the intensity of the wave field of a wave that travels along the gradient. The ponderomotive force of the positive and negative slopes no longer cancel each other (*e.g.* Stark *et al.*, 1995; Boynton & Torkelsson 1996; Torkelsson & Boynton, 1998).

The ponderomotive force is applied in plasma physics to, for example, problems of 'end-plugging' of magnetic mirror systems by radio-frequency waves, laser-plasma interactions and self-focusing of lasers (Nishikawa & Wakatami, 1990). It is also successfully applied to astrophysical situations. In the Earth's magnetospheric environment the ponderomotive force of MHD waves is studied in connection with mass transport from the ionosphere into the magnetosphere and the dynamics of field line resonances (Allan *et al.*, 1990; Allan *et al.*, 1991; Rankin *et al.*, 1993; Rankin *et al.*, 1994; Tikhonchuk *et al.*, 1995; Allan & Manuel, 1996). In the study of the solar wind, the ponderomotive force of MHD waves (Hollweg, 1971;1978) is used as an extra acceleration mechanism (Stark *et al.*, 1995) and an explanation for density fluctuations (Vasques & Hollweg, 1995). Martin *et al.* (1997) considered the ponderomotive force of an Alfvén wave in the context of molecular cloud support.

Allan & Manuel (1996) compare the plasma motions excited by the ponderomotive force of MHD waves with the motion of frictionless beads along a transversely oscillating, stretched string. In Chapter 2, we shall investigate this mechanical analogue in detail.

1.2.6 Boundary conditions

In a bounded or discontinuous plasma ,we need to add to the MHD equations boundary or jump conditions respectively. In this section we discuss the boundary conditions used in this thesis. We consider two basic models. In Chapters 1 and 2, we consider fixed boundaries and in Chapter 5 we consider a tangential discontinuity. We shall not explicitly derive the boundary conditions, for which the MHD equations are needed in a conservational form, but refer to the detailed discussion in Roberts (1967) and Goedbloed (1979).

Conditions for a bounded medium

We consider an isolated plasma which is bounded so that there is no flux of mass, momentum and energy through the boundaries, which are fixed. This implies that the component of

the velocity vector normal to the boundary is equal to zero: $\vec{v}.\vec{1}_n. = 0$ (Roberts, 1967). The vector $\vec{1}_n$ is a unit vector directed perpendicular to the boundary.

The induction equation (1.5) gives for this case the boundary condition $(\vec{B}.\vec{1}_n)[\vec{v}] = 0$ (Goedbloed, 1979), where the square brackets denote the difference of the quantity in the inside medium and the outside medium, measured infinitesimally close to the interface, taken along the normal to the surface of the boundary.

On a fixed boundary (a solid wall) the component of the magnetic field normal to the boundary is equal to zero, i.e. $\vec{B}.\vec{1}_n = 0$ (Goedbloed, 1979). The component of the velocity tangential to the boundary may, in an ideal medium, be non-zero.

At a boundary, threaded by a magnetic field, i.e. $\vec{B}.\vec{1}_n \neq 0$, the induction equation (1.5) shows that the tangential component of the velocity needs to be continuous (Goedbloed, 1979). We choose to set this component of the velocity equal to zero at this boundary. This is the line-tied boundary condition. The displacement vector $\vec{\xi}$, which is defined as (Goedbloed, 1979)

$$\vec{v} = \frac{d\vec{\xi}}{dt} , \qquad (1.34)$$

is consequently also equal to zero for line-tied conditions.

Jump-conditions at a tangential discontinuity

We consider the jump-conditions at a tangential discontinuity in the presence of dissipation. A tangential discontinuity is a discontinuity, which separates two plasmas and moves at the speed of the plasma. This means that there is no exchange of mass between the two plasmas:

$$(\vec{v} - \vec{w}) .\vec{1}_n = 0 , \qquad (1.35)$$

where $\vec{1}_n$ is the unit vector normal to the discontinuity surface and $\vec{w}$ is the velocity of the discontinuity. The solenoidal condition (1.6), integrated over an elemental volume, gives us: $[\vec{B}.\vec{1}_n] = 0$, where the square brackets denote the difference of the quantity in Medium '1' and Medium '2', measured infinitesimally close to the interface, taken along the normal to the surface of the interface. In order for the velocity to be discontinuous, we need to set

$$\vec{B}.\vec{1}_n = 0 . \qquad (1.36)$$

This means that the magnetic field is always parallel to the interface, which is the boundary between two topological distinct magnetic regions (Goedbloed, 1979). Integrating the

conservational form of the momentum Equation (1.3) across the interface, gives us:

$$\left[p + \frac{B^2}{\mu_0} + \hat{\Pi}. \right] \vec{1}_n = 0 \ .$$

(1.37)

Condition (1.37) represents the continuity of the stresses, normal to the surface. The energy equation (1.7) cannot be transformed into a conservational form. We rather need a conservation equation for the total energy density (Equation (5-13) in Goedbloed, 1979). Including the effect of dissipation, this equation is integrated across the discontinuity surface (Goossens, 1995). We find:

$$\left[\vec{q}.\vec{1}_n \right] = 0 \ .$$

(1.38)

This result can also be found by integrating the equation of heat transfer (*e.g.* Landau & Lifshitz, 1959). It is not obvious how to satisfy Condition (1.38). The classical (Fourier) form of the heat flux is $\vec{q} = -\kappa \vec{\nabla} T$, where κ is the thermal conduction coefficient. The heat flux tends to smooth out temperature differences parallel as well as normal to the discontinuity surface. In strongly magnetised plasmas the heat flux is anisotropic (Braginskii, 1965) and given by Expression (1.25). There is no heat flux across the surface, so that the temperatures on both sides of the discontinuity surface may differ.

1.3 Waves in an ideal and homogeneous plasma

In this section we consider an ideal and homogeneous plasma, in a cartesian coordinate system (x, y, z). This is the basis for the models we investigate in Chapters 2,3 and 4. The equilibrium quantities, which trivially satisfy the ideal MHD equations (1.26)-(1.30), are denoted with a subscript '0'. The equilibrium magnetic field is uniform and taken parallel to the x-direction: $\vec{B}_0 = B_0 \vec{1}_x$. We consider the equilibrium to be static, *i.e.* $\vec{v}_0 = \vec{0}$. Furthermore, we take perturbations from this equilibrium and we denote the perturbation quantities with a prime:

$$\rho = \rho_0 + \rho' \ , \quad \vec{v} = \vec{v}' \ , \quad \vec{B} = \vec{B}_0 + \vec{B}' \ , \quad p = p_0 + p' \ .$$

(1.39)

Expression (1.39) is substituted into the set of equations (1.26)-(1.30), which becomes:

$$\frac{\partial \rho'}{\partial t} + \rho_0 \vec{\nabla}.\vec{v}' = -\vec{\nabla}.\left(\rho' \vec{v}' \right) \ ,$$

(1.40)

$$\rho_0 \frac{\partial \vec{v}'}{\partial t} + \vec{\nabla} p' + \frac{B_0}{\mu_0} \left(\vec{\nabla} B'_x - \frac{\partial \vec{B}'}{\partial x} \right) = -\rho' \frac{\partial \vec{v}'}{\partial t} - \left(\rho_0 + \rho' \right) \left(\vec{v}.\vec{\nabla} \right) \vec{v}'$$

14

$$-\vec{\nabla}\left(\frac{B'^2}{2\mu_0}\right)+\left(\vec{B}'.\vec{\nabla}\right)\frac{\vec{B}'}{\mu_0}\ , \qquad (1.41)$$

$$\frac{\partial\vec{B}'}{\partial t}+\vec{B}_0\vec{\nabla}.\vec{v}'-B_0\frac{\partial\vec{v}'}{\partial x} = -\vec{B}'\vec{\nabla}.\vec{v}'+\left(\vec{B}'.\vec{\nabla}\right)\vec{v}'-\left(\vec{v}'.\vec{\nabla}\right)\vec{B}'\ , \quad (1.42)$$

$$\vec{\nabla}.\vec{B}' = 0\ , \qquad (1.43)$$

$$\frac{\partial p'}{\partial t}+\gamma p_0\vec{\nabla}.\vec{v}' = -\left(\vec{v}'.\vec{\nabla}\right)p'-\gamma p'\vec{\nabla}.\vec{v}'\ , \qquad (1.44)$$

The terms on the left-hand sides of Equations (1.40)-(1.42), which we call the perturbed MHD equations, are linear with respect to the perturbation quantities. These terms describe the well-known linear MHD wave behaviour of an homogeneous plasma (*e.g.* Goedbloed, 1979), which we shall discuss in a next section. The terms on the right-hand sides contain combinations of the perturbation quantities, and are therefore nonlinear. We identify the terms on the right-hand side of the momentum equation (1.41) as the ponderomotive force:

$$\vec{F}_{PMF} = -\rho'\frac{\partial\vec{v}'}{\partial t}-(\rho_0+\rho')\left(\vec{v}'.\vec{\nabla}\right)\vec{v}'-\vec{\nabla}\left(\frac{B'^2}{2\mu_0}\right)+\left(\vec{B}'.\vec{\nabla}\right)\frac{\vec{B}'}{\mu_0}\ . \qquad (1.45)$$

We are interested in situations where this force has a non-vanishing effect on a time-scale longer than the typical oscillation period of the perturbation.

1.3.1 Weakly nonlinear regime

The set of Equations (1.40)-(1.44), is also a nonlinear system of partial differential equations, and difficult to solve mathematically. We make the simplification that the perturbation quantities are small in comparison with the equilibrium quantities, so that they can be expanded in a power series of a small parameter ϵ ($0 \leq \epsilon < 1$), which is of the order of the perturbation amplitude (Neyfey, 1985):

$$\rho' = \epsilon\rho_1+\epsilon^2\rho_2+\epsilon^3\rho_3+\dots\ ,\quad \vec{v}' = \epsilon\vec{v}_1+\epsilon^2\vec{v}_2+\epsilon^3\vec{v}_3+\dots\ ,$$
$$\vec{B}' = \epsilon\vec{B}_1+\epsilon^2\vec{B}_2+\epsilon^3\vec{B}_3+\dots\ ,\quad p' = \epsilon p_1+\epsilon^2 p_2+\epsilon^3 p_3+\dots\ . \qquad (1.46)$$

Expansions (1.46) are substituted into the set of equations (1.40)-(1.44). The terms of the same order in ϵ are gathered together and form a closed system of linear, partial differential equations. The quantities of that order depend on the lower-order and equilibrium quantities. The full solution to Equations (1.40)-(1.44) is, in principle, calculated by solving the linearized system of equations at all orders of ϵ. In practice, the series expansion (1.46) is

truncated. The number of terms of the series, which are included in the analysis, depends on the subject of study. Often, when the amplitude of the perturbation is assumed to be very small, only the first-order terms in the series expansion (1.46) are considered. This is called *linear* MHD (*e.g.* Goedbloed, 1979; Goossens, 1995). In our model, this corresponds to seeking a solution of Equations (1.40)-(1.44), with setting the terms on the right-hand-side equal to zero. We shall investigate this case in the next section. When more terms in the series expansion (1.46) are considered, we take into account the effect of the nonlinear terms on the right-hand side of Equations (1.40)-(1.44). The study of nonlinear equations by use of a series expansion of the variables, is called the *weakly nonlinear* regime (*e.g.* Mio *et al.*, 1976). The expansion can be modified, by a multiple-scales analysis (Taniuti & Yajima, 1969), to change the ordering of the nonlinear terms. In this way, the lowest-order equation in ϵ is often reduced to a nonlinear equation in one of the plasma quantities, which is common in physics (*e.g.* Cohen & Kulsrud, 1974; Mio *et al.*, 1976; Roberts & Mangeney, 1982).

1.3.2 Linear waves in an homogeneous and infinite plasma

In this section we investigate the linear MHD waves in a homogeneous and infinite plasma. This relatively simple model is convenient for introducing the basic waves, which are supported by the kinetic pressure and magnetic pressure and tension forces, and their basic properties. We consider linear waves by setting the terms on the right-hand sides of Equations (1.40)-(1.44) equal to zero. The perturbation quantities correspond to the first-order terms in the Expansions (1.46) and we shall refer to them with the adjectives 'first-order' or 'linear'. The Equations (1.40)-(1.44) are linearized:

$$\frac{\partial \rho_1}{\partial t} = -\rho_0 \vec{\nabla}.\vec{v}_1 , \tag{1.47}$$

$$\rho_0 \frac{\partial \vec{v}_1}{\partial t} = -\vec{\nabla}\left(p_1 + \frac{B_0 B_{x,1}}{\mu_0}\right) + B_0 \frac{\partial}{\partial x}\left(\frac{\vec{B}_1}{\mu_0}\right) , \tag{1.48}$$

$$\frac{\partial \vec{B}_1}{\partial t} = -\vec{\nabla}.\vec{v}_1 \vec{B}_0 - B_0 \frac{\partial \vec{v}_1}{\partial x} , \tag{1.49}$$

$$\vec{\nabla}.\vec{B}_1 = 0 , \tag{1.50}$$

$$\frac{\partial p_1}{\partial t} = -\gamma p_0 \vec{\nabla}.\vec{v}_1 . \tag{1.51}$$

At this point it is convenient to introduce the typical speeds. The equilibrium Alfvén and sound speeds, V_A and C_s respectively, are defined as

$$V_A = \frac{B_0}{\sqrt{\rho_0 \mu_0}} \quad , \quad C_s = \sqrt{\frac{\gamma p_0}{\rho_0}} \, . \tag{1.52}$$

We introduce the parameter β as the ratio

$$\beta = \frac{C_s^2}{V_A^2} \, , \tag{1.53}$$

and it is equal to $\gamma/2$ times the plasma β. It is therefore a good measure of the importance of the ratio of kinetic and magnetic pressure. Another speed that frequently appears in MHD wave theory is the equilibrium cusp (or tube) speed, V_c. It is defined as:

$$V_c = \frac{C_s V_A}{\sqrt{C_s^2 + V_A^2}} \, , \tag{1.54}$$

and is smaller than both the Alfvén and sound speeds.

We transform the set of equations (1.47)-(1.51) into a system of equations in the dilatation $\Delta = \vec{\nabla} . \vec{v}_1$ and the components of the rate-of-strain and vorticity parallel to the equilibrium magnetic field, $\Gamma = \partial v_{x,1} / \partial x$ and $\Omega_x = (\vec{\nabla} \times \vec{v}_1) . \vec{1}_x$ respectively (Lighthill, 1960):

$$\frac{\partial^2 \Gamma}{\partial t^2} = C_s^2 \frac{\partial^2 \Delta}{\partial x^2} \, , \tag{1.55}$$

$$\frac{\partial^2 \Delta}{\partial t^2} = \left(C_s^2 + V_A^2 \right) \vec{\nabla}^2 \Delta - \vec{\nabla}^2 \Gamma \, , \tag{1.56}$$

$$\frac{\partial^2 \Omega_x}{\partial t^2} = V_A^2 \frac{\partial^2 \Omega_x}{\partial x^2} \, . \tag{1.57}$$

Equations (1.55)-(1.56) form a coupled system of equations in the variables Δ and Γ. Equation (1.57) is decoupled from the other equations and has the form of a one-dimensional wave-equation in Ω_x, with a wave speed V_A. It is the *Alfvén wave equation*. We consider the coupled system of equations (1.55)-(1.56) first.

Magneto-acoustic waves

We consider the case $\Omega_x = 0$ and eliminate the variable Γ in Equations (1.55)-(1.56) in favour of the variable Δ:

$$\left[\frac{\partial^4}{\partial t^4} - \left(C_s^2 + V_A^2 \right) \vec{\nabla}^2 \frac{\partial^2}{\partial t^2} + C_s^2 V_A^2 \vec{\nabla}^2 \frac{\partial^2}{\partial x^2} \right] \Delta = 0 \, , \tag{1.58}$$

17
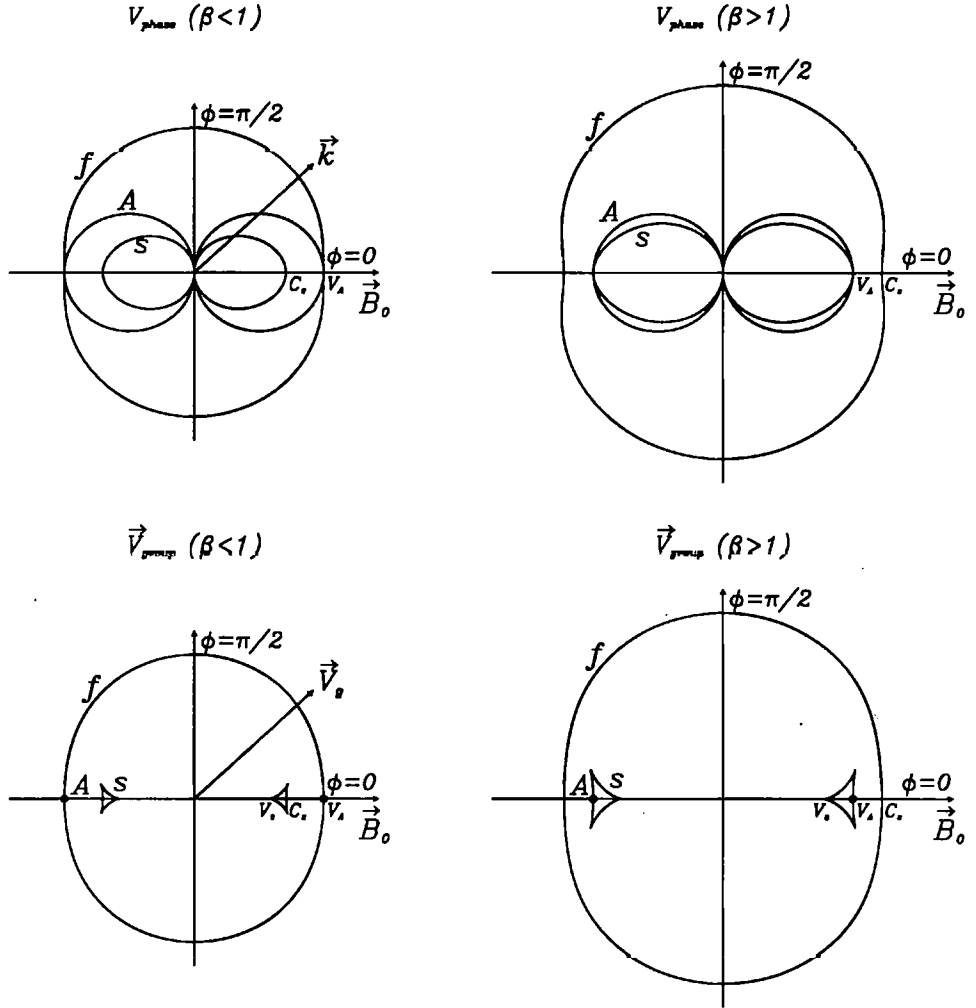
Figure 1.1: Polar plot of the phase speed, V_p, and the group velocity $\vec{V}_g$ as functions of the angle ϕ between the directions of the wave vector and equilibrium magnetic field. The symbols 'f', 's' and 'A' denote the fast and slow magneto-acoustic waves and the Alfvén wave respectively.

which is a partial differential equation, governing *magneto-acoustic waves*. We seek a solution of this equation in the form of a plane wave with frequency ω and wave vector $\vec{k}$:

$$\Delta(\vec{r}, t) = \int_{-\infty}^{+\infty} d\vec{r} \int_{-\infty}^{+\infty} dt \, \tilde{\Delta}(\vec{k}, \omega) \, e^{i(\vec{k}.\vec{r} - \omega t)} \ . \qquad (1.59)$$

Substituting Expression (1.59) into Equation (1.58), we find the dispersion relation for magneto-acoustic waves, which relates ω to the components of $\vec{k}$:

$$\omega^4 - \left(C_s^2 + V_A^2\right) k^2\omega^2 + C_s^2 V_A^2 k^2 k_x^2 = 0 \, , \tag{1.60}$$

which is solved for the squared phase speed $V_p^2 = \omega^2/k^2$, as a function of the angle between the wave vector and the equilibrium magnetic field, ϕ:

$$V_p^2 = \frac{1}{2} \left(C_s^2 + V_A^2\right) \left[1 \pm \sqrt{1 - \frac{4V_c^2 \cos^2\phi}{(C_s^2 + V_A^2)}}\right] \, , \tag{1.61}$$

The solutions with the largest and smallest magnitudes of the phase speed are called the *fast* and *slow* magneto-acoustic waves respectively.

From inspecting Equations (1.47), (1.49) and (1.51), we learn that the magneto-acoustic wave solution perturbs the density and the kinetic and magnetic pressures. These waves are therefore compressive and supported by pressure forces. Furthermore, this solution perturbs the components of the velocity and magnetic field perturbation vectors, both parallel and perpendicular to the magnetic field. Therefore these waves are also supported by the magnetic tension force. Magneto-acoustic waves can be interpreted as a marriage between sound and magnetic waves, with both longitudinal and transverse wave-behaviour.

Figure 1.1 shows the phase speed and group velocity of the fast and slow magneto-acoustic waves as functions of the angle ϕ, for the cases $\beta < 1$ and $\beta > 1$. It becomes immediately clear that the slow magneto-acoustic wave is highly anisotropic; it does not propagate perpendicular to the equilibrium magnetic field and the wave-energy propagates only quasi-parallel to the magnetic field. The slow wave has a maximum propagation speed of C_s and V_A when the parameter β is smaller and larger than unity respectively. On the other hand, the fast magneto-acoustic wave is nearly isotropic, with the largest propagation speed in the direction perpendicular to the equilibrium magnetic field. Both types of waves are dispersive, which can be seen by calculating the group velocity from Expression (1.61). Figure 1.2 shows the frequency range of the fast and slow magneto-acoustic waves as functions of the transverse wave-vector component, k_y. Because the dispersion relation (1.61) only depends on k_z through k, we can set k_z equal to zero without loss of generality. This corresponds to taking $\partial/\partial z = 0$. The square of the fast wave frequency is always larger than $\max\{C_s^2 k_x^2, V_A^2 k_x^2\}$ and the square of the slow wave frequency is in the interval $(V_c^2 k_x^2, \min\{C_s^2 k_x^2, V_A^2 k_x^2\})$.

19
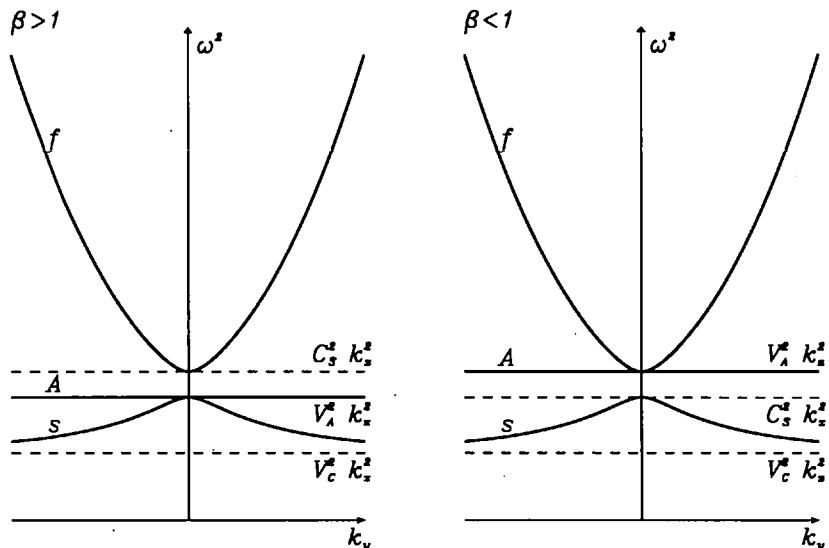
Figure 1.2: Plot of the wave frequency, ω, of the fast (f) and slow (s) magneto-acoustic waves (1.61) and the Alfvén wave (A) (1.62) as functions of k_y, for fixed value of k_x and $k_z = 0$ and for β larger and smaller than unity.

We see from Expression (1.61) and Figures 1.1 and 1.2 that, when β tends to zero (cold-plasma limit), the slow magneto-acoustic wave solution vanishes and the fast magneto-acoustic wave solution is governed by the dispersion relation $\omega^2 = k^2 V_A^2$. In this limit, the component of the linear velocity perturbation vector parallel to the equilibrium magnetic field, $v_{1,x}$, is equal to zero.

Alfvén waves

We consider the case that $\Delta = \Gamma = 0$ and solve the Alfvén wave-equation (1.57) for a plane wave $\Omega_x = \int d\vec{r} \int dt \tilde{\Omega}_x \exp[i(\vec{k}.\vec{r} - \omega t)]$, which results in the dispersion relation:

$$\frac{\omega^2}{k^2} = V_A^2 \cos^2 \phi \ . \tag{1.62}$$

From inspecting Equations (1.47)-(1.51), we see that the Alfvén wave solution perturbs the components of the velocity and magnetic field perturbation vectors perpendicular to the equilibrium magnetic field. The density, kinetic pressure and the components of the velocity and magnetic field perturbation vectors parallel to the equilibrium magnetic field

20

are not perturbed ($\rho = p = v_x = B_x = 0$). This means that the kinetic and magnetic pressure forces are zero, so that the Alfvén wave solution does not compress the plasma. Therefore we conclude that the linear Alfvén wave is a transverse and incompressible wave ($\vec{k}.\vec{v} = 0$), which is driven by the magnetic tension force. It is therefore a purely magnetic wave.

Figure 1.1 shows the phase speed and group velocity of the Alfvén wave as a function of the angle ϕ, which shows that the Alfvén wave is highly anisotropic; it does not propagate perpendicular to the magnetic field and the wave energy propagates only in the direction parallel to the equilibrium magnetic field. The Alfvén wave is clearly non-dispersive.

We compare the three types of waves for the case of propagation parallel to the equilibrium magnetic field ($k_y = k_z = 0$). Figure 1.1 shows that when β is smaller (larger) than unity, the fast and slow magneto-acoustic wave behave like Alfvén (sound) and sound (Alfvén) wave respectively.

Identification of linear perturbation quantities with wave-types

In Chapters 2, 3 and 4, we assume that the plasma quantities do not vary in the z-direction ($\partial/\partial z = 0$). We have previously shown that this assumption does not make the results of the linear model in this section less general. This argument, though, does not apply, generally, to the full perturbed nonlinear set of Equations (1.40)-(1.44). There is therefore no justification for making this assumption in that case, except that it simplifies the equations (*e.g.* Nakariakov *et al.*, 1997). We do not set the z-components of the plasma vector quantities equal to zero. With this assumption, we see that in the linear set of Equations (1.47)-(1.51), the z-components of the momentum and induction equation are decoupled from the rest of the equations. The z-component of the linear velocity and magnetic field vector, $v_{z,1}$ and $B_{z,1}$ respectively, satisfy the Alfvén wave equation, which is of the form (1.57). Therefore they govern a linearly polarized Alfvén wave. The other linear perturbation quantities (ρ_1, p_1, $v_{x,1}$, $v_{y,1}$, $B_{x,1}$ and $B_{x,2}$) govern the magneto-acoustic waves. By not considering variations in the z-direction, we eliminated the linear coupling between the Alfvén and magneto-acoustic waves.

1.3.3 Surface waves

In this subsection, we shall take $k_z = 0$ as well. If we look at Figure 1.2 and dispersion relation (1.61), we see that for squared frequencies, ω^2 in the intervals $(0, V_c^2 k_x^2)$ and $(\min\{C_s^2 k_x^2, V_A^2 k_x^2\}, \max\{C_s^2 k_x^2, V_A^2 k_x^2\})$, the z-component of the wave vector, k_y is complex. This means that, in these intervals, the wave solution is not oscillatory in the direction perpendicular to the equilibrium magnetic field (y-direction), but exponentially evanescent or growing. This solution is unphysical in a homogeneous, infinite plasma, because the wave energy density, $\rho_1 v_1^2/2$, becomes infinite as y tends to infinity. But this solution does have relevance in plasmas, which have structuring in the transverse direction. In many solar and astrophysical applications, the structuring is modelled by several homogeneous media, separated by a sharp discontinuity (*e.g.* Roberts, 1991; Edwin, 1992). For this type of model, we can apply Equations (1.2)-(1.7) to which the jump-conditions (1.36)-(1.38) are added. In Chapter 5 we consider a single interface separating two homogeneous media. Suppose that the two media are ideal and that perturbations are small so that we only consider solutions of first order. The plasma quantities on both sides of the interface are governed by Equations (1.47)-(1.51). The perturbation quantities can be fourier-analysed in x and t, but the y-dependency has to remain explicit. Equations (1.47)-(1.51) can then be transformed into an ordinary differential equation in y for one of the perturbation quantities. The solution has to satisfy the linearized and ideal versions of the jump-conditions and the requirement that the wave energy remains finite. This leads to a dispersion relation for ω as a function of k_x. It is possible to consider a solution which has an evanescent profile in the y-direction, in both media. This solution is localised at the interface and is called a *surface wave*. The surface wave solutions are classified into 'fast' and 'slow' surface waves (Roberts, 1981), although they are not the exact equivalent of the fast and slow magneto-acoustic waves in an infinite plasma.

1.3.4 Visual inspection of the quadratically nonlinear terms

We discuss, with the assumption that $\partial/\partial z = 0$, the terms in the set of equations (1.40)-(1.44), which are of order ϵ^2. We refer to the perturbation quantities of this order with the adjectives 'second-order' or 'quadratically nonlinear'. We discuss the second-order moderations of the linear waves by inspecting the the second-order terms in the momentum

Equation (1.41). It can be shown that the conclusions we make also hold for the second-order terms of Equations (1.40), (1.42) and (1.44) (Nakariakov $et\ al.$, 1997). The momentum Equation (1.41) of order ϵ^2 is:

$$\rho_0 \frac{\partial v_{x,2}}{\partial t} + \frac{\partial p_2}{\partial x} = F_{x,fs} + F_{x,A} \ , \qquad (1.63)$$

$$\rho_0 \frac{\partial v_{y,2}}{\partial t} + \frac{\partial p_2}{\partial y} + \frac{B_0}{\mu_0} \left(\frac{\partial B_{x,2}}{\partial y} - \frac{\partial B_{y,2}}{\partial x} \right) = F_{y,fs} + F_{y,A} \ , \qquad (1.64)$$

$$\rho_0 \frac{\partial v_{z,2}}{\partial t} - \frac{B_0}{\mu_0} \frac{\partial B_{z,2}}{\partial x} = F_{z,fsA} \ , \qquad (1.65)$$

where the functions F make up the components of the second-order ponderomotive force. They are defined as follows:

$$F_{x,fs} = -\rho_1 \frac{\partial v_{x,1}}{\partial t} - \rho_0 \left(\vec{v}_1 . \vec{\nabla} \right) v_{x,1} - \frac{\partial}{\partial x} \left(\frac{B_{y,1}^2}{2\mu_0} \right) + B_{y,1} \frac{\partial}{\partial y} \left(\frac{B_{x,1}}{\mu_0} \right) \ , \qquad (1.66)$$

$$F_{x,A} = -\frac{\partial}{\partial x} \left(\frac{B_{z,1}^2}{2\mu_0} \right) \ , \qquad (1.67)$$

$$F_{y,fs} = -\rho_1 \frac{\partial v_{y,1}}{\partial t} - \rho_0 \left(\vec{v}_1 . \vec{\nabla} \right) v_{y,1} - \frac{\partial}{\partial x} \left(\frac{B_{x,1}^2}{2\mu_0} \right) + B_{x,1} \frac{\partial}{\partial x} \left(\frac{B_{y,1}}{\mu_0} \right) \ , \qquad (1.68)$$

$$F_{y,A} = -\frac{\partial}{\partial y} \left(\frac{B_{z,1}^2}{2\mu_0} \right) \ , \qquad (1.69)$$

$$F_{z,fsA} = -\rho_1 \frac{\partial v_{z,1}}{\partial t} - \rho_0 \left(\vec{v}_1 . \vec{\nabla} \right) v_{y,1} + \left(\vec{B}_1 . \vec{\nabla} \right) \frac{B_{z,1}}{\mu_0} \ , \qquad (1.70)$$

where the nabla operator is defined as $\vec{\nabla}(\partial/\partial x, \partial/\partial y, 0)$. The left-hand side of the system of Equations (1.63)-(1.65) contains second-order perturbation quantities and has the same form as the components of the linear momentum equation (1.48). Therefore we have the same identification of the perturbation quantities of this order with the different linear wave-types: Equations (1.63) and (1.64) describe fast and slow magneto-acoustic waves and Equation (1.65) describes the linearly polarized Alfvén wave. This is actually true for all orders in ϵ. The second-order solution is driven by the components of the second-order ponderomotive force, which are the terms of the right-hand side of Equations (1.63)-(1.65). We call the driven part of the solution the *ponderomotive response*. They contain a product of two first-order perturbation quantities. The terms $F_{x,fs}$ and $F_{y,fs}$ contain a product of two first-order magneto-acoustic wave perturbations, and the terms $F_{x,A}$ and $F_{y,A}$ contain a product of two first-order Alfvén wave perturbation quantities. The term $F_{z,fsA}$ acts on the component of the momentum equation governing the Alfvén wave. It depends on a

23

product of a first-order magneto-acoustic and Alfvén perturbation quantity and is equal to zero when one of the two wave-types is not excited. Consequently the Alfvén wave is not moderated by the second-order ponderomotive force. From looking at the z-component of the ponderomotive force in Expression (1.45), we see that this is true for all orders of ϵ. It is a direct consequence of ignoring variations in the z-direction. We shall discuss two cases: the second-order ponderomotive force of a linear Alfvén wave and of the linear magneto-acoustic waves. .

Linear Alfvén wave

We assume that only a linearly polarized Alfvén wave is excited. This means that the amplitudes of the linear fast and slow magneto-acoustic wave solutions are equal to zero: $\rho_1 = p_1 = v_{x,1} = v_{y,1} = B_{x,1} = B_{y,1} = 0$. Consequently the force terms $F_{x,fs}$, $F_{y,fs}$ and $F_{z,fsA}$ are equal to zero as well. The force terms $F_{x,A}$ and $F_{y,A}$ are the components of the second-order ponderomotive force of the Alfvén wave. From Expressions (1.67) and (1.69) we see that they have the form of a Alfvén magnetic wave pressure force (Hollweg, 1971). This force excites magneto-acoustic waves. The driven magneto-acoustic solutions perturb the density and pressure. Therefore the Alfvén wave is, through a nonlinear coupling to the magneto-acoustic waves, compressive, where the perturbation v_x and the density perturbation are proportional to the square of the wave amplitude ($O(\epsilon^2)$). In the cold-plasma limit the linear slow wave solution vanishes and the plasma is directly accelerated along the equilibrium magnetic field by the force $F_{x,A}$ towards the nodes of the z-component of the first-order magnetic field perturbation. At these positions. the density is expected to increase. We conclude that the Alfvén wave does not moderate itself quadratically nonlinearly and that it perturbs the plasma density through the action of the second-order ponderomotive force. These results are relevant for Chapters 2 and 4 where the nonlinear evolution of Alfvén waves is investigated.

Linear magneto-acoustic waves

We assume that the coupled fast and slow magneto-acoustic waves are excited and the Alfvén wave amplitude is set equal to zero ($v_{z,1} = B_{z,1} = 0$). As a consequence the force terms $F_{x,A}$, $F_{y,A}$ and $F_{z,fsA}$ are equal to zero. The force terms $F_{x,fs}$ and $F_{y,fs}$ are the components of the second-order ponderomotive force of the magneto-acoustic waves, which moderate

the magneto-acoustic waves themselves. The Alfvén wave is not moderated. In the cold-plasma limit, the slow magneto-acoustic wave vanishes and the quantities $\rho_1, v_{y,1}, B_{x,1}$ and $B_{y,1}$ govern the first-order fast magneto-acoustic wave. The force terms $F_{x,fs}$ and $F_{y,fs}$ are then the components of the second-order ponderomotive force of the fast wave. The force $F_{x,fs}$ accelerates plasma along the equilibrium magnetic field and the force $F_{y,fs}$ moderates the fast magneto-acoustic wave. We conclude that the magneto-acoustic waves moderate themselves through the action of the second-order ponderomotive force. These results are relevant for Chapter 3 where the nonlinear evolution of magneto-acoustic waves in a cold plasma is investigated.

1.4 Numerical simulations

In this section we want to give details about the numerical code, which has been used for simulations in Chapters 3 and 4. We used the ideal MHD Lagrangian code of Dr Aaron Longbottom (Arber *et al.*, 1998; Longbottom *et al.*, 1998), which solves the fully nonlinear, Lagrangian version of the ideal MHD equations (1.26)-(1.30):

$$\rho \frac{d\vec{v}}{dt} = -\vec{\nabla}p + \left(\vec{\nabla} \times \vec{B}\right) \times \vec{B} , \qquad (1.71)$$

$$\frac{d\vec{r}}{dt} = \vec{v} , \qquad (1.72)$$

where $\vec{v}$ and $\vec{r}$ are respectively the velocity and position vectors of a fluid element at the current time. The pressure, density and magnetic field vector at position $\vec{r}$ are calculated from the values of these quantities at the initial position $\vec{r}_i$, using the Lagrangian versions of Equations (1.31), (1.26) and (1.28) respectively:

$$\frac{p}{\rho^\gamma} = \text{constant} \quad , \quad \rho = \frac{\rho_i}{\Delta} \quad , \quad \vec{B} = \frac{1}{\Delta}\left(\vec{B}_i . \vec{\nabla}_i\right) \vec{r} , \qquad (1.73)$$

where

$$\Delta = \left|\frac{\partial \vec{r}}{\partial \vec{r}_i}\right| , \qquad (1.74)$$

is the Jacobian of the transformation from the initial to the current position vector. Equations (1.72) are advanced in time using a Lax-Wendroff type method, which is second-order in time and space. This method of solving the ideal MHD equations preserves the total mass, entropy and solenoidal conditions identically. Arber *et al.* (1999) state that the numerical scheme gives excellent energy conservation.

25

The advantage of a Lagrangian code over an equivalent Eulerian code is that as time progresses, the grid deforms so that grid points are moved to regions of compression. This property is attractive because in our models we encounter large, localised compressions. This property also means that the Lagrangian code needs fewer grid points in comparison with the Eulerian code to resolve the evolution of a system. Another important reason for preferring this code is the clarity and user-friendliness of the code and the close proximity of its designer. A disadvantage of the code is that, because it is an ideal code, it cannot capture shocks. The further evolution of a system, once a shock has formed, is meaningless.

In Chapter 3, we use a 2.5 D version of the code. Variations in the z-direction are not considered. At the boundaries in the x- and y-direction, all components of the velocity vector are set equal to zero. This implies that all components of the displacement vector are equal to zero at the boundary as well. The code has been modified so that the temporal evolution of the quantities, at a fixed point in space, can be calculated. This is achieved by interpolation from values of nearby grid-points. It proved efficient to consider six grid-points: the nearest grid-point, its four neighbours on the grid, and the next nearest grid-point.

In Chapter 4, we use a 1.5 D version of the code. Variations in the y- and z-direction are not considered. The same boundary conditions are applied but are not of importance because the boundaries are removed far enough not to influence the phenomena under study.

In Chapters 2 and 4, we use a fourth-order Runge-Kutta scheme with adaptive step size for the integration of ordinary differential equations.

1.5   Thesis outline

This thesis contains two separate topics: Elements of the nonlinear evolution of MHD waves in the context of the ponderomotive force (Chapters 2, 3 and 4) and the linear, dissipative instability of the tangential discontinuity (Chapter 5).

In this chapter we introduced the basic MHD Equations (1.2)-(1.7) and the boundary conditions, which are used in this thesis. We introduced the concepts of cold plasmas, ponderomotive force and weakly nonlinear theory. We presented the perturbed MHD Equations (1.40)-(1.44) for an ideal and homogeneous equilibrium, discussed the types of linear waves in an infinite plasma and inspected the quadratically nonlinear perturbed equations. Lastly we briefly discussed the numerical simulations which have been used.

In Chapter 2, we compare the evolution of bounded, nonlinear Alfvén waves to the mechanical analogues of the motion of a frictionless bead along an oscillating stretched string and of the motion of a fluid in a tube of infinitesimal width. In Chapter 3, we investigate the evolution of bounded, nonlinear fast magneto-acoustic waves in a cold plasma. In Chapter 4, the nonlinear evolution of two oppositely propagating linearly polarized Alfvén pulses is discussed in a cold plasma and in a plasma of finite plasma β.

Chapter 5 considers the linear instability of a tangential discontinuity in the presence of an equilibrium flow, which takes into account the effects of viscosity and thermal conduction, as a model for a coronal hole boundary.

In Chapter 6, we summarize and discuss the results of the previous chapters.

Chapter 2

A mechanical analogue of bounded, nonlinear Alfvén waves

2.1 Introduction

In an infinitely conducting plasma, the magnetic flux in conserved. It is said that the plasma is frozen to the magnetic field-lines. The magnetic field-lines are compared to stretched strings with their own tension $B^2/2\mu_0$. This magnetic tension drives transverse magnetic waves in fluids, *i.e.* Alfvén waves. In this mechanical analogy, Alfvén waves can be seen as the transverse disturbances of the string which travel along its length (*e.g.* Wentzel, 1989; Benz, 1993). Various authors have used this analogy in MHD applications. Joarder & Roberts (1992) and Mundie (1998) considered the analogy of the vibrations of a stretched string loaded with a large, concentrated mass at its centre to model the vertical modes of oscillation of a prominence.

In the Introduction, we have shown that linearly polarized Alfvén waves excite, through the action of the ponderomotive force, nonlinearly slow magnetosonic waves, which are characterised by density perturbations and a velocity component parallel to the equilibrium magnetic field. Allan & Manuel (1996) suggested, but without any arguments, that the nonlinear behaviour of the ponderomotive force of Alfvén waves can be compared by analogy to the frictionless motion of beads along a transversely oscillating, stretched string. In this chapter we investigate this claim in an attempt to understand the basic properties of the ponderomotive force.

Consider a string of length L and mass M. The linear density of the string is equal to $\sigma_s = M/L$. We use the convention of axes of Chapter 1. At rest, the string lies along the x-direction. The string only moves transversly in the z-direction. The displacement of the string is called $\eta(x,t)$ (which is equal to the z-component of the displacement vector, $\vec{\xi}$). Displacements in the x-direction are not permitted. The restoring force that resists the transverse displacement, is the tension force per unit length, which is directed along the principal normal of the string:

$$\vec{F}(x,t) = \frac{\partial}{\partial x}\left(\mathcal{T}\frac{\partial \eta(x,t)}{\partial x}\right)\vec{1}_{\perp}\,, \qquad (2.1)$$

where $\vec{1}_{\perp} = \sin\left(\arctan\left(\frac{\partial \eta}{\partial x}\right)\right)\vec{1}_x - \cos\left(\arctan\left(\frac{\partial \eta}{\partial x}\right)\right)\vec{1}_z$ and $\vec{1}_x$ and $\vec{1}_z$ are the unit vectors in the x- and z-directions respectively. The quantity $\mathcal{T}$ is the tension, which is related to the elasticity of the material of which the string is made. We shall assume that $\mathcal{T}$ is constant. Expression (2.1) is valid when the condition

$$\frac{\partial \eta(x,t)}{\partial x} \ll 1\,, \qquad (2.2)$$

is met. This limits the magnitude of the displacement. This approximation therefore corresponds to a weakly nonlinear limit and the displacement is of order ϵ $(0 \leq \epsilon < 1)$.

We attach beads, each of mass m, uniformly onto the string. The beads can move freely along the string. The string is made to oscillate in the transverse direction. The question is then: how do the beads move ? In the first section, a geometric argument is given for the force that moves a bead. We shall discuss the validity of the derived equations as a mechanical analogue for Alfvén waves. In the second section, a more rigorous approach is given for the motion of discrete particles along the string and how they influence the string's oscillation. In the third section we make the transition to a continuum description.

2.2 Geometric approach

We attach a bead to the string. The position of the bead is given by the coordinates $(x_b(t), z_b(t))$ as shown in Figure 2.1. The bead is accelerated by the restoring force of the string. The acceleration in the z-direction forces the bead to oscillate along with the string as the bead is constrained by it $(z_b(t) = \eta(x_b, t))$. The acceleration in the x-direction moves
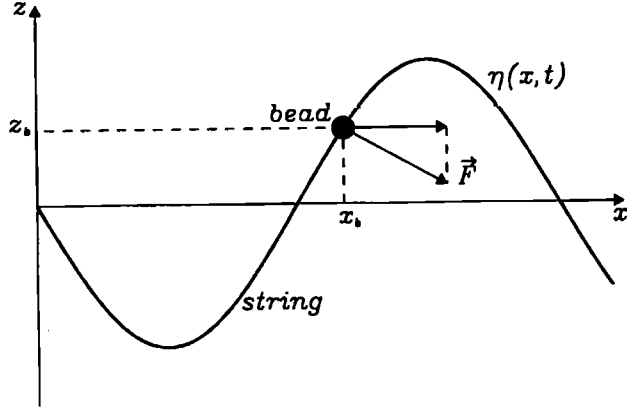
Figure 2.1: Model of the mechanical analogue.

the bead along the string.

$$m\frac{d^2x_b}{dt^2} = \vec{1}_\perp.\vec{1}_x \, T\frac{\partial^2\eta}{\partial x^2} \, |_{x=x_b} \, , \tag{2.3}$$

$$m\frac{d^2z_b}{dt^2} = m\frac{d^2\eta}{dt^2} \, |_{x=x_b} = \vec{1}_\perp.\vec{1}_z \, T\frac{\partial^2\eta}{\partial x^2} \, |_{x=x_b} \, . \tag{2.4}$$

The typical speed at which disturbances travel along the string is given by the speed V_s:

$$V_s = \sqrt{\frac{T}{\sigma_s}}, \tag{2.5}$$

The total derivative, acting on the continuous variable η, is defined as

$$\frac{d\eta}{dt} \, |_{x=x_b} = \frac{\partial\eta}{\partial t} \, |_{x=x_b} + \frac{dx_b}{dt}\frac{\partial\eta}{\partial x} \, |_{x=x_b} \, . \tag{2.6}$$

We eliminate the common part of the two Equations (2.3) and (2.4) and obtain an equation for $x_b(t)$:

$$m\frac{d^2x_b}{dt^2} = m\frac{(\vec{1}_\perp.\vec{1}_x)}{(\vec{1}_\perp.\vec{1}_z)}\frac{d^2z_b}{dt^2} = -m\left(\frac{\partial\eta}{\partial x}\frac{d^2\eta}{dt^2}\right) \, |_{x=x_b} \, . \tag{2.7}$$

The force that moves the bead along the string is a nonlinear force, of at least order ϵ^2, consisting of the product of the spatial derivative and the acceleration of the displacement of the string at the position of the bead. The displacement of the bead in the x-direction is then at least of order ϵ^2 as well. We identify this force as the ponderomotive force. Note

30

that this force does not directly depend on the mass density or tension of the string. At the nodes and anti-nodes of the string's displacement field, the ponderomotive force is zero, making these positions equilibrium positions for the bead. In the next section a linearization of the ponderomotive force will show which equilibrium positions are stable or unstable.

We compare the form of the ponderomotive force of this mechanical analogue to that of the case of Alfvén waves, in the weakly nonlinear regime. In Chapter 1, we established that the Alfvén wave is driven by the magnetic tension force. We identified this force as the second term in Expression (1.11):

$$\vec{F} = \frac{B^2}{\mu_0} \frac{\vec{1}_\perp}{R} \, , \tag{2.8}$$

where R is equal to the radius of curvature. An important difference between the magnetic tension force and (2.8) and the elastic tension force (2.1), is that the magnetic tension B^2/μ_0 is not a constant. If we repeat the derivation of the ponderomotive force, replacing the force (2.1) by the force (2.8), we find the same Expression (2.7) for the ponderomotive force. This force depends on the magnetic tension indirectly through the relationship between the displacement and the magnetic field, given by Equations (1.27) and (1.28):

$$\frac{d^2\eta}{dt^2} = \frac{B_0}{\rho_0\mu_0} \frac{\partial B_z}{\partial x} + o(\epsilon^3) \, , \quad \frac{\partial \eta}{\partial x} = \frac{B_z}{B_0} + o(\epsilon^3) \, . \tag{2.9}$$

Note that the correction is at least of order ϵ^3 because, as we have shown in Chapter 1, the Alfvén wave is not moderated at order ϵ^2.

With Expression (2.9), the tension force (2.8) is rewritten as:

$$\vec{F} = \frac{B_0^2}{\mu_0} \left[1 + \left(\frac{\partial\eta}{\partial x}\right)^2\right]^{-2} \frac{\partial^2\eta}{\partial x^2} \vec{1}_\perp = \frac{\partial}{\partial x}\left(\frac{B_0^2}{\mu_0}\frac{\partial\eta}{\partial x}\right) \vec{1}_\perp + o(\epsilon^3) \, . \tag{2.10}$$

This shows that up to order ϵ^3, the tension force of the string and the magnetic tension force are equivalent if we put $\mathcal{T} = B_0^2/\mu_0$.

Lastly we show the correspondence between the form of the ponderomotive force (2.7) and the x-component of the second-order ponderomotive force of Alfvén waves, (1.67). We eliminate the displacement, using Expression (2.9), in Expression (2.7) and find to leading order in ϵ:

$$\rho_0 \left(\frac{\partial\eta}{\partial x}\frac{d^2\eta}{dt^2}\right) = -\frac{\partial}{\partial x}\left(\frac{B_{z,1}^2}{2\mu_0}\right) \, . \tag{2.11}$$

31

The right-hand side of Expression (2.11) corresponds to the x-component of the second-order ponderomotive force of linearly polarized Alfvén waves (1.67).

We find, to leading order in ϵ, the same tension and ponderomotive force. The variance of the magnetic tension is of importance at order ϵ^3. We conclude that the model of a transversely oscillating, stretched string, of constant tension, is a good mechanical analogue for the weakly nonlinear dynamics of a linearly polarized Alfvén waves when the displacement is small. We therefore examine this analogue further.

Using Definition (2.6), Equation (2.7) is rewritten as

$$\frac{d^2 x_b}{dt^2} = -\frac{\frac{\partial \eta}{\partial x}\left(\frac{\partial^2 \eta}{\partial t^2} + 2\frac{\partial^2 \eta}{\partial t \partial x}\frac{dx_b}{dt} + \frac{\partial^2 \eta}{\partial x^2}\left(\frac{dx_b}{dt}\right)^2\right)}{1 + \left(\frac{\partial \eta}{\partial x}\right)^2} \mid_{x=x_b} . \tag{2.12}$$

The equation of motion for the displacement η is that of a string with an added, mobile bead:

$$\sigma_s \frac{\partial^2 \eta}{\partial t^2} + m\delta(x - x_b)\frac{d^2 \eta}{dt^2}\mid_{x=x_b} - \mathcal{T}\frac{\partial^2 \eta}{\partial x^2} = 0 , \tag{2.13}$$

or

$$\left[\frac{\partial^2}{\partial t^2} - V_s^2\frac{\partial^2}{\partial x^2}\right]\eta = -\frac{m\delta(x - x_b)}{\sigma_s}\frac{d^2 \eta}{dt^2}\mid_{x=x_b} . \tag{2.14}$$

The term on the right-hand side of Equation (2.14) is the counteraction of the bead on to the motion of the string. Using Definition (2.6) and Equation (2.12), the previous Equation (2.14) is rewritten as

$$(\sigma_s + m\delta(x - x_b))\frac{\partial^2 \eta}{\partial t^2} - \left(\mathcal{T} - m\delta(x - x_b)\left(\frac{dx_b}{dt}\right)^2\right)\frac{\partial^2 \eta}{\partial x^2} =$$
$$- m\delta(x - x_b)\left(\frac{d^2 x_b}{dt^2}\frac{\partial \eta}{\partial x} + 2\frac{dx_b}{dt}\frac{\partial^2 \eta}{\partial t \partial x}\right) . \tag{2.15}$$

From Expression (2.15) we see that at the position of the bead the tension has decreased by the inertia of the bead in the x-direction, $m(dx_b/dt)^2$. The inertia of the bead carries the string further than its original maximum displacement in the absence of the bead. We model the bead as a point particle. The nonlinear term is therefore localised at the position of the bead. This poses the following problem. Close to the bead's position the derivative $\partial \eta / \partial x$ will violate Assumption (2.2). At the exact position of the bead the derivative $\partial \eta / \partial x$ will not even exist as the string is forced into a cusp there. To overcome this difficulty a bead of a finite width has to be considered.

32

We shall not consider this here because we shall neglect the contribution of the bead to the string's oscillation by taking the mass of the bead to be negligible compared with the mass of the string. However when dealing with a large number of beads, a large concentration of beads can locally make the density of the beads of the same order as that of the string's density, implying that the contribution of the beads to the string's oscillation cannot be ignored. This problem will be addressed in the next section, where we derive the equations for the bead and string in a more rigorous manner.

2.3   Beads as discrete particles

Consider n identical beads attached to the string. Each bead has a mass m. The position of the ith bead is given by $(x_i(t), z_i(t))$. Equations for the motion of the beads and the string are obtained using the variational principle with the method of undetermined multipliers (Goldstein, 1950). We construct the Lagrangian, $\mathcal{L}$, of this system. It contains the kinetic and potential energies of the string and the kinetic energy of each bead. The potential energy of the string is calculated for the restoring force per unit length (2.1), with constant tension, $\mathcal{T}$ (Morse & Feshbach, 1953). The Lagrangian, $\mathcal{L}$ is equal to:

$$\mathcal{L} = \int_0^L dx \left[\frac{\sigma_s}{2} \left(\frac{\partial \eta}{\partial t} \right)^2 - \frac{\mathcal{T}}{2} \left(\frac{\partial \eta}{\partial x} \right)^2 \right] + \sum_{i=1}^n \frac{m}{2} \left(\left(\frac{dx_i}{dt} \right)^2 + \left(\frac{dy_i}{dt} \right)^2 \right). \qquad (2.16)$$

The first term of the previous expression is the Lagrangian of the string and the second term is the Lagrangian of all the beads. The position of each bead is constrained by the condition that it has to remain on the string:

$$z_i = \int_0^L dx\, \delta(x - x_i)\, \eta(x, t). \qquad (2.17)$$

We form the following functional:

$$I = \int_{t_1}^{t_2} dt \left[\mathcal{L} + \sum_{i=1}^n \lambda_i \left(z_i - \int_0^L dx\, \delta(x - x_i)\, \eta(x, t) \right) \right], \qquad (2.18)$$

where the λ_i's are the Lagrangian undetermined multipliers. The functional I has as dependent variables $\eta(x, t)$, $x_i(t)$ and $z_i(t)$. Following Hamilton's principle, we minimize the functional I by taking variations of I with respect to the dependent variables and setting the variation equal to zero. At times t_1 and t_2, the variations are zero. We obtain $2n+1$

33

equations:

$$m\frac{d^2x_i}{dt^2} = -\lambda_i \frac{\partial \eta}{\partial x}\mid_{x=x_i} , \tag{2.19}$$

$$m\frac{d^2z_i}{dt^2} = \lambda_i , \tag{2.20}$$

$$\left[\frac{\partial^2}{\partial t^2} - V_s^2 \frac{\partial^2}{\partial x^2}\right] \eta(x,t) = -\frac{1}{\sigma_s}\sum_{i=1}^{n} \lambda_i \, \delta(x - x_i) . \tag{2.21}$$

The multipliers λ_i's are obtained from Equations (2.17) and (2.20):

$$\lambda_i = m\frac{d^2\eta}{dt^2}\mid_{x=x_i} = m\left(\frac{\partial \eta}{\partial x}\frac{d^2x_i}{dt^2} + \frac{\partial^2 \eta}{\partial t^2} + 2\frac{\partial^2 \eta}{\partial t \partial x}\frac{dx_i}{dt} + \frac{\partial^2 \eta}{\partial x^2}\left(\frac{dx_i}{dt}\right)^2\right)\mid_{x=x_i} . \tag{2.22}$$

Substituting Expression (2.22) into Equations (2.19) and (2.21), we get

$$\frac{d^2x_i}{dt^2} = -\frac{\frac{\partial \eta}{\partial x}\left(\frac{\partial^2 \eta}{\partial t^2} + 2\frac{\partial^2 \eta}{\partial t \partial x}\frac{dx_i}{dt} + \frac{\partial^2 \eta}{\partial x^2}\left(\frac{dx_i}{dt}\right)^2\right)}{1 + \left(\frac{\partial \eta}{\partial x}\right)^2}\mid_{x=x_i} , \tag{2.23}$$

$$\left[\frac{\partial^2}{\partial t^2} - V_s^2 \frac{\partial^2}{\partial x^2}\right] \eta(x,t) = -\frac{m}{\sigma_s}\sum_{i=1}^{n} \frac{d^2\eta}{dt^2}\mid_{x=x_i} \delta(x - x_i) . \tag{2.24}$$

These equations are identical to Equations (2.12) and (2.14).

We prescribe the following boundary and initial conditions for the string's displacement:

$$\eta(0,t) = 0 , \ \eta(L,t) = 0 , \ \eta(x,0) = \frac{a}{k}\sin(kx) , \tag{2.25}$$

where k is a multiple of π/L and a is the dimensionless amplitude of the perturbation. The boundary conditions on the displacement correspond to the line-tied boundary conditions. In the absence of beads, Condition (2.25) makes the string oscillate in one of its standing wave modes. With beads included, the oscillation of the string is moderated. We therefore use the terminology 'bounded' instead of 'standing'. The initial conditions for the beads are:

$$x_i(0) = x_{i,0} , \ \frac{dx_i(0)}{dt} = 0 , \tag{2.26}$$

and we assume that the beads do not overlap initially, *i.e.* $x_{i,0} \neq x_{j,0}$. Condition (2.2) implies that the weakly nonlinear regime applies. Therefore the amplitude a is small and proportional to a parameter ϵ ($0 \leq \epsilon < 1$). The quantities η and x_i are expanded in a power series in the parameter ϵ:

$$\eta(x,t) = \epsilon\eta_1(x,t) + \epsilon^2\eta_2(x,t) + \dots ,$$
$$x_i(t) = x_{i,0} + \epsilon x_{i,1}(t) + \epsilon^2 x_{i,2}(t) + \dots . \tag{2.27}$$

34

We substitute Expansions (2.27) into Equations (2.23) and (2.24) and gather terms of the same order of ϵ.

We assume that the mass of the beads is much less than the mass of the string. The term on the right-hand side of Equation (2.24) represents the influence of the beads on the string's oscillation. We neglect this unless the density of the beads, which is defined as

$$\sigma(x,t) = \sum_{i=1}^{n} m\delta(x - x_i) , \qquad (2.28)$$

becomes locally of the same order as the string's density. We need to keep an eye on the condition:

$$\sigma(x,t) \ll \sigma_s . \qquad (2.29)$$

2.3.1 Oscillations of string without beads

The terms in Equations (2.23) and (2.24) of order ϵ are:

$$\frac{d^2 x_{i,1}}{dt^2} = 0 , \qquad (2.30)$$

$$\left[\frac{\partial^2}{\partial t^2} - V_s^2 \frac{\partial^2}{\partial x^2} \right] \eta_1 = 0 . \qquad (2.31)$$

At order ϵ we simply have the oscillation of the string without the presence of the beads. There is no displacement of the beads along the string ($x_{i,1}=0$). The density of the beads fulfills Condition (2.29). The solution of the wave equation (2.31) is a discrete set of 'standing' modes. Together with Condition (2.25) we find:

$$\eta_1 = \frac{a}{k} \sin(kx) \cos(\omega t) , \qquad (2.32)$$

where ω is the oscillation frequency, which is defined as $\omega = kV_s$.

2.3.2 Motion of beads due to the ponderomotive force

The equations of order ϵ^2 are:

$$\frac{d^2 x_{i,2}}{dt^2} = -\frac{\partial \eta_1}{\partial x} \frac{\partial^2 \eta_1}{\partial t^2} \Big|_{x=x_i} , \qquad (2.33)$$

$$\left[\frac{\partial^2}{\partial t^2} - V_s^2 \frac{\partial^2}{\partial x^2} \right] \eta_2 = 0 . \qquad (2.34)$$

35

Because the wave equation (2.34) is the same as the wave equation (2.31), we take $\eta_2 = 0$. The term on the right-hand side of Equation (2.33) corresponds to the second-order ponderomotive acceleration. Using the first-order Solution (2.32), Equation (2.33) is written as

$$\frac{d^2 x_{i,2}}{dt^2} = \frac{1}{2} a^2 k V_s^2 \sin\left(2k x_{i,2}\right) \sin^2\left(\omega t\right). \tag{2.35}$$

We are interested in the movement of the bead over a time-scale longer than the oscillation period of the string. Therefore we average Equation (2.35) over the oscillation period:

$$\frac{d^2 x_{i,2}}{dt^2} = \frac{1}{4} a^2 k V_s^2 \sin\left(2k x_{i,2}\right). \tag{2.36}$$

We see that the second-order ponderomotive force of the bounded wave has a net effect over a wave oscillation period. Equation (2.36) is the differential equation of an anharmonic oscillator (*e.g.* Pippards, 1978). The solution of this equation is given in terms of Jacobian elliptic functions. Equation (2.36) can be integrated once immediately:

$$\frac{1}{2} m \left(\frac{dx_{i,2}}{dt}\right)^2 + \frac{m}{8} a^2 V_s^2 \cos\left(2k x_{i,2}\right) = C, \tag{2.37}$$

which reflects conservation of energy. The terms on the left-hand side of Expression (2.37) are the kinetic energy of the bead i and the potential energy of the second-order ponderomotive force respectively. Here C is an integration constant linked to the initial energy:

$$C = E(x_{i,0}) = -\frac{m}{8} a^2 V_s^2 \cos\left(2k x_{i,0}\right). \tag{2.38}$$

From the potential energy, we see that the anti-nodes ($x = p\pi/2$, p an odd integer) of the string's wave-field are stable equilibrium points, while the nodes ($x = p\pi$, p integer) are unstable equilibrium points.

Equation (2.37) can be written in the form:

$$\frac{d\chi}{dt} = \frac{\Omega\zeta}{k} \sqrt{1 - \zeta^{-2} \sin^2\left(k\chi\right)}, \tag{2.39}$$

with

$$\begin{aligned} \chi &= x_{i,2} + \frac{\pi}{2k}, \\ \Omega &= \frac{akV_s}{\sqrt{2}}, \\ \zeta &= \cos\left(k x_{i,0}\right). \end{aligned} \tag{2.40}$$
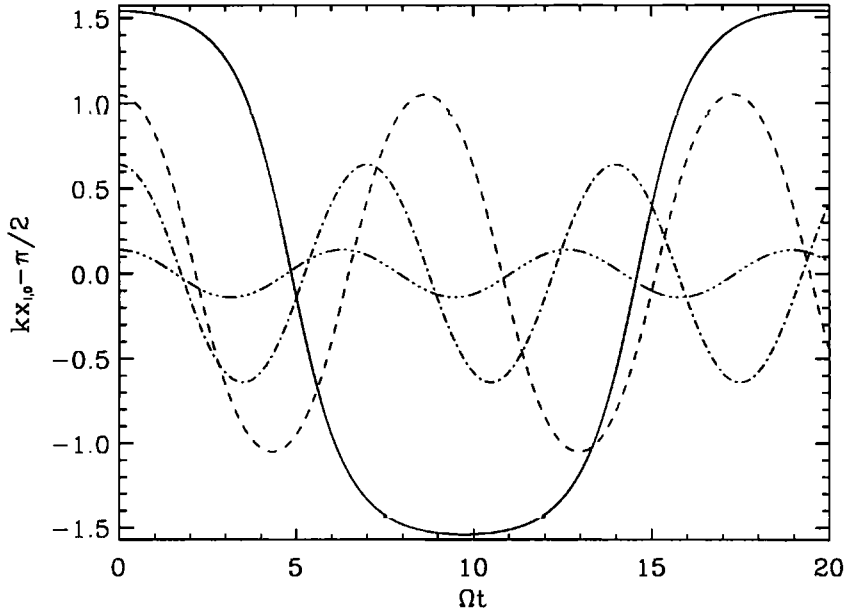
Figure 2.2: Position of bead $x_{i,2}(t)$ for different initial positions $kx_{i,0} - \pi/2$ (solid line: 1.54, dashed line: 1.05, dot-dashed line: 0.64, triple-dot line: 0.14). The anti-node is at 0. Two nodes are located at $\pm\pi/2$.

The solution of Equation (2.39), satisfying the initial and boundary conditions (2.25) is:

$$x_{i,2}(t) = \frac{1}{k} \arccos\left[\text{sn}\left(\zeta\Omega t + \text{sn}^{-1}\left(\zeta, \zeta^{-2} \right), \zeta^{-2} \right) \right]. \tag{2.41}$$

The function $\text{sn}(u, \kappa)$ is a Jacobian elliptic function with parameter κ (Abramowitz & Stegun, 1965). Using the properties of Jacobian elliptic functions, Expression (2.41) is written as

$$x_{i,2}(t) = \frac{1}{k} \arccos\left[\cos\left(kx_{i,0} \right) \frac{\text{cn}\left(\Omega t, \zeta^2 \right)}{\text{dn}\left(\Omega t, \zeta^2 \right)} \right]. \tag{2.42}$$

$\text{cn}(u, \kappa)$ and $\text{dn}(u, \kappa)$ are Jacobian elliptic functions with parameter κ. Figure 2.2 shows the x-coordinate of a bead in time, starting at several initial positions.

Every bead, when given no initial velocity, will oscillate around the nearest anti-node in the string's displacement field with an amplitude equal to the distance between the nearest anti-node and its original position. When this amplitude is small, the motion is approximately harmonic.

37

There are now two approaches. The first approach is to have a finite number n of non-interacting beads attached to the string. The motion of each of these beads, when the string is oscillating according to Equation (2.32), is given by Solution (2.42). The total mass of the beads is sufficiently small compared with the mass of the string so that at no instance the does local linear density of the beads become of the same order as the linear density of the string. The contribution of the beads to the string's oscillation is negligible. This approach is adequate as a mechanical analogue for charged particles in a low density environment along an oscillating magnetic field-line, where there are no external fields.

The second approach is an attempt to use the previous equations to describe a continuous spread of beads. Initially the beads are uniformly spread along the string; at every position along the string, there is one bead of mass m. This means that the linear density of the beads is initially equal to $\sigma(t=0) = nm/L$ and we assume this is much less than the linear density of the string. However, this will not necessarily be true for later times. We need to check whether Condition (2.29) remains valid. This condition is rewritten as:

$$\frac{\sigma(x,t)}{\sigma(t=0)} \ll \frac{M}{nm} \; . \tag{2.43}$$

We calculate the linear density of beads at later times. The position at later times is known from Expression (2.42). We assume that the beads do not interact with each other, passing through each other freely. This is obviously an unrealistic assumption. We shall discuss the consequences of this later on. The density of the beads at time t is given by the transformation (Goedbloed,1979):

$$\begin{aligned}
\sigma(x_{i,0}, t) &= \frac{\partial x_{i,0}}{\partial x_{i,2}} \sigma(t=0) \; , \\
&= \frac{\mathrm{dn}^2(\Omega t, \zeta^2)\, \sigma(t=0)}{\mathrm{cn}(\Omega t, \zeta^2)\left[1 + \zeta(1-\zeta^2)\frac{\partial}{\partial \zeta}\ln\left(\mathrm{cn}(\Omega t, \zeta^2)\right)\right]} \; ,
\end{aligned} \tag{2.44}$$

where we treat $x_{i,0}$ and $x_{i,2}$ as the Eulerian and Lagrangian position coordinates respectively. Figure 2.3a shows the time T_n a bead takes to reach the closest anti-node from its original position. It is calculated from the fact that the function $\mathrm{cn}(u, \kappa)$ is periodic with a period equal to $4\,\mathrm{F}(\pi/2, \kappa)$ where $\mathrm{F}(u, \kappa)$ is the Jacobian integral of the first kind. Beads that start out close to the anti-node arrive at the anti-node at approximately the same time, while the beads that start further out, come in later. For $kx_{i,0}$ nearing $\pi/2$, ΩT_n is converging to $\pi/2$, as it should since then we are in the harmonic regime. Obviously the graph is incorrect for
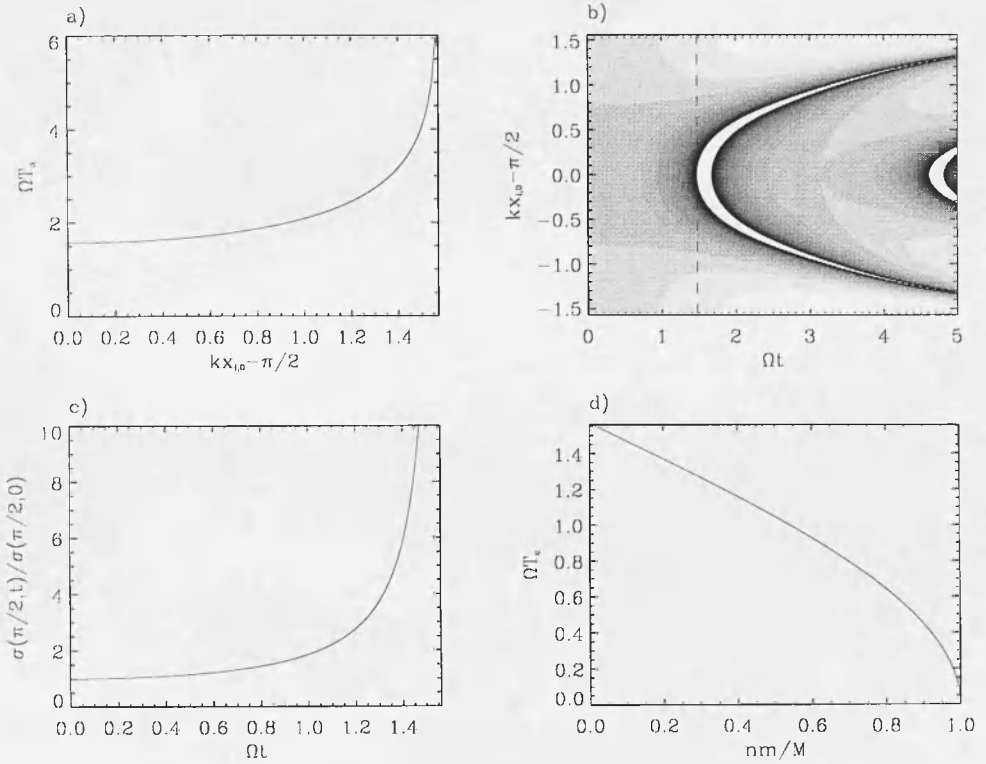
Figure 2.3: a) Time T_n for a bead starting at $x_{i,0}$ to reach the nearest anti-node. b) Density ratio $\sigma(x,t)/\sigma(t=0)$. The density increases as the shading darkens. The white areas bordered by a black line are where $\sigma \geq 0.1\sigma_0$. The dashed line refers to the first instance at which that inequality is valid. c) Density profile at the anti-node. At $\Omega t = \pi/2$ the density becomes infinite. d) Time T_c at which locally the density ratio $\sigma(x,t)/\sigma(t=0)$ for the first time becomes equal to the ratio $\sigma_s/\sigma(t=0) = M/nm$ as a function of the mass ratio between the beads and the string (nm/M).

beads starting out at the node $(kx_{i,0}=\pi/2)$ or anti-nodes $(kx_{i,0} - \pi/2=\pm\pi/2)$ since they are at equilibrium positions. We can expect that the density at the anti-node will go up sharply as we near $\Omega t=\pi/2$. Figure 2.3b confirms this. It shows the density ratio $\sigma(x,t)/\sigma(t=0)$ along the string from node to node as a function of time. As the shading darkens, the density ratio increases. The white areas bordered by black, are where this ratio becomes equal to or larger than a tenth of the ratio $\sigma_s/\sigma(t=0)=M/nm$, giving an idea of when and where Condition (2.43) is no longer satisfied. The result to the right of the dashed line is therefore irrelevant. Figure 2.3c shows the time profile of the density ratio $\sigma/\sigma(t=0)$ at the node. It follows the function $\sec(\Omega t)$. At $\Omega t=\pi/2$ this density ratio becomes infinite. This

is a very local increase in density as the total mass of the beads has to remain constant. However, before this time, Condition (2.43) will be violated. Call T_c the time when the inequality in Condition (2.43) becomes an equality. Figure 2.3d shows the dependence of T_c on the mass ratio nm/M. For nm/M nearing zero (light beads), ΩT_c is converging to $\pi/2$ but nm/M equal to zero does not make physical sense in this context as Equation (2.23) becomes obsolete.

The frequency Ω is proportional to the amplitude a and wavenumber k of the string's oscillation. An increase in either of these quantities speeds up the beads' behaviour. This is easily understood considering that in both cases the gradient $\partial\eta/\partial x$ becomes larger, hence also does the force on the right-hand side of Equation (2.23).

It is because we permitted the beads to overlap, that we obtain a local infinite density. In reality, the beads cannot pass through each other. They would also have a finite width which, if large enough, prevents Condition (2.43) being violated. Incorporating these features means having $n+1$ coupled equations as we have to take into account the separation between the beads.

We shall not attempt to see how this density increment affects the oscillation of the string by solving the equations at order ϵ^3. Instead we shall approach the whole problem from a different angle, that of a continuum of beads. The beads become a 'fluid'. This will turn out to be quite advantageous.

2.4   Continuum approach

Instead of a discrete set of beads, we shall consider a one-dimensional continuum as our model for investigating the nonlinear behaviour of Alfvén waves. The mechanical analogue can be pictured as an hollow, elastic 'tube' of infinitely small diameter, filled with a fluid. Because this tube is quite artificially defined, we shall continue to use the term 'string'. The string has a constant density σ_s and tension constant T. The transverse displacement of the tube is $\eta(x,t)$. We take into account the compressibility of this fluid. Again equations for the continuum-string system will be obtained using the variational principle and the method of undetermined multipliers (Neukirch, 1997). The Lagrangian, $\mathcal{L}$ of the system is:

$$\mathcal{L} = \int dx \left[\frac{1}{2}\sigma_s \left(\frac{\partial\eta}{\partial t}\right)^2 - \frac{1}{2}T \left(\frac{\partial\eta}{\partial x}\right)^2 + \frac{1}{2}\sigma \left(v_x^2 + v_y^2\right) - \frac{p}{\gamma - 1} \right] , \qquad (2.45)$$

40

where the four terms in the integral are the kinetic and potential energy densities of the string and the kinetic and potential (internal) energy densities of the fluid respectively. The quantities σ, p, v_x and v_y are the linear density, pressure, and x- and y- velocity components of the fluid. γ is the ratio of specific heats. The pressure has to be interpreted as a force per unit length. The Lagrangian is equal to the one-dimensional Lagrangian of an MHD system if we replace the potential energy of the string by $B^2/2\mu_0$ (Goedbloed, 1979). It is the effect of this change that is of interest. It is expected that we shall obtain a good match between the analogue and the MHD case up to order ϵ^2, but differences for higher orders.

Besides the constraint that the fluid has to remain on the string, we need to satisfy mass conservation, conservation of the identity of the fluid elements and conservation of entropy, thus applying Equations (1.26) and (1.31), we have:

$$\frac{\partial \eta}{\partial t} + v_x \frac{\partial \eta}{\partial x} = v_y \quad \text{(string constraint)}, \tag{2.46}$$

$$\frac{\partial \sigma}{\partial t} + \frac{\partial}{\partial x}(v_x \sigma) = 0 \quad \text{(mass conservation)}, \tag{2.47}$$

$$\frac{\partial X_0}{\partial t} + v_x \frac{\partial X_0}{\partial x} = 0 \quad \text{(identity of fluid elements)}. \tag{2.48}$$

$$\frac{\partial}{\partial t}(p\sigma^{-\gamma}) + v_x \frac{\partial}{\partial x}(p\sigma^{-\gamma}) = 0 \quad \text{(entropy conservation)}. \tag{2.49}$$

X_0 is a quantity related to the identity of the fluid elements. With the previous constraints in mind, we can form the following functional

$$I = \int_{t_1}^{t_2} dt \left[\mathcal{L} + \int dx \, \lambda_1 \left(v_y - \frac{d\eta}{dt} \right) + \int dx \, \lambda_2 \left(\frac{\partial \sigma}{\partial t} + \frac{\partial}{\partial x}(\sigma v_x) \right) + \right.$$
$$\left. + \int dx \, \lambda_3 \frac{dX_0}{dt} + \int dx \, \lambda_4 \frac{d}{dt}(p\sigma^{-\gamma}) \right], \tag{2.50}$$

with

$$\frac{d}{dt} = \frac{\partial}{\partial t} + v_x \frac{\partial}{\partial x}. \tag{2.51}$$

The λ's are Lagrangian undetermined multipliers. The functional I has as independent variables x and t, whilst $v_x(x,t)$, $v_y(x,t)$, $\sigma(x,t)$, $\eta(x,t)$, $X_0(x,t)$ and $p(x,t)$ are dependent variables. We take variations of I with respect to these dependent variables and set the variation equal to zero. We obtain the following system of six algebraic equations:

$$\frac{\partial \eta}{\partial x}\lambda_1 + \sigma \frac{\partial \lambda_2}{\partial x} - \frac{\partial X_0}{\partial x}\lambda_3 - \frac{\partial}{\partial x}(p\sigma^{-\gamma})\lambda_4 = \sigma v_x,$$

$$\lambda_1 = -\sigma v_y,$$

41

$$\frac{d\lambda_2}{dt} - \gamma p \sigma^{-\gamma-1} \left[\frac{\partial \lambda_4}{\partial t} + \frac{\partial}{\partial x} (v_x \lambda_4) \right] = \frac{1}{2} \left(v_x^2 + v_y^2 \right), \tag{2.52}$$

$$\frac{\partial \lambda_1}{\partial t} + \frac{\partial}{\partial x} (v_x \lambda_1) = \sigma_s \frac{\partial^2 \eta}{\partial t^2} - T \frac{\partial^2 \eta}{\partial x^2},$$

$$\frac{\partial \lambda_3}{\partial t} + \frac{\partial}{\partial x} (v_x \lambda_1) = 0,$$

$$\frac{\partial \lambda_4}{\partial t} + \frac{\partial}{\partial x} (v_x \lambda_4) = \frac{\sigma^\gamma}{\gamma - 1}.$$

Together with the constraints (2.46)- (2.49) we have ten equations and ten variables. After some straightforward manipulation, the following system of equations is obtained:

$$\frac{\partial \sigma}{\partial t} + \frac{\partial}{\partial x} (\sigma v_x) = 0, \tag{2.53}$$

$$\left[1 + \left(\frac{\partial \eta}{\partial x} \right)^2 \right] \frac{dv_x}{dt} = -\frac{\partial \eta}{\partial x} \left[\frac{\partial^2 \eta}{\partial t^2} + 2 \frac{\partial \eta}{\partial t \partial x} v_x + \frac{\partial^2 \eta}{\partial x^2} v_x^2 \right] - \frac{1}{\sigma} \frac{\partial p}{\partial x}, \tag{2.54}$$

$$\left[\frac{\partial^2}{\partial t^2} - V_s^2 \frac{\partial^2}{\partial x^2} \right] \eta = -\frac{d}{dt} \left(\frac{\sigma}{\sigma_s} \frac{d\eta}{dt} \right), \tag{2.55}$$

$$\frac{d}{dt} (p \sigma^{-\gamma}) = 0, \tag{2.56}$$

where the speed V_s is defined as in Expression (2.5), representing the typical speed at which a disturbance would travel along an empty string.

The speed V_t is defined as the typical speed at which a disturbance would travel along the string filled with the fluid:

$$V_t(x,t) = \sqrt{\frac{T}{\sigma_s + \sigma}}. \tag{2.57}$$

The added fluid reduces the speed of the string's oscillation as it increases the total density of the system. In the previous section we took the limit $\sigma_s \gg \sigma$, meaning $V_t = V_s$. We are not going to do this here as it does not complicate the equations. Furthermore, if we want to compare the string-tube system to a magnetic field-line in a plasma, we need to take $\sigma_s = 0$, since a magnetic field-line does not have a mass!

The terms on the right-hand side of Equation (2.54) are the force due to the string's displacement field (the ponderomotive force) and the pressure force of the fluid, respectively. We make an order of magnitude comparison of the two terms:

$$\frac{| \, \text{pressure force} \, |}{| \, \text{ponderomotive force} \, |} \approx \frac{1}{\gamma} \left(\frac{C_s}{V_s} \right)^2 \left(\frac{L}{\eta} \right)^2 \approx \frac{1}{a^2} \left(\frac{4\pi^2}{\gamma} \right) \left(\frac{C_s}{V_s} \right)^2, \tag{2.58}$$

where C_s is defined as the sound speed in the fluid, given as

$$C_s(x,t) = \sqrt{\frac{\gamma p}{\sigma}}. \tag{2.59}$$

42

The quantity a is again the dimensionless amplitude of the string's displacement. It is clear that the ponderomotive force is dominant when $a \gg 2\pi C_s/\sqrt{\gamma}V_s$. Also because of Condition (2.2), we need $a \ll 1$. For the ponderomotive force to be dominant, we must be in the regime where $C_s \ll V_s$ in order of magnitude. In MHD this limit corresponds to $C_s \ll V_A$, where C_s and V_A are the sound and Alfvén speeds respectively.

Equation (2.55) can be rewritten in a way that is more physically understandable:

$$\frac{\partial}{\partial t}\left[(\sigma_s + \sigma)\frac{\partial \eta}{\partial t}\right] - \frac{\partial}{\partial x}\left[\left(\mathcal{T} - \sigma v_x^2\right)\frac{\partial \eta}{\partial x}\right] + \frac{\partial}{\partial x}\left(\sigma v_x \frac{\partial \eta}{\partial t}\right) + \frac{\partial}{\partial t}\left(\sigma v_x \frac{\partial \eta}{\partial x}\right) = 0. \quad (2.60)$$

We see that the density is increased by the presence of the fluid and that the tension is decreased by the inertia of the fluid.

Instead of specifying initial conditions as in the previous section, we now give an equilibrium state from which to work:

$$\eta_0 = 0 \ , \ v_{x,0} = 0 \ , \ p_0 = \text{constant} \ , \ \sigma_0 = \text{constant} \ . \quad (2.61)$$

Again we shall use an expansion procedure in the small parameter ϵ, which is proportional to a,

$$f = f_0 + \epsilon f_1 + \epsilon^2 f_2 + \epsilon^3 f_3 + \dots, \quad (2.62)$$

where f represents any of the dependent variables η, v_x, p and σ. We substitute Expansion (2.62) into Equations (2.53)-(2.56) and gather terms of the same order of ϵ.

2.4.1 Oscillations of tube with static fluid

The terms of Equations (2.53)-(2.56) of order ϵ are:

$$\frac{\partial \sigma_1}{\partial t} + \sigma_0 \frac{\partial v_{x,1}}{\partial x} = 0, \quad (2.63)$$

$$\frac{\partial v_{x,1}}{\partial t} = -\frac{1}{\sigma_0}\frac{\partial p_1}{\partial x}, \quad (2.64)$$

$$\left[\frac{\partial^2}{\partial t^2} - V_{t,0}^2\frac{\partial^2}{\partial x^2}\right]\eta_1 = 0, \quad (2.65)$$

$$\frac{\partial p_1}{\partial t} - C_{s,0}^2\frac{\partial \sigma_1}{\partial t} = 0. \quad (2.66)$$

The extra index 0 in the speeds $V_{t,0}$ and $C_{s,0}$ means that they are calculated from the equilibrium quantities. At this point it is convenient to define the ratio:

$$\beta = \frac{C_{s,0}^2}{V_{t,0}^2}, \quad (2.67)$$

43

which the equivalent of the parameter β, (1.53). Equations (2.63), (2.64) and (2.66) are the one-dimensional hydrodynamical equations (Landau & Lifshitz, 1959). Combining Equations (2.63), (2.64) and (2.66) gives the longitudinal wave equation

$$\left[\frac{\partial^2}{\partial t^2} - C_{s,0}^2 \frac{\partial^2}{\partial x^2}\right] \sigma^{(1)} = 0, \tag{2.68}$$

which describes a sound wave travelling along the string through the fluid. It is a longitudinal wave mode. Equation (2.65) is the wave equation of a stretched string and describes transverse wave motions.

We assume the string is fixed at $x=0$ and $x=L$. The fluid cannot flow out of the string at those points. Therefore the two kinds of wave modes are bounded (standing) modes. We shall assume that the system is disturbed from its equilibrium in such a way that only one transverse mode is excited. We assume that the amplitude of the sound wave is equal to zero. The solutions of order ϵ are then:

$$\eta_1 = \frac{a}{k} \sin{(kx)} \cos{(\omega t)}, \tag{2.69}$$

$$v_{x,1} = p_1 = \sigma^{(1)} = 0. \tag{2.70}$$

The quantity ω is the frequency of the oscillation, given by the dispersion relation $\omega = kV_{t,0}$.

2.4.2 Motion of fluid due to the ponderomotive force

The terms of Equations (2.53)-(2.56) of order ϵ^2 are:

$$\frac{\partial \sigma_2}{\partial t} + \sigma_0 \frac{\partial v_{x,2}}{\partial x} = 0, \tag{2.71}$$

$$\frac{\partial v_{x,2}}{\partial t} = -\frac{\partial \eta_1}{\partial x}\frac{\partial^2 \eta_1}{\partial t^2} - \frac{1}{\sigma_0}\frac{\partial p_1}{\partial x}, \tag{2.72}$$

$$\left[\frac{\partial^2}{\partial t^2} - V_{t,0}^2 \frac{\partial^2}{\partial x^2}\right] \eta_2 = 0, \tag{2.73}$$

$$\frac{\partial p_2}{\partial t} - C_{s,0}^2 \frac{\partial \sigma_2}{\partial t} = 0. \tag{2.74}$$

The equation (2.73) for the displacement η is the same as at order ϵ. We therefore take η_2 to be zero. The other three equations can be combined to give

$$\left[\frac{\partial^2}{\partial t^2} - C_{s,0}^2 \frac{\partial^2}{\partial x^2}\right] \sigma_2 = \sigma_0 \frac{\partial}{\partial x}\left(\frac{\partial \eta_1}{\partial x}\frac{\partial^2 \eta_1}{\partial t^2}\right). \tag{2.75}$$

We see that the sound wave is driven by the transverse mode. Substituting Solution (2.69) into Expression (2.75) gives:

$$\left[\frac{\partial^2}{\partial t^2} - C_{s,0}^2 \frac{\partial^2}{\partial x^2}\right] \sigma_2 = -\sigma_0 a^2 k^2 V_{t,0}^2 \cos(2kx) \cos^2(\omega t). \qquad (2.76)$$

If we substitute Solution (2.69) into Equation (2.72), we find the same form as Equation (2.35). The big difference, though, is that here x in the sine function is an independent variable whilst in Equation (2.35) it is a dependent variable describing the position of a discrete bead. Solving the equations is much easier in the latter case. The solution to Equation (2.76) is

$$\sigma_2 = \begin{cases} \frac{1}{8}\sigma_0 a^2 V_{t,0}^2 \cos(2kx)\left(\frac{\cos(2kC_{s,0}t)-1}{C_{s,0}^2} + \frac{\cos(2kC_{s,0}t)-\cos(2\omega t)}{C_{s,0}^2-V_{t,0}^2}\right) & C_{s,0} \neq V_{t,0} \\ \frac{1}{8}\sigma_0 a^2 V_{t,0} \cos(2kx)\left(\cos(2\omega t) - 1 - \omega t \sin(2\omega t)\right) & C_{s,0} = V_{t,0} \end{cases} \qquad . (2.77)$$

The pressure p_2 is simply given as $p_2 = C_{s,0}\sigma_2$. The velocity $v_{x,2}$ is calculated from Equations (2.77) and (2.71):

$$v_{x,2} = \begin{cases} \frac{1}{8}a^2 \sin(2kx)\left(\frac{\sin(2kC_{s,0}t)}{C_{s,0}} + \frac{C_{s,0}\sin(2kC_{s,0}t)-V_{t,0}\sin(2\omega t)}{C_{s,0}^2-V_{t,0}^2}\right) & C_{s,0} \neq V_{t,0} \\ \frac{1}{16}\frac{a^2}{V_{t,0}}\sin(2kx)\left(3\sin(2\omega t) + 2\omega t\cos(2\omega t)\right) & C_{s,0} = V_{t,0} \end{cases} \qquad . (2.78)$$

We call the quantities σ_2 and $v_{x,2}$ the ponderomotive density and velocity response respectively. For $\beta < 1$, we can identify the sound wave with the slow magneto-acoustic wave of the MHD case and for $\beta > 1$, we can identify the sound wave with the fast magneto-acoustic wave of the MHD case. Figure 2.4 shows the density $\sigma_0 + \sigma_2$ at the anti-node of the string's displacement field for several values of β, which is defined as the ratio $C_{s,0}^2/V_{t,0}^2$.

The case $\beta = 0$ corresponds to the neglect of the pressure force in comparison with the tension force. This can be seen as the equivalent of the cold-plasma limit. This case can be compared to the previous mechanical analogue of discrete particles, where we ignored the 'compressibility' of the particles. Expressions (2.77) and (2.78) become:

$$\sigma_2 = -\sigma_0 \left(\frac{1}{2}(\Omega t)^2 + \frac{\Omega^2}{(2\omega)^2}(1 - \cos(2\omega t))\right)\cos(2kx), \qquad (2.79)$$

$$v_{x,2} = \frac{1}{2\sqrt{2}}a\left(\Omega t + \frac{\Omega}{2\omega}\sin(2\omega t)\right)\sin(2kx), \qquad (2.80)$$

where Ω is defined in Expression (2.41). The second-order density and x-component of the velocity vector vary secularly with time. This is shown in Figure 2.4a. As in the discrete

45
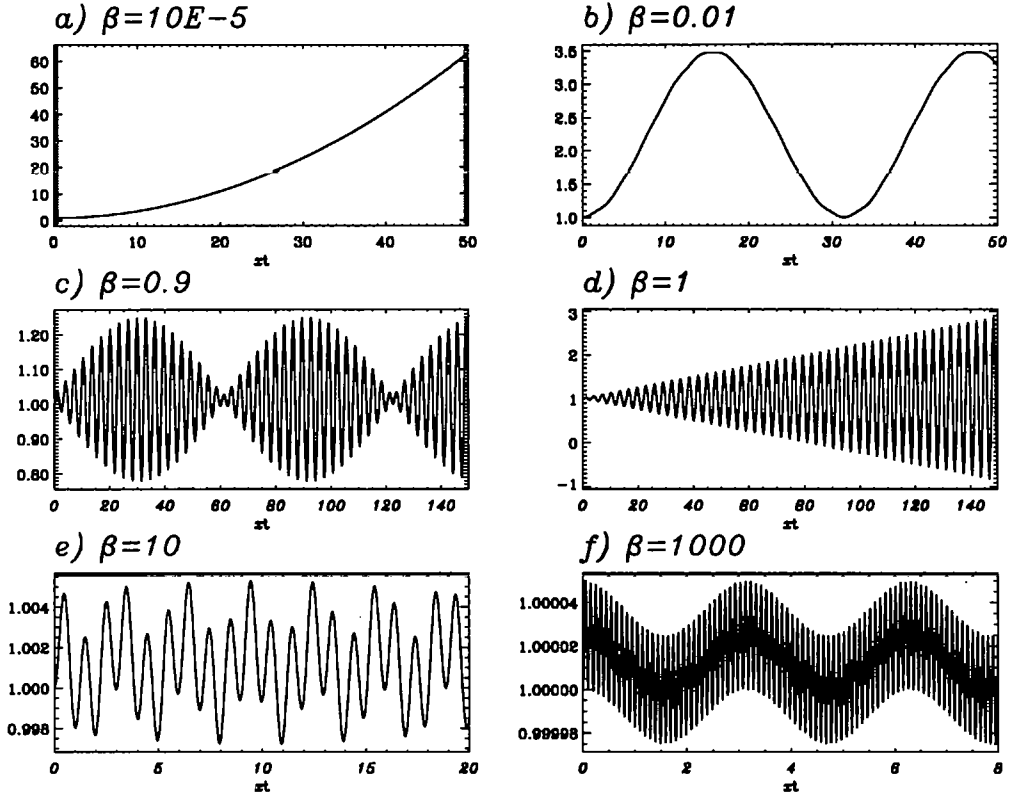
Figure 2.4: Time profiles of the density ratio $1 + \sigma_2/\sigma_0$ at the anti-node of the string's displacement field for different values of the parameter β. The amplitude of the string displacement is $a = 0.1$.

case, we find that the scaling factor Ωt is an essential feature of the nonlinear behaviour of the fluid. We see from Expression (2.79) that the density is increasing quadratically at the anti-nodes. The time-scale for this behaviour is $\Omega t \sim 2\sqrt{2}$ $(V_{t,0}t \sim a^{-1}k^{-1})$. The density we obtain up to second order can be seen as the Taylor expansion of Expression (2.44) for small times up to the quadratic term. The second-order solution does not show that the density becomes infinite at a finite time, as is predicted in the mechanical analogue of discrete particles. Higher-order terms are needed in the continuum approach to describe this behaviour. Expressions (2.79) and (2.80) match the expressions found by Rankin *et al.* (1994) for the second-order ponderomotive response of bounded Alfvén waves in a cold plasma.

Figure 2.4b shows the time profile of the density for small β. The density is periodically enhanced with a period of $\omega t = \pi/\sqrt{\beta}$. The maximum density enhancement is shown in

46
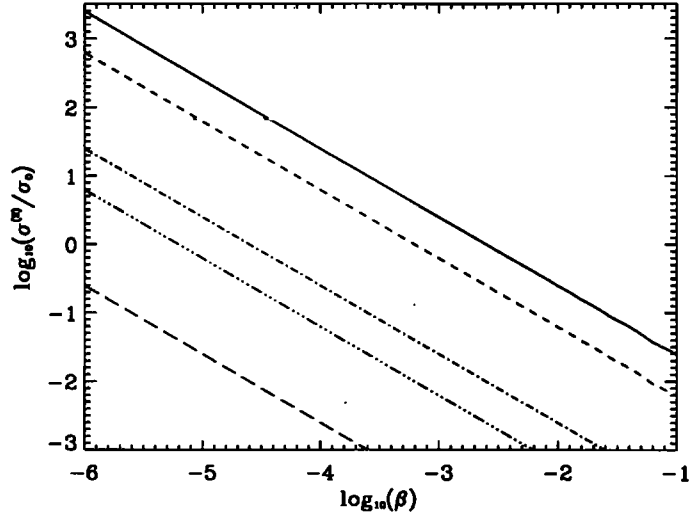
Figure 2.5: Maximum value of the density ratio σ_2/σ_0 as a function of β for several values of the amplitude a (solid line: a=0.1, short dashed line: a=0.05, dot-dashed line: a=0.01, triple dot-dashed line: a=0.005 and long dashed line: a=0.001).

Figures 2.5 and 2.6. The maximum density enhancement for a $\beta \ll 1$ follows the dependency predicted by the order-of-magnitude comparison of the forces:

$$\max\left(\frac{\sigma_2}{\sigma_0}\right) \sim \frac{a^2}{\beta} \, . \tag{2.81}$$

This result has been noted by Allan *et al.* (1991) and Rankin *et al.* (1994) for bounded fast magneto-acoustic and Alfvén waves respectively. The density enhancement decreases rapidly as β increases. For β close to one the frequency of the driver is close to one of the normal modes of the sound wave. Beats occur. For β equal to one the transverse mode and sound wave are in resonance, growing on a time-scale $t \sim a^{-1}k^{-1}V_{t,0}^{-1}$. The amplitude and density of the sound wave grow linearly in time. Lastly for a β larger than one there is no significant density enhancement at all.

We need to be very careful in interpreting Figures 2.4, 2.5 and 2.6. For values of the density exceeding the background density, the expansion procedure is no longer valid. Therefore, the results in those regimes have to be interpreted qualitatively. Numerical simulations are needed to quantitatively investigate the regimes where the analytical approach fails.
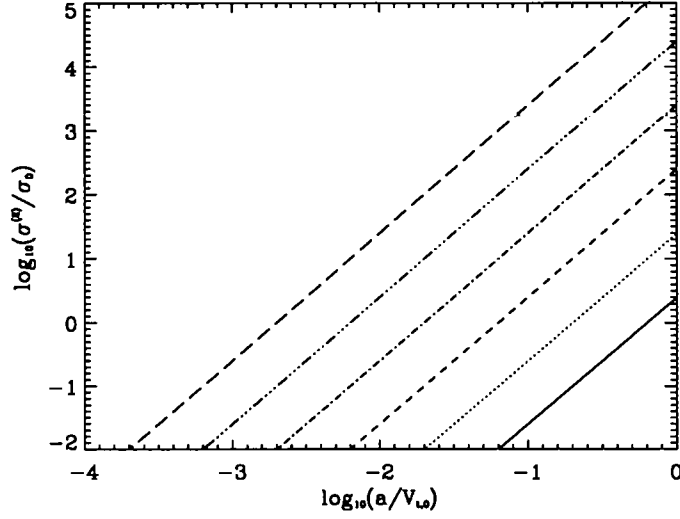
Figure 2.6: Maximum value of the density ratio σ_2/σ_0 as a function of the ratio a for several values of β (solid line: $\beta=10^{-1}$, dotted line: $\beta=10^{-2}$, short dashed line: $\beta=10^{-3}$, dot-dashed line: $\beta=10^{-4}$, triple dot-dashed line: $\beta=10^{-5}$ and long dashed line: $\beta=10^{-6}$).

2.4.3 Moderation of the tube oscillations

From the comparison between the tension force of the mechanical analogue and the magnetic tension force in Expression (2.10), we expect, at third order in ϵ, the results of the mechanical analogue to differ from the MHD case. It is worthwhile studying the third-order equations in the two cases for which the density and flow become very large. These occur when $\beta \ll 1$ and $\beta=1$ respectively. We shall consider the specific cases $\beta=0$, $\beta=1$ and the general solution. The terms of Equations (2.53)-(2.56) of order ϵ^3 are:

$$\frac{\partial \sigma_3}{\partial t} + \sigma_0 \frac{\partial v_{3,x}}{\partial x} = 0, \tag{2.82}$$

$$\frac{\partial v_{3,x}}{\partial t} = -\frac{1}{\sigma_0} \frac{\partial p_3}{\partial x}, \tag{2.83}$$

$$\left[\frac{\partial^2}{\partial t^2} - V_{t,0}^2 \frac{\partial^2}{\partial x^2} \right] \eta_3 = -\frac{1}{1+\frac{\sigma_2}{\sigma_0}} \left(\frac{\sigma_2}{\sigma_0} \frac{\partial^2 \eta_1}{\partial t^2} + 2v_{x,2} \frac{\partial^2 \eta_1}{\partial t \partial x} \right.$$
$$\left. + \frac{\partial v_{x,2}}{\partial t} \frac{\partial \eta_1}{\partial x} - \frac{\partial v_{x,2}}{\partial x} \frac{\partial \eta_1}{\partial t} \right), \tag{2.84}$$

$$\frac{\partial p_3}{\partial t} - C_{s,0}^2 \frac{\partial \sigma_3}{\partial t} = 0. \tag{2.85}$$

48

At this order we see the back-reaction of the mass redistribution on the string's displacement field. The driver term on the right-hand side of Equation (2.84) contains first and third spatial harmonics of the wave field. The mass flow excites higher harmonics and moderates the original field. Note that the second harmonic is not excited at first. The driver term is also proportional to the ratio $(1 + \sigma_s/\sigma_0)^{-1}$. The more the fluid makes up the density of the system, the stronger is the moderation of the oscillation.

$\beta = 0$

We only consider the dominant term, which contains σ_2 and is proportional to t^2, on the right-hand side of Equation (2.84):

$$\left[\frac{\partial^2}{\partial t^2} - V_{t,0}^2 \frac{\partial^2}{\partial x^2} \right] \eta_3 = -\frac{1}{2} \frac{ak\omega^2}{1 + \frac{\sigma_s}{\sigma_0}} \sin(kx) \cos(2kx)(\Omega t)^2 \cos(\omega t) . \qquad (2.86)$$

The solution of Equation (2.86) is:

$$\eta_3 \approx -\frac{1}{16} \frac{a}{k} \frac{1}{1 + \frac{\sigma_s}{\sigma_0}} \left[\frac{1}{2}(\Omega t)^2 \sin(3kx) \cos(\omega t) + (\Omega t)^2 \sin(kx) \cos(\omega t) + \right.$$
$$\left. + \frac{1}{3} \frac{2\omega}{\Omega} (\Omega t)^3 \sin(kx) \sin(\omega t) \right] . \qquad (2.87)$$

We have neglected any terms linear or constant in t. The first term of Expression (2.87) represents a third spatial harmonic for which the amplitude is growing quadratically in time. It will become prominent on a time-scale $\Omega t \sim \sqrt{1 + \sigma_s/\sigma_0}$ ($t \sim a^{-1}k^{-1}V_{t,0}^{-1}$). The second and third terms are the amplitude and phase modification of the original oscillation respectively. The amplitude modification acts on a similar time-scale to that of the third spatial harmonic. The phase shift ϕ that the original mode feels, is:

$$\phi \approx -\frac{1}{48} \frac{1}{1 + \frac{\sigma_s}{\sigma_0}} \frac{2\omega}{\Omega} (\Omega t)^3 . \qquad (2.88)$$

The frequency shift $\Delta\omega$ therefore is:

$$\frac{\Delta\omega}{\omega} = \frac{1}{\omega} \frac{\partial\phi}{\partial t} \approx \frac{1}{8} \frac{1}{1 + \frac{\sigma_s}{\sigma_0}} (\Omega t)^2 . \qquad (2.89)$$

The phase shift acts on a faster time-scale than the amplitude modification: $\Omega t \sim (1 + \sigma_s/\sigma_0)^{(1/3)}(\Omega/\omega)^{1/3}$ ($t \sim a^{-3/2}k^{-1}V_{t,0}^{-3/2}$). If we compare the expression for the frequency-shift (2.89), with $\sigma_s = 0$, with the result found by Rankin *et al.* (1994) for bounded Alfvén

waves, we see that they exactly match. This suggests, for this case, that the difference between the tension forces of the mechanical analogue and the MHD case, is of lesser importance than the ponderomotive density perturbation σ_2. This can be understood as follows. The third-order correction to the magnetic tension force involves the velocity component v_x but not the density. We have shown in the previous section that v_x varies linearly in time. Therefore the third-order terms of the magnetic tension force varies more slowy than the term containing the ponderomotive density. This fact strengthens the case in favour of the mechanical analogue.

$\beta = 1$

We only consider the dominant term, which is proportional to t, on the right-hand side of Equation (2.84):

$$
\left[\frac{\partial^2}{\partial t^2} - V_{t,0}^2 \frac{\partial^2}{\partial x^2}\right] \eta_3 = \frac{1}{32} \frac{a^3 k^2 V_{t,0}^3 t}{1 + \frac{\sigma_s}{\sigma_0}} \left[\sin(3kx)\left(\sin(3\omega t) + \sin(\omega t)\right)\right.
$$
$$
\left. + \sin(kx)\left(-7\sin(3\omega t) + \sin(\omega t)\right)\right] . \tag{2.90}
$$

The solution of Equation (2.90) is:

$$
\eta_3 \approx -\frac{1}{128} \frac{a^3}{k} \frac{1}{1 + \frac{\sigma_s}{\sigma_0}}
$$
$$
\left[\sin(kx)\left(\left(\omega t - \frac{7}{2}\sin(2\omega t)\right)(\omega t)\cos(\omega t) - \left(1 + \frac{7}{2}\cos(2\omega t)\right)(\omega t)\sin(\omega t)\right)\right.
$$
$$
+ \sin(3kx)\left(\frac{1}{3}(\omega t \cos(2\omega t) - \frac{1}{3}\sin(2\omega t))(\omega t)\cos(\omega t)\right.
$$
$$
\left.\left. - (\frac{1}{3}\omega t \sin(2\omega t) + \frac{1}{9}\cos(2\omega t) + \frac{1}{2})(\omega t)\sin(\omega t)\right)\right] . \tag{2.91}
$$

Through the resonance of the transverse mode and sound wave, we have the significant generation of both spatial and temporal higher harmonics. The time-scale for the amplitude modification of the original mode and the third spatial harmonic is $t \sim 128 a^{-1} k^{-1} V_{t,0}^{-1}$. The phase modification of the original mode acts on a slower time scale than the amplitude modification, namely $t \sim 128 a^{-2} k^{-1} V_{t,0}^{-2}$. The phase shift, ϕ, and frequency shift, $\Delta\omega$, are:

$$
\phi \approx \frac{1}{128} \frac{a^2}{1 + \frac{\sigma_s}{\sigma_0}} (\omega t)\left(1 + \frac{7}{2}\cos(2\omega t)\right) , \tag{2.92}
$$

$$
\frac{\Delta\omega}{\omega} \approx -\frac{7}{128} \frac{a^2}{1 + \frac{\sigma_s}{\sigma_0}} (\omega t)\sin(2\omega t) . \tag{2.93}
$$

50
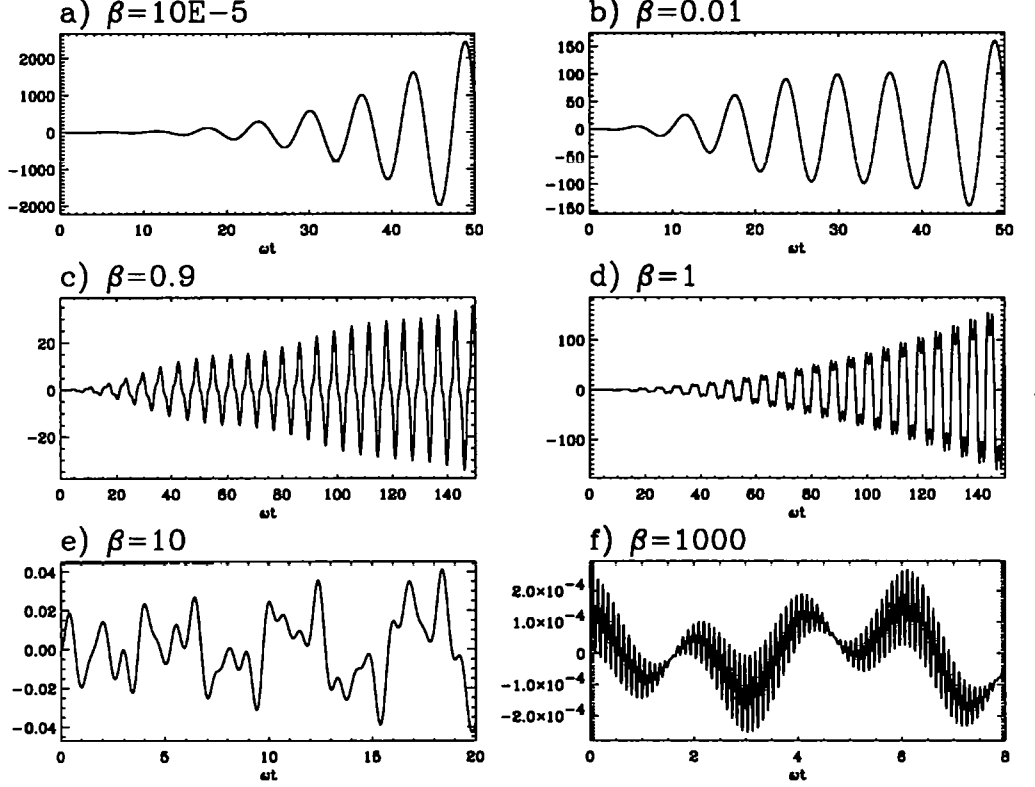
Figure 2.7: Time profile of the string displacement perturbation η_3 at the anti-node of the string's displacement field η_1 for different values of the parameter β. The velocity amplitude of the string displacement is $a=0.1$. When the amplitude of η_3 becomes of the same order as a, the results are no longer valid and serve only as a qualitative representation of the perturbation.

General solution

For completeness, we consider all the terms on the right-hand side of Equation (2.84), substituting σ_2 and $v_{x,2}$ from the solutions (2.77) and (2.78), for $\beta \neq 1$.

$$\left[\frac{\partial^2}{\partial t^2} - V_{t,0}^2 \frac{\partial^2}{\partial x^2}\right]\eta_3 = \tfrac{1}{16}a^3 \frac{kV_{t,0}^2}{1+\frac{g_z}{\sigma_0}} \left[\sin\left(kx\right)\left(\Theta_1 \cos\left(\omega t\right) + \Theta_2 \sin\left(\omega t\right)\right)\right.$$

$$\left. + \sin\left(3kx\right)\Theta_3\cos\left(\omega t\right)\right], \qquad (2.94)$$

with

$$\Theta_1(t,\beta) = \frac{4\beta^2 - 1}{\beta(\beta-1)}\cos\left(2\sqrt{\beta}\omega t\right) - \frac{3}{\beta-1}\cos\left(2\omega t\right) - \frac{1}{\beta},$$

$$\Theta_2(t,\beta) = -\frac{4(2\beta-1)}{\sqrt{\beta}(\beta-1)}\sin\left(2\sqrt{\beta}\omega t\right) + \frac{4}{\beta-1}\sin\left(2\omega t\right), \qquad (2.95)$$

51

$$\Theta_3(t,\beta) = -\frac{(2\beta-1)^2}{\beta(\beta-1)}\cos\left(2\sqrt{\beta}\omega t\right) + \frac{1}{\beta-1}\cos\left(2\omega t\right) - \frac{1}{\beta}.$$

The functions Θ are a combination of the time-dependent parts of the second-order solutions (2.77) and (2.78). The limits of the functions Θ as β tends to both 0 and 1 exist. The solution of Equation (2.94) is:

$$
\begin{aligned}
\eta_3 = \tfrac{1}{16}\tfrac{a^2}{k}\tfrac{1}{1+\frac{\sigma_s}{\sigma_0}} \quad & [\sin\left(kx\right)\left(\Psi_1\cos\left(\omega t\right)+\Psi_2\sin\left(\omega t\right)\right) \\
& + \sin\left(3kx\right)\left(\Psi_3\cos\left(\omega t\right)+\Psi_4\sin\left(\omega t\right)\right)]
\end{aligned}
\tag{2.96}
$$

with

$$
\begin{aligned}
\Psi_1(t,\beta) &= -\frac{(2\beta-1)(2\beta-3)}{4\beta(\beta-1)^2}\left(\cos\left(2\sqrt{\beta}\omega t\right)-1\right)+\frac{7}{16(\beta-1)}\left(\cos\left(2\omega t\right)-1\right), \\[6pt]
\Psi_2(t,\beta) &= \frac{(2\beta-1)^2}{4\beta^{\frac{3}{2}}(\beta-1)^2}\sin\left(2\sqrt{\beta}\omega t\right)-\frac{\beta-2}{4\beta(\beta-1)}\omega t-\frac{7}{16(\beta-1)}\sin\left(2\omega t\right), \\[6pt]
\Psi_3(t,\beta) &= \frac{(2\beta-1)^2(\beta-2)}{4\beta(\beta-1)^2(\beta-4)}\left(\sin\left(2\sqrt{\beta}\omega t\right)+\sin\left(2\omega t\right)\right) \\
&\quad + \frac{1}{12(\beta-1)}\omega t\sin\left(2\omega t\right)-\frac{\beta-2}{16\beta(\beta-1)}\left(1-\cos\left(2\omega t\right)\right), \\[6pt]
\Psi_4(t,\beta) &= \frac{(2\beta-1)^2}{8\beta(\beta-1)(\sqrt{\beta}+1)(\sqrt{\beta}-2)}\left(\sin\left(2\sqrt{\beta}\omega t\right)+\sin\left(2\omega t\right)\right) \\
&\quad - \frac{(2\beta-1)^2}{8\beta(\beta-1)(\sqrt{\beta}-1)(\sqrt{\beta}+2)}\left(\sin\left(2\sqrt{\beta}\omega t\right)-\sin\left(2\omega t\right)\right) \\
&\quad + \frac{1}{12(\beta-1)}\omega t\cos\left(2\omega t\right)-\frac{\beta-2}{16\beta(\beta-1)}\sin\left(2\omega t\right).
\end{aligned}
\tag{2.97}
$$

The limits of the function Ψ as β tends to 0 and 4 exist. In the limit of β tending to unity, the functions Ψ themselves are not finite, but the combinations $\Psi_1\cos\left(\omega t\right)+\Psi_2\sin\left(\omega t\right)$ and $\Psi_3\cos\left(\omega t\right)+\Psi_4\sin\left(\omega t\right)$ are. The phase shift ϕ and corresponding frequency shift $\Delta\omega$ that the original mode feels, are approximately given by:

$$\phi \approx \frac{1}{16}\frac{a^2}{1+\frac{\sigma_s}{\sigma_0}}\Psi_2(t,\beta),\tag{2.98}$$

$$\frac{\Delta\omega}{\omega} \approx \frac{1}{16}\frac{a^2}{1+\frac{\sigma_s}{\sigma_0}}\frac{\partial\Psi_2(t,\beta)}{\partial t}.\tag{2.99}$$

The phase shift and frequency shift given here are not valid close to β equal to unity. Figure 2.8 shows the phase shift ϕ as a function of time for different values of the parameter β.
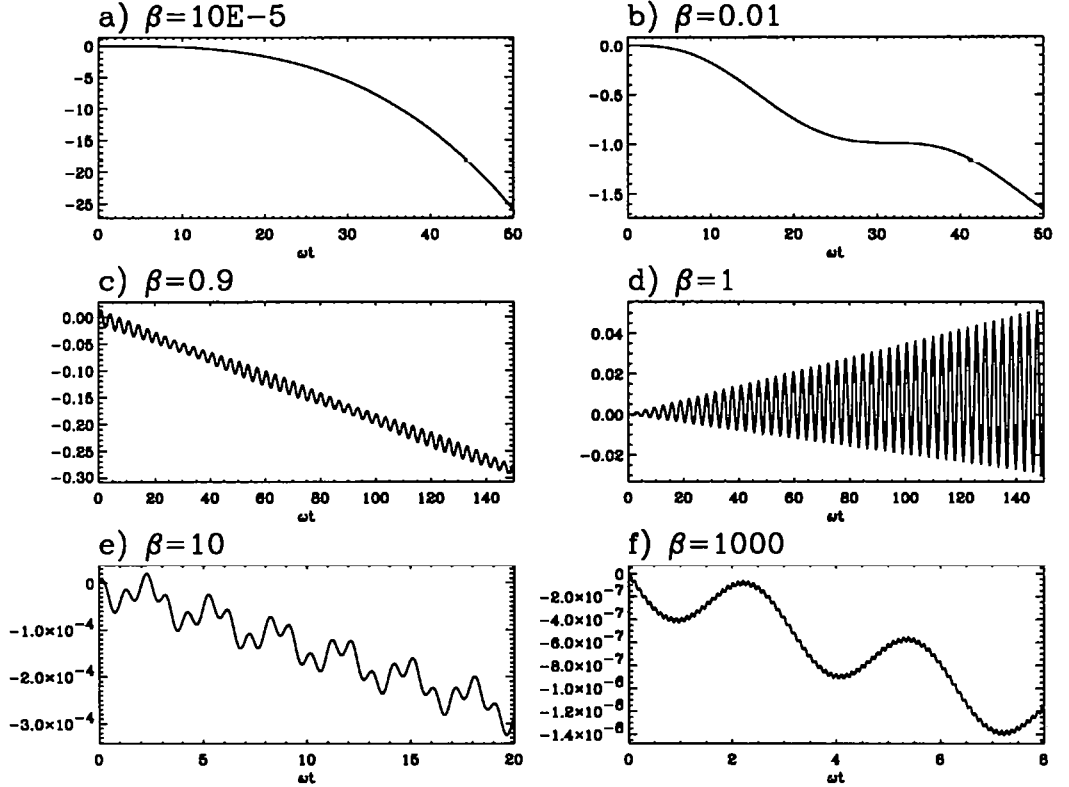
Figure 2.8: Time profile of the phase shift $\phi(t)$ of the original mode for different values of the parameter β. The velocity amplitude of the string displacement is $a=0.1$. When the amplitude of ϕ becomes of the same order as a, the results are no longer valid and serve only as a qualitative representation of the perturbation.

The solution (2.96) for the displacement perturbation η_3 can be neglected compared with the first-order solution, except when the parameter β is close to 0 or 1. The cases $\beta=0$ and $\beta=1$ have already been studied, with much less analytical effort. Figure 2.7 shows the displacement perturbation η_3 as a function of time for different values of the parameter β. When β is less than unity, the oscillation envelope is proportional to the integral $\int dt\,\sigma_2$, confirming that the term proportional to $(\sigma_2/\sigma_0)(\partial^2\eta_1/\partial t^2)$ is the dominant driver term in Equation (2.84). The function Ψ_2 is the dominant term in the solution (2.96) for the displacement perturbation η_3 when $\beta < 1$. The functions $\Psi_1\cos(\omega t)$ and $\Psi_3\cos(\omega t)$ contain a beat with a major frequency of $\sqrt{\beta}\,\omega$ and a minor frequency of $(\sqrt{\beta}+1)\,\omega$.

2.5 Discussion

We have shown that the mechanical analogues of mobile beads on a stretched string and of a fluid in an oscillating tube, where we have taken the tension to be a constant, match very well the results of the weakly nonlinear dynamics of bounded Alfvén waves (Rankin *et al.*, 1994). We shall see in the work that follows that the results we have obtained in this chapter link in very well with the work on the ponderomotive force of bounded fast magneto-sonic waves as well. Because of the nonlinear effects on these waves, we prefer to speak of bounded rather than standing waves. The description of discrete beads on a string gives a better feeling of what the ponderomotive force actually is. The ponderomotive force is the longitudinal component of the restoring force, which in this case is the tension force, and is proportional to the gradient and the acceleration of the string's transverse displacement field. It is a nonlinear force. We have shown that this force does not depend directly on the tension. We have shown that the leading-order term of the ponderomotive force of the string has the same form as the second-order ponderomotive force of linearly polarized Alfvén waves.

If the displacement field is a bounded wave, there is an average ponderomotive force. The force is directed towards the anti-nodes of the wave field. In the description of discrete beads on a string, we see that the beads (when given no initial velocity) are trapped between the two nearest nodes of the wave field, oscillating around the anti-node. The motion is described by the equation of an anharmonic oscillator. We have seen that the discrete description posed some mathematical problems. Firstly, the derivative $\partial\eta/\partial x$ does not really exist at the position of the bead if the bead is modelled as a point particle. This is because the inertia of the bead in the string generates a cusp at that position. We neglected this problem by saying that every bead has such a tiny mass compared with the mass of the string that the contribution of the bead to the string's oscillation is negligible. When we consider a continuous spread of beads, at a certain time T_c, the linear density of the beads will exceed the linear density of the string, and even becomes infinite shortly afterwards. This is possible because the beads do not interact with each other. The contribution of the beads to the string's oscillation cannot be neglected then. The solutions we have obtained for this case are valid up to the time T_c.

A better approach to the problem is to use a fluid analogy rather than a continuous
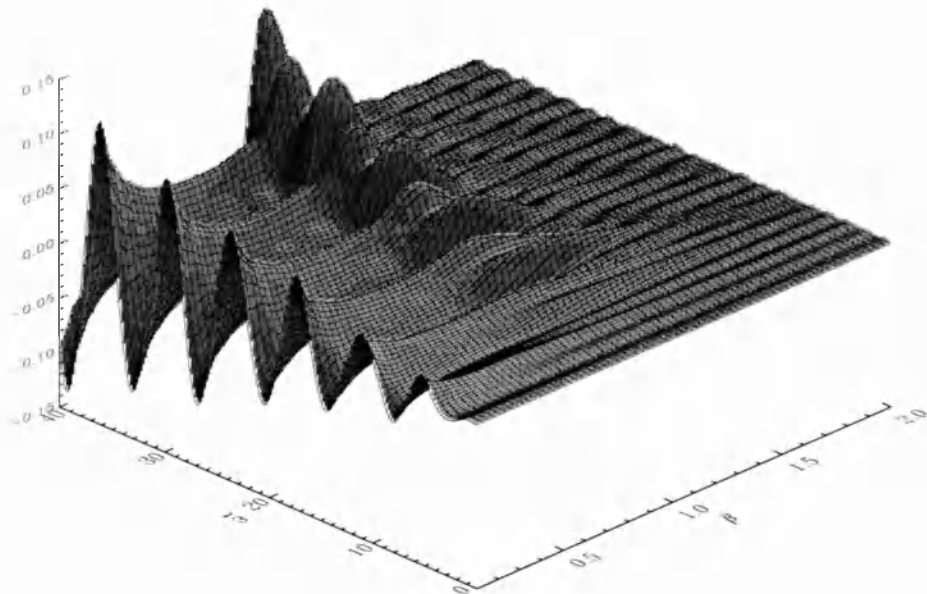
Figure 2.9: Surface plot of the displacement perturbation η_3 as a function of time and the parameter β. The velocity amplitude of the first-order displacement is $a=0.1$.

spread of discrete beads as the latter contains more information than is needed. Instead of a bead-string system we have a fluid-tube system, where the tube has a negligible diameter. We obtain equations which are very similar to the MHD equations. The Lorentz force has been replaced by the restoring force of the fluid-tube system with a tension consisting of the tension of the tube minus the inertia of the fluid.

We have included the pressure force as well in the equations. In the fluid there is a competition between the ponderomotive force and the pressure force. This is reflected by the solution of the lowest order non-zero solution of the equation of motion of the fluid. When the parameter β, which is the ratio of the sound speed of the fluid and the tension speed of the fluid-tube system, is much smaller than unity, the ponderomotive force dominates the system, causing large density fluctuations. In the limit of β tending to zero, the density at the position of the anti-node of the wave field grows secularly as t^2. For β

equal to unity, the sound wave in the fluid and the transverse oscillation of the tube are in resonance. The density at the position of the anti-node of the wave field grows linearly.

For the two previous ranges of β, it is worthwhile studying the counteraction of the fluid redistribution (due to the ponderomotive force) onto the transverse oscillation of the fluid-tube system. When β is less than unity, the transverse oscillation modification is driven by the ponderomotive density redistribution. In the case of zero β, we have the generation of a third spatial harmonic of the wave field, whilst the original mode is modified in amplitude and frequency. A temporal higher harmonic generation is less efficient. In the case of β equal to unity, we have the generation of higher harmonics both in space and time, whilst the original mode is again modified in amplitude and frequency.

These results match up very well with work done on bounded magnetic waves (Allan *et al.*, 1990, 1991, 1996; Rankin *et al.*, 1994; Tikhonchuk *et al.*, 1995). In this analogue we only consider two dimensions. Coupling to the third dimension is completely absent. Therefore this analogue does not include the coupling between modes with different transverse components (coupling between the fast magnetosonic and Alfvén waves). Non-uniformity across the magnetic field-lines cannot be described either in this analogue.

Chapter 3

The nonlinear evolution of bounded fast magneto-acoustic waves

3.1   Introduction

In this chapter the nonlinear evolution of fast magneto-acoustic waves in the cold-plasma limit in a two-dimensional homogeneous cavity is investigated. This is studied in the weakly nonlinear regime as put forward in the first chapter. From the quadratically nonlinear equations (1.63)-(1.65) we concluded that in the cold-plasma limit the ponderomotive force of a linear fast magneto-acoustic wave excites plasma flow along the equilibrium magnetic field, as well as causing moderation of the fast modes. Alfvén waves are not generated. This is true for every order in the expansion, so that the velocity component v_z and magnetic field component B_z are, at all times, equal to zero.

Allan *et al.* (1990) and Allan (1992) investigated the quadratically nonlinear solution generated by a bounded fast magneto-acoustic wave in the context of the Earth's magnetosphere. Guglielmi (1997) pointed out that in Allan's work, it is necessary to study the cubic nonlinearity as well, because it governs the self-moderation of the fast magneto-acoustic modes. Rankin *et al.* (1994) investigated the nonlinear evolution of standing Alfvén waves.

The chapter is organised as follows. The two first sections describe the model and the
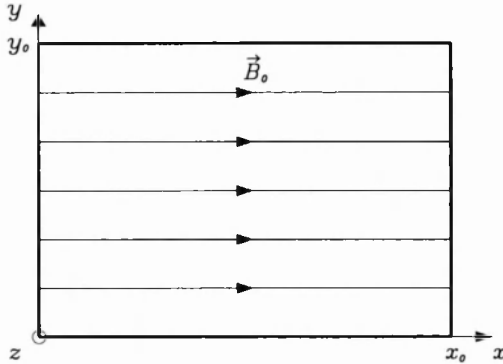
Figure 3.1: A simple model with four line-tied boundaries.

linear set of bounded fast wave modes. The third section presents a numerical simulation
which shows the main features that occur. In the fourth and fifth sections the second- and
third-order terms of the governing equations are investigated. The sixth section looks at a
slow time-scales analysis to obtain the results of the previous two sections in a more natural
way. The seventh section presents an approximate description of the nonlinear evolution
of the flow along the equilibrium magnetic field where an upper limit is found for the time
of the formation of a velocity discontinuity in v_x. The last section is a discussion of the
obtained results.

3.2   Model

We consider the model put forward in the first chapter: a homogeneous plasma with a
uniform magnetic field in the x-direction, $B_0 \vec{1}_x$. The equilibrium is static and uniform.
We assume that there are no variations in the z-direction. We consider a box of size
$[0,x_0]\times[0,y_0]$ and take $\vec{v} = \vec{0}$ at the boundaries. The boundaries in the x-direction are
thus line-tied. Figure 3.1 shows this. The kinetic pressure is neglected in comparison
with the magnetic pressure (cold-plasma limit) to avoid the linear coupling between the
fast and slow magneto-acoustic wave modes. We shall see later that this has important
implications. Initially fast magneto-acoustic waves of small but finite amplitudes, which
satisfy the boundary conditions, are prescribed. The velocity components $v_{x,1}$ and $v_{z,1}$ are

taken to be zero.

The z-component of the magnetic field is equal to zero in this model. It is therefore more convenient to work with the magnetic vector potential instead of the magnetic field components since only the z-component of the vector potential is non-zero. The magnetic field is written as

$$\vec{B} = B_0 \, \vec{\nabla} \times A \vec{1}_z \, , \tag{3.1}$$

where $\vec{1}_z$ is the unit vector in the z-direction and $B_0 A$ is the z-component of the vector potential. Throughout this chapter the quantity A itself is loosely called the vector potential. The ideal MHD Equations (1.26)-(1.28) are transformed into:

$$\frac{\partial \rho}{\partial t} + \vec{\nabla} \cdot (\rho \vec{v}) = 0 \, , \tag{3.2}$$

$$\rho \frac{d\vec{v}}{dt} = -\frac{B_0^2}{\mu_0} \left(\vec{\nabla}^2 A \right) \vec{\nabla} A \, , \tag{3.3}$$

$$\frac{dA}{dt} = 0 \, . \tag{3.4}$$

In order to generate the equilibrium magnetic field B_0, the equilibrium value of the vector potential A is $A_0 = y$. The magnetic field components are retrieved from Expression (3.1):

$$\frac{B_x}{B_0} = \frac{\partial A}{\partial y} \, , \, \frac{B_y}{B_0} = -\frac{\partial A}{\partial x} \, . \tag{3.5}$$

In the same manner as in the first chapter, we assume that any perturbation from the equilibrium (*e.g.* $\rho = \rho_0 + \rho'$) has a small but finite amplitude. This is the weakly nonlinear regime. The perturbation is expanded in a power series in ϵ, which is a small and positive parameter ($0 < \epsilon \ll 1$), proportional to the wave amplitude (*e.g.* $\rho' = \epsilon \rho_1 + \epsilon^2 \rho_2 + \ldots$).

Equations (3.2)-(3.4) are then linearized by gathering together terms of the same order in ϵ.

3.3   A discrete set of linear, bounded fast magneto-acoustic waves

The terms in Equations (3.2)-(3.4) of order ϵ combine into a system of equations which describe the possible linear MHD waves for the choice of model:

$$\frac{\partial \rho_1}{\partial t} + \rho_0 \vec{\nabla} \cdot \vec{v}_1 = 0 \, , \tag{3.6}$$

59

$$\frac{\partial v_{x,1}}{\partial t} = 0 \,, \tag{3.7}$$

$$\frac{\partial v_{y,1}}{\partial t} = -V_A^2 \vec{\nabla}^2 A_1 \,, \tag{3.8}$$

$$\frac{\partial A_1}{\partial t} = -v_{y,1} \,. \tag{3.9}$$

Combining Equations (3.8) and (3.9), a wave equation in the velocity perturbation $v_{y,1}$ for fast magneto-acoustic waves is obtained, which is of the form:

$$\left[\frac{\partial^2}{\partial t^2} - V_A^2 \vec{\nabla}^2 \right] v_{y,1} = 0 \,. \tag{3.10}$$

We look for normal mode solutions to this equation. They are proportional to $\Re(\exp(-i\omega t))$. Together with the boundary condition of $\vec{v} = \vec{0}$, the solution to Equation (3.10) is a linear combination of discrete fast magneto-acoustic wave modes.

$$\frac{v_{y,1}}{V_A} = \sum_{n=1}^{n_{max}} \sum_{l=1}^{l_{max}} a_{n,l} \sin\left(k_{x,n} x\right) \sin\left(k_{y,l} y\right) \cos\left(\omega_{n,l} t\right) , \tag{3.11}$$

where

$$k_{x,n} = \frac{n\pi}{x_0} \,, \quad k_{y,l} = \frac{l\pi}{y_0} \,, \quad k_{n,l} = \sqrt{k_{x,n}^2 + k_{y,l}^2} \,. \tag{3.12}$$

The wave-numbers n and l of a mode are integer numbers and indicate the number of anti-nodes in the x- and y-directions respectively. Each fast magneto-acoustic mode oscillates at a frequency $\omega_{n,l}$ with an arbitrary amplitude $a_{n,l}$, determined by the initial conditions of the perturbation. The frequency $\omega_{n,l}$ is given by the dispersion relation

$$\omega_{n,l}^2 = V_A^2 k_{n,l}^2 \,. \tag{3.13}$$

The phase speed for every mode is equal to the Alfvén speed. The group velocity is equal to

$$\vec{V}_g = \frac{\partial \omega}{\partial \vec{k}} = V_{A0} \frac{\vec{k}}{k} \,. \tag{3.14}$$

The group velocity, and hence the wave-energy, has no preferred direction of propagation but because it depends on the wave-vector, the fast wave modes are dispersive.

The spatial part of the set of modes forms a complete set of orthogonal functions:

$$\chi_n = \sqrt{\frac{2}{x_0}} \sin\left(k_{x,n} x\right) , \quad \psi_l = \sqrt{\frac{2}{y_0}} \sin\left(k_{y,l} y\right) , \quad w_{n,l} = \chi_n \psi_l \,,$$

$$\int_0^{x_0} \int_0^{y_0} w_{n,l} \, w_{m,k} \, dx \, dy = \int_0^{x_0} \chi_n \chi_m \, dx \int_0^{y_0} \psi_l \psi_k \, dy = \delta_{n,m} \delta_{l,k} \,. \tag{3.15}$$

Every function that satisfies the prescribed boundary conditions can be written as a linear combination of the functions $w_{n,l}$. The fundamental mode has one anti-node in the velocity profile in the centre of the box.

The set of modes is truncated at n_{max} and l_{max} since for higher harmonics the mode frequency does not satisfy the MHD requirements. For example if the frequency becomes of the same order as the ion Larmor gyration frequency, the Hall effect can no longer be ignored.

The other first-order quantities are derived from Equations (3.6), (3.9) and (3.5) using Expression (3.11):

$$\frac{\rho_1}{\rho_0} = -\sum_{n=1}^{n_{max}} \sum_{l=1}^{l_{max}} \frac{a_{n,l} k_{y,l}}{k_{n,l}} \sin(k_{x,n}x) \cos(k_{y,l}y) \sin(\omega_{n,l}t) , \qquad (3.16)$$

$$A_1 = -\sum_{n=1}^{n_{max}} \sum_{l=1}^{l_{max}} \frac{a_{n,l}}{k_{n,l}} \sin(k_{x,n}x) \sin(k_{y,l}y) \sin(\omega_{n,l}t) , \qquad (3.17)$$

$$\frac{B_{x,1}}{B_0} = -\sum_{n=1}^{n_{max}} \sum_{l=1}^{l_{max}} \frac{a_{n,l} k_{y,l}}{k_{n,l}} \sin(k_{x,n}x) \cos(k_{y,l}y) \sin(\omega_{n,l}t) , \qquad (3.18)$$

$$\frac{B_{y,1}}{B_0} = \sum_{n=1}^{n_{max}} \sum_{l=1}^{l_{max}} \frac{a_{n,l} k_{x,n}}{k_{n,l}} \cos(k_{x,n}x) \sin(k_{y,l}y) \sin(\omega_{n,l}t) , \qquad (3.19)$$

3.4 Numerical simulation

In this section the nonlinear evolution of one single bounded fast magneto-acoustic wave mode is studied numerically as an initial-value problem, with a fully nonlinear, non-dissipative Lagrangian MHD code from Arber, Longbottom and Van Der Linden (1998) of which we use a two-dimensional version. The code is second-order in space and time. We impose on the boundaries that the velocity is zero.

At $t = 0$ a velocity perturbation v_y of the form

$$v_y(t = 0) = aV_A \sin(k_{x,n}x), \sin(k_{y,l}y) , \qquad (3.20)$$

is imposed. We concentrate mainly on the fundamental mode ($n = 1, l = 1$). We choose x_0 = 2.0 and $y_0 = 1.0$ and a spatial resolution of 0.0125. The amplitude parameter a is chosen to be in the range 0.01-0.1. In that range the behaviour is weakly nonlinear and behaves on a time-scale suitable for numerical investigation.

61
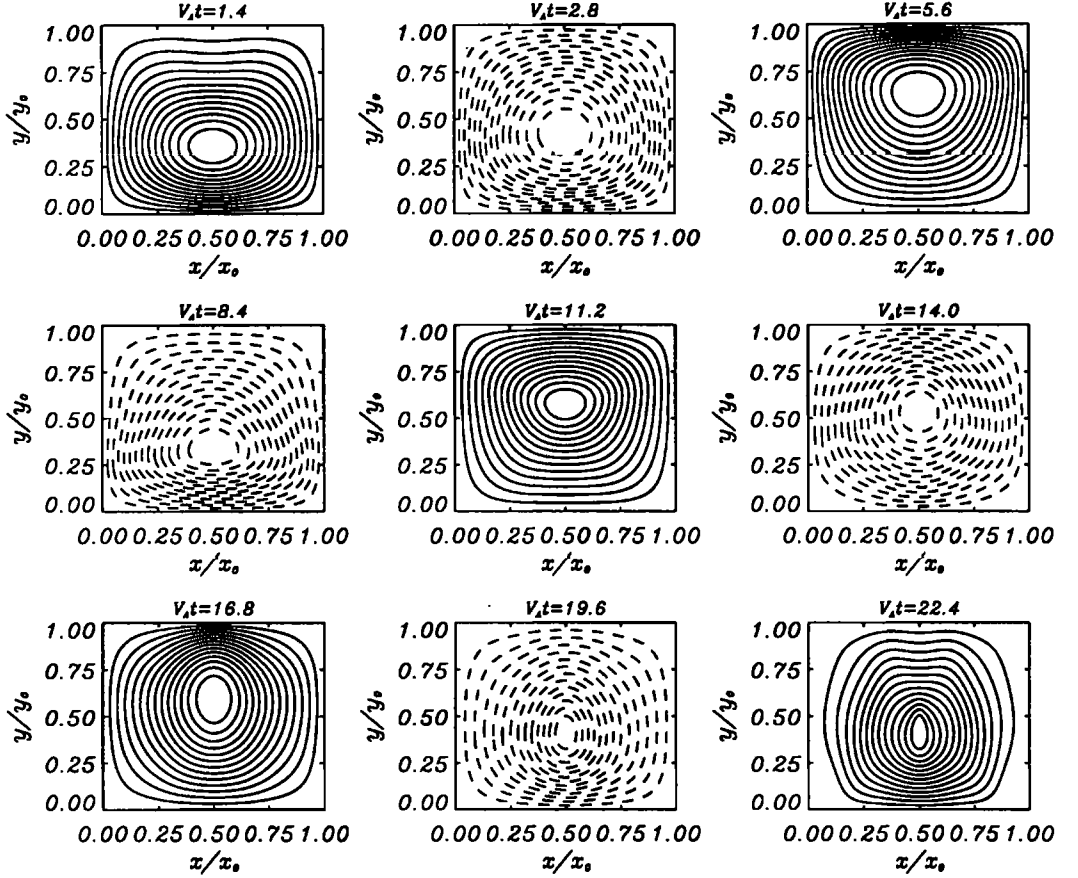
Figure 3.2: Spatial structure of the velocity component v_y at certain times using the full MHD Lagrangian code. Initially the fundamental mode ($n=1,l=1$) with an amplitude parameter $a = 0.05$ is imposed. The range of contour values is equal to $[-a,a]$, with positive values given by solid lines and the negative values given by dashed lines.

First of all we look at the general behaviour of the plasma quantities which describe the fast waves. Figure 3.2 shows, in a sequence of contourplots, the spatial structure of the velocity component v_y at certain times. The difference between the value of v_y at consecutive contour lines is equal to 0.007 V_A. Initially the spatial structure of the fundamental fast magneto-acoustic wave mode with amplitude $a = 0.05$ is imposed. The fundamental mode is clearly visible. It has an oscillation period of $V_A t = 1.8$.

Early on, the spatial structure in the transverse direction (y-direction) is moderated. The position of the anti-node in the velocity shifts in the y-direction. The presence of.low-amplitude higher harmonics is responsible for this. Figure 3.3 shows the spatial structure of
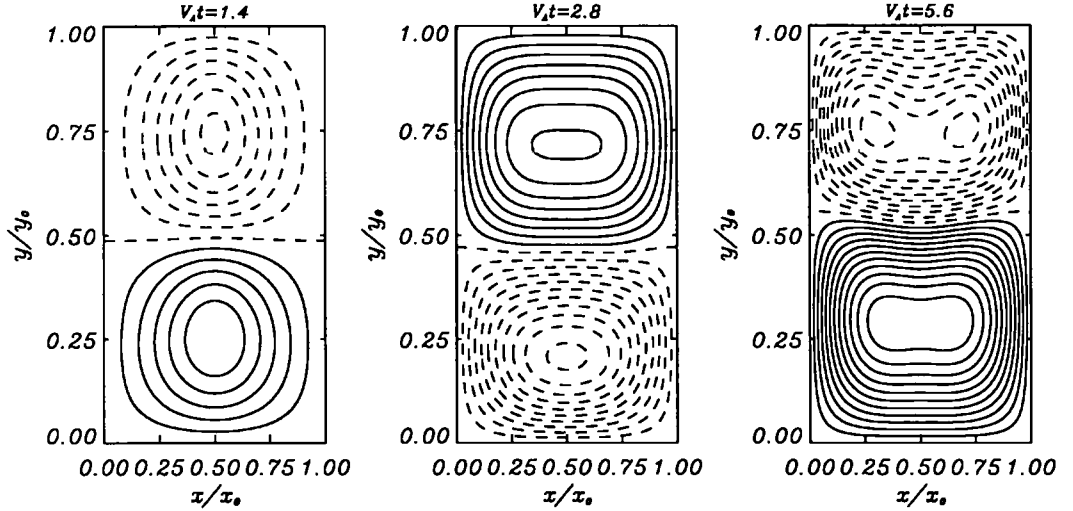
Figure 3.3: Spatial structure of the velocity difference v_y - $v_{y,1}$ at the times $V_A t$= 1.4, 2.8 and 5.6. The amplitude parameter $a = 0.05$. The range of contour values is [-0.007,0.007], with the positive values given by solid lines and the negative values given by dashed lines.

the difference between the velocity v_y and the linear velocity perturbation $v_{y,1}$. It reveals the presence of a velocity perturbation of amplitude 0.007 $V_A \approx 3$ $a^2 V_A$, with wave numbers n=1 and l=2. This mode is excited by a nonlinear process and oscillates at a different frequency from the original mode. Therefore, when the original mode passes through a temporal node, this higher harmonic becomes visible, hence the shift of the anti-node in the
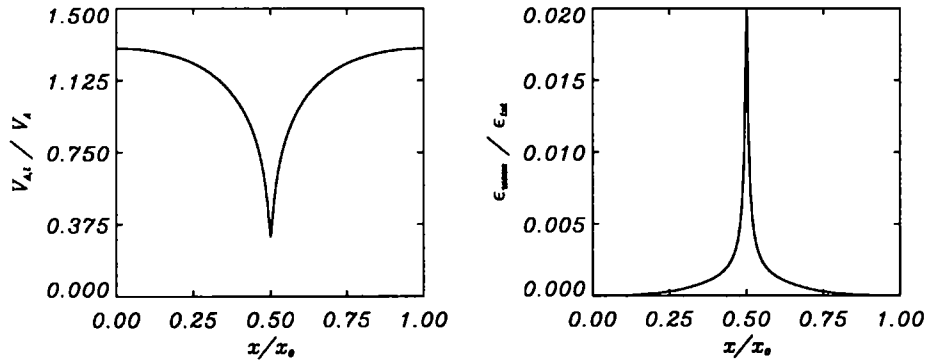
Figure 3.4: Plot of the local Alfvén speed (left) and wave energy density (right) as a function of x with $y = 0.5$ y_0 and $V_A t = 22.4$. Initially the fundamental mode of amplitude a=0.05 is imposed.

63
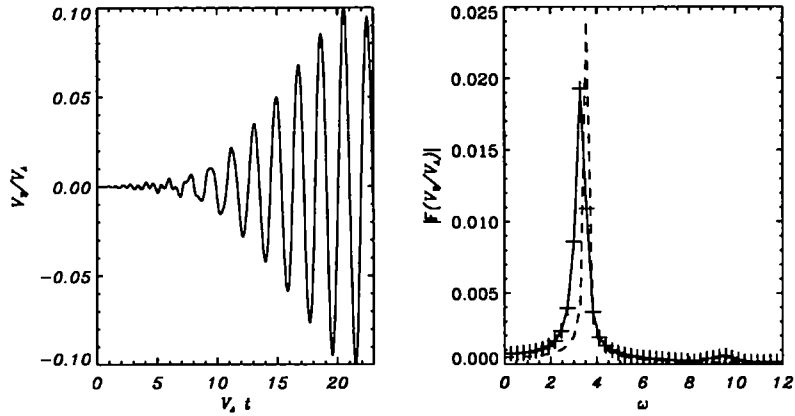
Figure 3.5: Left: Plot of the velocity difference v_y - $v_{y,1}$ as a function of time. Right: Frequency spectrum of the velocity v_y and velocity perturbation $v_{y,1}$ (dashed line). The velocity v_y is the numerical result from an initially imposed mode (3.20) with amplitude $a = 0.05$ and wave number $n=1$ and $l=1$ and $v_{y,1}$ is the corresponding first-order mode in (3.11). The velocities are measured at the position ($x=0.5$ x_0, $y = 0.5$ y_0).

velocity field. At the time $V_A t = 5.6$, the presence of a low-amplitude velocity perturbation with wave numbers $n = 3$ and $l=2$ is also visible. For the simulation with the amplitude $a = 0.05$, the amplitudes of the higher harmonics remain small compared with the initially excited wave mode during the time range of the numerical simulation.

By comparing the spatial structure of the velocity at the times $V_A t = 1.4$ and 22.4 in Figure 3.2, it becomes clear that the mode is refracted towards the central position with the strongest refraction in the x-direction. Figure 3.4 shows the x-dependency of the local Alfvén speed for $y=0.5$ y_0 at the time $V_A t = 22.4$. The Alfvén speed is dramatically reduced at the position $x=0.5$ x_0, which corresponds to the position of the anti-node of the fundamental mode. The wave energy density is strongly enhanced at that position. The fast wave mode refracts from regions of low Alfvén speed to those of high Alfvén speed, forming a wave guide for the fast magneto-acoustic wave.

The moderation of the local Alfvén speed also influences the oscillation frequency of the fast mode. Figure 3.5 shows the time variation of the difference between the velocity component v_y and the corresponding linear solution $v_{y,1}$ at an anti-node of the velocity wavefield. In the beginning the two quantities are in phase. With increasing time the numerical result shifts out of phase with the linear solution. At the time of approximately $V_A t \approx 20$,

the velocity v_y is in anti-phase with $v_{y,1}$. The phase shift, call it $\phi(t)$, can be calculated from the time variation of the velocity difference, measured at the position of an anti-node in the velocity of the initially imposed wave mode. At that position the nonlinearly excited modes with double the wavenumber in the y-direction have a spatial node and thus are equal to zero. We assume that the velocity v_y is proportional to $a\cos(\omega t + \phi)$. The linear solution $v_{y,1}$ is proportional to $a\cos(\omega t)$. The difference between the two velocity components is equal to $-2a\sin(\phi/2)\sin(\omega t + \phi/2)$. By comparing the amplitude modulation $2a\sin(\phi/2)$ with the numerical result, the phase shift is retrieved. In a later section this is done and compared with the analytically derived phase shift.

The right plot of Figure 3.5 shows the frequency spectrum of the velocity component v_y measured at the same position. The dashed line represents the frequency spectrum of the linear solution $v_{y,1}$, which unsurprisingly has one strong peak at its oscillation frequency $\omega_{1,1}$. The frequency spectrum of the numerical result shows one strong peak, which is centred slightly lower than the frequency $\omega_{1,1}$. It is broader than its analytical counterpart because it contains the history of the continuous frequency shift from $\omega_{1,1}$ to its preferred oscillation frequency. The mode (n=1, l=2) is not visible in the spectrum because at the position the spectrum is taken, it has a spatial node. Figure 3.6 shows the frequency contents of the velocity component v_y at the position $x = 0.5\ x_0$, $y = 0.25\ y_0$. The mode (n=1, l=2) is here clearly visible as the smaller peak to the right of the peak of the original
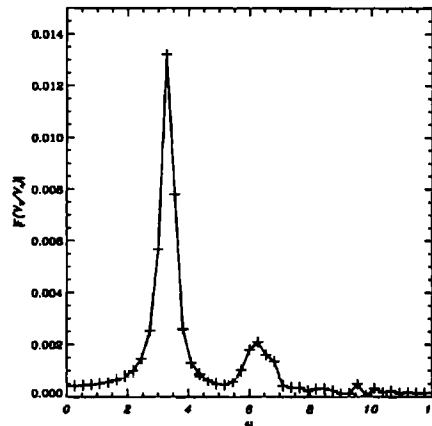
Figure 3.6: Frequency spectrum of the velocity v_y, measured at the position x=0.5 x_0, $y = 0.25$ y_0. Initially the fundamental mode with amplitude $a = 0.05$ is imposed.

65
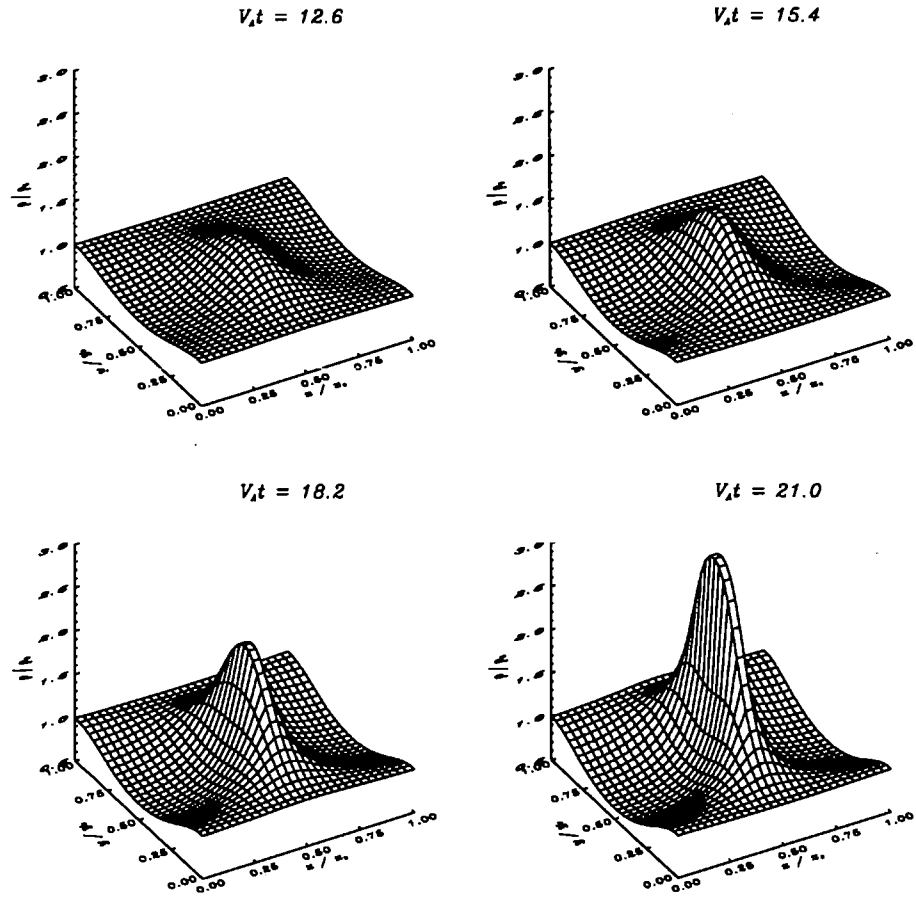
Figure 3.7: Surface plot of the spatial structure of the density at certain times. Initially the fundamental mode with amplitude $a = 0.05$ is imposed.

mode.

The change in the local Alfvén speed, and the consequential wave refraction and frequency shift, is caused by the presence of a strong inhomogeneity in the density, which does not have the spatial or temporal structure of the linear density perturbation (3.16). Figure 3.7 shows the spatial structure of the density at certain times. Plasma is accumulating at the position of the anti-node in the x-direction of the velocity wave field ($x = 0.5\ x_0$ in this case) and is depleted around the nodes in the x-direction. Figure 3.8 shows the time evolution of the density at the anti-node of the initial wave mode. The density at this position grows with a profile which resembles a secant function and becomes locally much larger than
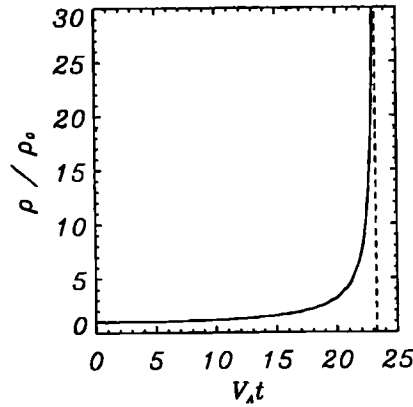
Figure 3.8: Plot of the density at the position of the anti-node in the velocity wave field v_y ($x = 0.5\ x_0$, $y = 0.5\ y_0$) as a function of time. Initially the fundamental mode with an amplitude $a=0.05$ is imposed.

the background density. For an initially imposed fundamental mode of amplitude $a = 0.05$, this time is approximately $V_A t = 23.25$. Figure 3.9 shows that the plasma redistribution is caused by a flow along the direction of the equilibrium magnetic field (v_x) from the regions around the nodes towards the node. The amplitude of the velocity component v_x grows initially linearly in time. At a finite time the longitudinal velocity component v_x forms a fixed discontinuity across the anti-node in the x-direction (the density would become locally
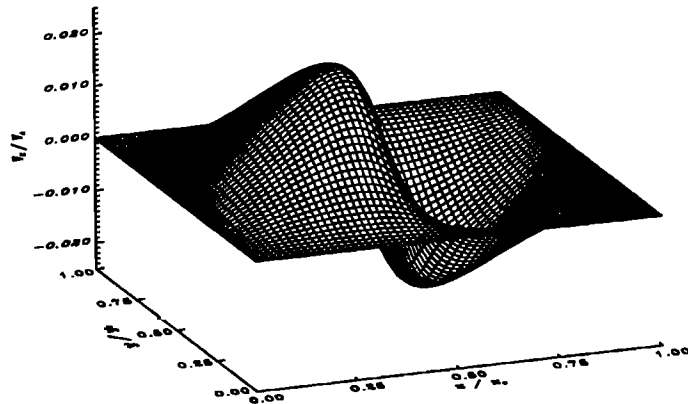
Figure 3.9: Surface plot of the spatial structure of the velocity component v_x at the time $V_A t = 21$. Initially the fundamental mode with an amplitude $a=0.05$ is imposed.

67
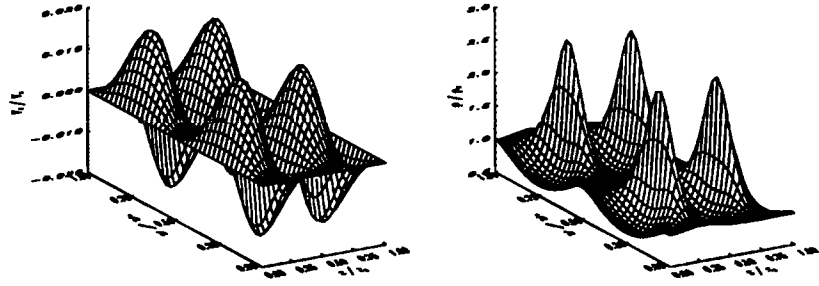
Figure 3.10: Surface plot of the spatial structure of the velocity component v_x and the density ρ at the time $V_A t = 9.9$. Initially the wave mode with wave numbers $n = 2$, $l = 2$ and an amplitude $a=0.05$ is imposed.

infinite). For an initially imposed fundamental mode of amplitude $a = 0.05$, this time is $V_A t = 23.25$. Figure 3.9 shows that there is already a strong velocity gradient present at $x = 0.5\, x_0$ at the time $V_A t = 21$. The numerical scheme tries to resolve the steepening profile correctly by diminishing the time-step. Therefore the numerical simulation ends when the velocity gradient becomes so large that the value of the time-step falls below computer accuracy. We say that, at this time, the velocity discontinuity has formed.

Figure 3.10 shows the spatial profile of the velocity component v_x and the density ρ at the time $V_A t = 9.9$ for an initially imposed mode of amplitude $a = 0.05$ and wave numbers $n=2$ and $l = 2$. The same general nonlinear behaviour is observed: a large density build-up at the anti-nodes of the velocity wave-field and the formation of a discontinuity in the velocity component v_x at those positions (at the time $V_A t \approx 11.9$).

From these numerical results, it is clear that a perturbation method, which assumes that perturbations are small compared with the equilibrium value, is not valid for all times.

Equation (3.3) shows that, in our model, a plasma flow in the x-direction is excited by the only force present in that direction: the x-component of the ponderomotive force of the fast magneto-acoustic wave. This force is quadratically nonlinear. The fact that the density and its spatial gradient become very large means that other forces, which are not taken into account in this model or the numerical simulation, become important at a certain stage and counteract the large density build-up.

For a larger amplitude a, another nonlinear feature is observed which acts on a time-scale faster than the nonlinear evolution of the velocity component v_x. The case of an initially
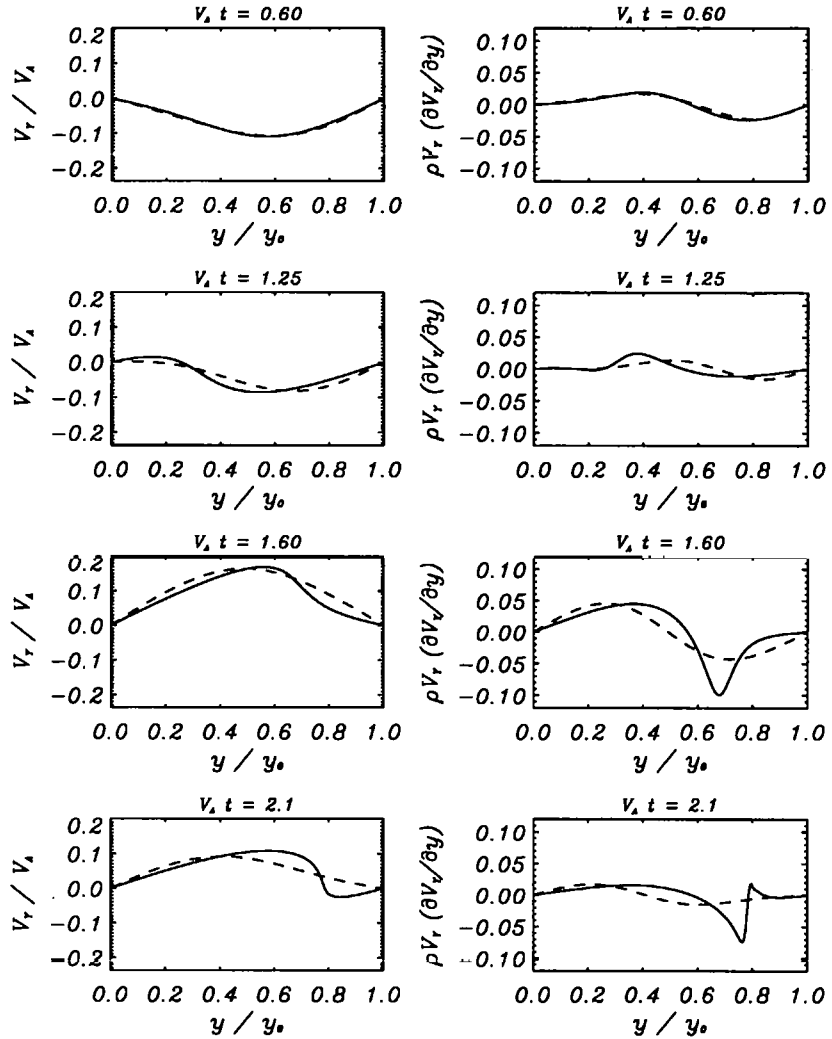
Figure 3.11: Plot of the velocity component v_y and the inertial term $\rho v_y(\partial v_y/\partial y)$ as a function of y at the position $x = 0.5\,x_0$ for certain times. Initially the fundamental mode with an amplitude $a = 0.2$ is imposed. The dashed lines represent the analytical equivalent, calculated in the later sections.

imposed fundamental mode of amplitude $a=0.2$ reveals a strong nonlinear evolution in the y-dependency of the fast wave mode. Figure 3.11 shows the y-dependency of the velocity v_y and the inertial term $\rho v_y(\partial v_y/\partial y)$ for $x = 0.5\,x_0$ at certain times. The change of the y-profile, first introduced by the generation of a second harmonic in the y-direction, causes the velocity component v_y to contain a 'travelling' part, which has, locally, a steepening

69

gradient in y (close to the position of the shifting anti-node). At that position the inertial term shown in Figure 3.11 departs strongly from the expected $\sin(2k_y y)$ profile. At the time $V_A t = 2.1$ the gradient in v_y has become locally large enough for the numerical scheme to start having trouble capturing the profile accurately. After that time, signs of Gibbs overshoot become clear and entropy is no longer preserved, which are signs of the inability of the numerical code to capture a steep gradient accurately (Dym & McKean, 1972). The numerical code stops well before the formation time of the discontinuity in the velocity component v_x. Figure 3.12 clearly shows the presence of a forming shock. It shows the velocity difference in v_y between two consecutive grid points in the y-direction at the time $V_A t = 2.1$. Expression (85.7) of Landau & Lifshitz (1959) states that the velocity difference between the velocity at the front and the back of a shock is given by $(-\Delta p \Delta V)^{1/2}$, where the quantity V is the specific volume $1/\rho$. We use the magnetic pressure instead of the kinetic pressure. Around the position $y = 0.78 \, y_0$ this velocity difference is enhanced, revealing the location of the forming shock at that time. Ideally when the shock is formed this enhancement will have an infinitesimal width and a maximum value exceeding the local Alfvén speed.
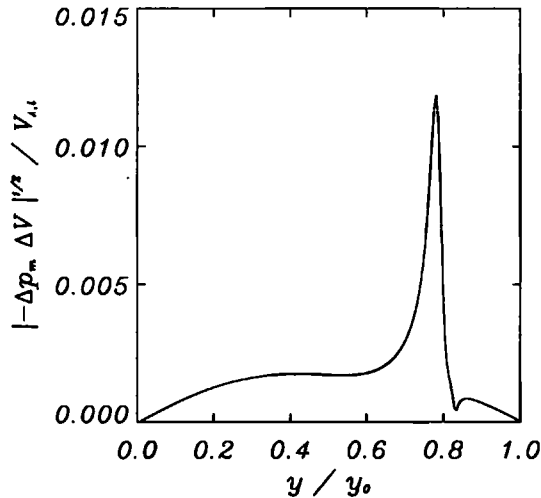
Figure 3.12: Plot of the function $(-\Delta p_m / 2\Delta V)^{1/2}$ as a function of the y-coordinate at the time $V_A t = 2.1$. The quantity Δp_m is the difference in the magnetic pressure between two consecutive grid points. The quantity ΔV is the difference in the specific volume $V = 1/\rho$ between two consecutive grid points. Initially the fundamental mode with an amplitude $a = 0.2$ is imposed.

It is clear that, in the cold-plasma limit, both components of the ponderomotive force have a strong effect on the bounded fast magneto-acoustic waves, acting on time-scales depending on the amplitude of the imposed wave. The response to the longitudinal component of the ponderomotive force dominates when the amplitude $a \ll 1$. When $a \sim 1$ the response to the transverse component of the ponderomotive force dominates.

In the following sections we shall look at the nonlinear forces and the effect they have on the bounded fast magneto-acoustic wave modes, explaining the features the numerical simulation has revealed, within the frame of weakly nonlinear theory. This means that we investigate the regime of the amplitude a for which the longitudinal component of the ponderomotive force produces the strongest effects.

3.5 Quadratically nonlinear solutions

The lowest non-zero contribution of the ponderomotive force is at order ϵ^2. Equations (3.2)-(3.4) of order ϵ^2 are:

$$\frac{\partial \rho_2}{\partial t} + \rho_0 \vec{\nabla}.\vec{v}^{(2)} = -\vec{\nabla}.\left(\rho_1 \vec{v}_1\right) , \tag{3.21}$$

$$\frac{\partial v_{x,2}}{\partial t} = -V_A^2 \left(\vec{\nabla}^2 A_1\right) \frac{\partial A_1}{\partial x} , \tag{3.22}$$

$$\frac{\partial v_{y,2}}{\partial t} + V_A^2 \vec{\nabla} A_2 = -\frac{\rho_1}{\rho_0}\frac{\partial v_{y,1}}{\partial t} - v_{y,1}\frac{\partial v_{y,1}}{\partial y} - V_A^2 \left(\vec{\nabla}^2 A_1\right) \frac{\partial A_1}{\partial y} , \tag{3.23}$$

$$\frac{\partial A_2}{\partial t} + v_{y,2} = -v_{y,1}\frac{\partial A_1}{\partial y} . \tag{3.24}$$

The right-hand sides of Equations (3.21)-(3.24) consist of a combination of two first-order quantities related to the bounded fast magneto-acoustic wave mode. The right-hand side terms of Equations (3.22) and (3.23) are the components of the second-order ponderomotive force of fast magneto-acoustic waves. Notice that each term is the product of a fast wave quantity and the a spatial gradient of a fast wave quantity. We call the solutions of Equations (3.21)- (3.24), which are driven by the right-hand-sides of these equations, the second-order ponderomotive response. This response consists of mass flow along the magnetic field-lines and moderation of the fast magneto-acoustic wave modes. First the effectiveness of the second-order fast magneto-acoustic wave moderation is investigated.

3.5.1 Quadratically nonlinear moderation of fast waves

The moderation of the bounded fast magneto-acoustic wave modes through the quadratic nonlinearity is investigated. It will be shown that, for this model, the moderation is weak. The velocity perturbations $v_{y,2}$ and $v_{y,1}$ are eliminated from Equation (3.23) with the use of Equations (3.24) and (3.9). A driven fast magneto-acoustic wave equation for A_2 is obtained. The solution is driven by terms which contain the first-order solution A_1 quadratically:

$$\left[\frac{\partial^2}{\partial t^2} - V_A^2 \vec{\nabla}^2 \right] A_2 = 2 \left(\frac{\partial A_1}{\partial t} \right) \frac{\partial}{\partial y} \left(\frac{\partial A_1}{\partial t} \right) + V_A^2 \left(\vec{\nabla}^2 A_1 \right) \frac{\partial A_1}{\partial y} . \tag{3.25}$$

Expression (3.17) for A_1 is substituted into Equation (3.25):

$$\left[\frac{\partial^2}{\partial t^2} - V_A^2 \vec{\nabla}^2 \right] A_2 = \frac{x_0 y_0}{4} V_A^2 \sum_{\substack{n=1 \\ n'=1}}^{n_{max}} \sum_{\substack{l=1 \\ l'=1}}^{l_{max}} w_{n,l} \frac{\partial w_{n',l'}}{\partial y} F_{n,l,n',l'}(t) , \tag{3.26}$$

with

$$F_{n,l,n',l'}(t) = a_{n,l} a_{n',l'} \left[2 \cos(\omega_{n,l} t) \cos(\omega_{n',l'} t) - \frac{\omega_{n,l}}{\omega_{n',l'}} \sin(\omega_{n,l} t) \sin(\omega_{n',l'} t) \right] . \tag{3.27}$$

The function $F_{n,l,n',l'}$ contains oscillations with frequencies $\omega_{n,l} \pm \omega_{n',l'}$.

Non-resonant excitation

It will be shown that the second-order moderation of the fully bounded fast magneto-acoustic waves is non-resonant. The spatial part of the solution A_2 is written as a linear combination of the set of functions $w_{n,l}$.

$$A_2 = \sum_{n=1}^{n_{max}} \sum_{l=1}^{l_{max}} A_{n,l}(t) w_{n,l} . \tag{3.28}$$

Expression (3.28) is consequently substituted into Equation (3.26), which is projected onto the function $w_{m,k}$. The following ordinary differential equation for every mode (m,k) is obtained:

$$\left[\frac{d^2}{dt^2} + \omega_{m,k}^2 \right] A_{m,k} = V_A^2 \sum_{\substack{n=1 \\ n'=1}}^{n_{max}} \sum_{\substack{l=1 \\ l'=1}}^{l_{max}} C_{m,k,n,l,n',l'} F_{n,l,n',l'}(t) \tag{3.29}$$

with

$$C_{m,k,n,l,n',l'} = \frac{x_0 y_0}{4} \int_0^{x_0} dx \int_0^{y_0} dy \, w_{m,k} w_{n,l} \frac{\partial w_{n',l'}}{\partial y} . \tag{3.30}$$

The number $C_{m,k,n,l,n',l'}$ is the coupling coefficient. Its value determines how strong the fast wave mode with wave numbers (m,k) is driven by a pair of fast wave modes with wave numbers (n,l) and (n',l'). When

$$\begin{cases} \omega_{m,k} = \omega_{n,l} \pm \omega_{n',l'} \, , \\ m = n \pm n' \, , \\ k = l \pm l' \, , \end{cases} \tag{3.31}$$

the possibility of resonant excitation of the fast mode (m,k) exists. The coefficient (3.30) consists of the product of two integrals: one in x and one in y. The integral in x is equal to

$$\begin{aligned} \frac{x_0}{2} \int_0^{x_0} \chi_m \chi_n \chi_{n'} \, dx &= \sqrt{\frac{2}{x_0}} \int_0^{x_0} \sin(k_{x,m}x) \sin(k_{x,n}x) \sin(k_{x,n'}x) \, dx \\ &= -\frac{1}{4}\sqrt{\frac{2}{x_0}} \int_0^{x_0} \left[\sin(k_{x,m-n+n'}x) - \sin(k_{x,m-n-n'}x) \right. \\ &\qquad \left. - \sin(k_{x,m+n+n'}x) + \sin(k_{x,m+n-n'}x) \right] dx \, . \end{aligned} \tag{3.32}$$

For the integral (3.32) to be nonzero, the sine functions need to have an odd number of anti-nodes in the domain $[0,x_0]$. This is true for all four terms in the integral when the combination $m + n + n'$ is an odd integer. This selection rule is not satisfied for the case (3.31). Therefore the coupling coefficients $C_{n\pm n',l\pm l',n,l,n',l'}$ are equal to zero, which implies that resonant three-wave interaction and second harmonic generation of fully bounded fast magneto-acoustic waves is not possible. The integral in y in the coefficient (3.30) is equal to:

$$\begin{aligned} \frac{y_0}{2} \int_0^{y_0} \psi_k \psi_l \psi_{l'} \, dy &= \sqrt{\frac{2}{y_0}} k_{y,l'} \int_0^{y_0} \sin(k_{y,k}y) \sin(k_{y,l}y) \cos(k_{y,l'}y) \, dy \\ &= \frac{1}{4}\sqrt{\frac{2}{y_0}} k_{y,l'} \int_0^{y_0} \left[\cos(k_{y,k-l-l'}y) - \cos(k_{y,k+l+l'}y) \right. \\ &\qquad \left. + \cos(k_{y,k-l+l'}y) - \cos(k_{y,k+l-l'}y) \right] dy \\ &= \frac{1}{4}\sqrt{\frac{2}{y_0}} k_{y,l'} \left[\delta_{k,l+l'} - \delta_{k,-l-l'} + \delta_{k,l-l'} - \delta_{k,-l+l'} \right] \, . \end{aligned} \tag{3.33}$$

From Expression (3.33) it is clear that the coupling coefficient $C_{n,l,n,l,n,l}$ is equal to zero. Therefore second-order self-moderation of the the original wave mode is not possible.

The conclusion is that the second-order quantity A_2, and therefore also the velocity perturbation $v_{y,2}$ and second-order magnetic field perturbation, does not contain a solution

which is resonantly driven by the quadratic nonlinearity of the original wave field. The amplitude of the second-order solutions A_2 and $v_{y,2}$ remains small (proportional to a^2) compared with the first-order solution amplitude. The solution of Equation (3.29) is equal to

$$A_{m,k} = V_A^2 \sum_{\substack{n=1 \\ n'=1}}^{n_{max}} \sum_{\substack{l=1 \\ l'=1}}^{l_{max}} C_{m,k,n,l,n',l'} \, G_{m,k,n,l,n',l'}(t) \, , \tag{3.34}$$

with

$$
\begin{aligned}
G_{m,k,n,l,n',l'}(t) &= \frac{\left(1 - \frac{\omega_{n,l}}{2\omega_{n',l'}}\right)}{\omega_{m,k}^2 - \left(\omega_{n,l} - \omega_{n',l'}\right)^2} \left[\cos((\omega_{n,l} - \omega_{n',l'})t) - \cos(\omega_{m,k}t)\right] \\
&+ \frac{\left(1 + \frac{\omega_{n,l}}{2\omega_{n',l'}}\right)}{\omega_{m,k}^2 - \left(\omega_{n,l} + \omega_{n',l'}\right)^2} \left[\cos((\omega_{n,l} + \omega_{n',l'})t) - \cos(\omega_{m,k}t)\right] \, . \tag{3.35}
\end{aligned}
$$

Second-order moderation of a single wave mode

Despite the previous arguments, we shall investigate the solutions for the second-order wave field moderation closer, as interesting features appear when and where the linear solution becomes zero. For this investigation we consider only one single fast magneto-acoustic wave mode (n,l), which simplifies matters without losing the basic properties. Because there is no confusion possible between different modes, the indices n and l are dropped. Equation (3.26) reduces to

$$\left[\frac{\partial^2}{\partial t^2} - V_A^2 \vec{\nabla}^2\right] A_2 = \frac{1}{4}a^2 V_A^2 k_y \sin^2(k_x x) \sin(2k_y y)(3\cos(2\omega t) + 1) \, . \tag{3.36}$$

When considering only one linear mode, the coupling coefficient (3.30) is zero for all values except when the index m is an odd integer number and the indices n and n' are equal. Therefore the function $\sin^2(k_{x,n}x)$ is expanded out in an odd half-Fourier series:

$$\sin^2(k_{x,n}x) = \sum_{m=1}^{n_{max}/2} c_{n,m} \sin(k_{x,2m-1}x) \, , \tag{3.37}$$

with

$$c_{n,m} = -\frac{8}{\pi} \frac{n}{(2m-1)\left[(2m-1)^2 - 4n^2\right]} \, . \tag{3.38}$$

The coefficients $c_{n,m}$ are a subset of the coefficients $C_{m,k,n,l,n',l'}$ of Expression (3.30). As expected, the driver does not contain the spatial structure of the mode with wave numbers

74
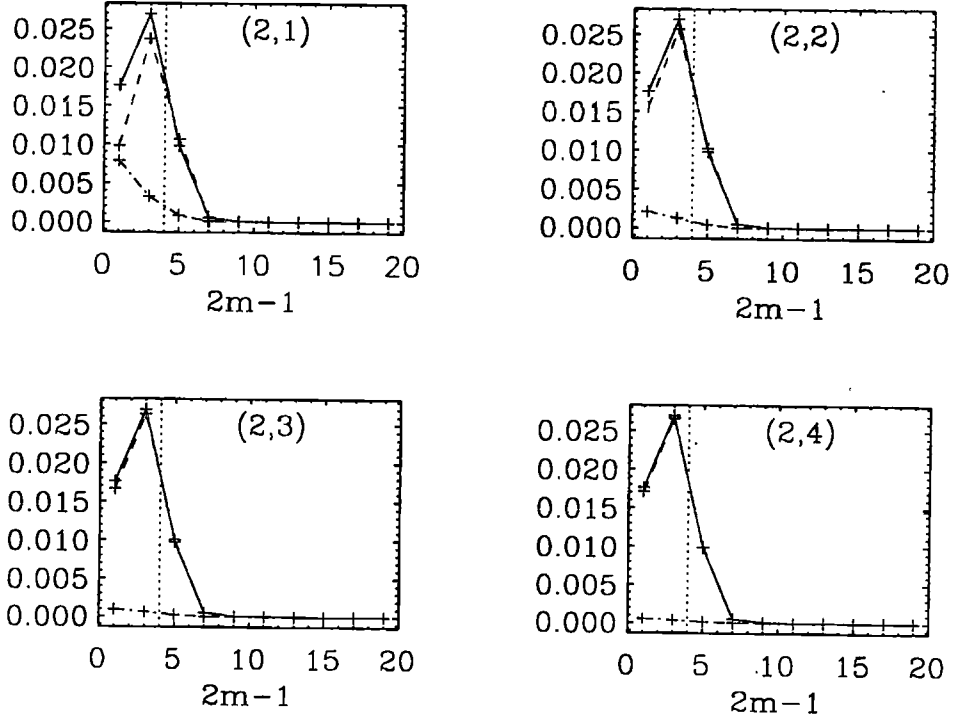
Figure 3.13: Plots of the three terms of the expression $c_{n,m}A_m$ as a function of $2m - 1$ for the modes (n=2,l=1), (2,2), (2,3) and (2,4). The full, dashed and dot-dashed lines show, respectively, the coefficients of the first, second and third terms of the right-hand side of Expression (3.41). The crosses denote the valid values. The dotted line shows the singular position.

$(2n,2l)$, which confirms that the second harmonic is not resonantly excited. The coefficients $c_{n,m}$ are proportional to m^{-3} and decrease quickly for larger values of m. Equation (3.36) is solved by assuming that the quantity A_2 has the form

$$A_2 = \frac{1}{4}a^2 V_A^2 k_y \sin{(2k_y y)} \sum_{m=1}^{n_{max}/2} c_{n,m} A_m(t) \sin{(k_{x,2m-1}x)} \,. \tag{3.39}$$

After substitution of Expression (3.39) into Equation (3.36), an ordinary differential equation for every A_m is obtained:

$$\left[\frac{d^2}{dt^2} + V_A^2 \left(k_{x,2m-1}^2 + 4k_y^2\right)\right] A_m = (3\cos{(2\omega t)} + 1) \,. \tag{3.40}$$

75

The solution of Equation (3.40), which satisfies the initial boundary conditions $A_m(t=0)$ $= dA_m/dt|_{t=0} = 0$, is:

$$A_m = \frac{1}{\Omega_m^2} + \frac{3}{(\Omega_m^2 - 4\omega^2)}\cos(2\omega t) - \frac{4(\Omega_m^2 - \omega^2)}{\Omega_m^2(\Omega_m^2 - 4\omega^2)}\cos(\Omega_m t), \qquad (3.41)$$

with

$$\Omega_m = V_A\left(k_{x,2m-1}^2 + 4k_y^2\right)^{1/2} = \omega_{2m-1,2l}. \qquad (3.42)$$

The other second-order quantities $v_{y,2}$, $B_{x,2}$ and $B_{y,2}$ which describe the fast magneto-acoustic wave are easily retrieved from Expression (3.41) using Equations (3.5) and (3.24):

$$\frac{v_{y,2}}{V_A} = \frac{1}{4}a^2 V_A k_y \sin(2k_y y) \sum_{m=1}^{n_{max}/2} c_{n,m} B_m(t)\sin(k_{x,2m-1}x), \qquad (3.43)$$

$$\frac{B_{x,2}}{B_0} = \frac{1}{2}a^2 V_A^2 k_y^2 \cos(2k_y y) \sum_{m=1}^{n_{max}/2} c_{n,m} A_m(t)\sin(k_{x,2m-1}x), \qquad (3.44)$$

$$\frac{B_{y,2}}{B_0} = -\frac{1}{4}a^2 V_A^2 k_y \sin(2k_y y) \sum_{m=1}^{n_{max}/2} c_{n,m} A_m(t) k_{x,2m-1}\cos(k_{x,2m-1}x), \qquad (3.45)$$

with

$$B_m = \frac{\sin(2\omega t)}{\omega} - \frac{dA_m}{dt}. \qquad (3.46)$$

The second-order solutions A_2 and $v_{y,2}$ and the mass perturbation they produce, are a small moderation to the linear solution. They have a wavenumber in the y-direction equal to $2l$, which confirms the numerical observation. We examine Expression (3.39) with the result (3.41) to find out what this moderation looks like and which are the dominant terms. Similar conclusions can be made for the velocity $v_{y,2}$ as well.

We see from Expressions (3.38) and (3.41) that for $m = n + \frac{1}{2}$ ($\Omega_m^2 = 4\omega^2$), the quantity $c_{n,m}A_m$ is singular. The index m cannot have this value but we expect the modes with a wave number $m = n$ or $m = n + 1$ to have an enhanced amplitude. This is confirmed in Figure 3.13 which shows the amplitudes of the three terms in the quantity $c_{n,m}A_m$ as a function of $2m - 1$ for the modes (n=2,l=1), (2,2), (2,3) and (2,4). The general profile is a sharp decrease with increasing m, with a local peak around the singular position $m = n + \frac{1}{2}$. The amplitudes of $c_{n,m}A_m$ for m larger than $n + 1$ are much smaller than the other amplitudes. Therefore Solution (3.41) is well approximated by truncating the series in m at $m = n + 1$. Expression (3.39) also shows that A_2 is proportional to the wave
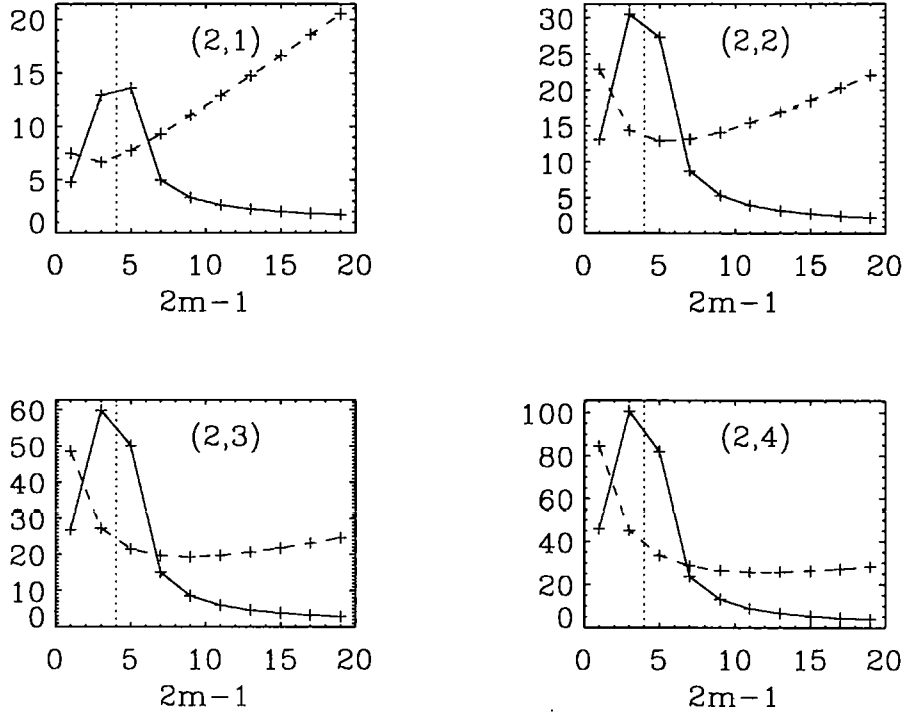
Figure 3.14: Ratios of major and minor periods of beats arising from the pair of modes with frequencies 2ω, Ω_m (solid line) and from the pair of modes with frequencies Ω_m, Ω_{m+1} (dashed line) as a function of $2m+1$ for the modes (n=2,l=1), (2,2), (2,3) and (2,4). The dotted line shows the singular position.

numbers n and l. The second-order moderation is therefore better visible for modes with higher wave numbers.

Expression (3.39) contains oscillations with frequencies 2ω, Ω_1, Ω_2,... There is the possibility of beats between the different oscillations. Figure 3.14 shows the ratios of major and minor periods of beats arising from the pair of modes with frequencies 2ω and Ω_m and from the pair of modes with frequencies Ω_m and Ω_{m+1}. We have prominent beats for the pairs $(\Omega_n,2\omega)$, $(\Omega_{n+1},2\omega)$ and also (Ω_1,Ω_2). Figure 3.15 shows the time variation of the quantity $B_{x,2}$ for the fundamental mode at a position of a spatial node in the linear solution, to show the higher-order solutions. The left picture is the result of a numerical simulation using a full MHD Lagrangian code and the right picture is Solution (3.44). First of all we see that the amplitude of the solution is of order a^2 which confirms previous statements on the
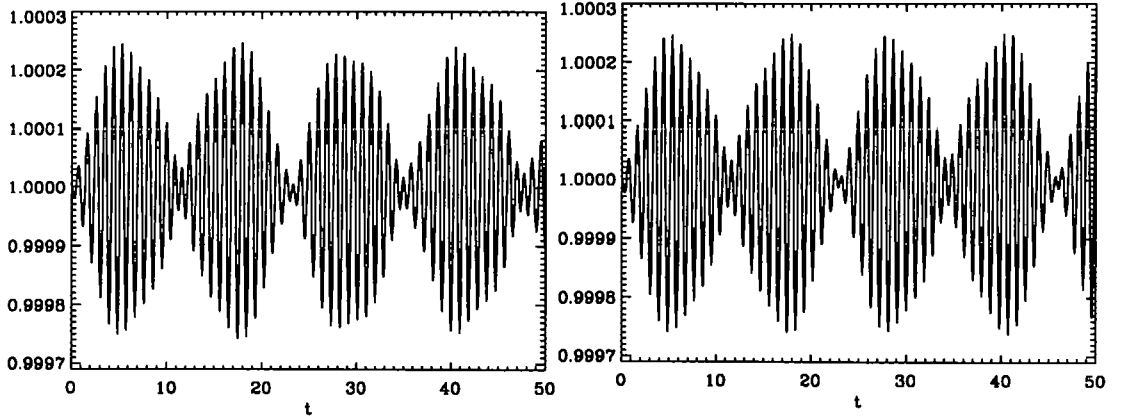
Figure 3.15: Time profile of the magnetic field component B_x for the fundamental mode for $a = 0.01$ at position $(0.25x_0, 0.5y_0)$. At that position the first-order solution is identically zero. Left: numerical result using a full MHD Lagrangian code. Right: analytical result (3.44).

second-order moderation. The dominant beat is between the two modes with frequencies Ω_1 and 2ω. The analytical solution slowly moves out of phase with the numerical result. We shall discuss this effect in the next section as it arises from a cubic nonlinearity which is linked to the redistribution of plasma along the equilibrium magnetic field lines.

We are interested in the times when the linear solution is equal to zero. The second-order velocity $v_{y,2}$ (3.43) oscillates at different frequencies from the first-order solution frequency ω. Therefore when the first-order solution is at a temporal node ($\omega T_j = j\pi/2$ with j an integer number), the second-order solution remains and is the dominant part of the velocity v_y around those times. Figure 3.16 shows the velocity v_y as a function of the y-coordinate and time with $x = 0.5\, x_0$. The left picture is the fully numerical result. The right picture is the sum of the velocity perturbations $v_{y,1}$ and $v_{y,2}$. The spatial structure of the velocity v_y in the y-direction is a combination of a $\sin(k_y y)$ and $\sin(2k_y y)$ function, corresponding to the first- and second-order solutions respectively. The velocity profile in the y-direction is changing with time. The dots show the y-position of the anti-node in the velocity field as a function of time. The curve is discontinuous when the first-order time oscillation passes through a temporal node. This leaves the second-order solution, which has extrema in its spatial structure in the y-direction at the positions $y = 0.25\, y_0$ and $y = 0.75\, y_0$. In between these times, the curve shows an extremum. As we go through all the separate

78
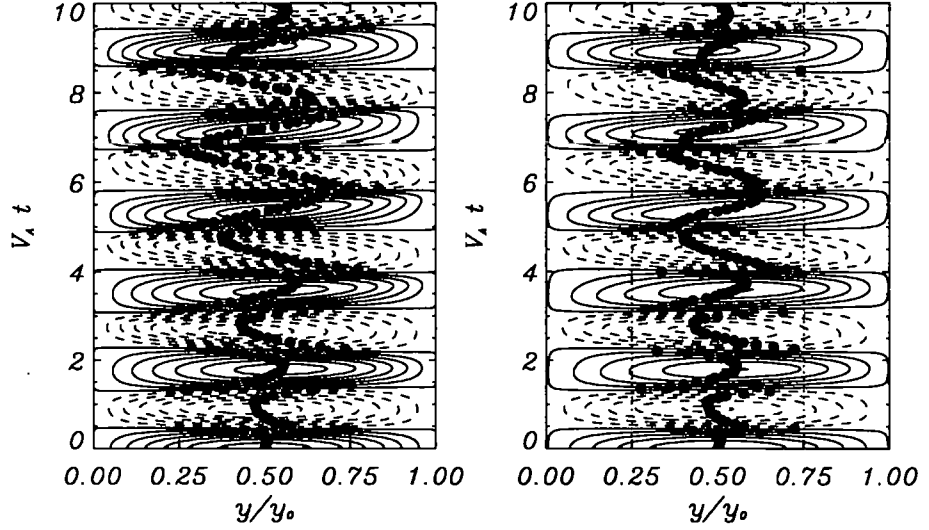
Figure 3.16: Plot of the velocity v_y as a function of the y-coordinate and time t with $x=0.5\,x_0$. Initially a fast wave with wave numbers $n=1$, $l=1$ and an amplitude of $a = 0.05$ is imposed. Left: numerical result using a full MHD Lagrangian code. Right: analytical result $v_{y,1} + v_{y,2}$. The dots shows the y-position of the maximum velocity as a function of time.

subcurves, the value of this extremum oscillates between the values $y= 0.25\,y_0$ and $y= 0.75$ y_0. This is the result of a beat occurring between the first-order oscillation with frequency ω and the second-order oscillation with frequency Ω_1. Figure 3.16 shows that there is good agreement between the numerical and analytical result. There are two differences. Firstly the numerical result slowly drifts out of phase with respect to the analytical result. It represents a moderation of the first-order wave mode and is a third-order effect. We shall investigate this later. Secondly, in the numerical simulation, the y-position of the velocity extremum shifts further towards the boundary of the domain than the analytical result predicts. The difference between the numerical and analytical profiles of the velocity component v_y in Figure 3.11 at the time $V_A t = 1.35$ shows the presence of a fast wave mode with a wave number $l = 3$ in the y-direction. As we shall see later, this mode is generated by the quadratically nonlinear moderation of the fast wave modes. The numerical simulation reveals that the change of the profile of the velocity component v_y results in a local steepening of the velocity gradient, which, for large enough amplitude a, shocks before the velocity component v_x forms a discontinuity. The nonlinear inertial term $\rho v_y(\partial v_y/\partial y)$,

79

where the velocity component v_y has a changing profile in y, with time, is an important ingredient in the shock formation.

3.5.2 Plasma flow along the magnetic field-lines

The equation of motion in the direction along the equilibrium magnetic field-lines is investigated. For this, we shall solve the second-order equation (3.22) for the velocity perturbation $v_{x,2}$. Equation (3.22) becomes

$$
\begin{aligned}
\rho_0 \frac{\partial v_{x,2}}{\partial t} &= -\rho_0 V_A^2 \left(\vec{\nabla}^2 A_1 \right) \frac{\partial A_1}{\partial x} \\
&= \rho_0 V_A^2 \frac{x_0 y_0}{4} \sum_{\substack{n=1 \\ n'=1}}^{n_{max}} \sum_{\substack{l=1 \\ l'=1}}^{l_{max}} \left\{ a_{n,l} a_{n',l'} \frac{\omega_{n,l}}{\omega_{n',l'}} \mathbf{w}_{n,l} \frac{\partial \mathbf{w}_{n',l'}}{\partial x} \sin(\omega_{n,l} t) \sin(\omega_{n',l'} t) \right\}
\end{aligned} \quad (3.47)
$$

The force term on the right-hand side of Equation (3.47) is the component of the ponderomotive force of the fast magneto-acoustic wave field parallel to the equilibrium magnetic field and accelerates plasma in this direction. The acceleration is, similar to the acceleration of a mass in a gravitational field, independent of the density (mass) of the plasma. We see that this force is the only force present in this direction. Therefore the velocity v_x has the same spatial structure as the driving force. If this force contains secular terms in time, the velocity, and consequently the density, is expected to behave in a secular manner as well. The right-hand side of Equation (3.47) contains terms which are a combination of the same wave mode, and cross-terms. The former terms always contain a non-oscillatory contribution because of their time dependency $\sin^2(\omega_{n,l} t)$. This means that the ponderomotive force has a net effect on the plasma and that the velocity perturbation $v_{x,2}$ evolves on a longer time-scale than the oscillation period of the linear wave field.

The cross-terms contain the product $\sin(\omega_{n,l}) \sin(\omega_{n',l'})$, with the wave numbers n,l not equal to the wave numbers n',l'. The frequencies $\omega_{n,l}$ and $\omega_{n',l'}$ actually match if

$$
\frac{n'^2 - n^2}{x_0^2} + \frac{l'^2 - l^2}{y_0^2} = 0 . \quad (3.48)
$$

If the ratio y_0/x_0 is an integer number, a wave mode (n,l) can always be found for given (n',l') which matches Condition (3.48). We shall not consider this special case. There is also the possibility of low frequency oscillations when Condition (3.48) is approximately satisfied. The amplitude of the beat oscillation is inversely proportional to the frequency difference
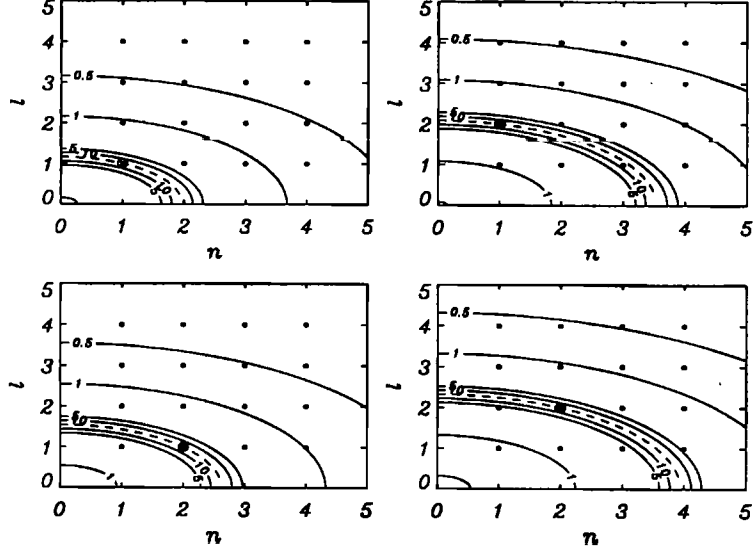
Figure 3.17: Plot of the function $1/\mid \omega_{n,l} - \omega_{n',l'} \mid$ as a function of the wave numbers n and l for given wave numbers $(n',l') = (1,1)$, $(2,1)$, $(1,2)$ and $(2,2)$. The spatial dimensions are $x_0 = 1.7$ and $y_0 = 1.0$. The dashed curve corresponds to Condition (3.48).

$\mid \omega_{n,l} - \omega_{n',l'} \mid$. Figure 3.17 shows the dependency of the function $1/\mid \omega_{n,l} - \omega_{n',l'} \mid$ on the wave numbers n and l for given wave numbers n' and l'. The region where this function is larger than ten is narrow and covers, for the case represented in Figure 3.17, only a few modes. Most cross-terms therefore have an amplitude which is of the order $a_{n,l}a_{n',l'}$. It is only in the extreme cases of $x_0 \gg y_0$ or $x_0 \ll y_0$ that Condition (3.48) is approximately satisfied for a number of modes, with $l = l'$ or $n = n'$ respectively.

The solution of Equation (3.47) is:

$$
\begin{aligned}
\frac{v_{x,2}}{V_A} &= \frac{1}{8} \sum_{n=1}^{n_{max}} \sum_{l=1}^{l_{max}} \left\{ a_{n,l}^2 \frac{k_{x,n}}{k_{n,l}} \sin\left(2k_{x,n}x\right) \sin^2\left(k_{y,l}y\right) \left[2\left(\omega_{n,l}t\right) - \sin\left(2\omega_{n,l}t\right)\right] \right\} \\
&+ \frac{1}{2}V_A \sum_{\substack{n,n' \\ n'\neq n}} \sum_{\substack{l,l' \\ l'\neq l}} \left\{ a_{n,l}a_{n',l'} \frac{k_{x,n}k_{n,l}}{k_{n',l'}} \cos(k_{x,n}x) \sin(k_{x,n'}x) \sin(k_{y,l}y) \sin(k_{y,l'}y) \right. \\
&\qquad \left. \left[\frac{\sin[(\omega_{n,l} - \omega_{n',l'})t]}{\omega_{n,l} - \omega_{n',l'}} - \frac{\sin[(\omega_{n,l} + \omega_{n',l'})t]}{\omega_{n,l} + \omega_{n',l'}} \right] \right\} .
\end{aligned}
\tag{3.49}
$$

This solution can also be retrieved from Equation (1.63) in the cold-plasma limit. The part of Solution (3.49) which arises from those terms in the ponderomotive force which are
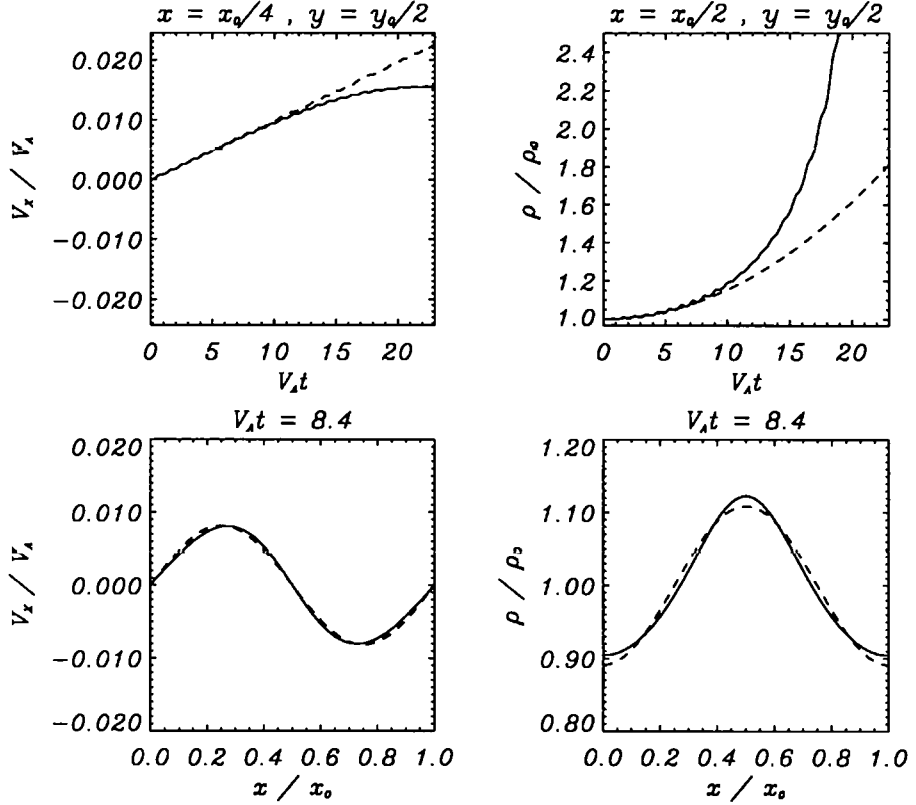
Figure 3.18: Temporal and spatial profile of the velocity component v_x and the density ρ. Initially the fundamental mode with an amplitude $a = 0.05$ is imposed. Solid line: full numerical result. Dashed line: analytical results $v_{x,2}$ and $\rho_0 + \rho_2$.

combinations of the same mode, contains terms which increase linearly with time. These secular terms are the dominant part of the solution. On a time scale $V_A t \sim 4a_{n,l}^{-1} k_{x,n}^{-1}$, the second-order solution grows to become of order $a_{n,l}$. The numerical simulation reveals that this actually does not happen. Figure 3.18 shows that after an initial linear growth, the velocity amplitude saturates. It is clear from the spatial form of this part of Solution (3.49), that there is a flow of plasma away from the minima of the velocity wave field intensity (nodes) of each mode towards its maxima (anti-nodes).

Because the plasma flow along the background magnetic field reaches large amplitudes compared with the second-order solutions of the wave-field moderation, the velocity perturbation $v_{y,2}$ is neglected in comparison with the velocity $v_{x,2}$.

The equation of mass continuity (3.21) is approximately equal to

82

$$\frac{\partial \rho_2}{\partial t} + \rho_0 \frac{\partial v_{x,2}}{\partial x} \approx -\vec{\nabla} \cdot (\rho_1 \vec{v}_1) \ . \tag{3.50}$$

The driver term on the right-hand side of Equation (3.50) is, together with the oscillatory parts of Expression (3.49), neglected in comparison with the secular terms in Expression (3.49). The solution of Equation (3.50) is approximately equal to

$$\frac{\rho_2}{\rho_0} \approx -\frac{1}{4} \sum_{n=1}^{n_{max}} \sum_{l=1}^{l_{max}} a_{n,l}^2 \frac{k_{x,n}^2}{k_{n,l}^2} \cos\left(2k_{x,n}x\right) \sin^2\left(k_{y,l}y\right) \left(\omega_{n,l}t\right)^2 \ . \tag{3.51}$$

ρ_2 is the ponderomotive density perturbation, which is approximately the sum of the contributions of the ponderomotive response of each linear mode separately. The cross-terms have been neglected. Plasma is depleted in the areas around the nodes in the x-direction of the linear velocity wave-field of each mode and enhanced around its anti-nodes. Figure 3.19 shows a plot of the density perturbation ρ_2 and the velocity $v_{x,2}$ for the mode (2,1) at a certain time. The growth-rate of each mode of the density perturbation is proportional to the wavenumber n. The density perturbation grows quadratically with time and is of order $a_{n,l}$ on a time scale $V_A t \sim 2a_{n,l}^{-1/2}k_{x,n}^{-1}$. Before that time the expansion procedure will have broken down. This time scale is faster than the time scale for the velocity component
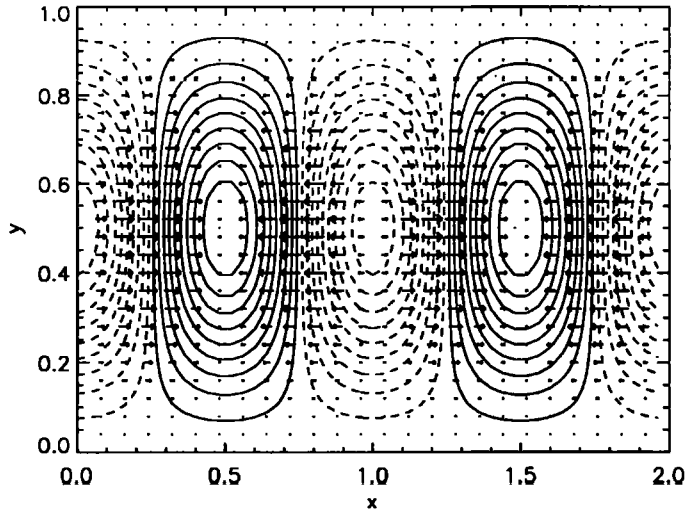
Figure 3.19: Contourplot of the density perturbation ρ_2 and vectorplot of the velocity component $v_{x,2}$ for the mode (2,1). Solid lines relate to density enhancements and dashed lines relate to density depletions.

$v_{x,2}$. Figure 3.18 shows the time profile of the x-component of the velocity and the density. There is a good agreement between the numerical and analytical result up to a time $V_A t \approx 10$, which is about double the time predicted for the expansion scheme to break down. After that time, the amplitude of the velocity v_x at that position does not grow linearly, but saturates. The comparison between the spatial structure of the numerical result, Figure 3.9, and the analytical result shows that the shape of the velocity profile changes slowly with time. Around the anti-node the velocity gradient steepens and near the nodes it flattens. This behaviour is a common effect of nonlinear inertia, *i.e.* the term $\rho v_x(\partial v_x/\partial x)$ in this case, which is of fourth-order in ϵ and has not been taken into account thus far.

3.6 Cubically nonlinear moderation and self-moderation of fast waves

The quadratic nonlinearity in our model introduced two features: the excitation of plasma flow along the field lines and a weak self-moderation of the original wave field. The cubic nonlinearity is now considered. This enables the investigation of the effect of the ponderomotive density perturbation on the original linear wave field. Because the response to the cross-terms in the ponderomotive force is non-secular, they have been neglected in calculating the second-order density. We consider one single mode with wave numbers (n, l) for the linear wave field and take its corresponding ponderomotive response in Solutions (3.49) and (3.51). Since confusion is not possible, the indices n and l are dropped. The terms of the system of equations (3.2)-(3.4) which are of order ϵ^3 combine into the following linearized system of equations:

$$\frac{\partial \rho_3}{\partial t} + \rho_0 \vec{\nabla} \cdot \vec{v}^{(3)} = -\frac{\partial}{\partial y}(\rho_2 v_{y,1}) - \vec{\nabla} \cdot \left(\rho_1 \vec{v}^{(2)}\right) , \tag{3.52}$$

$$\begin{aligned}
\frac{\partial v_{x,3}}{\partial t} = & -\frac{\rho_1}{\rho_0}\frac{\partial v_{x,2}}{\partial t} - v_{y,1}\frac{\partial v_{x,2}}{\partial y} \\
& - V_A^2 \left(\vec{\nabla}^2 A_2\right)\frac{\partial A_1}{\partial x} - V_A^2 \left(\vec{\nabla}^2 A_1\right)\frac{\partial A_2}{\partial x} ,
\end{aligned} \tag{3.53}$$

$$\begin{aligned}
\frac{\partial v_{y,3}}{\partial t} + V_A^2 \vec{\nabla}^2 A_3 = & -\frac{\rho_2}{\rho_0}\frac{\partial v_{y,1}}{\partial t} - \frac{\rho_1}{\rho_0}\frac{\partial v_{y,2}}{\partial t} - \left(\vec{v}^{(2)}\cdot\vec{\nabla}\right)v_{y,1} - v_{y,1}\frac{\partial v_{y,2}}{\partial y} \\
& -\frac{\rho_1}{\rho_0}v_{y,1}\frac{\partial v_{y,1}}{\partial y} - V_A^2 \left(\vec{\nabla}^2 A_2\right)\frac{\partial A_1}{\partial y} - V_A^2 \left(\vec{\nabla}^2 A_1\right)\frac{\partial A_2}{\partial y} ,
\end{aligned} \tag{3.54}$$

$$\frac{\partial A_3}{\partial t} + v_{y,3} = -\left(\vec{v}^{(2)}\cdot\vec{\nabla}\right)A_1 - v_{y,1}\frac{\partial A_2}{\partial y} . \tag{3.55}$$

The terms on the right-hand side of the system of equations (3.52)-(3.55) contain the combination of a first- and second-order quantity and have different dependencies on t. Since we neglected purely oscillatory terms in the calculation of the ponderomotive density perturbation ρ_2, we neglect the purely oscillatory terms here as well. Then we look at which of the remaining terms are dominant. Rankin *et al.* (1994) used the same strategy for standing Alfvén waves. Equations (3.54) and (3.55) are combined into a second-order PDE for the vector potential perturbation A_3.

$$\frac{\partial \rho_3}{\partial t} + \rho_0 \vec{\nabla} . \vec{v}^{(3)} \approx -\frac{\partial}{\partial y}\left(\rho_2 v_{y,1}\right) , \tag{3.56}$$

$$\frac{\partial v_{x,3}}{\partial t} \approx -v_{y,1}\frac{\partial v_{x,2}}{\partial y} , \tag{3.57}$$

$$v_{y,3} \approx -\frac{\partial A_3}{\partial t} . \tag{3.58}$$

$$\left[\frac{\partial^2}{\partial t^2} - V_A^2 \vec{\nabla}^2\right] A_3 \approx \frac{\rho_2}{\rho_0}\frac{\partial v_{y,1}}{\partial t} , \tag{3.59}$$

where terms on the right-hand side, which are purely oscillatory terms or linear in time, have been neglected in comparison with terms which are quadratic in time. Examining the driver term on the right-hand side of Equation (3.57) reveals that the velocity component $v_{x,3}$ acts on a time scale $V_A t \sim a^{-2}$ compared with the first-order solution. This is a longer time scale than the time scale on which the ponderomotive density perturbation acts. Therefore the velocity component $v_{x,3}$ is neglected. The self-moderation of the bounded fast magneto-acoustic wave modes through the cubic nonlinearity is investigated. Again we confine ourselves to studying the effect of a single mode. The right-hand side driver term in Equation (3.59) is calculated by substituting the velocity perturbation $v_{y,1}$ and the density perturbation ρ_2 from Expressions (3.49) and (3.51) respectively:

$$\left[\frac{\partial^2}{\partial t^2} - V_A^2 \vec{\nabla}^2\right] A_3 = \frac{1}{4}a^3 V_A^2 \frac{k_x^2}{k} \sin\left(k_x x\right)\cos\left(2k_x x\right)\sin^3\left(k_y y\right)\left(\omega t\right)^2 \sin\left(\omega t\right) . \tag{3.60}$$

The spatial structure of the driver term reveals that modes are driven with wavenumbers (n, l), $(3n, l)$, $(n, 3l)$ and $(3n, 3l)$. The solution of Equation (3.60) is:

$$\begin{aligned}
A_3 &\approx \left[\frac{1}{64}a^3\frac{k_x^2}{k^3}\left(\omega t\right)^3 \cos\left(\omega t\right) - \frac{3}{128}a^3\frac{k_x^2}{k^3}\left(\omega t\right)^2\sin\left(\omega t\right)\right]\sin\left(k_x x\right)\sin\left(k_y y\right)\\
&+ \frac{3}{256}a^3\frac{k^2}{k^3}\left(\omega t\right)^2\sin\left(\omega t\right)\sin\left(3k_x x\right)\sin\left(k_y y\right)
\end{aligned}$$
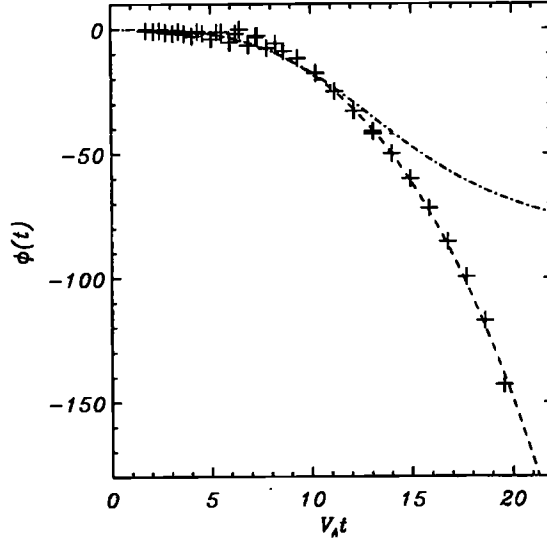
Figure 3.20: Time profile of the phase shift $\phi(t)$ of the velocity v_y in degrees for the fundamental mode of amplitude $a=0.01$. The dashed line is the approximated analytical value proportional to t^3. The dot-dashed line is the analytical value in the form of an inverse tangent. The crosses are the numerical result using a full MHD Lagrangian code.

$$+ \frac{1}{256}a^3\frac{k_x^2}{k_y^2 k}(\omega t)^2\sin(\omega t)\sin(k_x x)\sin(3k_y y)$$

$$- \frac{1}{256}a^3\frac{k_x^2}{k^3}(\omega t)^2\sin(\omega t)\sin(3k_x x)\sin(3k_y y) \ . \tag{3.61}$$

Terms which are purely oscillatory or proportional to t have been neglected in the previous result. The velocity perturbation $v_{y,3}$ is easily calculated from Equation (3.58):

$$\frac{v_{y,3}}{V_A} \approx \left[\frac{1}{64}a^3\frac{k_x^2}{k^2}(\omega t)^3\sin(\omega t) - \frac{3}{128}a^3\frac{k_x^2}{k^2}(\omega t)^2\cos(\omega t)\right]\sin(k_x x)\sin(k_y y)$$

$$- \frac{3}{256}a^3(\omega t)^2\cos(\omega t)\sin(3k_x x)\sin(k_y y)$$

$$- \frac{1}{256}a^3\frac{k_x^2}{k_y^2}(\omega t)^2\cos(\omega t)\sin(k_x x)\sin(3k_y y)$$

$$+ \frac{1}{256}a^3\frac{k_x^3}{k^2}(\omega t)^2\cos(\omega t)\sin(3k_x x)\sin(3k_y y) \ . \tag{3.62}$$

The first term of Expressions (3.61) and (3.62) has the same spatial structure as the linear wave field, *i.e.* it has the same wave numbers. This term is therefore the cubic self-moderation of the original wave mode. If we combine this term in Expression (3.62) with

86
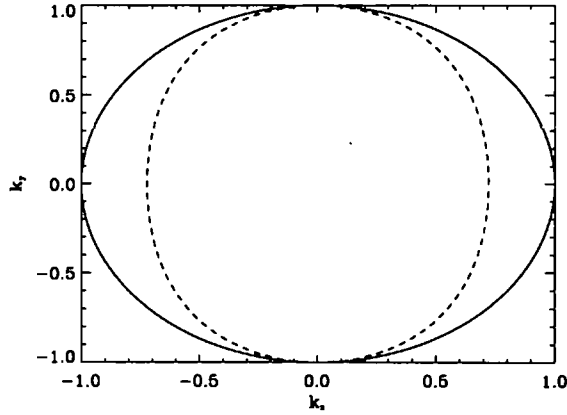
Figure 3.21: Plot of the group velocity. Solid line: the group velocity of the linear fast magneto-acoustic wave. Dashed line: the group velocity taking into account the frequency shift due to the ponderomotive force at a given time.

the linear solution (3.11), the mode of the velocity component v_y with the original wave numbers, is approximated as

$$\frac{v_y}{V_A} \approx a \left(1 - \frac{3}{128} a^2 \frac{k_x^2}{k^2} (\omega t)^2 \right) \sin (k_x x) \sin (k_y y) \cos (\omega t + \phi(t)) , \qquad (3.63)$$

with

$$\phi(t) = -\arctan \left(\frac{\frac{1}{64} a^2 k_x^2 k^{-2} (\omega t)^3}{1 - \frac{9}{128} a^2 k_x^2 k^{-2} (\omega t)^2} \right) \approx -\frac{1}{64} a^2 \frac{k_x^2}{k^2} (\omega t)^3 . \qquad (3.64)$$

Rankin *et al.* (1994) found that the cubic nonlinear self-moderation of standing Alfvén waves in a homogeneous, cold plasma is of the same form as we found here for fast magneto-acoustic waves, only differing by a constant. This is not surprising because in both cases the moderation is introduced through a term which is proportional to the first-order acceleration of the wave-field and the second-order density perturbation, excited by the component of the second-order ponderomotive force in the direction of the equilibrium magnetic field and which is quadratic in time. Figure 3.20 shows the time variation of the phase $\phi(t)$. Clearly the approximation from Expression (3.64) matches the numerical result much better than the expression which involves the arctan. The small discrepancy between the analytic and the numerical phase shift, when $V_A t < 10$, is due to the phase shift caused by the second-order velocity component $v_{y,2}$. The phase $\phi(t)$ of the original mode is decreasing on a time scale $V_A t \sim 64^{1/3} a^{-2/3} k^{1/3} k_x^{-2/3}$, which is quicker than the amplitude moderation of the

87

original mode and the third spatial harmonics, which act on a time scale $V_A t \sim a^{-1}$. The analytically derived phase shift approximates the numerical result beyond the regime of validity of the expansion procedure. From the phase shift $\phi(t)$ the frequency shift $\Delta\omega$ is calculated as

$$\Delta\omega = \frac{d\phi(t)}{dt} \approx -\frac{3}{64}a^2\frac{k_x^2}{k^2}\omega\left(\omega t\right)^2 \ . \tag{3.65}$$

The action of the ponderomotive force decreases the oscillation frequency of the mode that generated the force. The plasma is forced by the ponderomotive force to accumulate at the anti-nodes of the velocity wave field. At those positions, the local Alfvén speed is reduced, hence the fast magneto-acoustic wave oscillates at a lower frequency. From the correction (3.65), the group velocity of the wave is calculated.

$$\vec{V}_g = \frac{\partial}{\partial\vec{k}}\left(\omega + \Delta\omega\right) = V_A\frac{\vec{k}}{k}\left(1 - \frac{3}{64}a^2\frac{k_x^2}{k^2}\left(\omega t\right)^2\right) - \frac{3}{32}a^2 V_A\frac{k_x}{k}\left(\omega t\right)^2\vec{1}_x \ . \tag{3.66}$$

Figure 3.21 shows that the propagation of wave-energy becomes anisotropic. Compared with the group velocity obtained at first-order, the group velocity does not change in the direction across the background magnetic field-lines (y-direction) but is reduced in the direction along the background magnetic field lines (x-direction) as plasma is redistributed along that direction. The fast magneto-acoustic wave mode consequently refracts towards the positions where the density increases, *i.e.* its anti-nodes.

3.7 Multiple time-scales method

The previous expansion procedure gives us the time-scales of the variations of the various plasma quantities. Table 3.1 shows the time-scales over which the various quantities vary, ordered from fastest to slowest. We want to construct a new expansion procedure with a multiple time-scales approach to obtain the same key features that we saw earlier but which will emerge in a more natural way. The dominant nonlinear effects are the ponderomotive force along the background magnetic field (quadratic nonlinearity) and the cubic nonlinear self-moderation of the wave field. An approximate set of equations which focuses on effects which act on time-scales which are equal or faster than a^{-2}, is constructed from the system of equations (3.2)-(3.4):

$$\frac{\partial\rho}{\partial t} \approx -\rho_0\frac{\partial v_x}{\partial x} \ , \tag{3.67}$$

88

plasma quantity	$(V_A t) \sim$
ϕ	$a^{-2/3}$
ρ_2/ρ_0	a^{-1}
$\Delta\omega$	a^{-1}
$\mid v_{y,3} \mid /v_{y,1}$	a^{-1}
$v_{x,2}/v_{y,1}$	a^{-1}
$v_{x,3}/v_{y,1}$	a^{-2}

Table 3.1: The time-scales over which the the various plasma quantities vary.

$$\frac{\partial v_x}{\partial t} \approx -V_A^2 \left(\vec{\nabla}^2 A\right) \frac{\partial A}{\partial x} , \qquad (3.68)$$

$$\frac{\partial v_y}{\partial t} + V_A^2 \vec{\nabla}^2 A \approx -\left(\frac{\rho}{\rho_0}\right) \frac{\partial v_y}{\partial t} , \qquad (3.69)$$

$$\frac{\partial A}{\partial t} \approx -v_y . \qquad (3.70)$$

Notice that the oscillatory plasma compression by the wave field is neglected. We only retain the secular part of the ponderomotive density perturbation (3.51). The nonlinear inertial terms have been omitted from the momentum equations (3.68) and (3.69) as well. Equations (3.67)-(3.70) are combined into the following pair of PDE's:

$$\left[\frac{\partial^2}{\partial t^2} - V_A^2 \vec{\nabla}^2\right] A \approx -\left(\frac{\rho}{\rho_0}\right) V_A^2 \vec{\nabla}^2 A , \qquad (3.71)$$

$$\frac{\partial^2}{\partial t^2}\left(\frac{\rho}{\rho_0}\right) \approx V_A^2 \frac{\partial}{\partial x}\left(\vec{\nabla}^2 A \frac{\partial A}{\partial x}\right) . \qquad (3.72)$$

The two equations (3.71) and (3.72) are a coupled set of nonlinear PDE's in the variables A and ρ/ρ_0. We impose that at the boundaries of $[0,x_0]\times[0,y_0]$, the velocity is zero.

Table 3.1 shows that the phase shift and amplitude moderation of the fast wave act on time-scales $a^{2/3}t$ and at respectively. This suggests a different ordering for the terms in the system of equations (3.2)-(3.4) and the pair of coupled equations (3.71)-(3.72). We introduce multiple time-scales, which take into account different time-scales:

$$t_0 = t , \quad t_1 = \epsilon^{2/3}t , \quad t_2 = \epsilon t . \qquad (3.73)$$

A derivative with respect to time becomes

$$\frac{d}{dt} = \frac{\partial}{\partial t_0} + \epsilon^{2/3}\frac{\partial}{\partial t_1} + \epsilon\frac{\partial}{\partial t_2} . \qquad (3.74)$$

The oscillation period of the linear mode oscillates on the fast time-scale t_0. The secular time variation of the various plasma perturbations involves the slower time-scales t_1 and t_2.

The spatial part of A is expanded in the set of functions $w_{n,l}$ (3.15):

$$A = \sum_{n=1}^{n_{max}} \sum_{l=1}^{l_{max}} A_{n,l}(t)\, w_{n,l} \,, \tag{3.75}$$

Because the left-hand side of Equation (3.72) does not contain any spatial derivatives, the quantity ρ/ρ_0 has the same spatial structure as that of the driver term on the right-hand side of the equation. The cross-terms in the driver term are neglected. Using Expansion (3.75), the density perturbation therefore has the form

$$\frac{\rho}{\rho_0} = \sum_{n-1}^{n_{max}} \sum_{l=1}^{l_{max}} R_{n,l}(t)\, \frac{\partial}{\partial x}\left(w_{n,l}\frac{\partial w_{n,l}}{\partial x}\right) \,. \tag{3.76}$$

The quantities $A_{n,l}$ and $R_{n,l}$ are expanded in power series of epsilon:

$$\begin{cases} A_{m,k} = \epsilon\left(A_{1,m,k} + \epsilon^{2/3}A_{2,m,k} + \epsilon A_{3,m,k} + \epsilon^{4/3}A_{4,m,k} + \ldots\right) \,, \\ R_{m,k} = \epsilon^2\left(R_{2,m,k} + \epsilon^{2/3}R_{3,m,k} + \epsilon R_{4,m,k}\ldots\right) \,. \end{cases} \tag{3.77}$$

The multiple time-scales (3.73) are substituted into the pair of equations (3.71)-(3.72) and projected onto the function $w_{m,k}$:

$$\left[\frac{\partial^2}{\partial t_0^2} + \omega^2 + 2\epsilon^{2/3}\frac{\partial^2}{\partial t_0 \partial t_1} + \epsilon^{4/3}\frac{\partial^2}{\partial t_1^2} + \ldots\right] A_{m,k} =$$

$$\sum_{\substack{n=1 \\ n'=1}}^{n_{max}} \sum_{\substack{l=1 \\ l'=1}}^{l_{max}} D_{m,k,n,l,n',l'}\, \omega_{n,l}^2 R_{n',l'} A_{n,l} \,, \tag{3.78}$$

$$\left[\frac{\partial^2}{\partial t_0^2} + 2\epsilon^{2/3}\frac{\partial^2}{\partial t_0 \partial \tau} + \epsilon^{4/3}\frac{\partial^2}{\partial t_1^2} + \ldots\right] R_{m,k} = -\omega_{m,k}^2 A_{m,k}^2 \,, \tag{3.79}$$

with

$$\begin{aligned} D_{m,k,n,l,n',l'} &= \int_0^{x_0} dx \int_0^{y_0} dy\, w_{m,k} w_{n,l}\frac{\partial}{\partial x}\left(w_{n',l'}\frac{\partial w_{n',l'}}{\partial x}\right) \\ &= \frac{2k_{x,n'}^2}{x_0 y_0}\left(\delta_{m,n-2n'} + \delta_{m,n+2n'} + \delta_{m,-n+2n'} + \delta_{m,-n-2n'}\right) \\ &\quad \left(2\delta_{k,l} - 2\delta_{k,-l} - \delta_{k,l-2l'} - \delta_{k,l+2l'} + \delta_{k,-l+2l'} + \delta_{k,-l-2l'}\right) \,. \end{aligned} \tag{3.80}$$

The coefficient $D_{m,k,n,l,n',l'}$ determines the coupling of the wave modes through their density perturbation. Because the density perturbation involves the amplitudes of the modes

quadratically, the coupling between the modes is nonlinear. For the case in which only one linear mode with spatial wave numbers (n,l) is excited ($n'=n$ and $l'=l$), Expression (3.80) shows that this mode moderates itself and excites the modes $(n, 3l)$, $(3n,l)$ and $(3n,3l)$. This confirms the result of the previous section.

The lowest order of the system of equations (3.78)-(3.79) which involves a non-zero right-hand side of Equation (3.78), gives an infinite set of highly coupled nonlinear ordinary differential equations. Solving this system of equations will not be attempted.

The previous section showed that the amplitudes of these modes grow secularly on the slow time-scale ϵt. We can therefore consider a single mode approximation for the study of the mode's time variation for times up to the time-scale ϵt. This means that one single mode $A_{m,k}$, together with its corresponding ponderomotive density perturbation, is considered and in the coupling coefficient (3.80), only the contribution $D_{m,k,m,k,m,k}$ is taken into account. Because there is no possibility of confusion between different modes, the indices m and k are omitted. The pair of equations (3.78)-(3.79) is equal to:

$$\left[\frac{\partial^2}{\partial t_0^2} + \omega^2 + 2\epsilon^{2/3}\frac{\partial^2}{\partial t_0 \partial t_1} + 2\epsilon\frac{\partial^2}{\partial t_0 \partial t_2} + \epsilon^{4/3}\frac{\partial^2}{\partial t_1^2} + \ldots\right] \epsilon \left(A_1 + \epsilon^{2/3}A_2 + +\epsilon A_3 + \ldots\right) =$$
$$-D\omega^2\epsilon^3 \left(R_2 + \epsilon^{2/3}R_3 + \ldots\right) \left(A_1 + \epsilon^{2/3}A_2 + \epsilon A_3 + \ldots\right) \quad (3.81)$$

$$\left[\frac{\partial^2}{\partial t_0^2} + 2\epsilon^{2/3}\frac{\partial^2}{\partial t_0 \partial t_1} 2\epsilon\frac{\partial^2}{\partial t_0 \partial t_2} + \epsilon^{4/3}\frac{\partial^2}{\partial t_1^2} + \ldots\right] \epsilon^2 \left(R_2 + \epsilon^{2/3}R_3 + \ldots\right) =$$
$$-\omega^2\epsilon^2 \left(A_1 + \epsilon^{2/3}A_2 + \epsilon A_3 + \ldots\right)^2 \quad (3.82)$$

The constant D is equal to $-D_{m,k,m,k,m,k} = 3k_{x,m}^2/2x_0y_0$. The set of equations (3.81)-(3.82) is solved for consecutive orders in ϵ.

The lowest order of each of the two equations gives the linear fast mode and its ponderomotive density perturbation. The terms of order ϵ of Equation (3.81) give the equation

$$\left[\frac{\partial^2}{\partial t_0^2} + \omega^2\right] A_1 = 0 , \quad (3.83)$$

which has the solution

$$A_1 = \mathcal{A}(t_1,t_2)e^{i\omega t_0} + \mathcal{B}(t_1,t_2)e^{-i\omega t_0} . \quad (3.84)$$

This solution is substituted into Equation (3.82). The terms of order ϵ^2 of Equation (3.82) give the equation

$$\frac{\partial^2 R_2}{\partial t_0^2} \approx -2\omega^2 \mathcal{A}\mathcal{B} , \quad (3.85)$$

91

where for consistency only the part of the driver terms which produces the secular behaviour is considered. The solution of Equation (3.85) is

$$R_2 = -\mathcal{A}\mathcal{B}\left(\omega t_0\right)^2 \ . \tag{3.86}$$

The quantity $\epsilon^2 R_2$ becomes of order one on a time-scale $\omega t_2 \sim (\mathcal{A}\mathcal{B})^{-1/2}$. Consequently the expansion procedure is not valid for all times. The secular nature of the density perturbation cannot be removed with a multiple-scales method. From the full numerical analysis, we see that the time variation of the density is inherently secular. The pressure force, which has been neglected in the cold-plasma limit, is needed to remove this secularity.

The terms of order $\epsilon^{5/3}$ of Equation (3.81) combine into the equation

$$\left[\frac{\partial^2}{\partial t_0^2} + \omega^2\right] A_2 = -2\frac{\partial^2 A_1}{\partial t_0 \partial t_1} - D\omega^2 R_2 \ . \tag{3.87}$$

To avoid a secularly growing solution A_2, the right-hand side of this equation is set equal to zero and solved for the amplitudes $\mathcal{A}$ and $\mathcal{B}$. This determines the temporal evolution of these amplitudes with respect to the slow time t_1. Expression (3.86) is substituted into the second term on the right-hand side of Equation (3.87):

$$2\frac{\partial^2 A_1}{\partial t_0 \partial t_1} = D\omega^4 \mathcal{A}\mathcal{B} t_1^2 A_1 \ , \tag{3.88}$$

The rate of change of the wave with respect to the slow time t_1 is proportional to the third power of the amplitude. This is expected, because in the straight expansion procedure of the previous sections of this chapter, the self-moderation of the wave mode occurred at third order in ϵ. Solution (3.84) is substituted for the perturbation A_1 into Equation (3.87). We find a system of coupled ordinary differential equations for the amplitudes $\mathcal{A}$ and $\mathcal{B}$:

$$\begin{aligned}
\frac{\partial \mathcal{A}}{\partial t_1} &= \frac{-iD\omega^3}{2}\mathcal{A}^2 \mathcal{B} t_1^2 \ , \\
\frac{\partial \mathcal{B}}{\partial t_1} &= \frac{iD\omega^3}{2}\mathcal{A}\mathcal{B}^2 t_1^2 \ .
\end{aligned} \tag{3.89}$$

If the first equation is multiplied by $\mathcal{B}$ and the second equation by $\mathcal{A}$, and both results are added up, the quantity $\mathcal{A}\mathcal{B}$ is found to be independent of the slow time t_1. Therefore the perturbation R_2 is independent of the slow time t_1 as well. The system of equations (3.89) is now easily solved. From this, the perturbation A_1 is found to be equal to

$$A_1 = \tilde{\mathcal{A}}(t_2)e^{i(\omega t_0 + \phi)} + \tilde{\mathcal{B}}(t_2)e^{-i(\omega t_0 + \phi)} \ , \tag{3.90}$$

with the phase ϕ equal to

$$\phi = -\frac{1}{6}D\mathcal{A}(0, t_2)\mathcal{B}(0, t_2)(\omega t_1)^3 \ . \tag{3.91}$$

The amplitudes $\tilde{\mathcal{A}}(t_2)$ and $\tilde{\mathcal{B}}(t_2)$ are equal to $\mathcal{A}(0, t_2)$ and $\mathcal{B}(0, t_2)$ respectively.

We investigate the next order terms in Equation (3.81) to find the dependency of the wave field amplitudes $\tilde{\mathcal{A}}$ and $\tilde{\mathcal{B}}$ on the slow time t_2. The term $\epsilon^{7/3}(\partial^2 \mathsf{A}_1/\partial t_1^2)$ contains a term which is of order ϵ^2. This can be seen from calculating the second derivative of the amplitude $\mathcal{A}$ with respect to t_1:

$$
\begin{aligned}
\epsilon^{7/3}\frac{\partial^2 \mathcal{A}}{\partial t_1^2} &= \epsilon^{7/3}\left[i\frac{\partial^2 \phi}{\partial t_1^2} - \left(\frac{\partial \phi}{\partial t_1}\right)^2\right]\tilde{\mathcal{A}}e^{i(\omega t_0 + \phi)} \\
&= \left[-\epsilon^2 D\tilde{\mathcal{A}}\tilde{\mathcal{B}}\omega^3 t_2 - \frac{1}{4}\epsilon^{7/3}D^2\tilde{\mathcal{A}}^2\tilde{\mathcal{B}}^2\omega^3 t_1^4\right]\tilde{\mathcal{A}}e^{i(\omega t_0 + \phi)} \ .
\end{aligned}
\tag{3.92}
$$

The second derivative of the amplitude $\mathcal{B}$ with respect to t_1 is calculated in the same fashion. The first term of Expression (3.92) is of order ϵ^2. When we gather together all the terms of order ϵ^2 in Equation (3.81), the following equation is obtained:

$$\left[\frac{\partial^2}{\partial t_0^2} + \omega^2\right]\mathsf{A}_3 = -2\frac{\partial^2 \mathsf{A}_1}{\partial t_0 \partial t_2}iD\tilde{\mathcal{A}}\tilde{\mathcal{B}}\omega^3 t_2\left[\tilde{\mathcal{A}}e^{i(\omega t_0 + \phi)} - \tilde{\mathcal{B}}e^{-i(\omega t_0 + \phi)}\right] \ . \tag{3.93}$$

To avoid a secularly growing solution A_3, the right-hand side of this equation is set equal to zero and we obtain an equation which governs the dependency of the perturbation A_1 on the slow time t_2. We find a system of coupled differential equations for the amplitudes $\tilde{\mathcal{A}}$ and $\tilde{\mathcal{B}}$:

$$
\begin{aligned}
\frac{\partial \tilde{\mathcal{A}}}{\partial t_2} &= \frac{1}{2}D\omega^2\tilde{\mathcal{A}}^2\tilde{\mathcal{B}}t_2 \ , \\
\frac{\partial \tilde{\mathcal{B}}}{\partial t_2} &= \frac{1}{2}D\omega^2\tilde{\mathcal{A}}\tilde{\mathcal{B}}^2 t_2 \ .
\end{aligned}
\tag{3.94}
$$

If the first equation is multiplied with $\tilde{\mathcal{B}}$ and the second equation with $\tilde{\mathcal{A}}$, and both results added up, we have an equation which governs the rate of change of the product $\tilde{\mathcal{A}}\tilde{\mathcal{B}}$ with respect to t_2:

$$\frac{\partial}{\partial t_2}\left(\tilde{\mathcal{A}}\tilde{\mathcal{B}}\right) = D\omega^2\left(\tilde{\mathcal{A}}\tilde{\mathcal{B}}\right)^2 t_2 \ , \tag{3.95}$$

which is easily solved by separation of variables:

$$\tilde{\mathcal{A}}\tilde{\mathcal{B}} = \frac{\tilde{\mathcal{A}}(0)\tilde{\mathcal{B}}(0)}{1 - \frac{1}{2}D\tilde{\mathcal{A}}(0)\tilde{\mathcal{B}}(0)(\omega t_2)^2} \ . \tag{3.96}$$

93

The phase shift ϕ and the density perturbation R_2 depend on this product. Expressions (3.85) and (3.91) are rewritten as

$$R_2 = -\frac{\tilde{A}(0)\tilde{B}(0)\,(\omega t_0)^2}{1 - \frac{1}{2}D\tilde{A}(0)\tilde{B}(0)\,(\omega t_2)^2}\,, \qquad (3.97)$$

$$\phi = -\frac{1}{6}\frac{D\tilde{A}(0)\tilde{B}(0)\,(\omega t_1)^3}{1 - \frac{1}{2}D\tilde{A}(0)\tilde{B}(0)\,(\omega t_2)^2}\,. \qquad (3.98)$$

The system of equations (3.94) is, with use of Expression (3.96), easily solved:

$$\frac{\tilde{A}}{\tilde{A}(0)} = \frac{\tilde{B}}{\tilde{B}(0)} = \frac{1}{\sqrt{1 - \frac{1}{2}D\tilde{A}(0)\tilde{B}(0)\,(\omega t_2)^2}}\,. \qquad (3.99)$$

The denominator of Expressions (3.96)-(3.99) becomes zero at the time

$$(\omega t_2) = \frac{2}{k_x}\sqrt{\frac{x_0 y_0}{3\tilde{A}(0)\tilde{B}(0)}}\,. \qquad (3.100)$$

This time is comparable with the time period in which the perturbation method is valid. The singular behaviour is not physical because the total energy is not conserved and the density becomes infinite globally (total mass is still conserved) instead of locally infinite. The reason for this failure is the neglect of the other wave modes and the nonlinear inertial terms, whose amplitudes evolve on a similar time-scale. Therefore Expressions (3.96), (3.97), (3.98) and (3.99) are only valid for times much earlier than (3.100). In Expressions (3.97) and (3.98), the product $\tilde{A}\tilde{B}$ is approximated by $\tilde{A}(0)\tilde{B}(0)$ and the denominator in Expression (3.99) is expanded in a Taylor series:

$$\frac{1}{\sqrt{1 - \frac{1}{2}D\tilde{A}(0)\tilde{B}(0)\,(\omega t_2)^2}} \approx 1 + \frac{1}{4}D\tilde{A}(0)\tilde{B}(0)\,(\omega t_2)^2\,. \qquad (3.101)$$

With the initial conditions

$$\tilde{A}(0) = -\frac{a}{4ik}\sqrt{x_0 y_0}\,, \quad \tilde{B}(0) = \frac{a}{4ik}\sqrt{x_0 y_0}\,, \qquad (3.102)$$

the phase shift ϕ is equal to

$$\phi = -\frac{1}{64}a^2\frac{k_x^2}{k^2}\,(\omega t_1)^3\,, \qquad (3.103)$$

which is equal to the result for the phase shift in Expression (3.64) without the arctan function. Figure 3.20 shows that this expression for the phase shift corresponds to the

numerical result. The multiple-scales method brings out the correct phase shift in a more natural way.

Using Expressions (3.90), (3.98) and (3.99), the perturbation A is equal to

$$A = \left(1 + \frac{1}{4}D\tilde{A}(0)\tilde{B}(0)\ (\omega t_2)^2\right)\left(\tilde{A}(0)e^{i(\omega t_0 + \phi)} + \tilde{B}(0)e^{-i(\omega t_0 + \phi)}\right)\ . \tag{3.104}$$

An expression for the velocity component v_y is calculated from Expression (3.104) with Equation (3.70):

$$\begin{aligned}
v_y &= -\frac{\partial A}{\partial t_0} - \epsilon^{2/3}\frac{\partial A}{\partial t_1} - \epsilon\frac{\partial A}{\partial t_2} \\
&\approx \left(-\omega - \frac{1}{4}\omega D\tilde{A}(0)\tilde{B}(0)\ (\omega t_2)^2 - \epsilon^{2/3}\frac{\partial \phi}{\partial t_1}\right)\left(\tilde{A}(0)e^{i(\omega t_0 + \phi)} + \tilde{B}(0)e^{-i(\omega t_0 + \phi)}\right) \\
&\approx -\omega\left(1 - \frac{1}{4}\omega D\tilde{A}(0)\tilde{B}(0)\ (\omega t_2)^2\right)\left(\tilde{A}(0)e^{i(\omega t_0 + \phi)} + \tilde{B}(0)e^{-i(\omega t_0 + \phi)}\right)\ . \tag{3.105}
\end{aligned}$$

With the initial conditions (3.102), Expression (3.105) for the velocity component v_y is

$$v_y = aV_A\left(1 - \frac{3}{128}a^2\frac{k_x^2}{k^2}\ (\omega t_2)^2\right)\cos(\omega t_0 + \phi(t_1))\ \sin(k_x x)\ \sin(k_y y)\ . \tag{3.106}$$

Expression (3.106) is equal to Expression (3.63), so that we find the same result as in the straight expansion procedure of the previous sections.

3.8 The velocity discontinuity in v_x

The expansion methods we have used in this chapter show that plasma is flowing along the direction of the equilibrium magnetic field from the nodes to the anti-nodes in the velocity component v_y of the fast magneto-acoustic wave mode. The spatial profile of the flow (v_x) is fixed and the strength of the flow grows linearly in time. The results of the expansion procedure do not show that after this initial behaviour, the profile of the velocity component v_x in x changes and forms a fixed velocity discontinuity in v_x in the x-direction. At that position, the density becomes infinite at a finite time. This is because the nonlinear inertial term $\rho v_x(\partial v_x/\partial x)$, which is of order a^2, has not been taken into account. In this section we approximately describe the formation of the velocity discontinuity and find an upper limit for the formation time.

We consider the x-component of Equation (3.3). The following approximations are made. The nonlinear evolution of the velocity component v_x is much stronger in the x-direction than in the y-direction. We therefore neglect the inertial term $\rho v_y(\partial v_x/\partial y)$ in

comparison with the inertial term $\rho v_x (\partial v_x / \partial x)$. The density perturbation and the resulting moderation of the fast wave mode are not considered. The moderation is a refraction of the wave towards the density enhancement. The gradients of the wave in the x-direction steepen, and consequently increase the magnitude of the the ponderomotive force, speeding up the nonlinear evolution. We therefore expect that the neglect of this process means that the formation time we calculate here is an approximate upper limit of the real value.

With these approximations, Equation (3.3) is equal to

$$\frac{\partial v_x}{\partial t} + v_x \frac{\partial v_x}{\partial x} = -V_A^2 \left(\vec{\nabla}^2 A_1\right) \frac{\partial A_1}{\partial x} . \tag{3.107}$$

Initially one single mode is imposed. Equation (3.107) is solved by the method of characteristics. The x-coordinate is now dependent on time. Equation (3.107) is transformed into the second-order ordinary differential equation

$$\frac{d^2 x(t)}{dt^2} = \frac{1}{4} a^2 V_A^2 k_x^2 \sin^2(k_y y) \sin(2 k_x x(t)) , \tag{3.108}$$

where the right-hand side is equal to the time average over one wave oscillation period of the right-hand side of Equation (3.107). This equation has the form of an anharmonic oscillator and is similar to Equation (2.36), which described the motion of a discrete particle in a prescribed wave field. We shall follow the same procedure as described in Chapter 2. The solution of Equation (3.108) is equal to

$$
\begin{aligned}
x(t) &= \frac{1}{k_x} \text{arccos} \left[\text{sn} \left(\lambda \Omega t + \text{sn}^{-1} \left(\lambda, \lambda^{-2} \right), \lambda^{-2} \right) \right] \\
&= \frac{1}{k_x} \text{arccos} \left[\cos(k_x x(0)) \frac{\text{cn} \left(\Omega t, \lambda^2 \right)}{\text{dn} \left(\Omega t, \lambda^2 \right)} \right] ,
\end{aligned} \tag{3.109}
$$

with

$$\Omega = \frac{a V_A k_x}{\sqrt{2}} \sin(k_y y) , \quad \lambda = \cos(k_x x(0)) . \tag{3.110}$$

The functions $\text{sn}(u, \kappa)$, $\text{cn}(u, \kappa)$ and $\text{dn}(u, \kappa)$ are Jacobian elliptic functions with parameter κ (Abramowitz & Stegun, 1965). The velocity v_x is given as the derivative of x with respect to time:

$$\frac{v_x}{V_A}(x(t), t) = \frac{1}{2\sqrt{2}} a \sin(2 k_x x(0)) \sin(k_y y) \frac{\text{cn} \left(\Omega t, \lambda^2 \right)}{\text{dn} \left(\Omega t, \lambda^2 \right)} . \tag{3.111}$$

For $\omega t \ll 1$, $x(t) \approx x(0)$ and the secular part of a single mode of the second-order solution (3.49) is retrieved as the lowest-order term in the expansion of Expression (3.111) in powers

96
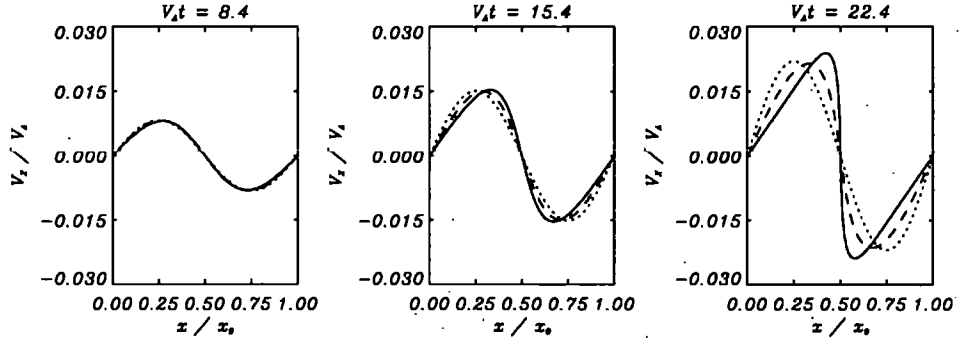
Figure 3.22: A plot of the velocity component v_x as a function of x at certain times with $y = 0.5$ y_0. Initially the fundamental mode with amplitude $a = 0.05$ is imposed. Solid line: full numerical result. Dashed line: Expression (3.111). Dotted line: Expression (3.49).

of ωt. Figure 3.22 shows the velocity v_x as a function of x at three times. The numerical solution clearly steepens around the position of the anti-node, which is positioned at $x = 0.5\ x_0$. The second-order velocity perturbation $v_{x,2}$ has a fixed profile and therefore only approximates the numerical solution at an initial stage. The profile of Solution (3.111) does change with time in accordance with the numerical simulation, but the rate-of-change is slower than the numerical solution. This is expected because we have neglected the ponderomotive density perturbation and the subsequent moderation of the fast wave mode and its ponderomotive force.

The density is calculated from the mass continuity Equation (3.2) using the method of characteristics:

$$\frac{d\rho}{dt} \approx -\rho \frac{\partial v_x}{\partial x} \,, \tag{3.112}$$

which becomes

$$\frac{\rho}{\rho_0} = e^{-\int dt \frac{\partial v_x}{\partial x}} = e^{-\int dt \frac{\partial x(0)}{\partial x} \frac{d}{dt}\left(\frac{\partial x}{\partial x(0)}\right)} = \frac{\partial x(0)}{\partial x} \,. \tag{3.113}$$

The density is calculated by substituting Expression (3.109) into Expression (3.113):

$$\frac{\rho}{\rho_0} = \frac{\mathrm{dn}^2(\Omega t, \lambda^2)}{\mathrm{cn}(\Omega t, \lambda^2)\left[1 + \lambda(1 - \lambda^2)\frac{\partial}{\partial \lambda}\ln\left(\mathrm{cn}(\Omega t, \lambda^2)\right)\right]} \,. \tag{3.114}$$

When, for the first time, two trajectories $x(t)$ meet (or the density has become infinite), a fixed discontinuity has formed. We already know that the discontinuity forms at the anti-nodes in the x-direction of the wave field of the velocity component v_y (at $k_x x =$

$m\pi/2$ with m an odd integer). When $k_x x(0)$ is close to the anti-node, the behaviour of $x(t)$ is approximately harmonic. The density is proportional to the function $\sec(\Omega t)$, in the harmonic regime. Therefore, all trajectories arrive at approximately the same time at the closest anti-node. This time corresponds to

$$\Omega t = \frac{\pi}{2} \quad \Leftrightarrow \quad V_A t = \frac{\pi}{\sqrt{2}ak_x} . \tag{3.115}$$

Because the density perturbation and subsequent moderation of the wave field and ponderomotive force are neglected, we expect this time to be an upper limit to the formation time. Figure 3.23 shows the time (3.115) compared with the numerical result for the fundamental mode. The time (3.115) is approximately 20% later than the numerical result, which confirms that the analytically derived time is a good upper limit. This means that the formation of the velocity discontinuity occurs at least on the time-scale $V_A t \sim a^{-1}$. For amplitudes larger than $a = 0.1$, the velocity v_y forms a shock before the large density enhancement occurs. Because the numerical code cannot capture shocks (it produces Gibbs overshoot) and therefore cannot conserve energy, the numerical results are no longer reliable beyond that time.
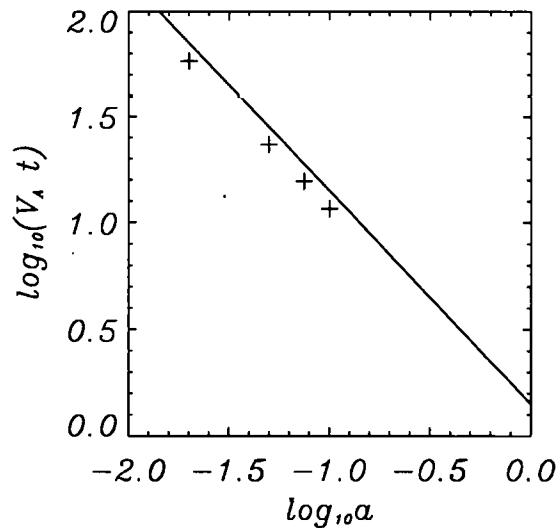
Figure 3.23: A logarithmic plot of the formation time of the discontinuity in v_x as a function of the amplitude a. Solid line: analytical upper limit (3.115). Crosses: numerical result. Initially the fundamental mode is imposed.

3.9 Discussion

In this chapter we have investigated the nonlinear behaviour of bounded fast magneto-acoustic waves in a cold and homogeneous plasma. We use weakly nonlinear theory. The fast wave is described by the y-component of the velocity and the vector potential perturbation. The fast wave propagation has a longitudinal (k_y) and a transverse (k_x) component of its wave vector. This is reflected in the second-order ponderomotive force which also has a longitudinal and a transverse component. We consider boundary conditions in the x- and y-direction for which the velocity is zero. This means that the fast magneto-acoustic wave solution consists of a discrete set of modes so that the wave vector components in the x- and y-direction are discrete, and hence also the oscillation frequency.

The longitudinal component of the second-order ponderomotive force acts on the fast modes and we have shown that the resulting moderation of the fast modes is weak. The conditions for which a mode with wave numbers m and k is generated are: $m + n + n'$ an odd integer and $k = \pm n \pm n'$. These selection rules do not permit resonant three-wave interaction, second-harmonic generation or quadratically nonlinear self-moderation. The former two processes are not possible because of the selection rule for the wave numbers in the x-direction, *i.e.* the x-dependency of the transverse second-order ponderomotive force. This is a direct consequence of the boundary conditions in that direction. This is in contrast with the case of an unbounded medium where resonant three-wave interaction of fast magneto-acoustic waves is possible (Nakariakov & Oraevsky, 1995; Nakariakov & Roberts, 1996). Nakariakov *et al.*, 1997 showed that second-harmonic generation is present for travelling, ducted fast magneto-acoustic waves.

When we initially impose a single linear fast wave mode with wave numbers n and l and an amplitude a, the second-order fast wave perturbation contains modes with odd wave numbers in the x-direction and the wave number $2l$ in the y-direction. They contain oscillations of frequency $2\omega_{n,l}$ and of their own eigenfrequency. The shape of the velocity component v_y in the y-direction is changing with time. This is clearly seen by a shifting of the anti-node in that direction. This behaviour is well described by the combination of the first- and second-order solutions. The numerical simulation reveals that for large amplitudes the shape of the velocity changes much more than predicted analytically, having locally steepening gradients because of inertial effects. Eventually a travelling shock is formed.

The numerical simulation ends there because the numerical code cannot capture shocks. Further analysis with a numerical code which can handle shocks is necessary to investigate the further evolution.

The transverse component of the second-order ponderomotive force excites a plasma flow along the direction of the equilibrium magnetic field. In a cold, ideal plasma there is no other force present in that direction opposing the ponderomotive force. Because the second-order ponderomotive force component contains a non-oscillatory term, the velocity v_x is expected to follow the spatial structure of the force and to grow secularly in time. At a node and an anti-node of the velocity wave-field v_y, the force is zero. The former is an unstable and the latter a stable equilibrium position. The plasma flows along the equilibrium magnetic fieldlines towards the positions of the anti-node. From the expansion procedure we see that the second-order velocity perturbation $v_{x,2}$ and density perturbation ρ_2 contain terms which grow as t and t^2 respectively. On a time-scale $V_A t \sim a^{-1}$, the density perturbation grows to be of the same order as the background density.

The equations containing the terms which are of third-order in ϵ describe the moderation of the fast wave modes by the ponderomotive flow $v_{x,2}$ and density perturbation ρ_2. Because these quantities are secular in time, the moderation is strong. We see that modes with wave numbers $(3n, l)$, $(n, 3l)$ and $(3n, 3l)$ are excited and grow as t^2. The amplitude and phase of the original mode are moderated. The amplitude moderation is also quadratically proportional in time. The phase moderation is proportional to $a^2 t^3$ and therefore acts on the time-scale $V_A t \sim a^{-2/3}$. This is also found by Rankin et al. (1994) for standing Alfvén waves in a homogeneous, cold plasma. The analytically derived phase moderation fits the numerical result well, even beyond its expected regime of validity.

The secular behaviour of the plasma parameters causes the evolution of the fast modes to become rapidly nonlinear. Therefore the weakly nonlinear description is no longer valid on the time-scale $V_A t \sim a^{-1}$. From the full numerical simulation we see that the profile of the x-component of the velocity changes slowly with time. The gradient in the x-direction of v_x flattens around the nodes and steepens around the anti-node. At a finite time a velocity discontinuity has formed at the latter position. Since the plasma can only flow along the magnetic field-lines and there is no exchange of plasma across the position of the anti-node, the density becomes infinite at the that position. We attempted to model this behaviour by adding the inertial term $\rho v_x (\partial v_x / \partial v_x)$ to Equation (3.47), but without taking

into account the ponderomotive density perturbation and the subsequent moderation of the fast wave modes and the ponderomotive force. We concluded that the time for the formation of a discontinuity in the velocity v_x is an upper limit of the true value. The equation in question is solved with the method of characteristics and the equation of an anharmonic oscillator is obtained, of which the solution is written as a function of Jacobian elliptic functions. We find that a discontinuity in the velocity v_x forms at the position of the anti-node at a time inversely proportional to the wave number n and the amplitude a. From this we learn that the nonlinear evolution of a bounded fast magneto-acoustic wave in a homogeneous, cold plasma mode acts on a time-scale at least as fast as $V_A t \sim a^{-1}$. Therefore weakly nonlinear theory cannot adequately describe the behaviour on that time-scale. This is reflected by the fact that on the same time-scale the second-order density perturbation becomes of the same order as the background density and the third-order wave mode amplitude moderation becomes of the same order as the first-order wave mode amplitude. The weakly nonlinear theory is nonetheless valuable because it describes the initial behaviour and helps in identifying the relevant terms and interpreting the further nonlinear evolution and the numerical results.

A key feature in our model is the occurrence of very large density perturbations, actually growing to become locally infinite. This is obviously an unphysical situation. This means that, realistically, forces in the x-component of the momentum equation, which have been neglected, grow to become important and prevent the density from becoming infinite. Around the position of the anti-node in the fast wave velocity-field, the gradient of the velocity and the density in the x-direction become very large. This implies that the kinetic pressure force and dissipation processes are important. From the density perturbation (3.51), we estimate the magnitude of the x-component of the pressure force:

$$-\frac{\partial p}{\partial x} \approx -\frac{\gamma p_0}{2} \sum_{n=1}^{n_{max}} \sum_{l=1}^{l_{max}} a_{n,l}^2 \frac{k_{x,n}^3}{k_{n,l}^2} \sin\left(2k_{x,n}x\right) \sin^2\left(k_{y,l}y\right) \left(\omega_{n,l}t\right)^2 . \qquad (3.116)$$

If we consider only one single mode, an order of magnitude comparison between the kinetic pressure force component (3.116) and the ponderomotive force component $-V_A^2 \vec{\nabla}^2 A_1 \, \partial A_1/\partial x$ is equal to:

$$\frac{\left|-\frac{\partial p}{\partial x}\right|}{\left|-V_A^2 \vec{\nabla}^2 A_1 \frac{\partial A_1}{\partial x}\right|} \sim 2\frac{k_x^2}{k^2} \left(\omega t\right)^2 \beta , \qquad (3.117)$$

where the parameter β is equal to the square of the ratio of the sound speed C_s and the

Alfvén speed V_A. The kinetic pressure force acts on a time-scale $V_A t \sim k_x^{-1}(2\beta)^{-1/2}$. When the density perturbation ρ_2 acts on a faster time-scale, the cold-plasma limit is a valid approximation up to the point where the expansion procedure breaks down. This is the case for $a > 2\sqrt{2\beta}$. Before the velocity forms a discontinuity the cold-plasma model is no longer valid. After the density reaches a large but finite value, the kinetic pressure force pushes the plasma back away from the position of the anti-node. The maximum density perturbation can be estimated by substituting the time-scale into the density perturbation (3.51):

$$\max \frac{\rho}{\rho_0} \approx \frac{1}{8}\frac{a^2}{\beta} . \tag{3.118}$$

The cold-plasma model is therefore a valid model for a small plasma β up to the time that the kinetic pressure force becomes important. This situation is a good example of how a cold-plasma model can be compromised because of the presence of nonlinear forces in the direction of the equilibrium magnetic field.

The next necessary step is to consider a model with a finite plasma β. Weakly nonlinear theory will be valid for all time as long as the density perturbation remains small in comparison with the background density, *i.e.* the amplitude $a < 2\sqrt{2\beta}$. This limitation is also noted by Rankin *et al.* (1994). It is expected that the difficulties of strong nonlinearities are removed in a warm plasma. In that case the first-order equations describe a set of linearly coupled fast and slow magneto-acoustic waves with the coupling proportional to the plasma β. Allan *et al.* (1991) performed a numerical simulation on the same model we put forward in this chapter, but used a small but finite plasma β. By introducing an initial plasma compression in the transverse direction, they excited a set of fast magneto-acoustic wave modes. Slow magneto-acoustic waves are not present initially. Because they have chosen $\beta \ll 1$ (linear coupling between fast and slow waves is weak) and amplitudes of the order of at least a^{-1}, the nonlinear effects take a prominent role in the evolution of the fast waves. In this regime the evolution of the system is close to the cold-plasma limit. The authors observed that, for a simulation with the plasma β equal to 5.10^{-3}, the frequency and amplitude of each mode are reduced in comparison with the linear, cold-plasma prediction, which is in agreement with our results. They do not observe the formation of a shock in the transverse direction, although they observe the shock formation of the transient pulse generated by the initial compression. It is not clear that they fail to observe this transverse effect because of the superposition of the nonlinear effects of a whole set of modes or the

difference in the initial conditions of the numerical simulation.

Nonetheless it is important, for arbitrary values of the plasma β, to recognize the influence of the linear coupling between the fast and slow waves. The large density enhancement produces a large pressure enhancement as well, which increases the plasma β locally and so produces a stronger linear coupling between the two wave modes.

Chapter 4

The nonlinear evolution of an Alfvén pulse

4.1 Introduction

In this chapter, we investigate the physical situation in which the nonlinear interaction of two oppositely propagating Alfvén pulses occurs. Wentzel (1974) briefly outlined the interaction of two Alfvén waves in the context of coronal heating problem. We consider the development of an initially static plane, linearly polarized, transverse Alfvén pulse in a homogeneous plasma as an initial-value problem. Hollweg et al. (1982), Hollweg (1992), Cargill et al. (1997) and others investigated the nonlinear behaviour of Alfvén pulses in the context of shock-wave dissipation mechanisms and spicule modelling. Hollweg et al. (1982) studied numerically the nonlinear evolution of a torsional Alfvén wave train in an open, untwisted magnetic flux tube in a stratified atmosphere. They found that the Alfvén wave steepens into a fast shock in the chromosphere, lifting up chromospheric plasma as it passes (and dissipates) further into the corona. The fast shock is followed by a slow shock which the Alfvén wave has generated nonlinearly. In this chapter, we study analytically a simpler model, which retains the main features of fast and slow shock generation, to understand the basic nonlinear processes involved.

In the presence of a smooth inhomogeneity in the Alfvén speed, e.g. due to gravitational stratification of the plasma density or radial divergence of the magnetic field, the nonlinear dynamics of the Alfvén waves become more complicated (see, e.g. Boynton & Torkelsson

1996, Torkelsson & Boynton 1998). However, even in this case, the homogeneous theory may give qualitatively correct results as far as one can neglect the wave reflection from the inhomogeneity or, in other words, while the WKB approximation is applicable.

The initial Alfvén pulse produces two oppositely propagating Alfvén pulses, which we call the Alfvén wings, which carry the information of the disturbance along the characteristics (parallel to the equilibrium magnetic field) at the Alfvén speed. In the initial stage of the splitting, when the pulses have not moved too far away from each other, their back slopes interact nonlinearly through the ponderomotive force, giving rise to a density perturbation symmetric about the position of the mass centre of the two recessive pulses. This is a main feature of the initially static Alfvén pulse. Depending on the amplitude of the initially static Alfvén pulse and the plasma β (i.e. the ratio between the kinetic and magnetic pressures of the plasma), a large density perturbation may form at the position of the mass centre of the two recessive Alfvén pulses, before splitting up into two oppositely propagating slow pulses, which we call slow wings, travelling at the sound speed. The Alfvén pulses are accompanied by a nonlinearly generated density perturbation which causes no net disturbance to a position the pulse passes. Later on a shock is formed on the recessive Alfvén and slow pulses. We show that, in the absence of a dispersive mechanism, the formation of the running Alfvén shock is governed by the scalar Cohen-Kulsrud equation (Cohen & Kulsrud 1974), which is nothing more than a regular simple wave equation with a cubic nonlinearity. The nonlinear evolution of the slow pulse is a classic hydrodynamical problem (Landau & Lifshitz, 1959), governed by the regular simple wave equation with a quadratic nonlinearity. Both types of simple wave equations describe steepening of a wave profile, leading to the formation of shocks (the fast shock forms a current sheet). Consequently, the simple wave equations work only till the shock appearance.

It has to be noted that, in the absence of dispersion, only linearly and elliptically polarized Alfvén waves are nonlinearly compressive and therefore steepen into a shock. Circularly polarized Alfvén waves are characterised by a magnetic perturbation that is constant in magnitude ($B = $ constant). Therefore it has no ponderomotive force associated with it to excite density fluctuations. It does not steepen into a shock. Cohen & Kulsrud (1974) have shown that a travelling linear (or elliptically) polarized Alfvén wave is transformed through shock formation into a circularly polarized wave.

The chapter is organised as follows. In the second section, we describe our model,

governing equations and the ponderomotive force. In the third section, we investigate the cold-plasma limit and in the fourth section the more complicated finite-plasma-β case. For each of the two cases, a numerical simulation is shown that outlines the main features of the problem, followed by an analytical description of the quadratically nonlinear solution. We present an analytical description of the evolution of the recessive Alfvén pulse in the single mode approximation and give an analytical theory of the central density perturbation. The results are summarized in the Discussion. Sections Two and Three form the basis of a paper, accepted for publication by the Journal of Plasma Physics (Verwichte *et al.*, 1999).

4.2 Model

As proposed in Chapter 1, we consider the ideal MHD Equations (1.26)-(1.30), in a rectangular coordinate system (x, y, z) in which the magnetic field is taken parallel to the x-direction. Plane Alfvén pulses, linearly polarized in the z-direction, are considered. Variations in the directions perpendicular to the equilibrium magnetic field are assumed negligible ($\partial/\partial y = \partial/\partial z = 0$). The Alfvén and fast magneto-acoustic wave modes are indistinguishable in this model. Perturbations of the z-component of the plasma velocity and magnetic field vectors are taken into account but the y-components are assumed to be zero. From Expression (1.9) we see that this implies that only the y-component of the current density is non-zero.

The MHD equations are studied in the weakly nonlinear regime. Consider small, but finite perturbations around a static equilibrium comprising a uniform density ρ_0 and pressure p_0 and a uniform magnetic field $B_0 \vec{1}_x$ (e.g. $\rho = \rho_0 + \rho'$). Thus, the perturbed Equations (1.40)-(1.42) reduce to

$$\frac{\partial \rho'}{\partial t} + \rho_0 \frac{\partial v_x'}{\partial x} = -\frac{\partial}{\partial x}(\rho' v_x') \, , \tag{4.1}$$

$$\rho_0 \frac{\partial v_x'}{\partial t} + \frac{\partial p'}{\partial x} = -\frac{1}{2\mu_0} \frac{\partial B_z'^2}{\partial x} - \rho' \frac{\partial v_x'}{\partial t} - \rho_0 v_x' \frac{\partial v_x'}{\partial x} - \rho' v_x' \frac{\partial v_x'}{\partial x} \, , \tag{4.2}$$

$$\rho_0 \frac{\partial v_z'}{\partial t} - \frac{B_0}{\mu_0} \frac{\partial B_z'}{\partial x} = -\rho' \frac{\partial v_z'}{\partial t} - \rho_0 v_x' \frac{\partial v_z'}{\partial x} - \rho' v_x' \frac{\partial v_z'}{\partial x} \, , \tag{4.3}$$

$$\frac{\partial p'}{\partial t} + \gamma p_0 \frac{\partial v_x'}{\partial x} = -v_x' \frac{\partial p'}{\partial x} - \gamma p' \frac{\partial v_x'}{\partial x} \, , \tag{4.4}$$

$$\frac{\partial B_x'}{\partial t} = 0 \, , \tag{4.5}$$

$$\frac{\partial B'_z}{\partial t} - B_0 \frac{\partial v'_z}{\partial x} = -\frac{\partial}{\partial x}(v'_x B'_z) \ . \tag{4.6}$$

The previous set of equations is still exact. The purely linear terms are gathered on the left-hand side and all the nonlinear terms on the right-hand side. Equation (4.5) reveals that there are no magnetic field perturbations in the longitudinal direction (x-direction) in time.

The perturbed quantities are expanded out in powers of a parameter ϵ (e.g. $\rho' = \epsilon \rho_1 + \epsilon^2 \rho_2 + \ldots$), which is taken to be $0 < \epsilon < 1$ and is of the same order as the amplitude (say a parameter a) of the linear solution. The index denotes the order of the quantity. We introduce two independent time-scales $t_0 = t$ and $\tau = \epsilon^2 t$ so that

$$\frac{\partial}{\partial t} = \frac{\partial}{\partial t_0} + \epsilon^2 \frac{\partial}{\partial \tau} \ . \tag{4.7}$$

The time-scale τ is slow compared with t_0. It is proportional to a^2. Hence, any non-zero term in Equations (4.1)-(4.6) containing the time-scale τ, is at least of order ϵ^3. To simplify the notation the index 0 of the first time-scale will be omitted.

The linear system of equations contains two wave modes: a slow magneto-acoustic wave and an Alfvén wave. The slow wave is characterised by compression and rarefaction of the plasma. It involves the plasma variables v_x, ρ and p. The Alfvén wave is incompressible. It is characterised by the plasma variables v_z and B_x. We assume that the plasma is disturbed in such a way that only an Alfvén mode is excited. We do not consider a linear slow magneto-acoustic wave. That implies that $v_{x,1} = \rho_1 = p_1 = 0$. The first-order linearizations of Equations (4.3) and (4.6) combine into the Alfvén wave equation:

$$\left[\frac{\partial^2}{\partial t^2} - V_A^2 \frac{\partial^2}{\partial x^2} \right] B_{z,1} = 0 \ , \tag{4.8}$$

with the quantity $V_A = B_0/\sqrt{\rho_0 \mu_0}$ being the background Alfvén speed. The general solution to Equation (4.8) is expressed as the d'Alembert solution, $B_{z,1} = aB_0 \left[f\left(x + V_A t\right) + g\left(x - V_A t\right) \right]$, describing two waves, one travelling in the positive and the other in the negative x-direction, both at the background Alfvén speed. The shapes of the functions f and g are determined by the initial conditions $B_{z,1}(t{=}0)$ and $(\partial B_{z,1}/\partial t)(t{=}0)$. We consider the solution excited by an initial pulse in the velocity ($B_{z,1}(t{=}0) = 0$, $v_{z,1}(t{=}0) = 2aV_A$ $\mathcal{F}(x,0)$, $\xi_{z,1}(t{=}0) = 0$):

$$\frac{B_{z,1}}{B_0} = a \left[\mathcal{F}\left(x + V_A t, \tau\right) - \mathcal{F}\left(x - V_A t, \tau\right) \right] \ , \tag{4.9}$$

107

where $\vec{\xi}$ is the displacement vector. The first-order solution contains two Alfvén pulses, one localised at the position $x = -V_A t$, the other at position $x = V_A t$. For most of the chapter, the dependency of the function $\mathcal{F}$ on the variable τ is not explicitly written. Throughout the chapter both the numerical and the analytical results are illustrated by taking the function $\mathcal{F}(s)$ to have the form of a Gaussian pulse:

$$\mathcal{F}(s) = e^{-\left(\frac{s}{\Delta x}\right)^2} , \tag{4.10}$$

which is localised at $s=0$ ($\mathcal{F}(0)=1$) and has a spatial width Δx, with monotonically decaying wings which tail off to zero as s tends to infinity.

If there is no initial perturbation of the longitudinal velocity and the density, the only term that can excite them, is the first term on the right-hand side of Equation (4.2), which is the nonlinear Alfvén magnetic pressure force and is of order a^2. This force is the only component of the second-order ponderomotive force in this model. Therefore the quantities v_x and ρ are of order a^2 as well (Hollweg, 1971). Using the linear solution (4.9), the second-order ponderomotive force is:

$$-\frac{1}{2\mu_0}\frac{\partial B_{z,1}^2}{\partial x} = -\frac{1}{2}\rho_0 a^2 V_A^2 \frac{\partial}{\partial x}\left[\mathcal{F}^2\left(x + V_A t\right) + \mathcal{F}^2\left(x - V_A t\right)\right.$$
$$\left. - 2\mathcal{F}\left(x + V_A t\right)\mathcal{F}\left(x - V_A t\right)\right] . \tag{4.11}$$

The ponderomotive force is parallel to the equilibrium magnetic field. Because this force is nonlinear, it is not equal to the sum of the ponderomotive forces of each Alfvén pulse separately, but contains an extra cross-term. The first two terms are the respective ponderomotive forces of the two travelling Alfvén pulses, which are always localised at the positions of the pulses. We call them the 'ponderomotive wings'. Where a pulse passes through a fixed position, the flow accelerated by the ponderomotive force of the front-slope of the pulse is decelerated by the flow induced by the ponderomotive force of the back-slope. In the case of a symmetric pulse, deceleration perfectly balances acceleration. The time integral of the force is equal to zero and no net plasma flow is induced. The ponderomotive response to these force terms will always remain of the order a^2. The third term is the cross-term of the two pulses. It is localised at $x = 0$ and decreases in magnitude rapidly in time with a time-scale $\Delta x/V_A$ as the two Alfvén pulses separate. We call this term the 'cross-ponderomotive force'. It eventually becomes one order of magnitude less than the

force of the ponderomotive wings. We estimate the time t_{sep} at which this occurs:

$$\frac{|\mathcal{F}^2\left(x \pm V_A t_{sep}\right)|}{|2\mathcal{F}\left(x + V_A t_{sep}\right)\mathcal{F}\left(x - V_A t_{sep}\right)|} \sim 10 \ . \tag{4.12}$$

In the case of Gaussian-shaped pulses, the time t_{sep} is equal to

$$\frac{V_A t_{sep}}{\Delta x} \approx \sqrt{0.5\ln(20)} \approx 1.22 \ . \tag{4.13}$$

In a cold, ideal plasma there is no force decelerating the flow of the plasma excited by this cross-ponderomotive force. Therefore, we expect large density perturbations to occur locally in time.

The density cannot physically become infinite. The cold-plasma limit states that the kinetic pressure is negligibly small compared with the magnetic pressure, but it is not equal to zero. When the gradients in the density become sufficiently large, the cold-plasma limit is not a good approximation. The kinetic pressure force has to be included. An order of magnitude comparison between the ponderomotive force and the kinetic pressure force is:

$$\frac{|-\frac{1}{2\mu_0}\frac{\partial B_{z,1}^2}{\partial x}|}{|-\frac{\partial p}{\partial x}|} \sim a^2 \beta^{-1} \ . \tag{4.14}$$

First the cold-plasma limit is investigated in order to understand the workings of the non-linear behaviour of an Alfvén pulse. The next step is to take into account the kinetic pressure.

For future reference, Table 4.1 gives a list of the critical times used in this chapter.

4.3 Cold-plasma limit

4.3.1 Numerical simulation

In this section the kinetic pressure is neglected in comparison with the magnetic pressure. We perform a numerical simulation with a fully nonlinear, non-dissipative Lagrangian MHD code from Arber, Longbottom and Van Der Linden (1998). The code is second-order in space and time. We use a grid resolution of $dx = 0.0125V_A t$. We solve an initial-value problem. At $t=0$ a pulse in the velocity component v_z, centred at $x = 0$, is set up. It has the shape (4.10) with a width $\Delta x = 0.1 \ V_A t$ and amplitude $2a = 0.3$. There is initially no perturbation in magnetic field, current density, longitudinal velocity or mass density.

time	description
t_{sep}	Time for the cross-ponderomotive force to become one order in magnitude less than the force of the ponderomotive wings.
$t_{sep,\beta}$	Time for the slow and Alfvén pulses to separate by a distance $V_A t_{sep}$.
$t_{sep,s}$	Time for slow pulses to separate by a distance $V_A t_{sep}$.
t_{sw}	Shock-formation time of travelling Alfvén pulse.
t_{sc}	Shock-formation time of central density perturbation in cold-plasma limit.
$t_{sc,\beta}$	Time when nonlinear inertia becomes of the same order as the pressure force.
t_{ssw}	Shock-formation time of travelling slow pulse.

Table 4.1: Definition of critical times used in this chapter

Figures 4.1 and 4.2 give a general view of the evolution of the main plasma quantities. The time $V_A t / \Delta x = 2 \times 10^{-4}$ corresponds to the first time step of the numerical code. The initial velocity pulse splits up into two oppositely travelling, linearly polarized Alfvén pulses of width Δx and amplitude a, as expected from the linear d'Alembert solution. The quantities in Figure 4.1 are the non-zero transverse components of the plasma vector fields. They are, at lowest order, governed by the linear transverse component of the Lorentz force $-B_0 j_y$ (proportional to a). They travel at the Alfvén speed away from the origin. Because we have chosen an initial disturbance of large amplitude, we see the influence of nonlinear terms, which is of interest to us. The Alfvén pulses have a nonlinear force, the ponderomotive force, associated with them, which is parallel to the equilibrium magnetic field. Therefore plasma flows in that direction and density perturbations are excited. These are shown in Figure 4.2. We see that the velocity component v_x and the mass density have a part that travels with the Alfvén pulse and a part that remains close to the origin. The part travelling with the Alfvén pulse is of order a^2. It shows that the Alfvén wave is nonlinearly compressible (this is true for linearly and elliptically polarized Alfvén waves, but not for circularly polarized Alfvén waves). We explain the existence of a standing structure around the origin as follows. In the case of a single, travelling, symmetric Alfvén pulse in a fixed position the time integral of the ponderomotive force is zero, so that there

110
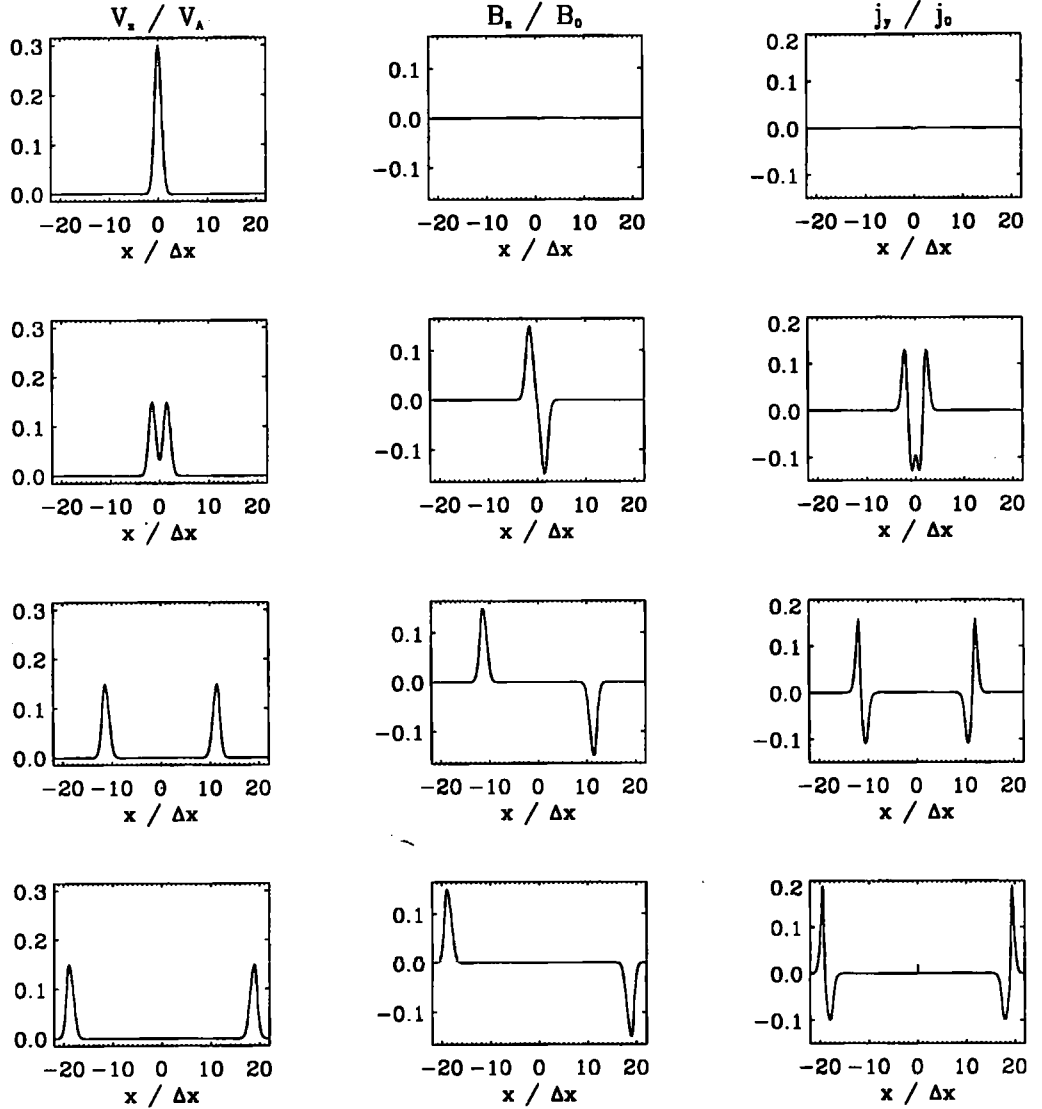
Figure 4.1: A plot of the velocity component v_x, magnetic field component B_z and the current density component j_y as a function of $x/\Delta x$ for four different times (from top to bottom) $V_A t/\Delta x$ = 2 ×10^{-4}, 1.5, 11.3 and 18.6. The quantity j_0 is defined as $j_0 = \Delta x B_0/\mu_0$. The parameter a = 0.15.

is no net plasma flow induced. Positions closer than approximately 2-3 Δx to the origin, experience the ponderomotive force of both Alfvén pulses, such that the time integral of the ponderomotive force is not zero at those positions. They feel the ponderomotive force of the back-slope of the pulses more than that of the front-slope. Figure 4.3 shows the time

111
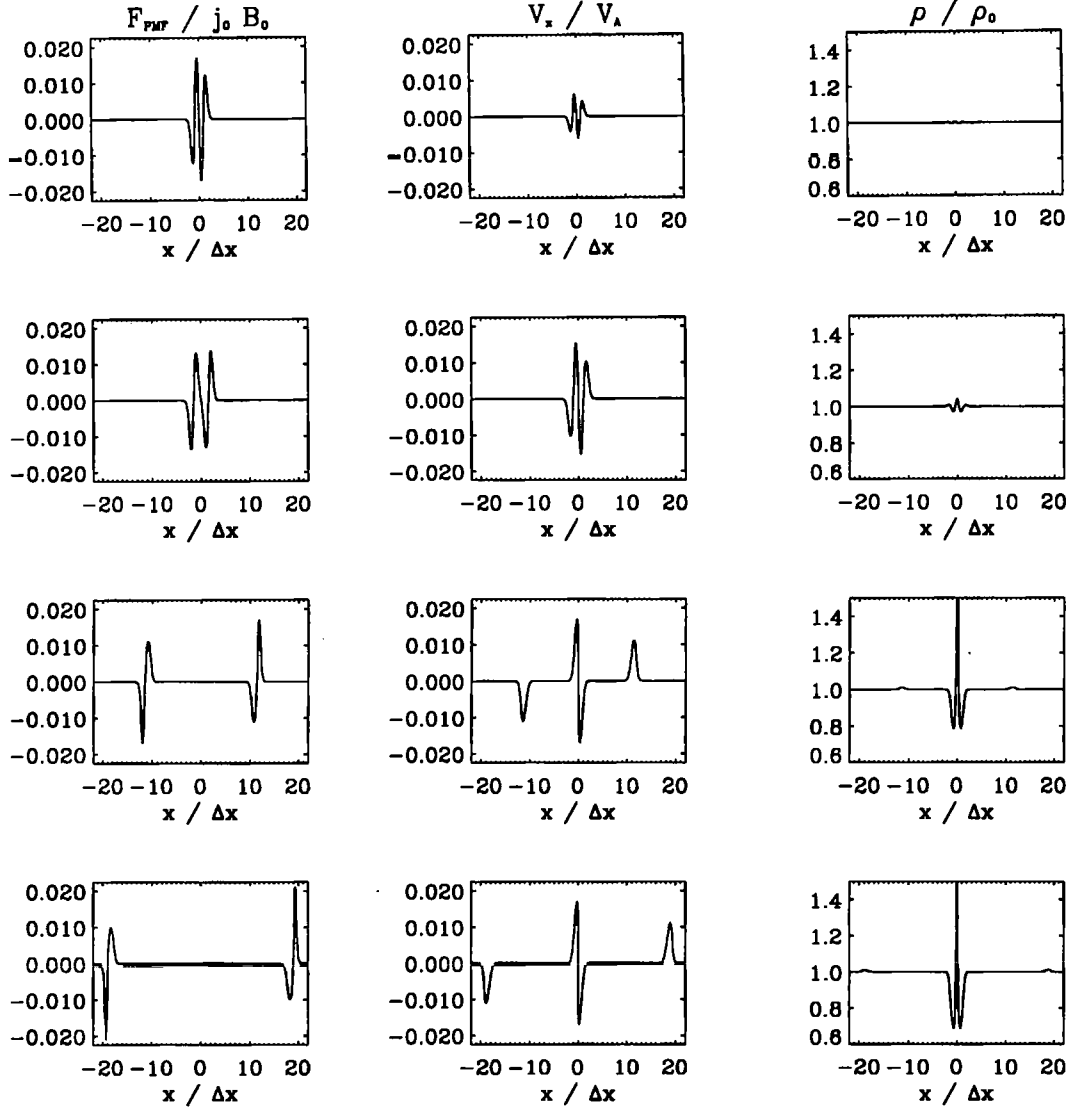
Figure 4.2: A plot of the ponderomotive force, the velocity component v_x and the mass density ρ as a function of $x/\Delta x$ for four different times (from top to bottom) $V_A t/\Delta x = 0.75$, 1.5, 11.3 and 18.6. The parameter $a = 0.15$.

evolution of the ponderomotive force at different positions. At the positions $x/\Delta x = 0.5$ and 1.0, it is clear that the plasma experiences a net acceleration in the negative x-direction. On a time-scale of t_{sep}, no force is acting on the plasma in the central region, which keeps moving at a constant speed towards the origin. This standing velocity profile is of order a^2. It is nicely shown at the time $V_A t/\Delta x = 11.3$ in Figure 4.2. At $V_A t/\Delta x = 18.6$ we notice

112
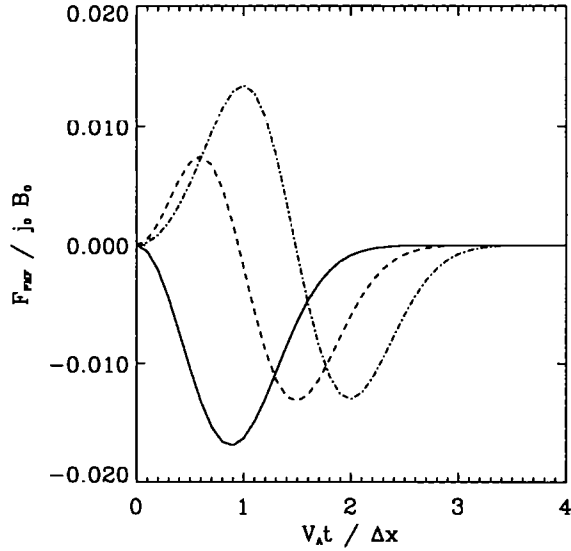
Figure 4.3: A plot of the ponderomotive force $-(1/2\mu_0)(\partial B_z^2/\partial x)$ as a function of time at the positions $x/\Delta x = 0.5$ (solid line), 1.0 (dashed line) and 1.5 (dot-dashed line). The parameter $a = 0.15$.

that the gradient of the standing velocity profile across the origin has become extremely large. Furthermore, the density perturbation at the centre has grown secularly in time, to values far exceeding the equilibrium value, and becomes extremely large as well. We expect that just after this time the velocity has formed a shock and the density has become infinite. We call the time when this occurs, t_{sc}. In practice the numerical code never reaches this time because it reduces its time step to resolve the growing gradient until the time step is below computer accuracy, and the numerical simulation ends. The time at which this happens, equal to $V_A t/\Delta x = 18.6$ in this case, is a good approximation of the time t_{sc}.

When we look at the evolution of the Alfvén pulses, we see that the shape of the pulse becomes non-symmetrical with time. The front-flank of the pulse in the velocity and magnetic field component is steepening. This continues until a shock is formed. We call the time at which this occurs t_{sw}. Unfortunately this time is longer than the time t_{sc}, so that the numerical code cannot investigate this further. The current density component j_y forms a narrowing region of enhanced current density, ultimately forming a current sheet.

113
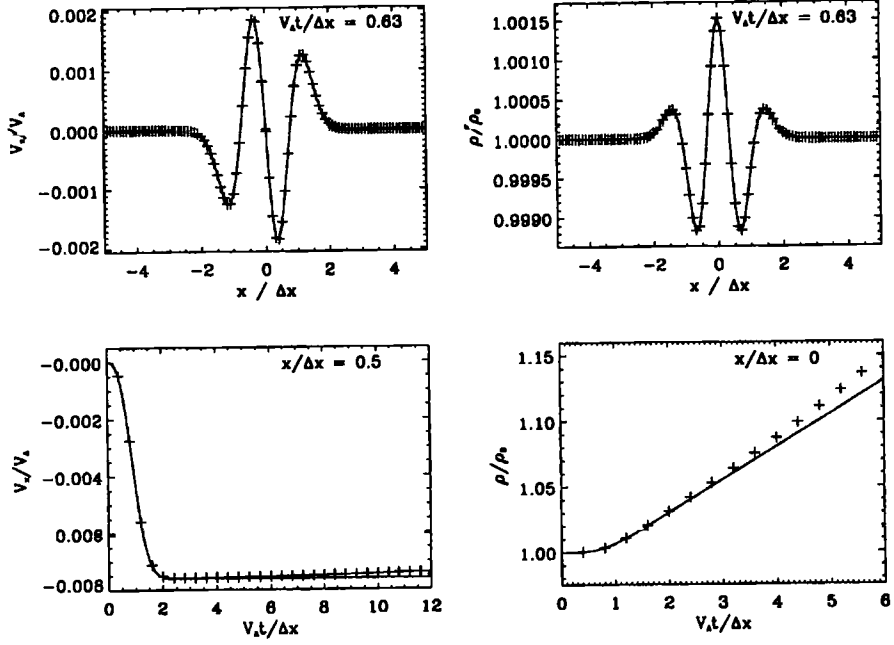
Figure 4.4: A plot of the longitudinal velocity v_x and density ρ. The top panels show the spatial behaviour at an early time $V_A t/\Delta x = 0.63$. The bottom panels show the early time evolution of the velocity v_x at $x/\Delta x = 0.5$ and the density ρ at $x/\Delta x = 0$. The crosses are the full numerical result. The solid line is the quadratically nonlinear solution (4.17). The amplitude parameter a is equal to 0.1.

4.3.2   Quadratic nonlinear solution

We first study the solution to the cold-plasma versions of the quadratically nonlinear equations (4.1) and (4.2) at order ϵ^2,

$$\frac{\partial \rho_2}{\partial t} = -\rho_0 \frac{\partial v_{x,2}}{\partial x} , \qquad (4.15)$$

$$\rho_0 \frac{\partial v_{x,2}}{\partial t} = -\frac{1}{2\mu_0} \frac{\partial B_{z,1}^2}{\partial x} , \qquad (4.16)$$

which are, in the case of Gaussian-shaped pulses:

$$\frac{\rho_2}{\rho_0} = \frac{1}{2} a^2 \left[\mathcal{F}^2\left(x + V_A t\right) + \mathcal{F}^2\left(x - V_A t\right) - 2\mathcal{F}^2\left(x\right) \right.$$
$$\left. + 2\sqrt{\pi}\left(1 - 2\left(\frac{x}{\Delta x}\right)^2\right) e^{-2\left(\frac{x}{\Delta x}\right)^2} \int_0^{\sqrt{2}\frac{V_A t}{\Delta x}} \mathrm{erf}\left(t'\right) \, dt' \right] ,$$

114

$$\frac{v_{x,2}}{V_A} = -\frac{1}{2}a^2\left[\mathcal{F}^2\left(x + V_A t\right) - \mathcal{F}^2\left(x - V_A t\right)\right.$$
$$\left. + 2\sqrt{2\pi}\left(\frac{x}{\Delta x}\right)e^{-2\left(\frac{x}{\Delta x}\right)^2}\mathrm{erf}\left(\sqrt{2}\frac{V_A}{\Delta x}t\right)\right] . \tag{4.17}$$

The last terms in the expressions for $v_{x,2}$ and ρ_2 represent the response to the cross-ponderomotive force. The temporal evolution of the velocity due to that term is an error function. After a time of approximately $\Delta x/\sqrt{2}V_A$, the velocity is constant, with the spatial structure of an inward flow towards $x/\Delta x=0$. At $x/\Delta x=\pm 1/\sqrt{2}$ the velocity has a local extremum. The density at $x/\Delta x=0$ has a maximum in space. The density has a term which grows secularly in time. At first the density grows quadratically but after a time of approximately $\Delta x/\sqrt{2}V_A$ the growth becomes linear. This shows that the quadratic nonlinear solution cannot be the correct description for all times, since it lets the density perturbation become of the same order as the background density. At that point the perturbation method is no longer valid. Figure 4.4 shows both the spatial structure at the time $V_A t/\Delta x = 0.63$ and the early time evolution of the numerically derived quantities v_x and ρ, compared with the quadratically nonlinear solution (4.17). The quadratically nonlinear solution matches the numerical result very well up to a time $V_A t/\Delta x \approx 2$. Beyond that time other nonlinear processes become important. Solution (4.17) remains of order a^2 for times earlier than t_{sep} when

$$\frac{\rho_2}{\rho_0} \ll \frac{B_{z,1}}{B_0} , \tag{4.18}$$

which, in the case of Gaussian-shaped pulses, yields the condition:

$$a \ll \left[\sqrt{\pi}\int_0^{\sqrt{2}\frac{V_A t_{sep}}{\Delta x}}\mathrm{erf}\left(t'\right)dt'\right]^{-1} \approx 0.48 . \tag{4.19}$$

We used the fact that

$$\int_0^t\mathrm{erf}(\alpha t')\,dt' = t\,\mathrm{erf}(\alpha t) - \frac{1 - e^{-\alpha^2 t^2}}{\alpha\sqrt{\pi}} . \tag{4.20}$$

For amplitudes that satisfy Condition (4.18) the ponderomotive response is of order a^2 for times earlier than t_{sep}. After t_{sep} the ponderomotive response to the three terms of the ponderomotive force (4.11) can be treated separately. This implies that the full solution is built up in three stages. First, the solution at times earlier than t_{sep} is adequately described by the linear and quadratic nonlinear solutions (4.9) and (4.17). For times later than t_{sep}

115

we treat the nonlinear behaviour of the Alfvén wings and the central part separately. This is the central idea of the model.

The terms on the right-hand sides of Equations (4.3) and (4.6) contain the nonlinear corrections to the Alfvén pulses. They are of order a^3 and consist of a combination of the perturbations governing the Alfvén pulses and the quantities $v_{x,2}$ and ρ_2, which are excited by the second-order ponderomotive force. These corrections then appear in the ponderomotive force as terms of order a^4.

The Alfvén correction terms, which contain the ponderomotive response of the cross-ponderomotive force, are expected to grow in magnitude for times earlier than t_{sep} but after that decrease exponentially to zero. The maximum magnitude of these terms is negligible under Condition (4.18). Thus, for the treatment of the central region the nonlinear terms in Equations (4.3) and (4.6) are neglected, even though we keep the terms of order a^4 in Equations (4.1) and (4.2). Consider the cold-plasma version of Equation (4.2):

$$(\rho_0 + \rho') \left[\frac{\partial v'_x}{\partial t} + v'_x \frac{\partial v'_x}{\partial x} \right] = -\frac{1}{2\mu_0} \frac{\partial B'^2_z}{\partial x} \approx \rho_0 a^2 V_A^2 \frac{\partial}{\partial x} \left[\mathcal{F}\left(x + V_A t\right) \mathcal{F}\left(x - V_A t\right) \right] \ . \quad (4.21)$$

The force on the right-hand side of the previous equation is, to leading order, equal to the third term of Expression (4.11), which is proportional to ρ_0. For times earlier than t_{sep} the density perturbation ρ' is negligible compared with the equilibrium density ρ_0. For times later than t_{sep}, the cross-ponderomotive force is negligible. The density can then be eliminated from the equation. Therefore instead of Equation (4.21) for the cross-ponderomotive response, we solve:

$$\frac{\partial v'_x}{\partial t} + v'_x \frac{\partial v'_x}{\partial x} \approx a^2 V_A^2 \frac{\partial}{\partial x} \left[\mathcal{F}\left(x + V_A t\right) \mathcal{F}\left(x - V_A t\right) \right] \ . \quad (4.22)$$

For the ponderomotive wings it is not possible to neglect the nonlinear Alfvén correction terms of order a^3 without neglecting the terms of order a^4 in Equations (4.1) and (4.2) as well. Therefore we shall investigate the effect of these nonlinear Alfvén correction terms by looking at the self-moderation of a finite amplitude Alfvén pulse.

4.3.3 Self-moderation of a travelling Alfvén pulse

In this section we address the self-moderation of a travelling Alfvén pulse of finite amplitude. This is a cubic nonlinear effect. Instead of the first-order solution (4.9), we take only one

pulse, either travelling in the positive or in the negative x-direction:

$$\frac{B_{z,1}}{B_0} = a\mathcal{F}\left(x \pm V_A t, \tau\right) .$$ (4.23)

The second-order solutions are easily obtained from looking at the Expressions (4.17):

$$\frac{\rho_2}{\rho_0} = \frac{1}{2}\left(\frac{B_{z,1}}{B_0}\right)^2 ,$$ (4.24)

$$\frac{v_{x,2}}{V_A} = \mp\frac{1}{2}\left(\frac{B_{z,1}}{B_0}\right)^2 .$$ (4.25)

The third-order equations, using the previous results (4.23)-(4.25), are:

$$\rho_0\frac{\partial v_{z,3}}{\partial t} - \frac{B_0}{\mu_0}\frac{\partial B_{z,3}}{\partial x} = -\rho_0\frac{\partial v_{z,1}}{\partial \tau} ,$$ (4.26)

$$\frac{\partial B_{z,3}}{\partial t} - B_0\frac{\partial v_{z,3}}{\partial x} = -\frac{\partial B_{z,1}}{\partial \tau} - \frac{\partial}{\partial x}\left(v_{x,2}B_{z,1}\right) .$$ (4.27)

Eliminating the secular terms yields a quasi-linear equation in the magnetic field perturbation $B_{z,1}$:

$$\frac{\partial B_{z,1}}{\partial \tau} \mp \frac{3}{4}V_A\left(\frac{B_{z,1}}{B_0}\right)^2\frac{\partial B_{z,1}}{\partial x} = 0 ,$$ (4.28)

which is known as the Cohen-Kulsrud equation (Cohen & Kulsrud, 1974). Its solution is written in an implicit form

$$\frac{B_{z,1}}{B_0} = a\,\mathcal{F}\left(x \pm V_A t \pm \frac{3}{4}V_A\left(\frac{B_{z,1}}{B_0}\right)^2 \tau\right) .$$ (4.29)

Since the propagation speed of the function $\mathcal{F}$ now depends on the square of the function itself, we have the possibility of shock formation since the centre of the pulse moves faster than the preceding wing of the pulse, thus catching up the preceding wing. A shock is formed when, locally, the time and space derivatives become infinite. Figure 4.5 shows Solution (4.29), for a pulse travelling in the negative x-direction, as a function of $x + V_A t$ at four different times. The numerical result and Solution (4.29) match very well.

We calculate the derivative of $B_{z,1}$ with respect to x from Expression (4.29):

$$\frac{\partial}{\partial x}\left(\frac{B_{z,1}}{B_0}\right) = a\left[1 \pm \frac{3}{2}V_A\frac{B_{z,1}}{B_0}\frac{\partial}{\partial x}\left(\frac{B_{z,1}}{B_0}\right)\tau\right]\mathcal{F}' ,$$ (4.30)

which at $\tau = 0$ yields an expression for the derivative of the function $\mathcal{F}$ with respect to its argument:

$$\mathcal{F}' = \frac{1}{a}\left[\left(\frac{B_{z,1}}{B_0}\right)\right]^{-1}_{\tau=0} .$$ (4.31)
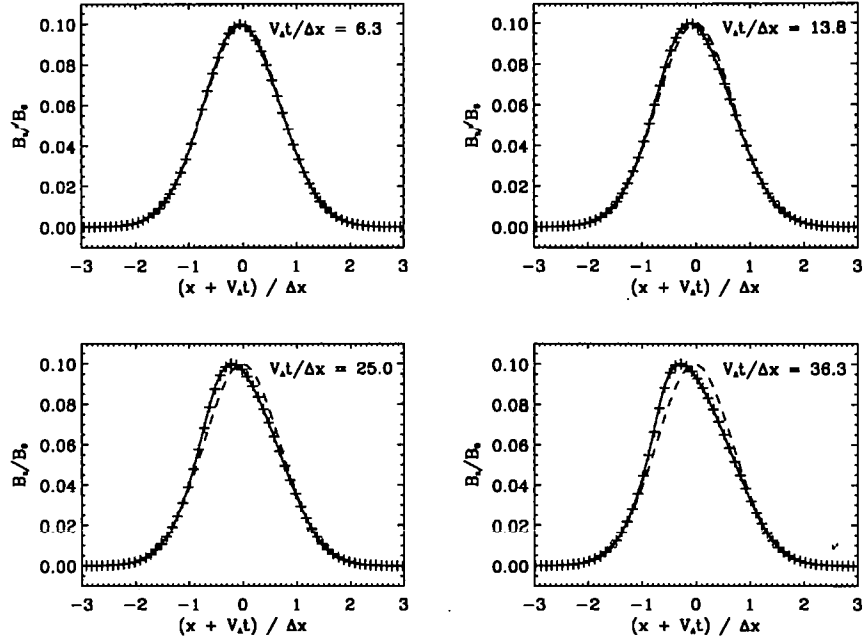
Figure 4.5: A plot of the magnetic perturbation B_z of the Alfvén pulse travelling in the negative x-direction as a function of $x + V_A t$ at different times. The crosses are the full numerical result. The solid line is Expression (4.29). The dashed line is the linear expression (4.9). The amplitude parameter a is equal to 0.1.

Eliminating the x-derivative of the magnetic field perturbation $B_{z,1}$ from Expression (4.30) and using the previous expression, we find

$$\frac{\partial}{\partial x}\left(\frac{B_{z,1}}{B_0}\right) = \frac{\frac{\partial}{\partial x}\left(\frac{B_{z,1}}{B_0}\right)_{\tau=0}}{1 \mp \frac{3}{2}V_A \frac{B_{z,1}}{B_0}\frac{\partial}{\partial x}\left(\frac{B_{z,1}}{B_0}\right)_{\tau=0}\tau} . \tag{4.32}$$

The earliest time (say at τ_{sw}) that the x-derivative of the magnetic field perturbation is infinite, thus forming a shock, is

$$\tau_{sw} = \min\left\{\pm\frac{1}{\frac{3}{4}V_A\left[\frac{\partial}{\partial x}\left(\frac{B_{z,1}}{B_0}\right)^2\right]_{\tau=0}}\right\} . \tag{4.33}$$

The magnetic field perturbation $B_{z,1}$ in the denominator of Expression (4.32) has been approximated by its initial profile at $\tau=0$. The magnetic field perturbation and its spatial derivative need to have the same sign somewhere in the spatial domain in order to have

the possibility of shock formation. The time-scale for the shock-formation is inversely proportional to a^2. With the function $\mathcal{F}$ defined as (4.10), the shock forms at the time $V_A \tau_{sw} / \Delta x = (2\sqrt{e}/3)a^{-2} \approx 1.1 a^{-2}$ at the position $(x \pm V_A t_{sw})/\Delta x = \mp 1$ (Mann, 1995).

4.3.4 Evolution of the central density perturbation

The central density perturbation is excited by the cross-ponderomotive force. Previously we have stated that for times earlier than t_{sep}, terms which are proportional to the density perturbation ρ are negligible because $\rho \ll \rho_0$. For times later than t_{sep}, the cross-ponderomotive force is negligible and the term $\rho + \rho_0$ is eliminated from the x-component of the momentum equation. Thus, the equations to be solved for the cross-ponderomotive force are, using Equations (4.1) and (4.2):

$$\frac{\partial \rho}{\partial t} + \frac{\partial}{\partial x}(\rho v_x) = 0 , \qquad (4.34)$$

$$\frac{\partial v_x}{\partial t} + v_x \frac{\partial v_x}{\partial x} \approx a^2 V_A^2 \frac{\partial}{\partial x}\left[\mathcal{F}(x + V_A t)\,\mathcal{F}(x - V_A t)\right] . \qquad (4.35)$$

The momentum equation is decoupled from the mass conservation equation. The difference between Equations (4.16) and (4.35) is the inclusion of the inertial term on the left-hand side. The force term on the right-hand side of Equation (4.35) is rapidly decreasing to zero on the fast time-scale $V_A t / \Delta x$.

First of all we assume that the time-scale of the cross-ponderomotive force ($\sim t_{sep}$) is faster than the time-scale of the nonlinear inertial term $v_x \partial v_x / \partial x$ in Equation (4.35). For times $t < t_{\text{sep}}$, the nonlinear inertial term is neglected. Then the solution for v_x is given as

$$v_x = a^2 V_A^2 \int_0^t dt' \frac{\partial}{\partial x}\left[\mathcal{F}(x + V_A t')\mathcal{F}(x - V_A t')\right] , \qquad (4.36)$$

which corresponds to the quadratic nonlinear solution. In the case of Gaussian-shaped pulses, this is the last term of Expression (4.17). From the time t_{sep} onwards the velocity is approximately time-independent because the cross-ponderomotive force has become negligible. We therefore switch off the force and switch on the nonlinear inertial term. We use Solution (4.36) for a Gaussian-shaped pulse, evaluated at large t,

$$v_x(t \to \infty) = a^2 V_A \, \mathcal{G}(x) , \qquad (4.37)$$

with

$$\mathcal{G}(x) = -\sqrt{2\pi}\left(\frac{x}{\Delta x}\right) e^{-2\left(\frac{x}{\Delta x}\right)^2} , \qquad (4.38)$$

119
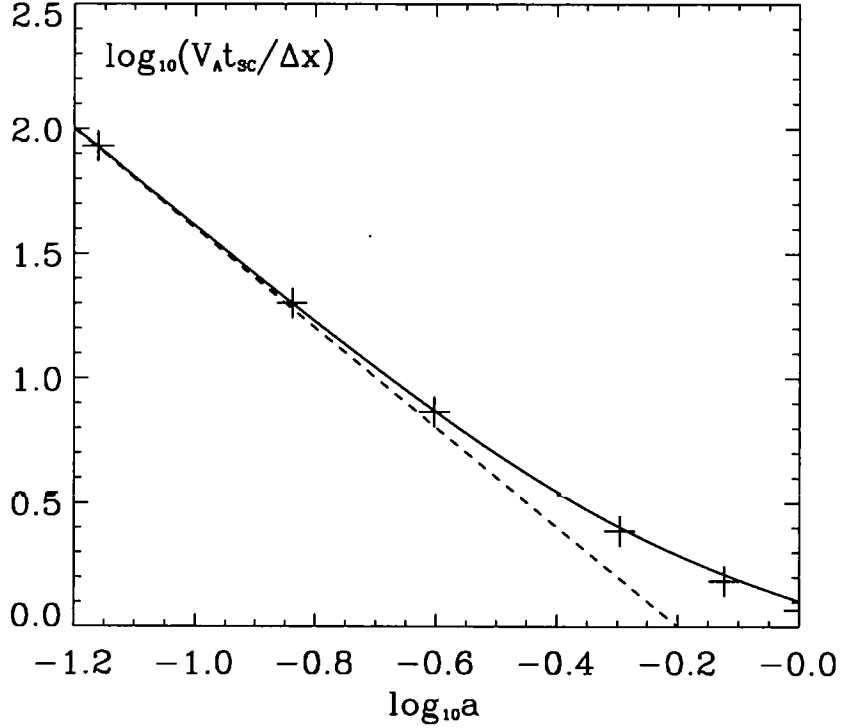
Figure 4.6: A logarithmic plot of the dependence of the time t_{sc} for the formation of a discontinuity in the flow velocity v_x on the amplitude parameter a. The crosses show the full numerical result. The solid line is the numerically derived solution of Equation (4.43). The dashed line shows the analytical result (4.42).

as an initial condition at $t = t_{sep}$ and solve the simple wave equation $\partial v_x/\partial t + v_x \partial v_x/\partial x = 0$. The implicit solution is

$$v_x = a^2 V_A \, \mathcal{G} \left(x - v_x(t - t_{sep}) \right) \ . \tag{4.39}$$

By the first time (e.g. $t = t_{sc}$) that two neighbouring characteristics intersect, corresponding to the condition that the spatial gradient becomes infinite, a discontinuity in v_x has formed. Using the same procedure as in Section 3.3, it can easily be found that

$$\frac{\partial v_x}{\partial x} = \frac{v_0{}'}{1 + v_0{}'(t - t_{sep})} \quad \text{with} \quad v_0{}' = \left(\frac{\partial v_x}{\partial x} \right)_{t=t_{sep}} \ . \tag{4.40}$$

The gradient (4.40) becomes infinite for the first time when

$$t_{sc} - t_{sep} = \min \left\{ \frac{-1}{v_0{}'} \right\} \ . \tag{4.41}$$

120
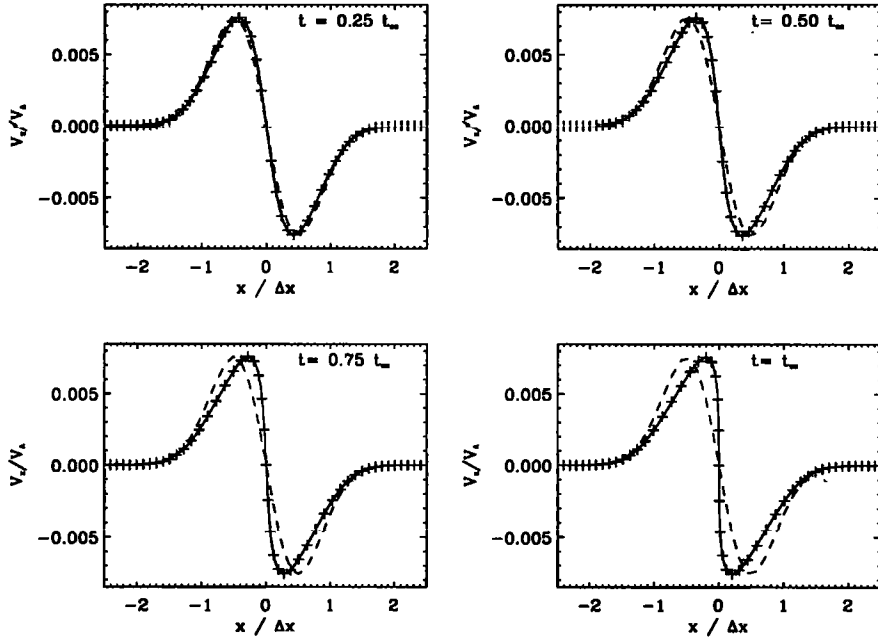
Figure 4.7: A plot of the velocity perturbation v_x as a function of x at different times t. The crosses are the full numerical result. The solid line is the numerical solution to Equation (4.43). The dashed line is the quadratically nonlinear solution $v_{x,2}$. The amplitude parameter a is equal to 0.1.

For the case of Gaussian-shaped pulses, this becomes

$$\frac{V_A t_{sc}}{\Delta x} = \min\left\{\frac{1}{\sqrt{2\pi}a^2\frac{\partial}{\partial x}\left(xe^{-2x^2/\Delta x^2}\right)}\right\} = \frac{1}{\sqrt{2\pi}\,a^2} . \qquad (4.42)$$

The infinite gradient in v_x forms at the position $x = 0$, where the original Alfvén pulse disturbance was centred at $t=0$.

From Expression (4.42) we conclude that the time-scale for the formation of a discontinuous velocity profile is inversely proportional to a^2. Figure 4.6 shows the time t_{sc} deduced both analytically and numerically. The result deduced using the one-dimensional MHD Lagrangian code is the most accurate as it assumes nothing besides the one-dimensionality of the problem. The analytical result matches the other results very well for small values of the parameter a but starts diverging once $a > 0.2$ reaching the limitation (4.18). For larger values of a, the time-scale for the cross-ponderomotive force and the inertia become comparable. The two terms counteract each other at times earlier than t_{sep}. This means that the second-order solution (4.17) does not approximate the full solution well enough.

121
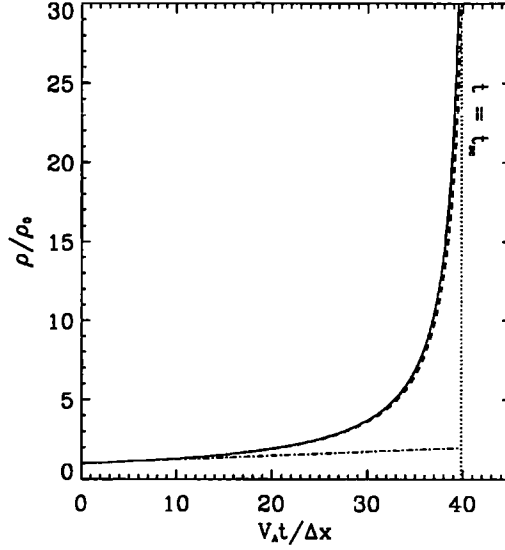
Figure 4.8: A plot of the temporal behaviour of the density at the position $x/\Delta x = 0$ with the parameter $a = 0.1$. Solid curve: numerical result from full MHD code. Dashed curve: analytical expression (4.45). Dot-dashed curve: quadratically nonlinear result (4.17).

This is reflected by the fact that the shock formation time is no longer proportional to a^{-2} but more like a^{-4}. After the time t_{sep} the inertia dominates, driving the velocity to shock. The solid curve in Figure 4.6 takes into account the competition between the ponderomotive force and inertia as it is the numerical solution of the forced simple wave equation

$$\frac{\partial v_x}{\partial t} + v_x \frac{\partial v_x}{\partial x} = -\frac{1}{2\mu_0\rho_0}\frac{\partial B_{z,1}^2}{\partial x} , \qquad (4.43)$$

assuming that the magnetic perturbation $B_{z,1}$ is given by Expression (4.9). The full ponderomotive force (4.11) is considered but we only focus on its effect on the relevant central region. Figure 4.7 shows a plot of the velocity v_x, derived using Equation (4.43) as a function of x for several times. The steepening of the gradient with time at $x=0$ is clearly visible. Up to values of $a=0.6$, this result matches up very well with the full numerical result. The deviation between the two results for higher values of a is due to the neglect of the self-moderation of the Alfvén pulses. For these values of a, the Alfvén pulses modify themselves substantially before they separate ($t < t_{sep}$), thus effecting the ponderomotive response in the central region after all. On top of that, the amplitude a becomes of the order 1, violating the perturbation approach. We therefore expect, in this regime, deviations

between the analytical solutions and the numerical results anyway.

An approximate expression for the evolution of the density for $t > t_{sep}$ is found from Equation (4.34) using Expression (4.40):

$$\frac{d\rho}{dt} = -\rho \frac{\partial v_x}{\partial x} = -\rho \frac{v_0'}{1 + v_0'(t - t_{sep})} , \qquad (4.44)$$

which has the solution

$$\frac{\rho}{\rho_0} = -\frac{\rho(t_{sep})}{\rho_0(1 + v_0'(t - t_{sep}))} = -\frac{1 - v_0't_{sep}}{1 + v_0'(t - t_{sep})} . \qquad (4.45)$$

We used the fact that the central density perturbation at t_{sep} is equal to the quadratically nonlinear density perturbation (4.17) with the integral of the error function increasing approximately linearly with time at the time t_{sep}.

This approximation is valid for $a \leq 0.2$. The cross-ponderomotive force and the resulting inertia produce a secular growth in the density profile. The formation of a discontinuous velocity profile, but where there is no mass flux across the surface, means that the density has become locally infinite at the time t_{sc}. This is an unphysical situation. Large gradients in velocity give rise to such large gradients in density, that the kinematic pressure force, however small the background pressure might be, eventually becomes of the same order as the inertia. The kinematic pressure force pushes the mass outwards before a discontinuity is formed. It is therefore more physical not to neglect the kinematic pressure force in comparison with the Lorentz force.

4.4 Finite plasma β

In this section we consider the effect of the kinetic plasma pressure on the nonlinear behaviour of an Alfvén pulse. We consider initially an Alfvén pulse in the velocity component $v_{z,1}$ of Equation (4.3). We investigate the nonlinear excitation of density and pressure perturbations in a plasma of finite plasma β, and therefore set the first-order perturbations, ρ_1, p_1 and $v_{x,1}$, which describe the linear slow magneto-acoustic wave, equal to zero.

We are interested in the case of the plasma $\beta < 1$ where magnetic forces dominate over pressure forces. In the case of this chapter the ponderomotive force is a purely magnetic force. Comparing the pressure force and the ponderomotive force to the Eulerian inertial

term:

$$\frac{\left|-\frac{\partial p}{\partial x}\right|}{\left|\rho \frac{\partial v}{\partial t}\right|} \sim \frac{C_s^2 \tau_s^2}{\gamma L^2} \quad , \quad \frac{\left|-\frac{1}{2\mu_0}\frac{\partial B^2}{\partial x}\right|}{\left|\rho \frac{\partial v}{\partial t}\right|} \sim \frac{V_A^2 \tau_{pmf}^2}{2 L^2} \quad , \tag{4.46}$$

where τ_s and τ_{pmf} are the typical time-scales for the pressure and the ponderomotive force respectively. The quantity L is a typical length-scale. If we compare the two time-scales,

$$\frac{\tau_s}{\tau_{pmf}} = \sqrt{\frac{\gamma}{2\beta}} \quad , \tag{4.47}$$

we see that for the plasma $\beta < 1$, the time-scale τ_{pmf} is shorter than the time-scale τ_s. If the plasma $\beta > 1$, the time-scale of the evolution of a disturbance set up by the ponderomotive force, τ_{pmf}, is longer than the time-scale of the advection of the disturbance at the speed of sound, τ_s, so that large density perturbations are not expected.

Although the focus of this section is on values of the plasma β below unity, most expressions are valid for the plasma β larger than unity as well, except when a specific regime of validity in β is specified or special resonances occur (at $\beta = 1$ for example).

4.4.1 Numerical simulation

We do a numerical simulation with the same initial conditions as in the cold-plasma limit, with the one exception that we now have a finite plasma β ($\beta = 0.1$). The behaviour of the transverse vector components v_z, B_z and j_y is qualitatively the same as in the cold-plasma limit. Figure 4.9 shows that the evolution of the plasma quantities v_x and ρ is very different because any density fluctuations excited by the ponderomotive force create a resisting pressure force. At the times $V_A t/\Delta x = 0.75$ and 1.50, the behaviour in v_x and ρ still resembles the cold-plasma limit, but from Figure 4.10 we see that at $V_A t/\Delta x = 1.50$, close to the central region, the pressure force is acting in the opposite direction from that of the ponderomotive force, resisting the compression of plasma and accelerating plasma outwards. Figure 4.11 shows the temporal behaviour of the forces in the direction parallel to the equilibrium field for a position $x/\Delta x = 0.6$, close to the origin. We see that the time integral of the sum of the pressure and ponderomotive forces is zero. Therefore the mass density shows no secular behaviour and remains of order a^2 at all times.

At $V_A t/\Delta x = 3.75$, the central standing velocity profile has split into two parts, each travelling in opposite directions. We call the time for the two pulses to separate $t_{sep,s}$. Instead of observing two travelling Alfvén pulses and a standing velocity profile at the

124
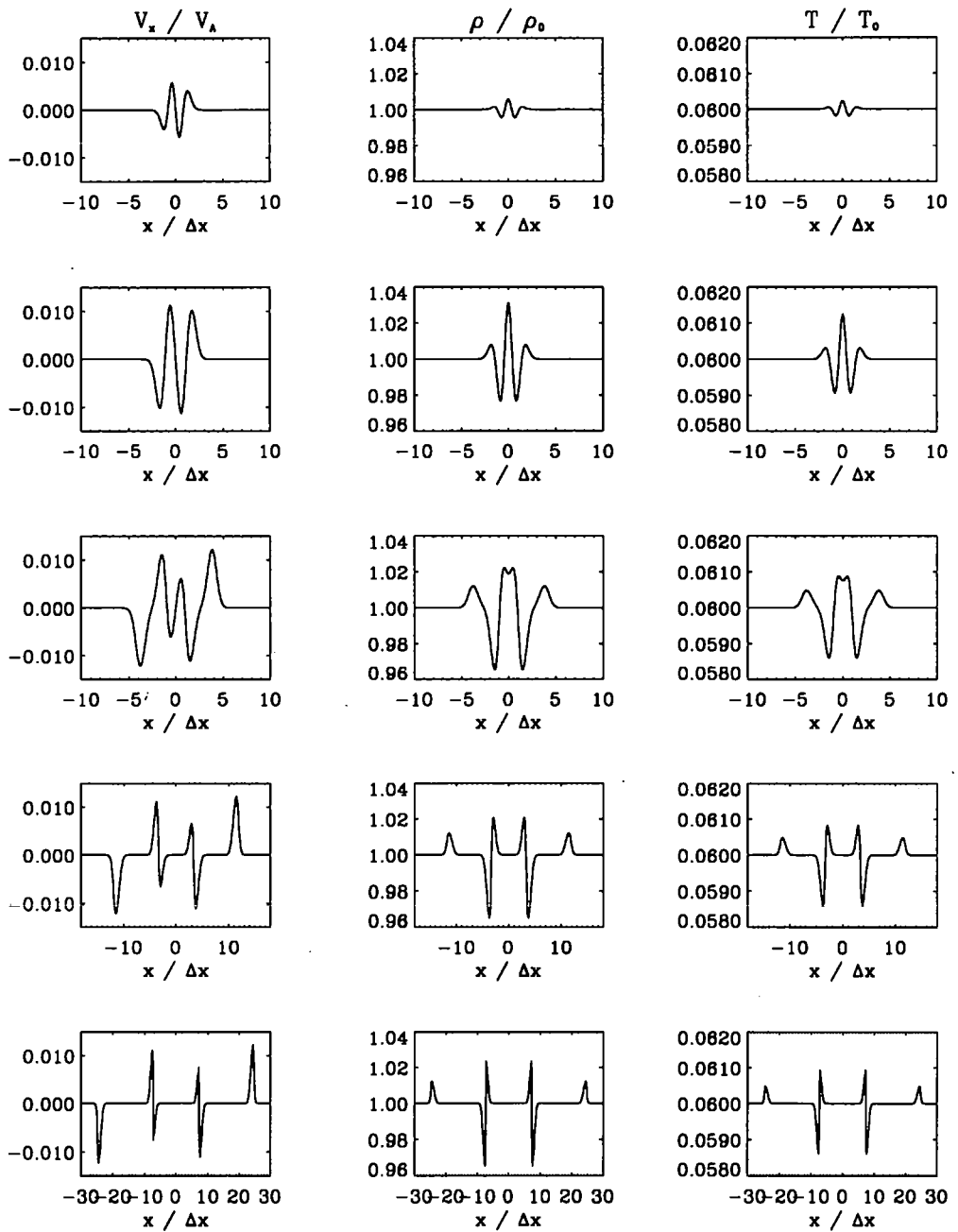
Figure 4.9: Plots of the velocity component v_x, the mass density ρ and the temperature T as functions of $x/\Delta x$ for five different times (from top to bottom) $V_A t/\Delta x = 0.75$, 1.50, 3.75, 11.25 and 24.00. The parameters $a = 0.15$ and $\beta = 0.1$. Note that the range of the x-axis for each time can be different. The temperature is calculated from the pressure and density from the ideal gas law (1.8).
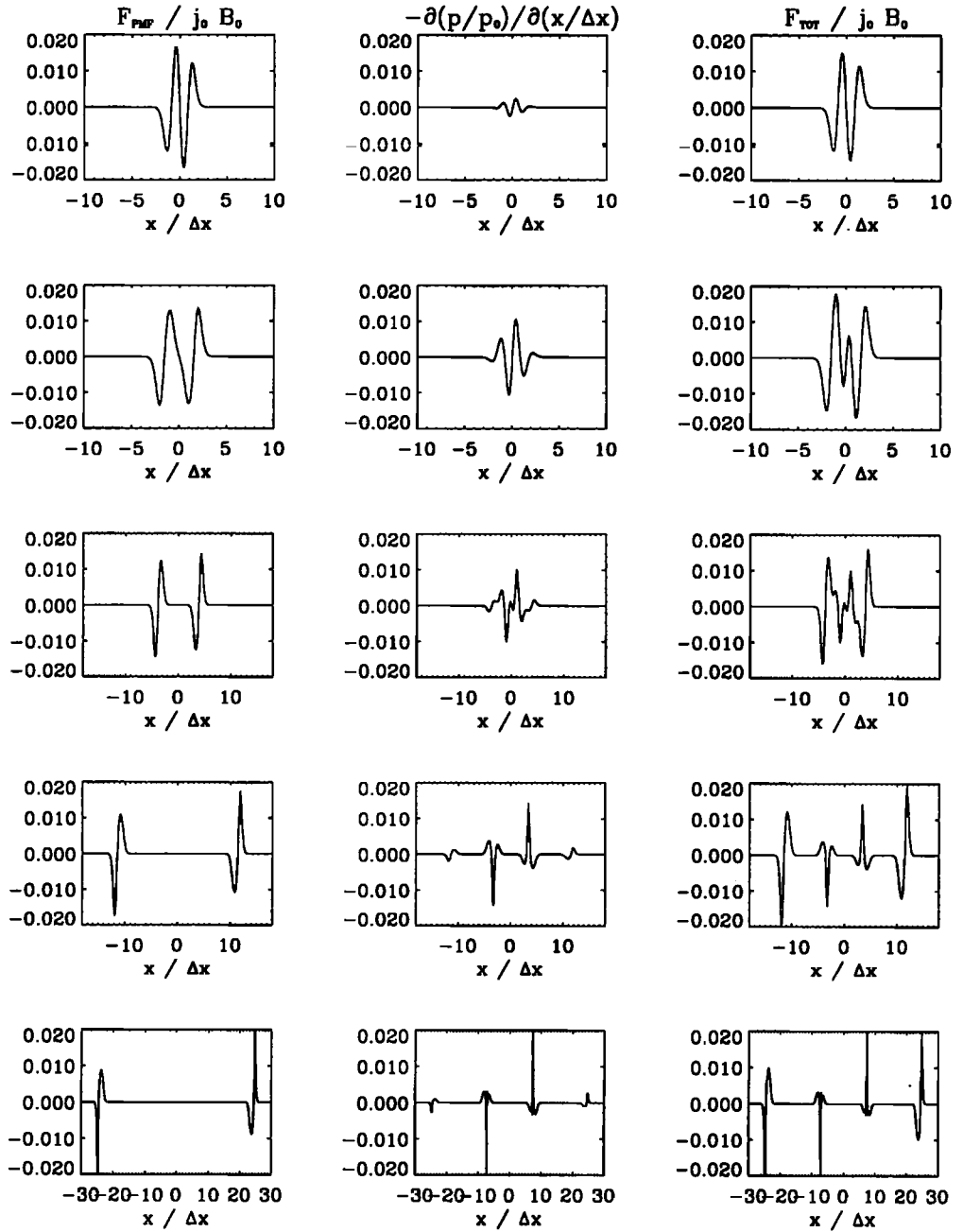
Figure 4.10: Plots of the ponderomotive force component, pressure force and total force parallel to the equilibrium field as functions of $x/\Delta x$ for five different times (from top to bottom) $V_A t/\Delta x$ = 0.75, 1.50, 3.75, 11.25 and 24.00. The parameters $a = 0.15$ and $\beta = 0.1$. Note that the range of the x-axis for each time can be different.

126
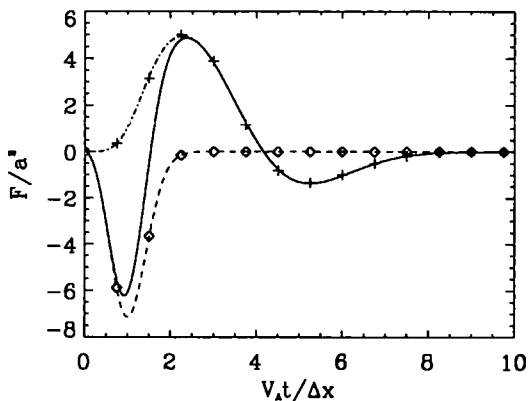
Figure 4.11: A plot of the component of the forces directed along the background magnetic field as a function of time at the position $x/\Delta x = 0.6$. Dashed line: quadratically nonlinear ponderomotive force (4.11). Dot-dashed line: quadratically nonlinear pressure force $-\partial p_2/\partial x$ calculated from the analytic result (4.68). Solid line: total quadratically nonlinear force. Diamonds: ponderomotive force $-(\partial B_z^2/\partial x)/2\mu_0$ from a numerical simulation. Crosses: pressure force $-\partial p/\partial x$ from a numerical simulation. We have taken a=0.1 and β=0.1.

origin as in the cold-plasma limit, we have two pairs of travelling pulses: two Alfvén and two slow pulses. The slow pulse is a longitudinal wave travelling at the sound speed and only perturbs hydrodynamic quantities, which basically makes it a sound wave. The amplitude of the slow pulse is of the order a^2. Its shape is not Gaussian and it is non-symmetrical.

Both types of pulses evolve. The slope of the pulse with a negative gradient in the direction of propagation steepens until it forms a shock. At the time $V_A t/\Delta x = 24.00$, we see that the slow pulse has steepened into a shock. This is before the Alfvén pulse has shocked and is because the slow pulse starts off with larger gradients than those of the Alfvén pulse. Because the numerical code is not equipped to capture a shock, the simulation ends there.

4.4.2 Quadratically nonlinear equations

We investigate the response of the plasma to the presence of Alfvén pulses by looking at Equations (4.1), (4.2) and (4.4) at order ϵ^2,

$$\frac{\partial \rho_2}{\partial t} = -\rho_0 \frac{\partial v_{x,2}}{\partial x} , \tag{4.48}$$

127

$$\rho_0 \frac{\partial v_{x,2}}{\partial t} + \frac{\partial p_2}{\partial x} = -\frac{1}{2\mu_0} \frac{\partial B_{z,1}^2}{\partial x} , \tag{4.49}$$

$$\frac{\partial p_2}{\partial t} + \gamma p_0 \frac{\partial v_{x,2}}{\partial x} = 0 . \tag{4.50}$$

Equations (4.49) and (4.50) combine into a forced slow (sound) wave equation for $v_{x,2}$:

$$\begin{aligned}
\left[\frac{\partial^2}{\partial t^2} - C_s^2 \frac{\partial^2}{\partial x^2} \right] v_{x,2} &= -\frac{1}{2\mu_0 \rho_0} \frac{\partial}{\partial t} \frac{\partial}{\partial x} B_{z,1}^2 \\
&= -\frac{1}{2} a^2 V_A^2 \frac{\partial}{\partial x} \left[V_A \frac{\partial}{\partial x} \mathcal{F}^2 \left(x + V_A t \right) - V_A \frac{\partial}{\partial x} \mathcal{F}^2 \left(x - V_A t \right) \right. \\
&\qquad \left. -2 \frac{\partial}{\partial t} \mathcal{F} \left(x + V_A t \right) \mathcal{F} \left(x - V_A t \right) \right] .
\end{aligned} \tag{4.51}$$

This equation is solved with the initial conditions $v_{x,2}(t = 0) = \partial v_{x,2}/\partial t(t = 0) = 0$. The homogeneous equation is the sound wave equation and has two solutions. The first and second solutions are constant along the characteristics $x + C_s t$ and $x - C_s t$ respectively. The driver terms on the right-hand side of Equation (4.51) depend on the characteristic variables $x \pm V_A t$, the first two terms of which drive the ponderomotive wings solution. The magnitude of these two terms does not decrease in time. The third term is the cross-ponderomotive contribution. Its magnitude decreases in time because the two Alfvén pulses separate. Again a Gaussian profile of the form (4.10) is taken for the function $\mathcal{F}$. The independent variables are transformed into

$$T = \sqrt{2} \frac{V_A t}{\Delta x} , \quad X = \sqrt{2} \frac{x}{\Delta x} . \tag{4.52}$$

With the use of the definitions

$$\mathsf{F}(g(X)) = \int_{-\infty}^{+\infty} e^{-ikX} g(X) dX , \quad \mathsf{F}^{-1}(G(k)) = \frac{1}{2\pi} \int_{-\infty}^{+\infty} e^{iXk} G(k) dk , \tag{4.53}$$

for the Fourier and inverse Fourier transformation respectively, Equation (4.51) is Fourier transformed in space to give:

$$\left[\frac{d^2}{dT^2} + \beta k^2 \right] \mathsf{F}(v_{x,2}) = \frac{1}{2} a^2 V_A \sqrt{\pi} \, e^{-\frac{k^2}{4}} \left[k^2 e^{ikT} - k^2 e^{-ikT} + 2ik \frac{de^{-T^2}}{dT} \right] . \tag{4.54}$$

Equation (4.54) is a linear ordinary differential equation which is treated as an initial-value problem. We find the response due to the first two driver terms (wings) and the third driver term (cross-ponderomotive driver) separately ($v_{x,2} = v_{x,2w} + v_{x,2c}$), with each

solution separately satisfying the initial boundary conditions. For the case of $\beta = 1$, the first two terms are resonant drivers.

The solution $v_{x,2w}$ to Equation (4.54) ,with only the first two driver terms on the right-hand side considered, is straightforward and we find:

$$
F(v_{x,2w}) = \begin{cases} \frac{a^2 V_A \sqrt{\pi}}{2(1-\beta)} e^{-\frac{k^2}{4}} \left[\frac{e^{i\sqrt{\beta}kT} + e^{-i\sqrt{\beta}kT}}{\sqrt{\beta}} + e^{-ikT} - e^{ikT} \right] & \beta \neq 1 \\ \frac{1}{4} a^2 V_A \sqrt{\pi} e^{-\frac{k^2}{4}} \left[e^{ikT} - e^{-ikT} - ikT \left(e^{ikT} + e^{-ikT} \right) \right] & \beta = 1 \end{cases}
$$
(4.55)

The inverse Fourier transformation of Expression (4.55) reduces this to

$$
\frac{v_{x,2w}}{V_A} = \begin{cases} \frac{a^2}{2(1-\beta)} \left[\frac{e^{-(X+\sqrt{\beta}T)^2} - e^{-(X-\sqrt{\beta}T)^2}}{\sqrt{\beta}} - e^{-(X+T)^2} + e^{-(X-T)^2} \right] & \beta \neq 1 \\ \frac{1}{4} a^2 \left[1 - T \frac{\partial}{\partial T} \right] \left[e^{-(X+T)^2} - e^{-(X-T)^2} \right] & \beta = 1 \end{cases}
$$
(4.56)

Solution (4.56) satisfies the initial conditions.

The solution $v_{x,2c}$ to the cross-ponderomotive driver is not so easily found. Equation (4.54) with only the third driver term on the right-hand side is Laplace transformed in time. We use the definitions

$$
\mathsf{L}\left(f(T) \right) = \int_0^\infty e^{-sT} f(T) dT \ , \ \mathsf{L}^{-1}\left(F(s) \right) = \frac{1}{2\pi i} \int_{\sigma - i\infty}^{\sigma + i\infty} e^{Ts} F(s) ds \ ,
$$
(4.57)

for the Laplace and inverse Laplace transformations respectively. We have:

$$
\left[s^2 + \beta k^2 \right] \mathsf{L}(F(v_{x,2c})) = a^2 V_A i k \sqrt{\pi} e^{-\frac{k^2}{4}} \mathsf{L} \left(\frac{d e^{-T^2}}{dT} \right) \ .
$$
(4.58)

The inverse Laplace transformation of the solution $\mathsf{L}(F(v_{x,2c}))$ is consequently taken:

$$
\begin{aligned} F(v_{x,2c}) &= a^2 V_A i k \sqrt{\pi} e^{-\frac{k^2}{4}} \frac{d e^{-T^2}}{dT} * \mathsf{L}^{-1} \left(\frac{1}{s^2 + \beta k^2} \right) \\ &= \frac{\sqrt{\pi} a^2 V_A}{2\sqrt{\beta}} e^{-\frac{k^2}{4}} \frac{d e^{-T^2}}{dT} * \left[e^{i\sqrt{\beta}kT} - e^{-i\sqrt{\beta}kT} \right] \ . \end{aligned}
$$
(4.59)

We use the Faltung Theorem:

$$
\mathsf{L}^{-1} \left[F(s) G(s) \right] = \mathsf{L}^{-1} \left[F(s) \right] * \mathsf{L}^{-1} \left[G(s) \right] \ ,
$$
(4.60)

where the operator $*$ is the convolution integral defined as:

$$
f(t) * g(t) = \int_0^t f(t') g(t - t') dt' \ .
$$
(4.61)

Finally the inverse Fourier transformation of Expression (4.59) is taken:

$$\frac{v_{x,2c}}{V_A} = \frac{a^2}{2\sqrt{\beta}} \frac{de^{-T^2}}{dT} * \left[e^{-\left(X+\sqrt{\beta}T\right)^2} - e^{-\left(X-\sqrt{\beta}T\right)^2} \right] . \tag{4.62}$$

The problem of the response of the velocity perturbation $v_{x,2c}$ to the cross-ponderomotive force is rewritten as the convolution integral (4.62). The function on the left-hand side of the operator corresponds to the temporal behaviour of the cross-ponderomotive force. This function reaches a maximum magnitude at $V_A t/\Delta x = 0.5$ and after that decays away. After the time t_{sep} it has decreased one order of magnitude compared with its maximum value. After some straightforward manipulations, Expression (4.62) is transformed into:

$$\frac{v_{x,2c}}{V_A} = -\frac{a^2}{2\sqrt{\beta}(1+\beta)} \left[e^{-(X+\sqrt{\beta}T)^2} - e^{-(X-\sqrt{\beta}T)^2} \right]$$
$$+ \mathcal{A}_+(T,X)\, e^{-\frac{\left(X+\sqrt{\beta}T\right)^2}{1+\beta}} + \mathcal{A}_-(T,X)\, e^{-\frac{\left(X-\sqrt{\beta}T\right)^2}{1+\beta}} , \tag{4.63}$$

with

$$\mathcal{A}_\pm(T,X) = \pm\frac{a^2\sqrt{\pi}}{2(1+\beta)} \frac{(X \pm \sqrt{\beta}T)}{\sqrt{1+\beta}} \left[\mathrm{erf}\left(\frac{\sqrt{\beta}X \mp T}{\sqrt{1+\beta}} \right) - \mathrm{erf}\left(\sqrt{\beta}\frac{X \pm \sqrt{\beta}T}{\sqrt{1+\beta}} \right) \right] . \tag{4.64}$$

The functions $\mathcal{A}_\pm$ are zero initially. If we fix the variables $X \pm \sqrt{\beta}T$, then the functions $\mathcal{A}_\pm$ have the basic form

$$\mathcal{A}_\pm(T, X \pm \sqrt{\beta}T = C) \sim C \left[\mathrm{erf}\left(\pm\sqrt{1+\beta}T + \frac{\sqrt{\beta}}{\sqrt{1+\beta}}C \right) - \mathrm{erf}\left(\frac{\sqrt{\beta}}{\sqrt{1+\beta}}C \right) \right] . \tag{4.65}$$

For times $T > (1+\beta)^{1/2}$, Expression (4.65) tends to a constant value, implying that the functions $\mathcal{A}_\pm$ are constant along the characteristics $X \pm \sqrt{\beta}T$ from that time onwards.

The two contributions $v_{x,2w}$ (4.56) and $v_{x,2c}$ (4.63) are added up. We do not consider the case of $\beta = 1$. The solution to Equation (4.51) is then

$$\frac{v_{x,2}}{V_A} = -\frac{a^2}{2(1-\beta)} \left[e^{-(X+T)^2} - e^{-(X-T)^2} \right] + \frac{a^2\sqrt{\beta}}{(1-\beta^2)} \left[e^{-(X+\sqrt{\beta}T)^2} - e^{-(X-\sqrt{\beta}T)^2} \right]$$
$$+ \mathcal{A}_+(T,X)\, e^{-\frac{\left(X+\sqrt{\beta}T\right)^2}{1+\beta}} + \mathcal{A}_-(T,X)\, e^{-\frac{\left(X-\sqrt{\beta}T\right)^2}{1+\beta}} . \tag{4.66}$$

Expression (4.66) has two contributions. The first contribution is the ponderomotive response travelling at the Alfvén speed with the Alfvén pulse. It has the shape of a Gaussian pulse of width $\Delta x/\sqrt{2}$.

The second contribution resembles, initially, the cross-ponderomotive solution of the cold-plasma limit. Mass is transported towards $x=0$, where the local density rises. This builds up gradients in the density and hence pressure. The pressure force resists the ponderomotive force. After the time t_{sep} the cross-ponderomotive force has decayed away in magnitude. The pressure force therefore pushes mass outwards away from the origin. The second contribution is the ponderomotive response travelling with the sound speed in the opposite direction away from the origin. Its shape is that of the linear combination of a Gaussian pulse of width $\Delta x/\sqrt{2}$ and the derivative of a Gaussian pulse of width $\Delta x/\sqrt{2(1+\beta)}$.

After substituting the previous expression into Equations (4.48) and (4.50), expressions for the density and pressure perturbation are found:

$$\frac{\rho_2}{\rho_0} = \frac{a^2}{2(1-\beta)}\left[e^{-(X+T)^2} + e^{-(X-T)^2}\right] - \frac{a^2}{(1-\beta^2)}\left[e^{-(X+\sqrt{\beta}T)^2} + e^{-(X-\sqrt{\beta}T)^2}\right]$$

$$- \frac{\mathcal{A}_+(T,X)}{\sqrt{\beta}}e^{-\frac{\left(X+\sqrt{\beta}T\right)^2}{1+\beta}} + \frac{\mathcal{A}_-(T,X)}{\sqrt{\beta}}e^{-\frac{\left(X-\sqrt{\beta}T\right)^2}{1+\beta}} + \frac{a^2}{1+\beta}e^{-X^2-T^2} , \qquad (4.67)$$

$$\frac{p_2}{p_0} = \gamma\frac{\rho_2}{\rho_0} . \qquad (4.68)$$

Figure 4.12 shows the spatial and temporal behaviour of the longitudinal velocity and density for the parameters $a=0.1$ and $\beta=0.1$, The full numerical result is well fitted by the quadratically nonlinear solutions (4.66) and (4.67). We shall see later on that the quadratrically nonlinear solution is not a good approximation of the nonlinear behaviour for all values of a and β.

The temperature perturbation is found from the ideal gas law (1.8):

$$\frac{T_2}{T_0} = (\gamma - 1)\frac{\rho_2}{\rho_0} . \qquad (4.69)$$

As β tends to zero, Expressions (4.63) and (4.67) tend to Expression (4.17). This is easily seen considering

$$\lim_{\beta \to 0} \mathcal{A}_\pm(X,T) = -\frac{1}{2}\sqrt{\pi}a^2\,X\,\text{erf}(T) . \qquad (4.70)$$

For the case of a finite plasma β, the density can never locally become infinite. Expression (4.67) does not contain a secular term.

In the cold-plasma limit, the time t_{sep} is defined as the time it takes for the cross-ponderomotive force to become one order of magnitude less than the force of the ponderomotive wings, in effect, the time needed for the two Alfvén pulses to split up. We claimed
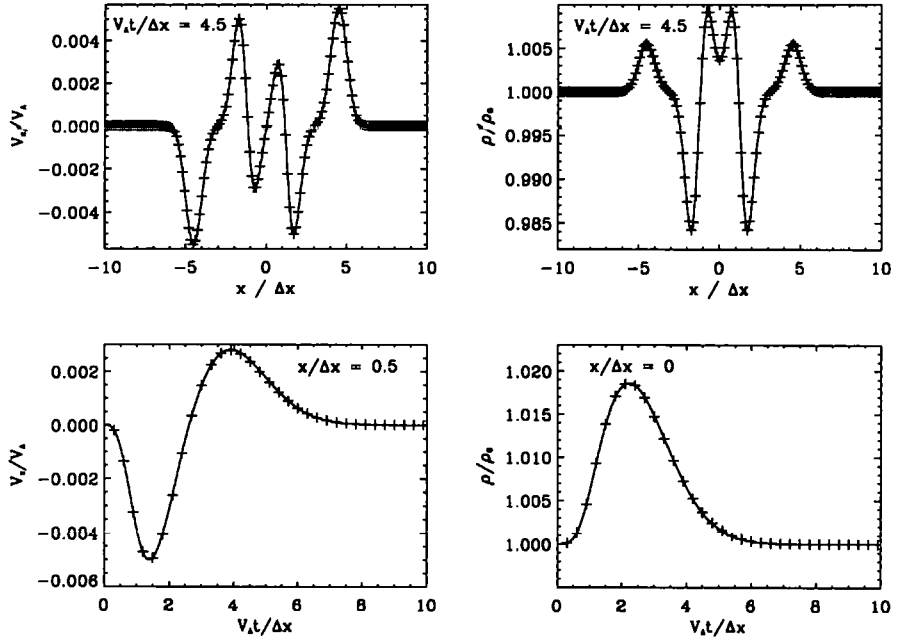
Figure 4.12: A plot of the longitudinal velocity v_x and density ρ. The top panels show the spatial behaviour at the time $V_A t/\Delta x$=4.5. The bottom panels show the early time evolution of the velocity v_x at $x/\Delta x$=0.5 and the density ρ at $x/\Delta x = 0$. The crosses are the full numerical result. The solid line is the quadratically nonlinear solution (4.17). We have chosen the parameters a=0.1 and β=0.1.

that as long as the density perturbation remains smaller in magnitude than the linear solution, before the time t_{sep}, the ponderomotive wing solution, which travels with the Alfvén speed, can be treated separately from the remaining solution which is stationary. This introduced an upper limit for the amplitude parameter a. In the case of a finite plasma β, this remaining solution travels at the sound speed. It therefore takes longer for the ponderomotive wing solution to separate from the remaining solution. In the time t, the Alfvén pulses have travelled a distance of $x_A = V_A t$ and the sound pulses have travelled a distance of $x_s = C_s t$. We impose that the distance between the two pulses is at least the distance $V_A t_{sep}$. Therefore we find the new separation time $t_{sep,\beta}$:

$$t_{sep,\beta} = \frac{V_A t_{sep}}{\mid V_A - C_s \mid} = \frac{t_{sep}}{\mid 1 - \sqrt{\beta} \mid} . \qquad (4.71)$$

The solid line in Figure 4.13 shows the upper limit for a for which Condition (4.18) is

132
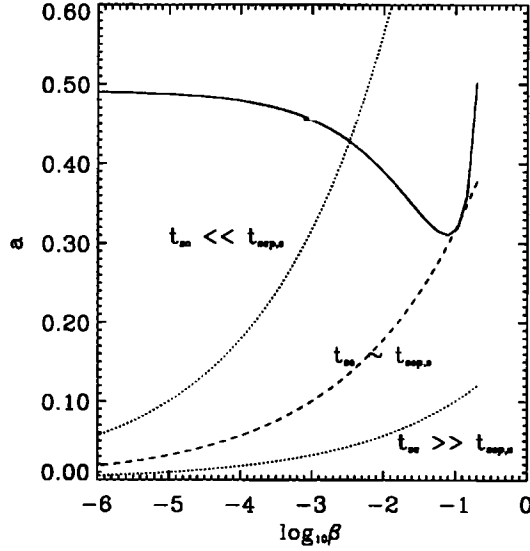
Figure 4.13: Solid line: A plot of the maximum amplitude a as a function of the parameter β for which the density perturbation (4.67) becomes of the same order as the linear solution (4.9) within the time span $t_{sep,\beta}$. Dashed line: The curve in the parameter space (β, a) where $t_{sep,s} = t_{sc}$. The dotted lines represent the curves where one time is one order of magnitude larger than the other.

satisfied, on substituting Expressions (4.67) and (4.9). For small values of β, the maximum amplitude tends to the value 0.48 as obtained in (4.19). When β increases, the maximum amplitude a decreases. This is because the maximum density in the time interval $[0, t_{sep,\beta}]$ increases with decreasing β. If a is much smaller than this upper limit, the nonlinear behaviour of the solution travelling at the Alfvén speed can be treated separately, at all times, from the remaining solution which travels at the sound speed.

4.4.3 Self-moderation of Alfvén pulses

The investigation of the self-moderation of a travelling Alfvén pulse of finite amplitude in a finite-plasma-β medium is a trivial extension of the cold-plasma case. We consider a single pulse as defined in Expression (4.23). From Expressions (4.66), (4.67) and (4.68), the corresponding quadratic nonlinear solution is easily found:

$$\frac{v_{x,2}}{V_A} = \mp\frac{1}{2(1-\beta)}\left(\frac{B_{z,1}}{B_0}\right)^2 , \tag{4.72}$$

133

$$\frac{\rho_2}{\rho_0} = \frac{1}{2(1-\beta)}\left(\frac{B_{z,1}}{B_0}\right)^2 , \tag{4.73}$$

$$\frac{p_2}{p_0} = \frac{\gamma}{2(1-\beta)}\left(\frac{B_{z,1}}{B_0}\right)^2 . \tag{4.74}$$

In all formulae from Expression (4.25) to (4.33), the finite-plasma-β result is obtained by substituting a by $a/(1-\beta)$. We find that the Alfvén pulse is governed by the Cohen-Kulsrud equation:

$$\frac{\partial B_{z,1}}{\partial \tau} \mp \frac{3}{4(1-\beta)}V_A \left(\frac{B_{z,1}}{B_0}\right)^2 \frac{\partial B_{z,1}}{\partial x} = 0 , \tag{4.75}$$

which has the implicit solution

$$\frac{B_{z,1}}{B_0} = a\,\mathcal{F}\left(x \pm V_A t \pm \frac{3}{4(1-\beta)}V_A \left(\frac{B_{z,1}}{B_0}\right)^2 \tau\right) . \tag{4.76}$$

The shock-formation time is equal to:

$$\tau_{sw} = \min\left\{\pm\frac{1}{\frac{3V_A}{4(1-\beta)}\left[\frac{\partial}{\partial x}\left(\frac{B_{z,1}}{B_0}\right)^2\right]_{\tau=0}}\right\} . \tag{4.77}$$

In the case of a Gaussian profile, the shock forms at the time $V_A\tau_{sw}/\Delta x = (2\sqrt{e}/3(1-\beta))a^{-2} \approx 1.1\,a^{-2}/(1-\beta)$. The effect of a finite plasma β compared with the cold-plasma limit, is to lengthen the time for the Alfvén pulse to shock. This expression is also equal to the typical length-scale $\ell/\Delta x$ over which the shock amplitude decreases, converting hydromagnetic wave energy into heat.

4.4.4 Self-moderation of sound pulses

The quadratic nonlinear solution (4.66) contains two slow pulses which travel away from the origin in opposite directions. The higher nonlinear terms on the right-hand sides of Equations (4.2) and (4.4) modify this result. Therefore we compare the time-scale of these higher nonlinear terms with the time-scale for the two sound pulses to separate.

The time it takes the pulses to separate by a distance L is equal to

$$t_{sep,s} = L/2C_s . \tag{4.78}$$

We impose a condition for the two slow pulses to have separated, that the distance L has to be at least equal to $V_A t_{sep}$. When $\beta \ll 1$, the sound pulses take longer to separate than
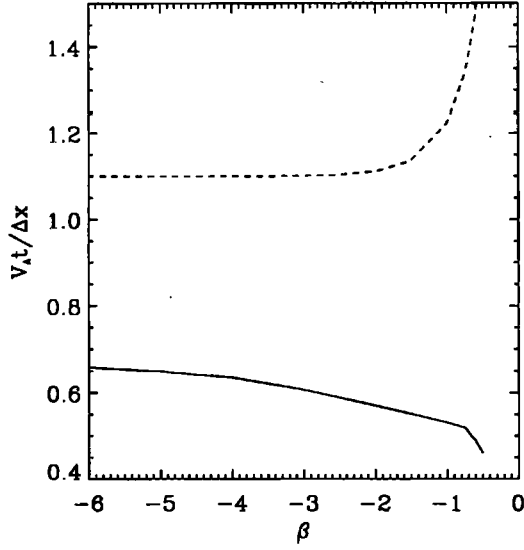
Figure 4.14: Solid line: A plot of the time $\tau_{ssw}a^2$ as a function of the parameter β. Dashed line: A plot of the time $\tau_{sw}a^2$ as a function of the parameter β.

the Alfvén pulses: $t_{sep,s} \gg t_{sep,\beta}$. By comparing the nonlinear inertial term $\rho_0 v_{x,2}\partial v_{x,2}/\partial x$ with the term $\rho_0\partial v_{x,2}/\partial t$, we see that it acts typically on a time-scale proportional to a^{-2}. This term is responsible for compressing or rarefying the velocity profile. In the cold-plasma limit it is responsible for establishing a shock at the centre at the time t_{sc} (4.41). We use this time-scale as the approximate typical time-scale for the higher nonlinear terms in the finite-plasma-β case. We have different behaviour according to how the two time-scales $t_{sep,s}$ and t_{sc} compare. This translates into the ordering of the parameters β and a with respect to each other and is easily seen by an order-of-magnitude comparison between the x-component of the pressure force and the nonlinear inertia:

$$\frac{\left|-\frac{\partial p}{\partial x}\right|}{\left|-\rho v_x\frac{\partial v_x}{\partial x}\right|} \sim \frac{\beta}{10a^4} \; . \tag{4.79}$$

The dashed line in Figure 4.13 shows the dependence of a upon β when $t_{sep,s} = t_{sc}$ and the dotted lines show when one time-scale is one order of magnitude larger than the other. If we keep the amplitude a constant and allow the parameter β to vary, we encounter several different cases. See Table 4.1 for a list of the typical times used in this chapter.

135

$t_{sep,s} \ll t_{sc}$ $(\beta \gg 10a^4)$

In this regime, the quadratic nonlinear solution (4.66) is a good approximation of the full solution when the two slow pulses have not yet separated. Therefore the evolution of both pulses can, at any time, be treated separately. We investigate the nonlinear evolution of a sound pulse. For $\beta < 1$, the time $t_{sep,\beta} < t_{sep,s}$. The ponderomotive force is therefore not further considered. We consider one slow pulse:

$$\frac{v_{x,2}}{V_A} = \pm a^2 \mathcal{G}\left(x \pm C_s t, \tau\right) , \tag{4.80}$$

where the function $\mathcal{G}(s)$ has the profile

$$\mathcal{G}(s) = \frac{1}{1+\beta} \left\{ -\frac{e^{-2\left(\frac{s}{\Delta x}\right)^2}}{2\sqrt{\beta}} + \sqrt{2\pi} \left(\frac{s}{\Delta x}\right) \left[\pm 1 - \mathrm{erf}\left(\sqrt{\frac{2\beta}{1+\beta}}\left(\frac{s}{\Delta x}\right)\right) \right] e^{-\frac{2}{1+\beta}\left(\frac{s}{\Delta x}\right)^2} \right\} . \tag{4.81}$$

The slow time τ represents the time-scale for the higher nonlinear terms. Equations (4.2) and (4.4), of order a^4, are:

$$\rho_0 \frac{\partial v_{x,4}}{\partial t} + \frac{\partial p_4}{\partial x} = -\rho_0 \frac{\partial v_{x,2}}{\partial \tau} - \rho_2 \frac{\partial v_{x,2}}{\partial t} - \rho_0 v_{x,2} \frac{\partial v_{x,2}}{\partial x} , \tag{4.82}$$

$$\frac{\partial p_4}{\partial t} + \gamma p_0 \frac{\partial v_{x,4}}{\partial x} = -\frac{\partial p_2}{\partial \tau} - v_{x,2} \frac{\partial p_2}{\partial x} - \gamma p_2 \frac{\partial v_{x,2}}{\partial x} . \tag{4.83}$$

When the secular terms on the right hand side of the previous set of equations are eliminated, the well-known simple wave equation for a one-dimensional sound wave in a polytropic gas is found (Landau & Lifshitz, 1959):

$$\frac{\partial v_{x,2}}{\partial \tau} + \frac{1}{2}\left(\gamma + 1\right) v_{x,2} \frac{\partial v_{x,2}}{\partial x} = 0 , \tag{4.84}$$

which has the implicit solution

$$\frac{v_{x,2}}{V_A} = a^2 \mathcal{G}\left(x \pm C_s t - \frac{1}{2}\left(\gamma + 1\right) v_{x,2}\tau\right) . \tag{4.85}$$

A discontinuity is formed in Solution (4.85) when the velocity profile has an infinite gradient. We call the earliest time for this to occur τ_{ssw}. It is straightforward, by following the same procedure as in Section 3.2, to find the time τ_{ssw} as

$$\tau_{ssw} = \min\left\{ -\frac{1}{\frac{1}{2}\left(\gamma + 1\right)\left[\frac{\partial v_{x,2}}{\partial x}\right]_{\tau=0}} \right\} . \tag{4.86}$$

136
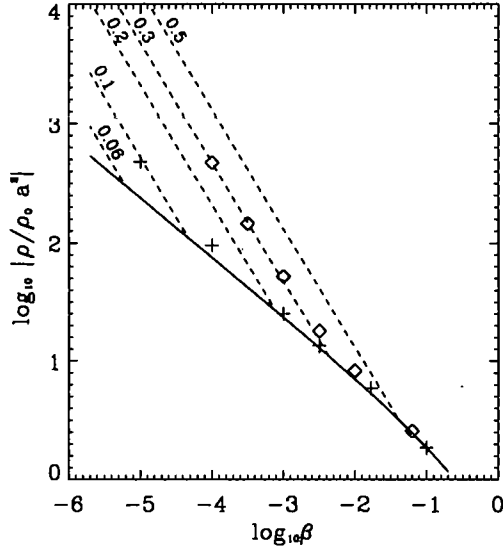
Figure 4.15: A logarithmic plot of the maximum density perturbation $\rho'/\rho_0 a^2$ as a function of the parameter β. Solid curve: maximum density derived from the quadratically nonlinear solution (4.67). Dashed curves: maximum density from Expression (4.91) for several values of the amplitude parameter a. Crosses: full numerical result for $a = 0.1$. Diamonds: full numerical result for $a = 0.3$.

The time τ_{ssw} does not depend on the sound speed. With the velocity $v_{x,2}$ of the form (4.80), it is only possible to determine the time τ_{ssw} numerically. Because the profile (4.81) depends on the sound speed, we investigate the dependency of the time $\tau_{ssw}a^2$ on the parameter β. This is shown is Figure 4.14. The shock time decreases with increasing β because the spatial profile exhibits larger gradients with increasing β.

$t_{sep,s} \gg t_{sc}$ $(\beta \ll 10a^4)$

In this regime the full behaviour is qualitatively the same as in the cold-plasma limit. The part of Solution (4.66) which travels at the sound speed remains approximately stationary in the time span t_{sc}. Therefore a large gradient in the longitudinal velocity at $x/\Delta x = 0$ is expected to form, producing, locally, a large enhancement in density which is larger than predicted by the quadratically nonlinear solution (4.67). We estimate the maximum density using Expressions (4.40) and (4.45) from the cold-plasma case. The pressure gradient is

137

then approximately equal to

$$-\frac{\partial p}{\partial x} \approx \frac{\gamma p_0 v_0'' t}{(1 + v_0'(t - t_{sep}))^2} \cdot \tag{4.87}$$

The functions v_0 and v_0'' are equal to Expression (4.37) and its second derivative respectively. The ratio between the pressure force and the nonlinear inertial term is then

$$\frac{\left|-\frac{\partial p}{\partial x}\right|}{\left|-\rho_0 v_x \frac{\partial v_x}{\partial x}\right|} \approx \frac{C_s^2 v_0'' t}{v_0 v_0'(1 + v_0'(t - t_{sep}))} \cdot \tag{4.88}$$

The earliest time (say, $t_{sc,\beta}$) at which this ratio is of order one is equal to:

$$t_{sc,\beta} = \min\left\{ \frac{1 - v_0' t_{sep}}{\frac{C_s^2 v_0''}{v_0 v_0'} - v_0'} \right\} \cdot \tag{4.89}$$

In the cold-plasma limit, the time $t_{sc,\beta}$ tends to the shock time t_{sc}. For Gaussian-shaped pulses, the time $t_{sc,\beta}$ is

$$t_{sc,\beta} = \frac{t_{sc}}{1 + \frac{6\beta}{\pi a^4}} \cdot \tag{4.90}$$

From Expression (4.45) the maximum density is estimated to be

$$\max\left\{ \frac{\rho}{\rho_0}(t_{sc,\beta}) \right\} \approx \frac{\pi a^4}{6\beta} \cdot \tag{4.91}$$

Because the density grows basically as t^{-1}, Expression (4.91) is quite sensitive to small changes in the time $t_{sc,\beta}$. Nevertheless the proportionality of $a^4 \beta^{-1}$ remains.

Figure 4.15 shows the maximum density (which always occurs at $x/\Delta x = 0$) as a function of the parameter β. The crosses and diamonds are the full numerical result for different values of a. The solid line represents the result derived from the quadratically nonlinear solution (4.67), which as expected, only fits the numerical result well in the regime where $\beta > 10a^4$. There the maximum density is approximately proportional to $a^2 \beta^{-1/2}$. When $\beta \ll 10a^4$, Expression (4.91) (dashed curves) fits the numerical result well. For a particular value of a, the transition between the two regimes occurs where the solid and dashed curves intersect. This corresponds approximately to $\beta \sim 10a^4$. This transition is very smooth. The result of the tendency of the nonlinear inertia to form a discontinuity in the velocity, is to increase the density more than was predicted by the quadratically nonlinear result. For a = 0.3 and $\beta = 10^{-3}$, we see that the maximum density is double that what the quadratically nonlinear solution predicted.

138

Even though the approximation used to obtain the velocity and density (as discussed in Section 3.3) starts diverging from the numerical result for $a > 0.2$, when looking at the dependency of the time t_{sc} on a, it is still a good approximation for higher values of a when determining the maximum value of the density. The numerical scheme runs into trouble when the gradient in the velocity becomes too large. The loss in accuracy in capturing this gradient is reflected by the failure to conserve energy. Hence the obtained results are invalidated. This occurs for $a=0.3$ when $\beta < 10^{-4}$.

Figure 4.15 can also be used to show the maximum temperature perturbation of the plasma, by using Expression (4.69).

Eventually the non-zero pressure force will counteract the plasma flow set up by the ponderomotive force and carry the density perturbation away from the centre. The spatial profile of the sound pulses will be very different from the shape (4.81).

The developed large gradient in velocity will also make viscous processes more important. We estimate the viscous stress, with the classical form (Landau & Lifshitz, 1959), to be:

$$\rho_0 \nu \frac{\partial^2 v_x}{\partial x^2} \approx \frac{\rho_0 \nu v_0''}{(1 + v_0't)^2} , \qquad (4.92)$$

where ν is the kinematic viscosity coefficient. The viscous stress will eventually become of order one as well, compared with the nonlinear inertia, but we do not consider it here because we assume the pressure force to be more important. This can be seen from comparing the pressure force to the viscous stress:

$$\frac{\left| \frac{\partial p}{\partial x} \right|}{\left| \rho_0 \nu \frac{\partial^2 v_x}{\partial x^2} \right|} \approx \frac{C_s^2 t}{\nu} = \left(\frac{V_A t}{\Delta x} \right) \left(\frac{V_A \Delta x}{\nu} \right) \beta = \left(\frac{V_A t}{\Delta x} \right) \mathrm{Re}\beta , \qquad (4.93)$$

with Re equal to the Reynolds number. In the solar corona, for example, the number Re β is of the order 10-100. The ratio (4.93) will become larger than unity on a much quicker time-scale than the process of the formation of the large velocity gradient. Therefore the pressure force is more important than the viscous stress in halting the secular density growth.

$t_{sep,s} \sim t_{sc}$ $(\beta \sim 10a^4)$

The time-scales for the nonlinear behaviour and the travel time of the slow pulses are similar. The slow pulses have nonlinearly evolved substantially before the time $t_{sep,s}$. Therefore the quadratically nonlinear solution (4.66) does not reflect the correct shape of the sound pulses
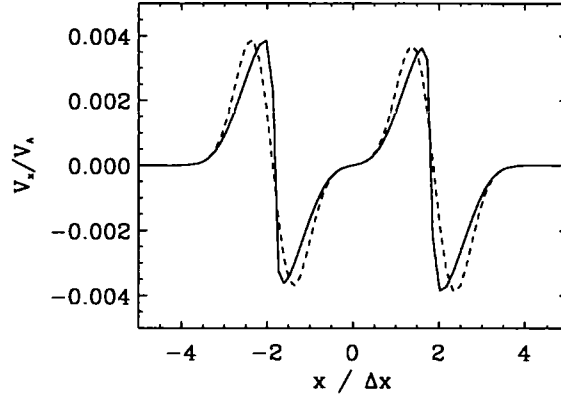
Figure 4.16: A plot of the spatial dependency of the velocity perturbation v_x, focused on the slow pulse contribution. The parameters are $a = 0.1$ and $\beta = 10^{-3}$. Solid curve: full numerical result. Dashed curve: quadratically nonlinear solution (4.66).

once the two slow pulses have split up. Figure 4.16 shows this clearly. The shape of the slow pulse is modified with respect to the profile (4.81). The early nonlinear interaction, when the two slow pulses have not yet separated, has increased the slope of the pulse in the direction of propagation and has flattened the others.

4.5   Elliptically polarized Alfvén pulses

In this section we consider an elliptically polarized Alfvén pulse for the same model and we shall show that this case is qualitatively the same as the case of a linearly polarized Alfvén pulse. We take plasma perturbations in the y- and z-directions into account. Equations (1.26)-(1.28) reduce to:

$$\frac{\partial \rho'}{\partial t} + \rho_0 \frac{\partial v'_x}{\partial x} = -\frac{\partial}{\partial x}(\rho' v'_x) , \tag{4.94}$$

$$-\rho' \frac{\partial v'_x}{\partial t} - \rho_0 v'_x \frac{\partial v'_x}{\partial x} = -\frac{1}{2\mu_0}\frac{\partial B'^2_\perp}{\partial x} - \rho'\frac{\partial v'_x}{\partial t} - \rho_0 v'_x \frac{\partial v'_x}{\partial x} - \rho' v'_x \frac{\partial v'_x}{\partial x} , \tag{4.95}$$

$$\rho_0 \frac{\partial \vec{v}'_\perp}{\partial t} - \frac{B_0}{\mu_0}\frac{\partial \vec{B}'_\perp}{\partial x} = -\rho'\frac{\partial \vec{v}'_\perp}{\partial t} - \rho_0 v'_x \frac{\partial \vec{v}'_\perp}{\partial x} - \rho' v'_x \frac{\partial \vec{v}'_\perp}{\partial x} , \tag{4.96}$$

$$\frac{\partial p'}{\partial t} + \gamma p_0 \frac{\partial v'_x}{\partial x} = -v'_x \frac{\partial p'}{\partial x} - \gamma p' \frac{\partial v'_x}{\partial x} , \tag{4.97}$$

$$\frac{\partial B'_x}{\partial t} = 0 , \tag{4.98}$$

140

$$\frac{\partial \vec{B}'_\perp}{\partial t} - B_0 \frac{\partial \vec{v}'_\perp}{\partial x} = -\frac{\partial}{\partial x}(v'_x \vec{B}'_\perp) \; . \tag{4.99}$$

The vectors $\vec{v}'_\perp$ and $\vec{B}'_\perp$ contain the components of the respective vector fields which are perpendicular to the equilibrium magnetic field. The system of equations (4.94)-(4.99) has basically the same form as the system of equations (4.1)-(4.6). The first-order terms in Equations (4.96) and (4.99) combine into an equation for elliptically polarized Alfvén pulses:

$$\left[\frac{\partial^2}{\partial t^2} - V_A^2 \frac{\partial^2}{\partial x^2}\right] \vec{B}_{\perp,1} = 0 \; . \tag{4.100}$$

We choose a solution of this equation which satisfies the initial conditions $\vec{B}_{\perp,1}(t=0) = 0$, $v_{y,1}(t=0) = 2a_y V_A \mathcal{F}_y(x,0)$ and $v_{z,1}(t=0) = 2a_z V_A \mathcal{F}_z(x,0)$:

$$\frac{B_{y,1}}{B_0} = a_y \left[\mathcal{F}_y(x + V_A t, \tau) - \mathcal{F}_y(x - V_A t, \tau)\right] \; ,$$

$$\frac{B_{z,1}}{B_0} = a_z \left[\mathcal{F}_z(x + V_A t, \tau) - \mathcal{F}_z(x - V_A t, \tau)\right] \; . \tag{4.101}$$

The second-order ponderomotive force $-(\partial B_{\perp,1}^2/\partial x)/(2\mu_0)$ is equal to the superposition of the second-order ponderomotive force of the y- and z-components of the Alfvén pulse, which each have the same form as Expression (4.11), but for a different pulse shape. The second-order longitudinal velocity and density perturbations are equal to the superposition of the responses to the ponderomotive force of each component. When the functions $\mathcal{F}_{y,z}$ have a typical pulse shape, we expect qualitatively the same results for the nonlinear evolution of the central density perturbation in the cold-plasma limit and the slow waves in a plasma of finite plasma β, as for the case of a linearly polarized Alfvén pulse. When the functions $\mathcal{F}_{y,z}$ both have the shape of a Gaussian pulse (4.10), the second-order ponderomotive force is exactly the same as Expression (4.11) with $a^2 = a_y^2 + a_z^2$. Consequently, the nonlinear behaviour of the longitudinal velocity and density perturbations is similar to the case of a linearly polarized Alfvén pulse.

Cohen & Kulsrud (1974) showed that the nonlinear evolution of a travelling elliptically polarized Alfvén pulse, either travelling in the positive or in the negative x-direction, of the form

$$\frac{B_{y,1}}{B_0} = a_y \mathcal{F}_y(x + V_A t, \tau) \; , \quad \frac{B_{z,1}}{B_0} = a_z \mathcal{F}_z(x + V_A t, \tau) \; , \tag{4.102}$$

is given by the Cohen-Kulsrud equation:

$$\frac{\partial \vec{B}_{\perp,1}}{\partial \tau} \mp \frac{1}{4(1-\beta)B_0^2} V_A \frac{\partial}{\partial x}\left(B_{\perp,1}^2 \vec{B}_{\perp,1}\right) = 0 \; . \tag{4.103}$$

Equation (4.103) reduces to the scalar Cohen-Kulsrud equation (4.75) when setting the y-component of the magnetic field perturbation to zero. Equation (4.103) is transformed into two equations for the direction $\vec{n} = \vec{B}_{\perp,1}/B_{\perp,1}$ and transverse field magnitude $b = B_{\perp,1}$:

$$\frac{\partial b}{\partial \tau} \mp \frac{3}{4(1-\beta)B_0^2}b^2\frac{\partial b}{\partial x} = 0 , \qquad (4.104)$$

$$\frac{\partial \vec{n}}{\partial \tau} \mp \frac{1}{4(1-\beta)B_0^2}b^2\frac{\partial \vec{n}}{\partial x} = 0 . \qquad (4.105)$$

The solution to Equation (4.104) is straightforwardly found to be:

$$b = \left[a_y^2\mathcal{F}_y^2\left(x + V_A t \pm \frac{3}{4(1-\beta)B_0^2}b^2\tau\right) + a_z^2\mathcal{F}_z^2\left(x + V_A t \pm \frac{3}{4(1-\beta)B_0^2}b^2\tau\right)\right]^{1/2} . \qquad (4.106)$$

We shall not consider Equation (4.105), which is more difficult to solve. Instead we consider the specific case that the functions $\mathcal{F}_y$ and $\mathcal{F}_z$ equal to each other. The components of the magnetic field perturbations are proportional to the transverse field magnitude b and the direction $\vec{n}$ is a constant. Equation (4.105) is trivially satisfied. The evolution of the transverse magnetic field perturbation components is easily derived from Expression (4.106):

$$\frac{B_{y,1}}{B_0} = a_y\mathcal{F}_y\left(x + V_A t \pm \frac{3}{4(1-\beta)B_0^2}b^2\tau\right) \ , \ \ \frac{B_{z,1}}{B_0} = a_z\mathcal{F}_z\left(x + V_A t \pm \frac{3}{4(1-\beta)B_0^2}b^2\tau\right) . \qquad (4.107)$$

A shock is formed when the spatial gradient becomes infinite for the first time. The method of derivation of this shock-formation time is identical to the one we have used before. We find that the shock-formation time for this case is the same as Expression (4.77) with the difference that the variable $B_{z,1}^2$ is replaced by B_1^2.

4.6 Discussion

This chapter puts forward a model for describing the weakly nonlinear behaviour of finite amplitude Alfvén pulses, linearly polarized in the z-direction. We showed that there is excellent agreement between the analytical and numerical results. Variations in the directions perpendicular to the background magnetic field direction are neglected. Perturbations of the plasma and the magnetic field in the z-direction are taken into account and those in the y-direction are taken to be zero. When, initially, a pulse in the transverse velocity or displacement is excited, two Alfvén pulses are created which travel in opposite directions

along the background magnetic field. The ponderomotive force that is associated with this magnetic disturbance is of order a^2. It excites longitudinal plasma flows and density perturbations. The ponderomotive force has three contributions: the first two terms contain only the magnetic perturbation of either the pulse travelling in the positive direction or of the pulse travelling in the negative direction (ponderomotive wings). The third term consists of a combination of the magnetic perturbation of both the pulses (cross-ponderomotive force). It decreases quickly to zero as the two pulses separate. We have studied the cold-plasma limit as well as the finite-plasma-β case, the former case giving us a first idea of the nonlinear processes involved.

We defined a time t_{sep} at which the cross-ponderomotive force becomes at least one order of magnitude smaller than the ponderomotive wings. We also took into account the spatial separation between part of the quadratically nonlinear solution travelling at the Alfvén speed (Alfvén wings) and the part travelling at the sound speed (slow wings). This modifies the time t_{sep} to $t_{sep,\beta}$. From the quadratically nonlinear solution, we found an upper limit for the amplitude parameter a for which the perturbed density remains of order a^2 for times earlier than time $t_{sep,\beta}$. Within this limit the problem is split up into three parts. The initial behaviour $(t < t_{sep,\beta})$ is well represented by the quadratically nonlinear solution. After that time the nonlinear evolution of the Alfvén wings and the slow wings can be treated separately.

For the Alfvén wings we found that the shape of the Alfvén pulse is governed by the scalar Cohen-Kulsrud equation. The leading side of the Alfvén pulse steepens into a shock front on a time-scale which is inversely proportional to a^2.

In the cold-plasma limit the slow wings reduce to a stationary profile, centred at the position $x = 0$. The excited plasma flow profile is such that it pushes mass together at the position $x/\Delta x = 0$. The nonlinear evolution of this flow profile is well represented by the solution of the forced simple wave equation (4.43), which we solved numerically by the method of characteristics. The profile forms a discontinuity in the flow velocity v_x on a time-scale which is proportional to a^2. At the position $x/\Delta x = 0$ the density becomes infinite. In reality this cannot occur. Eventually the kinetic pressure and viscosity, no matter how small they might be, will counteract the build-up of the large gradients in the flow velocity. It is therefore a necessary next step to include the plasma pressure in the calculations. In the finite-plasma-β case, we therefore see a build-up of pressure to counteract the established

143

inertia of the plasma. Two slow pulses are created which travel away from the centre. The further nonlinear evolution of the slow pulse is governed by the simple wave Equation (4.84). The part of the profile where the density decreases in the direction of propagation steepens into a shock on a time-scale which is inversely proportional to a^2. This shock time only depends on the plasma β through the shape of the sound pulse. We distinguished three cases according to how the time-scale of the nonlinear inertia and pressure force compare. When $t_{sep,s} \ll t_{sc}$, the nonlinear inertia has a negligible effect during the period before the two slow pulses have separated, so that the quadratically nonlinear solution describes the behaviour during that time. The nonlinear evolution of each slow pulse is treated separately. The maximum density is given by the maximum density of the quadratically nonlinear result (4.67). When $t_{sep,s} \gg t_{sc}$, the nonlinear inertia pushes mass together, at $x/\Delta x = 0$, until the density has become so high that the pressure force becomes of the same order as the nonlinear inertia term, resisting any further compression. The behaviour up to that point is well described by the results for the cold plasma. The maximum density is given by Expression (4.91), which is, in its range of applicability, higher than the maximum density calculated from the quadratically nonlinear Expression (4.67). When $t_{sep,s} \sim t_{sc}$ the nonlinear inertia term and the pressure force act on the same time-scale. The slow pulses have a modified shape compared with that given by the quadratically nonlinear solution. Before the time the two pulses split up, the gradient steepens in the direction of propagation.

For values of the amplitude parameter a close to, or exceeding, the upper limit (4.18), our model becomes inadequate, mainly because each Alfvén pulse is modified by the ponderomotive response of the other pulse and the cross-ponderomotive response.

When we consider elliptically polarized Alfvén pulses, the evolution of a central density perturbation in the cold-plasma limit and slow waves in a plasma of finite plasma β is qualitatively the same as for the case of linearly polarized Alfvén pulses because the second-order ponderomotive force has the same form in both cases.

144

Chapter 5

The dissipative instability of the MHD tangential discontinuity

5.1 Introduction

Coronal holes are the source of the steady, fast solar wind. This solar wind reaches typical speeds of 400-800 km s^{-1}. On the boundary between coronal holes and active regions, there exists the possibility of the development of a Kelvin-Helmholtz instability. In this chapter we model the coronal hole boundary as a tangential discontinuity. We study the stability of MHD surface waves on a single interface in the presence of a shear flow and weak dissipation.

Magnetohydrodynamic surface waves are intrinsically compressive (Wentzel, 1979). In the case of finite compressibility, there are two types of surface waves: 'slow' and 'fast' surface waves (e.g. Somasundaram & Uberoi, 1982). They have been studied in the incompressible limit (the sound speed considered infinite) by e.g. Chandrasekhar (1961) and Gerwin (1967). In this limit only one surface mode is present, which is often called the 'Alfvén ' surface wave (Roberts, 1981).

The compressible case has been investigated by Wentzel (1979), Roberts (1981), Hasegawa & Uberoi (1982), Somasundaram & Uberoi (1982), Miles & Roberts (1989), Jain & Roberts (1991) and González & Gratton (1990).

MHD surface waves can be dissipated, by for example, viscosity, heat conduction and radiation. Therefore they have been considered in the context of the coronal heating problem:

Ionson (1978), Wentzel (1979), Gordon & Hollweg (1983) Lee & Roberts (1986), Steinolfson *et al.* (1986).

The Kelvin-Helmholtz (K-H) instability occurs in plasmas whenever a shear flow is present, with a variance in the flow speed in the direction perpendicular to the flow. A commonly studied case is that of a discontinuity in the flow speed across the interface between two plasmas.

A well-developed branch of the study is that of MHD incompressible modes in relation to the K-H instability. Early work was done by Chandrasekhar (1961), Sen (1963) and Gerwin (1967). More recent work has been carried out by *e.g.* Mundie (1998). The incompressible limit, though, is not a good approximation of the solar coronal plasma.

The effect of compressibility in the context of the K-H instability has been investigated by Fejer (1964), Sen (1964), Duhau & Gratton (1973), Ruderman & Fahr (1993, 1995) and González & Gratton (1994a,b). Finite compressibility introduces new regimes of stability and instability. In particular, there is a regime of instability for which the threshold speed is below the threshold speed of the incompressible case (Fejer, 1964; Duhau & Gratton, 1973).

The MHD K-H problem is studied in a wide range of applications. Dungey (1955) first suggested that the boundary of the Earth's outer magnetosphere is subject to a K-H instability. Southwood (1968), Ong & Roderick (1972) and Lee & Olson (1980) and Pu & Kivelson (1983) worked further on this concept. The stability of the heliopause has been studied by Baranov (1990), Baranov, Fahr & Ruderman (1992), Ruderman & Fahr (1993) and Ruderman & Fahr (1995). The K-H instability has been studied in pulsar magnetosphere models by *e.g.* Ershkovich & Dolan (1985). Relativistic K-H models have been put forward by *e.g.* Turland & Scheuer (1976), Blandford & Pringle (1984) and Fiedler & Jones (1984), in connection with extragalactic jets.

In this chapter we include the effects of viscosity and thermal conduction in the problem of stability of MHD surface waves. MHD surface waves have been considered as a possible candidate for coronal heating, their energy being dissipated as heat, (*e.g.* Ionson, 1978; Gordon & Hollweg, 1983; Steinolfson *et al.*, 1986; Ruderman, 1991), but the damping rate has been found to be too small. Resonant absorption has been considered to enhance the damping rate of surface waves (*e.g.* Ionson, 1978; Rae & Roberts, 1982; Lee & Roberts, 1986; Davila, 1987; Hollweg, 1987a,b). Ruderman (1992) considered nonlinear surface wave-

steepening as another mechanism for increasing the damping rate.

Dissipation can also lead to instability, in the presence of an equilibrium flow, with a threshold speed below the K-H threshold (*e.g.* Cairns, 1979; Ruderman & Goossens, 1995; Ruderman *et al.*, 1996; Joarder *et al.*, 1997). Ruderman, Verwichte, Erdélyi & Goossens (1996) (hereafter called RVEG) showed, in both the incompressible and cold-plasma limits, that the presence of weak dissipation and an equilibrium plasma flow can lead to waves with growing amplitudes. Ryutova (1988), Ruderman & Goossens (1995) and Joarder *et al* (1997) use the concept of negative energy waves (Cairns, 1979; Ostrovskii *et al.*, 1986) to investigate flow instabilities. Hollweg *et al.* (1990), Yang & Hollweg (1991) and Tirry *et al.* (1998) studied the effect of an equilibrium flow on resonant absorption and found conditions for instability, which they related to the existence of negative energy waves.

In both the cold-plasma and incompressible limits, though, the contribution from thermal conduction vanishes. The solar corona is a plasma with a low plasma β. The cold-plasma limit is often chosen for modeling the corona. In this limit, though, thermal conduction, which is expected to be at least as important as viscosity for surface waves in the corona (Ruderman, 1991), cannot be included in a model for surface waves in a consistent manner. Therefore it is necessary to study the corona as a plasma with a low, but finite plasma β. In this chapter we shall use the dispersion relation derived by RVEG to investigate the influence of compressibility on the dissipative instability of waves on a single interface in a plasma of low but finite plasma β.

In Section 2 we present the model of a single interface and put forward the MHD equations used. In Section 3, we derive from the linearised MHD equations an ordinary differential equation in the velocity component normal to the interface, which governs the compressive MHD waves. We discuss the possible classes of wave behaviour. A dispersion relation, which governs the behaviour of surface waves in a weakly dissipative environment, is derived. In Section 4 we focus on a specific case, which is described by fewer free parameters, and which is put forward as a model of a coronal hole boundary. We shall show that the roots of the ideal dispersion relation are governed by a fourth-order polynomial in a quantity from which the frequency can be calculated. We discuss the surface wave solutions graphically (Chandrasekhar, 1961), before studying them analytically. The surface wave solutions are calculated by an expansion procedure from the cold-plasma solutions, where the plasma β is a small parameter. We study two intervals of K-H instability, and

the dissipative instability due to viscosity and thermal conduction. In Section 5, the analytical results are compared with the solution obtained by solving the dispersion relation numerically. We discuss the relevance of our results to the solar corona.

5.2 Model

A cartesian coordinate system (x, y, z) is used. We consider two plasmas, separated by an interface, which is a tangential discontinuity, defined as $z = \zeta(x, y, t)$ and which moves with a velocity $\vec{w}$. The subscripts '1' and '2' refer to plasma quantities at $z < \zeta$ and $z > \zeta$, as shown in Figure 5.1. Equilibrium plasma quantities are uniform and denoted with an index '0'. The interface has a zero thickness, which eliminates the possibility of resonant absorption (*e.g.* Ionson, 1978; Rae & Roberts, 1982; Lee & Roberts, 1986; Davila, 1987; Hollweg, 1987a,b; Goossens *et al.*, 1992; Tirry *et al.*, 1998). The equilibrium position of the interface is $z = \zeta_0 = 0$. We consider, in both media, equilibrium magnetic fields $\vec{B}_{0,1}$, $\vec{B}_{0,2}$ and equilibrium flows $\vec{v}_{0,1}$, $\vec{v}_{0,2}$, which are parallel to the discontinuity surface. A tangential discontinuity does not permit exchange of matter between the two media. It is then possible to have a density jump across the surface. The jump-conditions for a tangential discontinuity are given in Chapter 1.
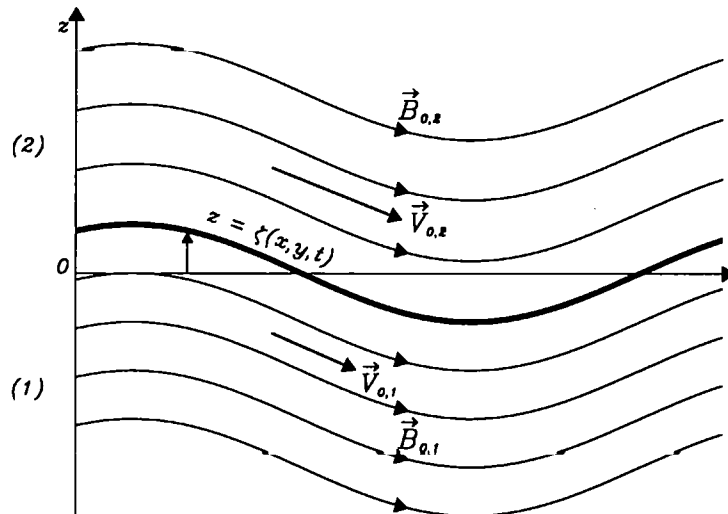
Figure 5.1: Model of the tangential discontinuity.

plasma quantity	active region	coronal hole
Temperature T (K)	2×10^6	1×10^6
Number density n (m^{-3})	3.0×10^{15}	1×10^{14}
Magnetic induction B (T)	5×10^{-3}	1×10^{-3}
Alfvén speed V_A (km s^{-1})	2.0×10^3	2.2×10^3
Plasma β	1.7×10^{-2}	0.7×10^{-2}
Scale height Λ (km)	1.2×10^5	0.6×10^5
Coulomb mean-free path ℓ (km)	1.1×10^2	7.6×10^2
Electron collision time τ_e (s)	1.3×10^{-2}	0.140
Ion collision time τ_i (s)	0.6	5.9
$\omega_{ce}\tau_e$	1×10^7	2×10^7
$\omega_{ci}\tau_i$	3×10^5	6×10^5
Kinematic viscosity coefficient ν (m^{2}s^{-1})	8×10^9	4.7×10^{10}
Thermal diffusivity χ(m^{2}s^{-1})	5×10^{11}	3×10^{11}
Reynolds number Re	1×10^4	0.2×10^4
Péclet number Pe	2.0×10^2	4×10^1
Magnetic Reynolds number R$_m$	1.4×10^{14}	5×10^{13}
Prandtl number Pr	2×10^{-2}	2×10^{-2}
Magnetic Prandtl number P$_m$	1×10^{10}	2×10^{10}
Pr β^{-1}	1.3	3.1

Table 5.1: Typical values of relevant physical quantities at the base of a coronal hole and an active region. Braginskii's (1965) formulae are used to calculate the transport coefficients. We take the Coulomb logarithm equal to 20 and choose a typical scale-length $L = 50000$ km to calculate the dimensionless numbers.

We consider a one-fluid model, *i.e.* we assume that the properties (temperature and density) of all species of particles are approximately the same. We discuss the relevant plasma quantities. Table 5.1 gives typical values of the relevant plasma quantities at the base of a coronal hole and an active region (Hollweg, 1985).

The plasma motion can be described by magnetohydrodynamics if the characteristic length-scale, L is much larger than the mean-free path of ions. Or, equivalently, if the wave period is much larger than the ion collision time τ_i. We neglect gravity and assume that

149

the plasmas are homogeneous, which is a valid assumption when the characteristic length-scale is much smaller than the coronal scale height Λ, which is defined as $k_b T / \bar{\mu} m_i g$ (g is the gravitational acceleration at the solar surface, and is equal to 274 ms^{-1}). The wave oscillation period P of a disturbance is approximately given by the ratio of its wave-length L and phase speed V_A. Our model is therefore, using Table 5.1, valid in the following spatial and temporal validity range (Ruderman, 1991):

$$\begin{cases} \ell \ll L \ll \Lambda & \Leftrightarrow & 10^2\,\text{km} \ll L \ll 10^5\,\text{km} \\ \tau_i \ll P \ll \frac{\Lambda}{V_A} & \Leftrightarrow & 1\,\text{s} \ll P \ll 50\,\text{s} \end{cases} . \tag{5.1}$$

There is an extensive set of coronal oscillations with periods in this range (see *e.g.* Laing, 1996 for observational references).

From Table 5.1 we see that in the corona the gyro-frequency ω_{ci} is much larger than the collision frequency τ_i^{-1}. The plasma is strongly magnetised. This means that ions spriral many times around the magnetic fieldline between collisions, which is then also true for electrons, since $\omega_{ce}\tau_e \gg \omega_{ci}\tau_i$. Therefore thermal, viscous and magnetic diffusion are expected to be highly anisotropic (Braginskii, 1965).

We discuss the importance of thermal, viscous and magnetic diffusion in the corona by considering the following dimensionless parameters. The Péclet number, Pe, measures the importance of inertial terms to thermal diffusion, and is in the corona of the order of unity or larger. The Reynolds number, Re, measures the importance of inertial terms to viscous diffusion. In the corona, Re is of order 10^4. The magnetic Reynolds number, R_m, measures the importance of inertial terms to magnetic diffusion and is in the corona of order 10^{14}. The Prandtl number, $Pr = Pe/Re$ compares viscous to thermal diffusion and is of order 10^{-2}. The magnetic Prandtl number, $P_m = R_m/Re$ compares viscous to magnetic diffusion and is of order 10^{10}. We conclude from the values of the numbers R_m and P_m that magnetic diffusion can be neglected in the corona, with the important exceptions of current sheets (Priest, 1982) or phase-mixing (Heyvaerts & Priest, 1983), and that thermal diffusion is the dominant diffusion mechanism of the three. Hollweg (1986) stated that viscosity may, in some circumstances, be important in the corona.

The importance of the Hall effect is measured by an order of magnitude comparison between the Hall term and the inductive electric field in Ohm's law (Priest, 1982), and is of order $\omega_{ce}\tau_e R_m$ (RVEG). In the corona, this number is of order 10^{-7} and we therefore conclude that the Hall-effect is, in general, not important in the corona.

In light of the previous discussion, we consider viscosity and thermal conduction as the dissipation mechanisms in our model. From the discussion in Chapter 1, we conclude that, in strongly magnetised plasmas, the compressive viscosity coefficient, ν_0, is much larger than the other viscosity coefficients. Furthermore, the thermal conduction coefficient parallel to the magnetic field, $\kappa_{\parallel}$, is much larger than the other thermal conduction coefficients. Therefore, the viscosity stress tensor and heat flux are given by Expressions (1.22) and (1.25) respectively. The viscosity stress tensor and heat flux are highly anisotropic. The form of the heat flux satisfies the jump-condition (1.38).

We assume that Re $\gg 1$ and Pe $\gg 1$, so that the dissipative terms in the MHD equations are small compared with the ideal terms. This implies that the length-scale over which a wave changes due to dissipation is much greater than the wave-length of wave-oscillation. This is the weakly dissipative regime.

We defined the parameter β, the ratio of the squared sound and Alfvén speeds, and it is of the order of the plasma β, which is of order 10^{-2} in the corona. The Reynolds and Péclet numbers are of order β^2 and β respectively. We shall show that the viscosity and thermal conduction are equally important and make contributions to the dimensionless equations of order β^2.

We define the thermal diffusivity χ as:

$$\chi = \frac{\kappa_{\parallel}}{\rho_0 C_p} , \tag{5.2}$$

which is proportional to $\kappa_{\parallel}$ and has the same units as the kinematic viscosity coefficient ν $(=\eta_0/\rho_0)$. The quantity C_p is the specific heat at constant pressure.

We consider the MHD equations (1.2)-(1.8). The equilibrium plasma quantities, ρ_0, $\vec{v}_0$, $\vec{B}_0$, p_0 and T_0, satisfy these equations trivially and also satisfy the jump-conditions (1.36)-(1.38), evaluated at the equilibrium position of the discontinuity surface, at $z = 0$, such that:

$$p_{0,1} + \frac{B_{0,1}^2}{2\mu_0} = p_{0,2} + \frac{B_{0,2}^2}{2\mu_0} . \tag{5.3}$$

We consider small perturbations from the equilibrium state which we denote with a prime (e.g. $\rho = \rho_0 + \rho'$ with $\mid \rho' \mid \ll \rho_0$). We consider the linearised MHD equations. Therefore terms in the system of equations (1.2)-(1.8), which are proportional to a product of perturbation quantities, are neglected. For example the expression of viscous heating, the last term in Equation (1.7), is neglected because its lowest-order contribution is proportional to
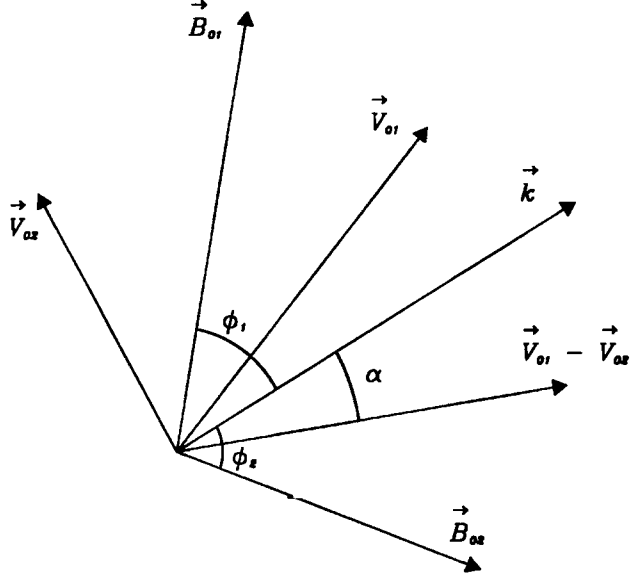
Figure 5.2: Definition of the angles α, ϕ_1 and ϕ_2.

$M = \frac{1}{2}\frac{|\vec{v}_{0,1}-\vec{v}_{0,2}|}{V_{A,2}}$	$\alpha = \left(\vec{k}, \widehat{\vec{v}_{0,1} - \vec{v}_{0,2}}\right)$
$\xi = M\cos\alpha$	$\eta = \frac{C_{s,1}}{C_{s,2}}$
$\phi_1 = \left(\widehat{\vec{k}, \vec{B}_{0,1}}\right)$	$\phi_2 = \left(\widehat{\vec{k}, \vec{B}_{0,2}}\right)$
$\beta_1 = \frac{C_{s,1}^2}{V_{A,1}^2}$	$\beta_2 = \frac{C_{s,2}^2}{V_{A,2}^2}$
$\epsilon = \frac{V_{c,2}^2}{k^2 V_{A,2}^2} = \frac{\beta_2}{1+\beta_2}$	$\delta = \left|\frac{\nu_1-\nu_2}{\nu_1+\nu_2}\right| = \left|\frac{\chi_1-\chi_2}{\chi_1+\chi_2}\right|$

Table 5.2: Non-dimensional parameters.

v'^2. We Fourier-analyse the perturbations in x, y and t, e.g.

$$\rho'(x,y,z,t) = \int\int\int_{-\infty}^{+\infty} dx\,dy\,dt\; \tilde{\rho}'(k_x, k_y, z, \omega)\, e^{i(\vec{k}.\vec{r}-\omega t)}\;, \qquad (5.4)$$

where $\vec{k} = (k_x,\, k_y,\, 0)$. We shall use the same symbols for the amplitudes of the perturbations as for the whole quantities in order to keep the notation simple.

At this point it is useful to introduce some more dimensionless parameters used in this chapter: the angles α, ϕ_1 and ϕ_2 (see Figure 5.2) are the angles between the wave vector $\vec{k}$ and the vectors $\vec{v}_{0,1} - \vec{v}_{0,2}$, $\vec{B}_{0,1}$ and $\vec{B}_{0,2}$ respectively. The parameters η, β_1 and β_2 are

ratios which involve the Alfvén and sound speeds. Using these parameters, each Alfvén or sound speed can be written as a function of the Alfvén speed $V_{A,2}$. The parameter M is a measure of the speed of the equilibrium flow. The parameter δ describes the difference in the value of the viscosity and thermal conduction coefficient between the two media. We can use the same δ for both cases because the viscosity and thermal conduction coefficients have the same proportionality with respect to the temperature and number density.

5.3 Dispersion relation for surface waves

5.3.1 Derivation of a linear equation for v_z'

The linearised set of MHD equations (1.2)-(1.8) are

$$i\Omega\rho' = \rho_0\vec{\nabla}.\vec{v}' \,, \tag{5.5}$$

$$\Omega\vec{v}_{\parallel}' = \frac{\vec{k}}{\rho_0}P' - \frac{B_0}{\mu_0\rho}\left(\vec{k}.\vec{b}_0\right)\vec{B}_{\parallel}' - \nu\left(\vec{b}_0\left(\vec{k}.\vec{b}_0\right) - \frac{1}{3}\vec{k}\right)Q \,, \tag{5.6}$$

$$\Omega v_z' = -\frac{i}{\rho_0}\frac{dP'}{dz} - \frac{B_0}{\mu_0\rho_0}\left(\vec{k}.\vec{b}_0\right)B_z' - \frac{i\nu}{3}\frac{dQ}{dz} \,, \tag{5.7}$$

$$\Omega p' = -iC_s^2\rho_0\vec{\nabla}.\vec{v}' - \frac{i\chi}{2}\left(\vec{k}.\vec{b}_0\right)^2\left(\gamma p' - C_s^2\rho'\right) \,, \tag{5.8}$$

$$\Omega\vec{B}_{\parallel}' = -i\vec{B}_0\vec{\nabla}.\vec{v}' - B_0\vec{v}_{\parallel}'\left(\vec{k}.\vec{b}_0\right) \,, \tag{5.9}$$

$$\Omega B_z' = -B_0 v_z'\left(\vec{k}.\vec{b}_0\right) \,, \tag{5.10}$$

$$\left(\vec{k}.\vec{B}'\right) = -\frac{dB_z'}{dz} \,, \tag{5.11}$$

$$\frac{p'}{p_0} = \frac{\rho'}{\rho_0} + \frac{T'}{T_0} \,. \tag{5.12}$$

The index '$\parallel$' refers to the vector components parallel to the equilibrium discontinuity surface, which is the xy-plane. The vector $\vec{b}_0$ is the unit vector in the direction of the equilibrium magnetic field. The quantity $\vec{\nabla}.\vec{v}'$ is equal to $i\vec{k}.\vec{v}' + dv_z'/dz$. The Doppler-shifted frequency, Ω, the total pressure perturbation, P', and the term, Q, are

$$\Omega = \omega - \left(\vec{k}.\vec{v}_0\right) \,, \tag{5.13}$$

$$P' = p' + \frac{\vec{B}'.\vec{B}_0}{\mu_0} \,, \tag{5.14}$$

$$Q = 3i\left(\vec{k}.\vec{b}_0\right)\left(\vec{b}_0.\vec{v}_{\parallel}'\right) - \vec{\nabla}.\vec{v}' \,. \tag{5.15}$$

153

Because we assumed that Re $\gg$ 1 and Pe $\gg$ 1, terms which are proportional to ν^2, χ^2, $\nu\chi$, or higher orders in ν or χ, are neglected in comparison with the other terms. At this point it is useful to introduce the Alfvén frequency $\Omega_A = V_A(\vec{k}.\vec{b}_0)$ and the cusp (or tube) frequency $\Omega_c = V_c(\vec{k}.\vec{b}_0)$.

The perturbed quantities need to satisfy the linearised version of the jump-conditions (1.36)-(1.38) across the discontinuity surface. Condition (1.35) is equal to:

$$[(\vec{v}' - \vec{w}')] \cdot \vec{1}_z = 0 , \qquad (5.16)$$

evaluated at $z = 0$. The square brackets denote the jump in the quantity across the discontinuity surface. The jump-condition (5.16) can be written as a function of the z-component of the linear displacement of the discontinuity surface ζ':

$$v'_{z,1}(z=0) = w'_z(z \to -0) = \frac{\partial \zeta'}{\partial t} + \left(\vec{v}_{0,1}.\vec{\nabla}\right)\zeta' = -i\Omega_1\zeta' ,$$

$$v'_{z,1}(z=0) = w'_z(z \to +0) = \frac{\partial \zeta'}{\partial t} + \left(\vec{v}_{0,2}.\vec{\nabla}\right)\zeta' = -i\Omega_2\zeta' . \qquad (5.17)$$

The linearized condition of continuity of stresses (1.37) across the discontinuity surface is equal to

$$\left[p' + \frac{\vec{B}'.\vec{B}_0}{\mu_0} + \hat{\Pi}'.\right]\vec{1}_z = 0 , \qquad (5.18)$$

evaluated at $z=0$. With Expression (1.22) we see that Condition (5.18) is equivalent to

$$\left[p' + \frac{\vec{B}'.\vec{B}_0}{\mu_0} + \frac{1}{3}\rho_0\nu Q\right] = 0 , \qquad (5.19)$$

evaluated at $z = 0$.

The magnetic field perturbation is eliminated from the components of the momentum equation (5.6) and (5.7) by using Expressions (5.9) and (5.10):

$$\rho_0\left(\Omega^2 - \Omega_A^2\right)\vec{v}'_\parallel = \Omega\vec{k}\left(P' + \frac{1}{3}\rho_0\nu Q\right) + i\rho_0\left(\vec{k}.\vec{b}_0\right)\vec{b}_0\left(V_A^2\vec{\nabla}.\vec{v}' + i\Omega\nu Q\right) , \quad (5.20)$$

$$\rho_0\left(\Omega^2 - \Omega_A^2\right)\vec{v}'_z = -i\Omega\frac{d}{dz}\left(P' + \frac{1}{3}\rho_0\nu Q\right) . \qquad (5.21)$$

The jump-conditions (5.17) and (5.19) and the system of equations (5.20)-(5.21) suggest that the normal velocity perturbation v'_z and the perturbation of the normal stresses $P' + \rho_0\nu Q/3$ are the useful quantities with which to describe the problem (Wentzel, 1979).

154

Expression for $\vec{\nabla}.\vec{v}'$

The quantity $\vec{\nabla}.\vec{v}'$ is calculated as a function of the total pressure perturbation P'. The kinetic pressure perturbation is calculated from Expressions (5.8) and (5.5):

$$p' = -\frac{i\rho_0 C_s^2}{\Omega^2}\left[\Omega - \frac{i}{2}(\gamma - 1)\left(\vec{k}.\vec{b}_0\right)^2 \chi\right]\vec{\nabla}.\vec{v}' . \qquad (5.22)$$

We assume that $\Omega \neq 0$. The magnetic pressure perturbation is calculated by projecting Expression (5.9) onto $\vec{B}_0/\mu_0$:

$$\frac{\vec{B}_0.\vec{B}'}{\mu_0} = -\frac{\rho_0 V_A^2}{\Omega}\left[i\vec{\nabla}.\vec{v}' + \left(\vec{b}_0.\vec{v}'\right)\left(\vec{k}.\vec{b}_0\right)\right] , \qquad (5.23)$$

with $\vec{b}_0.\vec{v}'$ calculated from Equation (5.20):

$$\left[\Omega^2 - \Omega_A^2 + 2i\Omega\left(\vec{k}.\vec{b}_0\right)^2 \nu\right]\left(\vec{b}_0.\vec{v}'\right) = \frac{\Omega\left(\vec{k}.\vec{b}_0\right)}{\rho_0}P' + i\left(\vec{k}.\vec{b}_0\right)\left[V_A^2 - \frac{2}{3}i\Omega\nu\right]\vec{\nabla}.\vec{v}' . \qquad (5.24)$$

An expression for the total pressure is found by summing up the expressions for the kinetic pressure (5.22) and magnetic pressure (5.23), from which the quantity $\vec{\nabla}.\vec{v}'$ is eliminated:

$$\vec{\nabla}.\vec{v}' = \frac{i\Omega^3}{\rho_0\left(V_A^2 + C_s^2\right)C}\left[1 - 2i\frac{\Omega_A^2}{\Omega^2}SK_\nu\nu + i\frac{D}{\Omega^4}K_\chi\chi\right]P' , \qquad (5.25)$$

which shows that the quantity $\vec{\nabla}.\vec{v}'$ is proportional to the total pressure perturbation (Lighthill, 1960). The quantities A, C, D, S, K_ν and K_χ are defined as:

$$A = \Omega^2 - \Omega_A{}^2 \ , \ \ C = \Omega^2 - \Omega_c{}^2 \ , \ \ S = \frac{D}{A\left(\Omega^2 - 3C_s^2\left(\vec{k}.\vec{b}_0\right)^2\right)} \ ,$$

$$D = \Omega^4 - \left(C_s^2 + V_A^2\right)k^2\Omega^2 + C_s^2 V_A^2 k^2\left(\vec{k}.\vec{b}_0\right)^2 \equiv \left(\Omega^2 - \Omega_I^2\right)\left(\Omega^2 - \Omega_{II}^2\right) \ ,$$

$$K_\nu = \frac{\Omega A\left(\Omega^2 - 3C_s^2\left(\vec{k}.\vec{b}_0\right)^2\right)^2}{3\left(C_s^2 + V_A^2\right)CD} \ , \ \ K_\chi = \frac{(\gamma - 1)\Omega^3 AC_s^2\left(\vec{k}.\vec{b}_0\right)^2}{2\left(C_s^2 + V_A^2\right)CD} . \qquad (5.26)$$

The product SK_ν does not depend on the term A and the solution $\Omega^2 = \Omega_A^2$ is still allowed. Expression (5.25) is singular at $\Omega^2 = \Omega_c^2$. The thermal conductive contribution K_χ is equal to zero when the wave propagates perpendicular to the equilibrium magnetic field and it tends to zero in the incompressible and cold-plasma limits.

The quantity Q (5.15), using Expressions (5.24) and (5.25), is written as a function of the total pressure perturbation as well:

$$Q = -3i\frac{SK_\nu}{\rho_0}P' . \qquad (5.27)$$

Equation for v_z'

Expressions (5.25), for $\vec{\nabla}.\vec{v}'$, and (5.24), for $\vec{b}_0.\vec{v}'$ are eliminated from the system of equations (5.20)-(5.21) in favour of the normal velocity perturbation v_z' and stress $P' + \rho_0 \nu Q/3$:

$$\rho_0 A \frac{dv_z'}{dz} = -i\Omega\Gamma^2 \left(P' + \frac{1}{3}\rho_0\nu Q\right) , \qquad (5.28)$$

$$-i\Omega\frac{d}{dz}\left(P' + \frac{1}{3}\rho_0\nu Q\right) = \rho_0 A\, v_z' , \qquad (5.29)$$

with

$$\Gamma^2 = \Gamma_0^2\left(1 + i\nu K_\nu + i\chi K_\chi\right) , \quad \Gamma_0^2 = -\frac{(\Omega^2 - \Omega_I^2)\,(\Omega^2 - \Omega_{II}^2)}{(C_s^2 + V_A^2)\left(\Omega^2 - \Omega_c{}^2\right)} . \qquad (5.30)$$

Elimination of P' from Equations (5.28) and (5.29) leads to a single second-order ordinary differential equation for v_z':

$$\left(\Omega^2 - \Omega_A^2\right)\left(\frac{d^2 v_z'}{dz^2} - \Gamma^2 v_z'\right) = 0 . \qquad (5.31)$$

This equation has the same form as in the ideal case (Roberts, 1981; Miles & Roberts, 1989), with the one difference that the function Γ^2 is modified by dissipative terms which, by assumption, are small compared with the ideal terms.

The importance of the viscous contribution compared with the thermal conductive contribution is measured by the ratio:

$$\frac{K_\nu}{K_\chi} \sim \frac{\nu\Omega^2}{\chi C_s^2 k^2} \sim \frac{\nu}{\chi\beta} = \frac{Pr}{\beta} . \qquad (5.32)$$

We see that this ratio is proportional to $Pr\,\beta^{-1}$ rather than Pr. For coronal conditions, we see from Table 5.1 that $Pr\,\beta^{-1} \approx 1$ (Ruderman, 1991), so that viscosity and parallel thermal conduction are of equal importance. We have assumed that $\Omega \sim kV_A$.

When $\Omega^2 = \Omega_A^2$, the first factor of Equation (5.31) is equal to zero. This describes an Alfvén wave. Equations (5.25) and (5.29) show that this mode is incompressible and does not perturb the total pressure. The normal component of the velocity perturbation v_z' is arbitrary (Roberts, 1981). We shall not consider this solution in our further analysis.

The second factor of Equation (5.31) is a second-order ordinary differential equation describing magneto-acoustic waves. This can be seen by rewriting the expression for Γ_0^2 in (5.31) as a second-order polynomial for Ω^2,

$$\Omega^4 - (C_s^2 + V_A^2)(k^2 - \Gamma_0^2)\Omega^2 - C_s^2(k^2 - \Gamma_0^2)\Omega_A^2 = 0 , \qquad (5.33)$$

which, when $\Gamma_0^2 < 0$, has the form of the dispersion relation (1.60), for magneto-acoustic waves propagating in a homogeneous medium. The wave modes governed by this equation are intrinsically compressive. It can be seen from Expressions (5.25), (5.28) and (5.29) that $\vec{\nabla}.\vec{v}' = 0$, implies that $P' = 0$ and hence $v'_z = 0$. Therefore these types of wave modes are only present when $\vec{\nabla}.\vec{v}' \neq 0$.

Equating the second term of Equation (5.31) to zero gives the solution

$$v'_{z,1} = -i\Omega_1 \left(a_{+,1}\, e^{\Gamma_1 z} + a_{-,1}\, e^{-\Gamma_1 z} \right) \quad , \quad v'_{z,2} = -i\Omega_2 \left(a_{+,2}\, e^{\Gamma_2 z} + a_{-,2}\, e^{-\Gamma_2 z} \right) \quad , \quad (5.34)$$

in each medium respectively. The coefficients $a_{\pm,1,2}$ are the integration constants, which are determined by imposing the linearised version of the jump-conditions (5.17) and (5.19) across the interface. The total pressure perturbation and the quantity Q are eliminated from the jump-condition (5.19) in favour of the normal velocity perturbation by using Equations (5.27) and (5.28):

$$\left[-\frac{1}{i\Omega} \frac{\rho_0 A}{\Gamma^2} \frac{dv'_z}{dz} \right] = 0 \ . \qquad (5.35)$$

Imposing the jump-conditions (5.17) and (5.35) on the solution (5.34) at $z=0$, we obtain the following system of equations for the constants $a_{\pm,1,2}$:

$$\begin{pmatrix} a_{+,1} \\ a_{-,1} \end{pmatrix} = \frac{\Gamma_1}{2\rho_{0,1}A_1} \begin{pmatrix} F & G \\ G & F \end{pmatrix} \begin{pmatrix} a_{+,2} \\ a_{-,2} \end{pmatrix} \ , \qquad (5.36)$$

with the functions F and G defined as:

$$F(\omega, k) = \frac{\rho_{0,1}A_1}{\Gamma_1} + \frac{\rho_{0,2}A_2}{\Gamma_2} \ , \quad G(\omega, k) = \frac{\rho_{0,1}A_1}{\Gamma_1} - \frac{\rho_{0,2}A_2}{\Gamma_2} \ . \qquad (5.37)$$

This system of equations describes surface modes and the reflection and transmission of propagating waves. A similar system of equations to (5.36) has been considered in an ideal plasma by *e.g.* González & Gratton (1991,1994a). To the system of equations (5.36) we add the boundary condition that the solution v'_z remains finite in the limit of z tending to infinity.

5.3.2 Classification of wave modes

Behaviour of the function Γ

From the conditions $Re \gg 1$ and $Pr\, Re \gg 1$ follows that $\mid \nu K_\nu \mid \ll 1$ and $\mid \chi K_\chi \mid \ll 1$. Therefore, the behaviour of $\Re(\Gamma^2)$ is approximately that of $\Re(\Gamma_0^2)$. Without loss of generality,

157
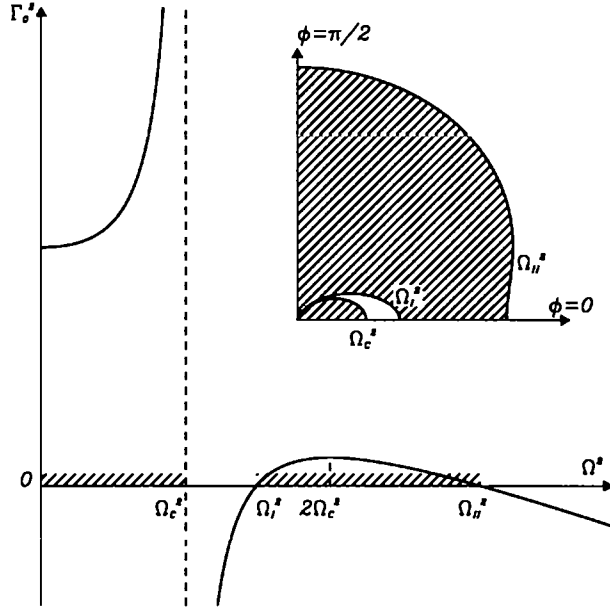
Figure 5.3: Plot of the function Γ_0^2 as a function of Ω^2 for the angle $\phi = 0$ and the inset plot shows the loci of $\Gamma_0^2=0$ as a function of the angle ϕ. The shading denotes regions where $\Gamma_0^2 > 0$. In both plots $\beta = 0.7$.

we choose $\Re(\Gamma) \geq 0$, which means that also $\Re(\Gamma_0) \geq 0$. The function $\Re(\Gamma)$ is approximately equal to:

$$\Gamma = \sqrt{\Gamma_0^2} \left(1 + \frac{1}{2} i\nu K_\nu + \frac{1}{2} i\chi K_\chi\right) . \tag{5.38}$$

We have different types of mode according to the sign of the function Γ_0^2. The function Γ_0 has been studied by many authors (e.g. Roberts & Webb, 1978; Wentzel, 1979; Somasundaram & Uberoi, 1982; Cally, 1986) in an ideal, static medium and extended to include an equilibrium flow by e.g. González & Gratton (1994a,b).

The function $\Re(\Gamma_0^2)$ has a singularity at $\Omega^2 = \Omega_c^2$, and has roots at $\Omega^2 = \Omega_I^2$ and $\Omega^2 = \Omega_{II}^2$. It is positive in the domain $(-\infty, \Omega_c^2) \cup (\Omega_I^2, \Omega_{II}^2)$ and negative elsewhere. This is illustrated in Figure 5.3, which plots the function Γ_0^2 as a function of Ω^2. This plot is in principle the same as Figure 1.2, which plots the frequency ω^2 as a function of $k_z = \Im(\Gamma_0)$. The sign of Γ_0 only changes when the frequency ω is real.

Firstly, we consider the case in which the frequency ω is real, which means that the function Γ_0^2 is real as well. The case $\Gamma_0^2 > 0$ ($\Re(\Gamma_0) > 0$) corresponds to a solution that

does not propagate in the z-direction. Instead, the ideal solution of the normal velocity perturbation v_z' consists of a linear combination of exponentially decaying and growing solutions. In order for the velocity to be finite for z tending to infinity, the integration constant in front of the relevant diverging term is set equal to zero. The function Γ^{-1} is the penetration depth of the mode in the z-direction. We call the cases $\Omega^2 \in (0, \Omega_c^2)$ and $\Omega^2 \in (\Omega_I^2, \Omega_{II}^2)$ the 'slow' and 'fast' evanescent perturbations respectively (González & Gratton, 1994a). The dissipative contribution ensures that $\Im(\Gamma) \neq 0$, so that a small oscillatory modulation is added to the evanescent profile of the ideal solution.

The case $\Gamma_0^2 < 0$ ($\Re(\Gamma_0) = 0$) corresponds to a wave propagating in the z-direction. The ideal solution for the normal velocity perturbation v_z' consists of a linear combination of an incoming and outgoing plane wave. From comparing Equations (5.33) and (1.61), and Figures 5.3 and 1.2, we see that the cases $\Omega^2 \in (\Omega_c^2, \Omega_I^2)$ and $\Omega^2 > \Omega_{II}^2$ correspond to a slow and fast branch respectively for waves propagating in an ideal, homogeneous medium. The fact that $\Re(\Gamma_0) = 0$ does not imply that $\Re(\Gamma) = 0$. The dissipative contribution adds to the ideal solution a small modulation to the oscillatory behaviour, which is either evanescent or growing. In order for the velocity to be finite as z tends to infinity, the integration constant in front of the relevant diverging term is set equal to zero.

Secondly we consider the case in which the frequency ω is complex. The function Γ_0^2 is complex and $\Re(\Gamma_0) > 0$. The ideal solution of the normal velocity perturbation v_z' consists of a linear combination of terms which are either evanescent or growing, modulated by an oscillation. In a similar manner to that of the previous case, the part of the solution that diverges as z tends to infinity is eliminated by setting the relevant integration constant equal to zero. Because the dissipative contribution is considered small compared with the ideal terms, it does not transform an evanescent term into a diverging term and vice versa.

Two interesting limits are the incompressible and cold-plasma limits, which correspond to the ratio C_s/V_A tending to infinity and zero respectively. In the incompressible limit, the quantity $\Gamma_0^2 = k^2$ and the characteristic frequencies are equal to $\Omega_c^2 = \Omega_A^2$, $\Omega_I^2 = 0$ and $\Omega_{II}^2 \to \infty$. Because Γ_0^2 is always positive, waves with a real frequency have, in the ideal limit, always an evanescent profile in the z-direction. This result is expected, if we consider the discussion of linear wave-types in Chapter 1. We showed that the magneto-acoustic waves are governed by the quantity $\vec{\nabla}.\vec{v}'$. From Expression (5.25) we see that this is equal to zero in the incompressible limit.

159

In the cold-plasma limit, the quantity $\Gamma_0^2 = (V_A^2 k^2 - \Omega^2)/V_A^2$ and the characteristic frequencies are equal to $\Omega_c^2 = 0$, $\Omega_I^2 = 0$ and $\Omega_{II}^2 = V_A^2 k^2$. Waves with a real frequency, in the ideal limit, propagate in the z-direction when $\Omega^2 > V_A^2 k^2$ and are evanescent in the z-direction when $\Omega^2 < V_A^2 k^2$. From Expression (5.24) we see, by using Expressions (5.25), (5.26) and (5.27), that the component of the velocity parallel to the equilibrium magnetic field, $\vec{b}_0.\vec{v}$, is in the limit $C_s \to 0$, equal to:

$$\left[\Omega^2 - \Omega_A^2 + 2i\Omega \left(\vec{k}.\vec{b}_0\right)^2 \nu\right] \left(\vec{b}_0.\vec{v}'\right) = \frac{2}{3}i\frac{\left(\vec{k}.\vec{b}_0\right)^2 \Omega^2}{\rho_0 V_A^2}\left[1 + \frac{\Omega_A^2}{\Omega^2}\right] \nu\, P' , \qquad (5.39)$$

which is proportional to the viscosity coefficient. Therefore $\vec{b}_0 \vec{v} \ll 1$ in the cold-plasma limit, if $\text{Re} \gg 1$.

The wave modes

We consider the case where the frequency ω is real. Depending on the sign of the functions $\Gamma_{0,1}^2$ and $\Gamma_{0,2}^2$, we have different kinds of wave modes.

Firstly, we consider the case $\Gamma_{0,1}^2 > 0$ and $\Gamma_{0,2}^2 > 0$ ($\Re(\Gamma_{0,1}) > 0$ and $\Re(\Gamma_{0,2}) > 0$). The constants $a_{-,1}$ and $a_{+,2}$ are set to zero to fulfill the boundary condition at infinity. The normal velocity perturbation v_z' is localised around $z = 0$, with an evanescent profile in each medium. This is a surface wave, but not in the strict sense as described by Roberts (1981), because the small dissipative contribution in the function $\Gamma_{1,2}$, adds a oscillatory modulation with a large wave-length to the evanescent behaviour (Van der Linden & Goossens, 1991). From the set of equations (5.36), we conclude that the frequency of the solution needs to fulfill the dispersion relation $F(\omega, k) = 0$. It is clear from looking at this, (5.37), that a real root of the dispersion relation needs to fulfill the extra condition that $A_1 A_2 < 0$ or equivalently

$$\left(\Omega_1^2 - \Omega_{A,1}^2\right)\left(\Omega_2^2 - \Omega_{A,2}^2\right) < 0 . \qquad (5.40)$$

A consequence of the previous condition is that wave propagation perpendicular to the equilibrium magnetic field is not permitted ($\vec{k}.\vec{b}_{0,1} = \vec{k}.\vec{b}_{0,2} = 0$). Roberts (1981) calls the surface waves 'fast' or 'slow' surface waves respectively, according to the condition:

$$\begin{cases} \text{fast} & : \quad C_1 C_2 > 0 \quad \Leftrightarrow \quad \left(\Omega_1^2 - \Omega_{c,1}^2\right)\left(\Omega_2^2 - \Omega_{c,2}^2\right) > 0 \\ \text{slow} & : \quad C_1 C_2 < 0 \quad \Leftrightarrow \quad \left(\Omega_1^2 - \Omega_{c,1}^2\right)\left(\Omega_2^2 - \Omega_{c,2}^2\right) < 0 \end{cases} . \qquad (5.41)$$

We shall adopt this terminology in the further analysis. The frequency of the slow surface wave is not necessarily below the cusp frequency of both media. The names 'slow' and 'fast' are not be confused with the fast and slow magneto-acoustic waves in an ideal, homogeneous medium, which we described in Chapter 1.

In the incompressible, ideal limit, we have shown that waves with a real frequency always have an evanescent profile in the z-direction. We therefore only have surface wave solutions (besides the Alfvén waves). Furthermore a solution needs to satisfy Condition (5.40). This implies that only when $C_1 C_2 < 0$, do surface waves exist. From Condition (5.41) we see that these waves are slow surface wave.

In the cold-plasma limit, we have evanescent behaviour when $\Omega_1^2 < V_{A,1}^2 k^2$ and $\Omega_2^2 < V_{A,2}^2 k^2$. A surface wave solution also needs to satisfy Condition (5.40). Because both the cusp frequencies are equal to zero, there is only one interval where surface waves, which are fast surface waves, exist.

Secondly, when $\Gamma_{0,1}^2 < 0$ and $\Gamma_{0,2}^2 < 0$ ($\Re(\Gamma_{0,1}) = 0$ and $\Re(\Gamma_{0,2}) = 0$), we have propagating waves in both media. We first discuss the ideal case. Because the solution (5.34) remains finite in the limit of z tending to infinity, there is no restriction on the integration constants $a_{\pm,1,2}$. We can treat problems as wave transmission and reflection or radiation of waves from the interface. We can calculate the frequencies for which the wave mode is totally transmitted (zeros of the reflection coefficient) or radiated (singularities of the reflection coefficient) (e.g. González & Gratton, 1994a).

When weak dissipation is included, clearly there are problems with the previous formalism. The condition $\Re(\Gamma_0) = 0$ does not imply that $\Re(\Gamma) = 0$. Therefore, the solution (5.34) consists of two propagating waves, each modulated by a growing or evanescent profile with a large penetration depth, which is proportional to $\Re(\Gamma)^{-1}$ This means that the relevant integration constant has to be set to zero to ensure that the perturbation remains finite as z tends to infinity. It depends on the sign of the function $\nu K_\nu + \chi K_\chi$ in each medium, and therefore on the various free parameters, as to which integration constant is eliminated. From the set of equations (5.36) we are restricted to imposing the dispersion relation $F(\omega, k) = 0$ or $G(\omega, k) = 0$, depending on which integration constants are eliminated.

In order to properly study the interaction of propagating waves at an interface in dissipative media, it is better to treat the problem as an initial-value problem. The case of Γ_0^2

positive in one medium and negative in the other, which describes wave tunneling in the ideal case, meets the same problems.

We shall therefore only focus on the case of surface waves.

Note on the definition of the types of surface waves

Authors do not use the same definition for naming slow and fast surface modes. Another definition in use is the following. Pu & Kivelson (1983) use a definition more closely related to the fast and slow magneto-acoustic waves and call surface modes with Ω^2 in the domain of the non-propagating lower branch ($\Omega^2 \in (0, \Omega_c^2) \cup (\Omega_I^2, 2\Omega_c^2)$) and the upper branch ($\Omega^2 \in (2\Omega_c^2, \Omega_{II}^2)$) of Equation (5.33) the 'quasi-slow' (s') and 'quasi-fast' (f') branches respectively. The value $\Omega^2 = 2\Omega_c^2$ corresponds to the position of a local maximum of the function Γ_0^2. When considering both media, four possible types of modes are possible for each intersection between the quasi-fast and quasi-slow mode domains: the $s' - s'$, $s' - f'$, $f' - s'$ and $f' - f'$ surface modes.

The terminology of Alfvén surface wave is misleading. In the strict sense, surface Alfvén waves do not exist because, as we can see from Equation (5.31) and from the discussion in Chapter 1, the Alfvén wave solution is separate from the equation governing the magneto-acoustic waves. Various limits of the magneto-acoustic surface waves, for which $\vec{\nabla}.\vec{v}' \ll 1$ and $P' \ll 1$, are called 'Alfvén surface waves'.

Most commonly, the slow surface wave in the incompressible limit is called the 'Alfvén surface wave' (*e.g.* Roberts, 1981; Somasundaram & Satya Narayanan, 1987; Ruderman & Goossens, 1995). The incompressible limit implies that $\vec{\nabla}.\vec{v}' \ll 1$, but is not equal to zero.

Wentzel (1979) calls the fast surface wave, in the cold-plasma limit, with propagation nearly perpendicular to the equilibrium magnetic field, an 'Alfvénic surface wave'. When $| \vec{k}.\vec{b}_0 | \ll k$, we see from the component of Equation (5.20) perpendicular to the equilibrium magnetic field, that $P' \ll 1$ and hence $\vec{\nabla}.\vec{v}' \ll 1$. The surface wave does not exist when $\vec{k}.\vec{b}_0 = 0$, because Condition (5.40) is not satisfied. Uberoi (1982) investigated the conditions for the existence of this type of Alfvén surface wave, taking into account the necessary conditions $\Gamma_0^2 > 0$ and (5.40).

We conclude that it is important to be aware of these different definitions for the types of surface waves when interpreting statements on their behaviour.

162

5.3.3 Dispersion relation for surface waves

We write the first dispersion relation in Equations (5.37), using Expression (5.38), in the form

$$F(\omega, k) = F_I(\omega, k) + iF_\nu(\omega k) + iF_\chi(\omega, k) = 0 , \qquad (5.42)$$

where

$$F_I(\omega, k) = \frac{\rho_{0,1} A_1}{\Gamma_{0,1}} + \frac{\rho_{0,2} A_2}{\Gamma_{0,2}} , \qquad (5.43)$$

$$F_\nu(\omega, k) = \frac{\rho_{0,1}\nu_1 A_1}{2\Gamma_{0,1}} K_{\nu,1} + \frac{\rho_{0,2}\nu_2 A_2}{2\Gamma_{0,2}} K_{\nu,2} , \qquad (5.44)$$

$$F_\chi(\omega, k) = \frac{\rho_{0,1}\chi_1 A_1}{2\Gamma_{0,1}} K_{\chi,1} + \frac{\rho_{0,2}\chi_2 A_2}{2\Gamma_{0,2}} K_{\chi,2} . \qquad (5.45)$$

Terms which are proportional to ν^2, χ^2 or $\nu\chi$ have been neglected in keeping with the assumption of weak dissipation. This dispersion relation has been obtained by Verwichte (1995) and RVEG. The term $F_I(\omega, k)$ is the ideal part of the dispersion relation. The static version of the ideal dispersion relation $F_I(\omega, k) = 0$ has been investigated by *e.g.* Kruskal & Schwartzschild (1954), Wentzel (1979) and Roberts (1981). The version of the ideal dispersion relation $F_I(\omega, k) = 0$ which includes flow has been investigated in the context of the Kelvin-Helmholtz instability by *e.g.* Chandrasekhar (1961), Sen (1963,1964), Fejer (1964), Gerwin (1967) and Duhau & Gratton (1973) and more recently by *e.g.* Pu & Kivelson (1983), Ruderman & Fahr (1993, 1995) González & Gratton (1994a,b) and Mundie (1998).

The terms $F_\nu(\omega, k)$ and $F_\chi(\omega, k)$ are the parts of the dispersion relation due to viscosity and thermal conduction respectively.

We are interested in their effect on the stability of the tangential discontinuity. We take the wavenumber k real and let the frequency ω be complex. The dispersion relation is then solved for ω as a function of the remaining parameters. If the wave frequency, ω, is real for a certain configuration, it is said to be stable. If a frame of reference can be found for which the frequency ω is purely imaginary and positive, the wave is said to be monotonically unstable. If the frequency is complex with a non-zero real part and a positive imaginary argument, the wave is said to be overstable. If ω has a negative imaginary argument, the wave is said to be damped.

In the previous section we discussed the conditions for the existence of surface waves.

For these waves, the solution of the ideal part of the dispersion relation (5.42) needs to satisfy the following conditions:

$$\Re(\Gamma_{0,1}) > 0 \quad , \quad \Re(\Gamma_{0,2}) > 0 \;,$$

$$\Gamma_{0,1}^2 > 0 \;\Leftrightarrow\; \Omega_1^2 \in (0, \Omega_{c,1}^2) \cup (\Omega_{I,1}^2, \Omega_{II,1}^2) \;,$$

$$\Gamma_{0,2}^2 > 0 \;\Leftrightarrow\; \Omega_2^2 \in (0, \Omega_{c,2}^2) \cup (\Omega_{I,2}^2, \Omega_{II,2}^2) \;,$$

$$\left(\Omega_1^2 - \Omega_{A,1}^2\right)\left(\Omega_2^2 - \Omega_{A,2}^2\right) \;<\; 0 \;. \tag{5.46}$$

We classified the surface waves into slow and fast modes, as put forward in Expression (5.41). We shall give a discussion of these modes in a diagram which plots the solution Ω_2 as a function of Ω_1 (Chandrasekhar, 1961) and show that for certain values of the equilibrium flow speed, the surface wave solutions have double roots, signifying marginal stability. We discuss the intervals of K-H instability.

Dissipative growth-rate

We shall not solve the dispersion relation (5.42) directly. Because our model is weakly dissipative, we expect the dissipative contribution to the solution of the dispersion relation (5.42) to be small compared with the ideal contribution. Therefore, the solution of (5.42) is expanded in a Taylor series about the solution of the ideal dispersion relation. Using regular perturbation theory (Nayfeh, 1985), we find:

$$\omega \approx \overline{\omega} + i\omega_d \;, \quad \omega_d \approx -\frac{F_\nu(\overline{\omega}, k) + F_\chi(\overline{\omega}, k)}{\frac{\partial F_I}{\partial \omega}\big|_{\omega=\overline{\omega}}} \;, \tag{5.47}$$

where $\overline{\omega}$ is a root with multiplicity one of the ideal dispersion relation $F_I(\overline{\omega}, k) = 0$. This approximation is only valid if $|\omega_d| \ll |\overline{\omega}|$. Regimes which for which the root $\overline{\omega}$ is marginally stable do not satisfy this requirement because the multiplicity of the root is increased and the derivative $\partial F_I/\partial \omega(\omega = \overline{\omega})$ is zero. In that case higher order terms need to be included in the Taylor series of the ideal dispersion relation. Hollweg *et al.* (1990) and Yang & Hollweg (1991) followed the same procedure when studying resonant absorption of surface waves in a dissipative plasma with an equilibrium flow.

If $\Re(\omega_d)$ is positive, then the configuration is dissipatively overstable and the solution grows exponentially in time on a time scale proportional to ω_d^{-1}. It is of interest to investigate if domains in parameter space, which are stable in the ideal case, could be overstable in

the weakly dissipative regime. Approximation (5.47) is valid in these domains. Because we linearised the MHD equations with respect to the transport coefficients, the growth-rate of the dissipative instability is directly proportional to the coefficients ν and χ. The qualitative behaviour of the dissipative instability does not depend on the magnitude of the transport coefficient, but on the difference between the two media, represented by the parameter δ, defined in Table 5.2.

We consider the case for which dissipation is only present in Medium '2' ($\nu_1 = \chi_1 = 0$) and we choose a frame of reference which moves with this medium ($\Omega_2 = \omega$). The surface waves are assumed to be stable in an ideal plasma. For this case, the dissipative growth-rate (5.47) is positive if

$$A_2 \left(K_{\nu,2} \, \nu_2 + K_{\chi,2} \, \chi_2 \right) \frac{\partial F_I}{\partial \omega} \bigg|_{\omega = \overline{\omega}} < 0 \quad \Leftrightarrow \quad \overline{\omega} \frac{\partial F_I}{\partial \omega} \bigg|_{\omega = \overline{\omega}} < 0 \;, \qquad (5.48)$$

which corresponds to the condition for the existence of negative energy waves derived by Cairns (1979). The idea is that a wave of negative energy gains, through dissipation, energy from the flow, and grows in amplitude. The concept of negative energy waves is a useful tool for investigating the criteria for the existence of flow instabilities such as K-H, resonant flow (Hollweg *et al.* 1990; Yang & Hollweg, 1991; Tirry *et al.* 1998), dissipative (Ruderman & Goossens, 1995; RVEG; Joarder *et al.*, 1997) or explosive instabilities (Craik & Adam, 1979; Joarder *et al.*, 1997). The presence of negative energy waves is also linked to the presence of a backward propagating wave, *i.e.* the oscillation frequency of a wave is Doppler shifted, such that it has changed sign, and hence propagates in the direction opposite to that in the absence of an equilibrium flow (Craik, 1985).

Using Condition (5.48), the criterion for the existence of dissipative instability ,in weakly dissipative plasmas, can be investigated without actually having to include dissipation itself (Joarder *et al.*, 1997). The choice of the frame of reference is important for the concept of negative energy waves and when dissipation is included in both media, it is not clear which frame of reference to choose (RVEG) so that Expression (5.47) may be transformed to the form of Expression (5.48). Therefore we shall not use the concept of negative energy waves and calculate the dissipative growth-rate directly. We shall show that the appearance of instability is connected to the existence of a backward propagating wave.

General characteristics of the ideal dispersion relation

The ideal dispersion relation F_I depends, besides the frequency ω, on eight independent parameters. We choose the following set of non-dimensional parameters, which have been defined in Table 5.2: the angles α, ϕ_1 and ϕ_2, the Alfvén Mach number $2M$, the ratio of sound speeds η, and the ratios of squared sound and Alfvén speeds β_1, β_2 In principle γ can also have a different value in each medium, but we do not consider this here. The plasma quantities can be written as functions of these parameters with the use of the equilibrium condition (5.3) and the definitions in Table 5.2:

$$\frac{\rho_{0,1}}{\rho_{0,2}} = \eta^{-2} \frac{\beta_1}{\beta_2} \frac{2\beta_2 + \gamma}{2\beta_1 + \gamma} , \tag{5.49}$$

$$\frac{p_{0,1}}{p_{0,2}} = \frac{\beta_1}{\beta_2} \frac{2\beta_2 + \gamma}{2\beta_1 + \gamma} , \tag{5.50}$$

$$\left(\frac{B_{0,1}}{B_{0,2}}\right)^2 = \frac{2\beta_2 + \gamma}{2\beta_1 + \gamma} . \tag{5.51}$$

For an ideal, static interface Roberts (1981) and Jain & Roberts (1991) showed, by transforming Expression (5.37) into an equation for the wave phase speed ω/k, that the phase speed does not explicitly depend on k:

$$(1-R)\left(\frac{\omega}{k}\right)^2 + 2(v_{0,1} - v_{0,2})\cos\alpha\left(\frac{\omega}{k}\right) + (v_{0,1} - v_{0,2})^2\cos^2\alpha - V_{A,1}^2\cos^2\phi_1 + RV_{A,2}^2\cos^2\phi_2 = 0 , \tag{5.52}$$

with $R = \rho_{0,2}\Gamma_1/\rho_{0,1}\Gamma_2$ a function of the phase speed ω/k. So wave modes which satisfy the dispersion relation are non-dispersive, because of a lack of a natural length-scale in our model.

Figure 5.4 shows, as an illustrative example, a plot of $\Re(\varpi)$, which is the solution of $F_I(\varpi) = 0$, in a Ω_1-Ω_2 diagram for a certain choice of parameters (Chandrasekhar, 1961). Only the modes with purely real frequencies are shown. Stable surface modes exist in the non-shaded parts of the boxed regions in the plot. Using the terminology of Roberts (1981), we call the solution branches for which either $-\Omega_{c,1} < \Omega_1 < \Omega_{c,1}$ or $-\Omega_{c,2} < \Omega_2 < \Omega_{c,2}$, the slow surface waves (s). The remaining solution branches are the fast surface waves (f).

We can always choose a frame of reference such that the surface wave solutions in the first and second quadrants have an opposite direction of propagation, and likewise for the second and fourth quadrants.
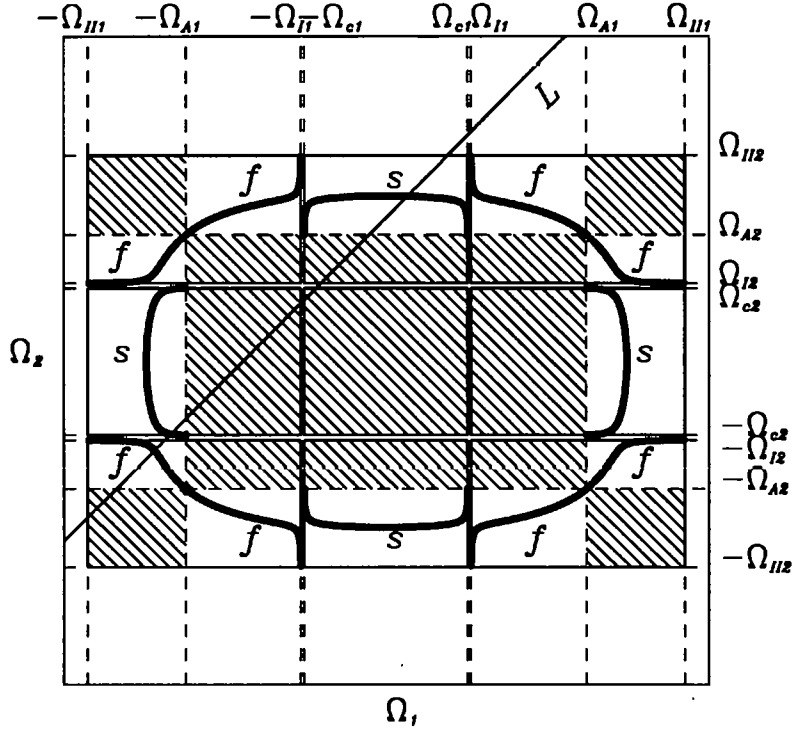
Figure 5.4: Plot of $\Re(\varpi)$, which is the solution of $F_I(\varpi) = 0$, in a Ω_1-Ω_2 diagram with $\beta_1 = 0.5$, $\beta_2 = 0.2$, $\alpha = \phi_1 = \phi_2 = 45$ degrees and $\eta = 1.0$. The quantities in the plot have been normalised by a factor $kV_{A,2}$. The boxed areas are the intervals where both $\Gamma_{0,1}^2 > 0$ and $\Gamma_{0,2}^2 > 0$. The shaded areas represent the regions where Condition (5.40) is not satisfied. The intersections between the line L: $\Omega_2/kV_{A,2} = \Omega_1/kV_{A,2} + 2M\cos\alpha$ and the solutions represent the stable surface wave solutions for a fixed value of parameter M. The letters 'f' and 's' denote the fast and slow surface waves. The solution branches have been calculated numerically.

For a fixed value of the flow velocity difference, the non-spurious roots of $F_I^2 = 0$ are the intersections between the line L: $\Omega_2/kV_{A,2} - \Omega_1/kV_{A,2} + 2M\cos\alpha$ and the solution curves. We discuss the different cases with increasing M.

When $M = 0$, which corresponds to a static interface, two oppositely propagating fast surface wave solutions exist, namely $\omega = \vec{k}.\vec{v}_{0,1} \pm \Omega_{A,1}^2 = \vec{k}.\vec{v}_{0,2} \pm \Omega_{A,2}^2$ in this case. When we increase M, we have cases of (i) only two fast, (ii) two fast and two slow, (iii) two

slow and (iv) four slow surface wave solutions. The extra pair of surface wave solutions lie on a branch that asymptotically approaches the cusp frequency $\pm\Omega_c$. We shall adopt the terminology 'asymptotic slow surface wave branch' for this type of solution. There exist one or two pairs of slow surface wave solutions for which the solution lies in the second quadrant. This means that they all have the same direction of propagation. One solution of a pair is therefore a backward propagating wave, where we define a backward propagating wave as a wave whose direction of propagation has reversed, due to the Doppler shift of the frequency in the presence of flow. For higher values of M, one or two pairs of fast surface wave solutions exist, of which one solution of a pair is a backward propagating wave, The extra pair of fast surface waves solutions lie on a branch that asymptotically approaches the frequency $\pm\Omega_I$. We shall adopt the terminology 'asymptotic fast surface wave branch' for this type of solution.

When the line L is tangent to the solution curve, a double root exists. This corresponds to marginal stability and the lower or higher limit of an interval of M where unstable modes exist. For the case of Figure 5.4, there are five points where the line L is tangent to the solution curve of surface waves. There exist three intervals of M, where at least one root of the ideal dispersion relation has a positive imaginary part and hence a wave is unstable. The upper interval, starting at a double root in the fast branch near the point $(-\Omega_{A,1}, \Omega_{A,2})$, corresponds to the K-H instability found in both the incompressible and cold-plasma limit (Chandrasekhar, 1961).

The two lower intervals of K-H instability exist between the slow surface wave solution branches and the fast surface wave solution branch. The unstable wave solutions in this interval are overstable. (Fejer, 1964; Duhau & Gratton, 1973; González and Gratton, 1994a). González & Gratton (1994b) call the wave solutions in these intervals 'secondary Kelvin-Helmholtz' modes. From Figure 5.4 is it clear that these intervals of instability lie between the cusp frequency Ω_c and the frequency Ω_I. Using the definition of these frequencies, we estimate that the width of the interval is minimal of order $\beta^{3/2}$ in a plasma with a low plasma β. We shall show in this chapter that the instability growth-rate is proportional to a power of β. Therefore, in the cold-plasma limit, the interval of instability vanishes as both frequencies Ω_c and Ω_I tend to zero and the instability growth-rate becomes zero as well. Duhau & Gratton (1973) showed that if β is equal to, or larger than, unity, that this interval of instability merges with the upper instability interval.

The upper interval of instability is more fundamental compared with the previous intervals, because:

a) the regime of instability covers a larger domain in parameter space,

b) the growth rate of the unstable wave solutions is much larger (González and Gratton, 1994a),

c) the regime of instability is present in both the cold-plasma and incompressible limit (*e.g.* RVEG). In those limits the instability is a monotonic instability.

At the upper limit in flow speed of this instability, the dispersion relation has a double root, but this is not a surface wave solution.

5.4 Model of coronal hole boundary

We consider the surface discontinuity as the boundary between two topologically distinct regions in the solar corona. Medium one is an active region with closed fieldlines. Medium two is a coronal hole with open fieldlines. It is well known that during the inactive period of the sun's cycle, coronal holes are the source of the steady, fast solar wind.

We choose $\eta = 1$ and $\phi = \phi_1 = \phi_2$ to reduce the number of free parameters. The corona is a low-plasma-β region, *i.e.* $\beta \ll 1$. Therefore, the kinetic pressure can approximately be neglected in the equilibrium condition (5.3). The error in this approximation is of order β. For the following analytical analysis, we shall take $\beta = \beta_1 = \beta_2$ to simplify the calculations. From Expressions (5.49)-(5.51), we see that this implies that the density, pressure and magnetic field strength ratios are strictly equal to unity. Therefore, the transport coefficients would be the same in each medium ($\delta = 0$). We shall, though, let the transport coefficients differ, because we shall show that a different value of the parameter β in each medium, within the assumption of $\beta \ll 1$, can easily be incorporated in the lowest-order contribution to the dissipative growth-rate ω_d.

In this specific model, we have five free parameters: M, α, ϕ, β and δ, which are defined in Table 5.2. We often consider the case $\phi = \alpha$. Figure 5.5 shows that the parameter δ increases rapidly to unity with increasing density or temperature ratio. A temperature ratio of two makes δ already equal to 0.67.

169
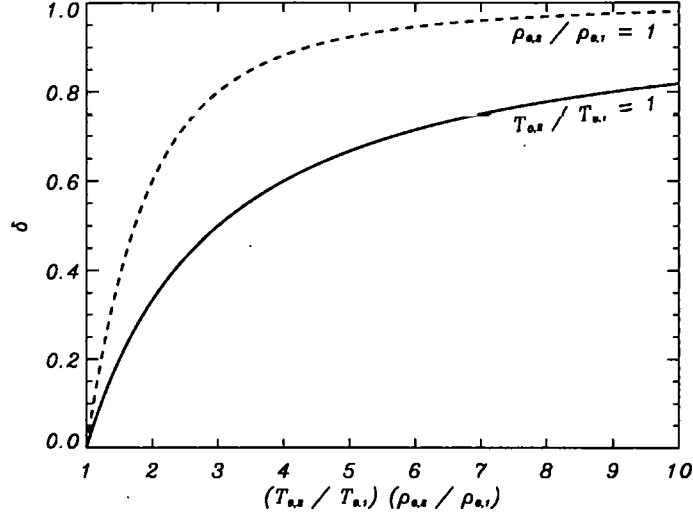
Figure 5.5: Plot of the dimensionless parameter δ as a function of the ratio $(T_{0,2}/T_{0,1})(\rho_{0,2}/\rho_{0,1})$. Solid line: δ as a function of $T_{0,2}/T_{0,1}$ for $\rho_{0,2}/\rho_{0,1} = 1$. Dashed line: δ in function of $\rho_{0,2}/\rho_{0,1}$ for $T_{0,2}/T_{0,1} = 1$.

5.4.1 Dispersion relation

The dispersion relation (5.42) is transformed, by squaring, into a polynomial equation:

$$f_I(\omega) + i f_\nu(\omega) + i f_\chi(\omega) = 0 , \tag{5.53}$$

with

$$f_I = A_1^2 C_1 D_2 - A_2^2 C_2 D_1 , \tag{5.54}$$

$$f_\nu = A_1^2 C_1 D_2 \nu_2 K_{\nu,2} - A_2^2 C_2 D_1 \nu_1 K_{\nu,1} , \tag{5.55}$$

$$f_\chi = A_1^2 C_1 D_2 \chi_2 K_{\chi,2} - A_2^2 C_2 D_1 \chi_1 K_{\chi,1} . \tag{5.56}$$

The quantities A, C and D are defined in Expression (5.26). The ideal term f_I is a tenth-order polynomial in ω. For our specific model we find:

$$
\begin{aligned}
f_I = & \left(\Omega_1^2 - \Omega_A^2\right)^2 \left(\Omega_1^2 - \Omega_c^2\right) \left(\Omega_2^2 - \Omega_I^2\right) \left(\Omega_2^2 - \Omega_{II}^2\right) \\
& - \left(\Omega_2^2 - \Omega_A^2\right)^2 \left(\Omega_2^2 - \Omega_c^2\right) \left(\Omega_1^2 - \Omega_I^2\right) \left(\Omega_1^2 - \Omega_{II}^2\right) ,
\end{aligned} \tag{5.57}
$$

170

which is, after some tedious but straightforward manipulations, transformed into:

$$f_I = \left(\Omega_1^2 - \Omega_2^2\right)\left(\Omega_1^4\Omega_2^4 + \mathcal{A}\,\Omega_1^2\Omega_2^2(\Omega_1^2 + \Omega_2^2) + \mathcal{B}\,(\Omega_1^4 + \Omega_2^4) + \mathcal{C}\,\Omega_1^2\Omega_2^2 + \mathcal{D}\,(\Omega_1^2 + \Omega_2^2) + \mathcal{E}\right),$$

(5.58)

with

$$\mathcal{A} = -(V_A^2 + C_s^2)k^2 \ , \quad \mathcal{B} = C_s^2 k^2 \Omega_A^2 \ , \quad \mathcal{C} = \mathcal{B} + (\Omega_c^2 - 2\Omega_A^2)\mathcal{A} - \Omega_A^2(\Omega_A^2 + 2\Omega_c^2) \ ,$$

$$\mathcal{D} = (\Omega_c^2 - 2\Omega_A^2)\mathcal{B} + \Omega_A^4\Omega_c^2 \ , \quad \mathcal{E} = \Omega_A^2(\Omega_A^2 + 2\Omega_c^2)\mathcal{B} + \Omega_A^4\Omega_c^2\mathcal{A} \ . \quad (5.59)$$

From this equation, the solution of Ω_2^2 as a function of Ω_1^2 can easily be found and used to visualise the roots in a Ω_1-Ω_2 diagram, but is less useful if the roots of the dispersion relation are to be found analytically. The solution $\Omega_1^2 = \Omega_2^2$ of $f_I(\omega) = 0$, corresponds to the ideal roots $\varpi \to \infty$ and $\varpi = \vec{k}.(\vec{v}_{0,1} - \vec{v}_{0,2})$. These roots are spurious because they clearly do not satisfy the ideal dispersion relation $F_I = 0$. The ideal, non-spurious roots are therefore contained in the second factor of Equation (5.58), which is an eighth-order polynomial in ω. We introduce the following dimensionless variables:

$$\xi = M\cos\alpha \ , \quad Y = \frac{\left(\omega - \frac{1}{2}\vec{k}.(\vec{v}_{0,1} + \vec{v}_{0,2})\right)^2}{k^2 V_A^2} - \xi^2 \ . \tag{5.60}$$

The Doppler-shifted frequencies are equal to:

$$\Omega_1 = \pm\sqrt{Y + \xi^2} + \xi \ , \quad \Omega_2 = \pm\sqrt{Y + \xi^2} - \xi \ , \tag{5.61}$$

so that we see that $\Omega_1\Omega_2 = Y$. Therefore the sign of the solution, Y, of a pair of surface waves, determines whether backward propagating waves exist. If $Y < 0$, this solution lies in the second (or fourth) quadrant of the Ω_1-Ω_2 diagram and the pair of solutions consists of both a forward and a backward propagating wave.

Using Definition (5.60) and Expression (5.61), Equation (5.58) is transformed into:

$$f_I(Y) = \pm 4\xi\sqrt{Y + \xi^2}\,P(Y)\,k^{10}V_A^{10} \ , \tag{5.62}$$

where $P(Y)$ is a fourth-order polynomial in Y:

$$P(Y) = Y^4 + aY^3 + (2a\xi^2 + b)Y^2 + (c\xi^2 + d)Y + (c\xi^4 + 2d\xi^2 + e) \ , \tag{5.63}$$

with real coefficients

$$a = -\frac{2}{1-\epsilon} \ , \quad b = \frac{(1 + 2\epsilon)\,(2 - \cos^2\phi(1 + \epsilon))\cos^2\phi}{1 - \epsilon} \ , \quad c = \frac{16\cos^2\phi}{1 - \epsilon}\epsilon \ ,$$

$$d = 2\left(\cos^2\phi - \frac{2 + \epsilon}{1 - \epsilon}\right)\cos^4\phi\,\epsilon \ , \quad e = \frac{2\cos^6\phi}{1 - \epsilon}\epsilon^2 \ , \tag{5.64}$$

171

where the parameter $\epsilon = V_c^2/V_A^2 = \beta/(1+\beta)$ is between zero and one. The values $\epsilon = 0$ and $\epsilon = 1$ correspond to the cold-plasma and incompressible limits respectively.

The polynomial $P(Y)$ contains all the non-spurious roots $Y = \overline{Y}$ of the ideal dispersion relation $F_I(\overline{Y}) = 0$. Therefore the derivative of $f_I(Y)$ with respect to Y (denoted with a prime) and evaluated at $Y = \overline{Y}$, is equal to:

$$f'_I(\overline{Y}) = \pm 4\xi\sqrt{\overline{Y}+\xi^2}\, P'(\overline{Y}) \,. \tag{5.65}$$

The necessary condition which a non-spurious root of the dispersion relation has to satisfy, Condition (5.40), is rewritten, using Expression (5.61), as:

$$\cos^2\phi - 2\,|\,\xi\,|\,|\cos\phi\,| < Y < \cos^2\phi + 2\,|\,\xi\,|\,|\cos\phi\,| \,. \tag{5.66}$$

5.4.2 The reduced equation: cold-plasma limit

First, we investigate the dispersion relation (5.62) in the cold-plasma limit. In this limit the interval in Ω where slow surface waves exist, is zero, because the frequency Ω_c is equal to zero in this limit. Therefore only fast surface wave solutions exist. The non-spurious roots are contained in the part of Equation (5.63) which is independent of the parameter β.

$$P_0 = Y_0^2 \left(Y_0 - 1 + \sqrt{4\xi^2 + \sin^4\phi}\right)\left(Y_0 - 1 - \sqrt{4\xi^2 + \sin^4\phi}\right) = 0 \,, \tag{5.67}$$

where cold-plasma quantities are denoted with a subscript '0'. The root $Y_0 = 1 + (4\xi^2 + \sin^4\phi)^{1/2}$ is a spurious root. This is easily checked by substituting this root, for example, into Condition (5.66) and evaluating the case $\alpha = \phi = \pi/2$.

The root

$$Y_0 = 1 - \sqrt{4\xi^2 + \sin^4\phi} \,, \tag{5.68}$$

is non-spurious and describes a pair of fast surface waves. This root degenerates into the root $Y_0 = 0$ when

$$\xi_c^2 = \frac{1 - \sin^4\phi}{4} \,, \tag{5.69}$$

or, if $\phi = \alpha$, when $M_c^2 = (1 + \sin^2\phi)/4$. In that case, Equation (5.67) has a root $Y_0 = 0$ of multiplicity three. Condition (5.69) also corresponds to the minimum value of ξ for which Solution (5.68) contains a backward propagating wave. When the root (5.68) is positive, corresponding to $\xi^2 < \xi_c^2$, we see from Definition (5.63), that the two solutions lie in the first and third quadrants of a Ω_1-Ω_2 diagram. Therefore there are two oppositely travelling fast

surface waves When the root (5.68) is negative, corresponding to $\xi^2 > \xi_c^2$, the two solutions both lie in the second quadrant. Therefore there is a backward travelling fast surface wave.

The double root $Y_0 = 0$ corresponds to $\Omega_1\Omega_2 = 0$ and is the cold-plasma value of the asymptotic branch solution at $\pm\Omega = \pm\Omega_I = 0$. Condition (5.66) shows that this root has to fulfill at least the condition $|\cos\phi|/2 < |\xi| < 1/2$ to be non-spurious. The lower limit in ξ for the asymptotic branches is given by the point where these branches meet the other solution branch. Therefore, we conclude that the double root $Y_0 = 0$ exists in the interval $|\xi_c| < |\xi| < 1/2$. The value of ξ_c describes also, for this wave solution, the minimum value of ξ for which the solution contains a backward propagating wave.

In the second quadrant of a Ω_1-Ω_2 diagram, the quantity $Y_0 + \xi^2$ for the root (5.68) is negative, and thus has a frequency with a positive imaginary part, when

$$\cos^2\phi < \xi^2 < 1 + \sin^2\phi \; . \tag{5.70}$$

This is the Kelvin-Helmholtz instability criterion in the cold-plasma limit. For waves propagating parallel to the magnetic field ($\phi = \alpha$), Condition (5.70) corresponds to

$$1 < M^2 < 1 + 2\tan^2\phi \; . \tag{5.71}$$

The interface is stable for all angles of propagation when

$$M < |\cos\varphi| \; , \tag{5.72}$$

where φ is the angle between the direction of the equilibrium flow and the equilibrium magnetic field. We are interested in equilibrium flow speeds which are below the threshold value of the Kelvin-Helmholtz instability in a cold plasma, thus fulfilling Condition (5.72).

5.4.3 Graphical discussion of surface wave solutions

In Subsection 5.3.3, we gave a general description of the ideal dispersion relation and introduced the Ω_1-Ω_2 diagram as a useful tool for describing the wave solutions. In this subsection we shall use this tool to discuss, for our specific model, the possible cases of ideal surface wave solutions in detail, to make the analytical calculations which follow more approachable.

Figure 5.6 shows the real, non-spurious roots of the dispersion relation in a Ω_1-Ω_2 diagram for our specific model. The frequencies $\Omega_{c,1,2}$ and $\Omega_{I,1,2}$ are so close to each other, they cannot be distinguished in the figure.

The diagram is in this case symmetric so that we only need to focus on the solution branches to one side of the line $\Omega_2 = -\Omega_1$. We choose the top half. There are three flow speeds for which the surface wave solutions have a double root, signifying marginal stability, highlighted by the numbers 'one', 'two' and 'three' in Figure 5.6. These points bound two intervals in M for which surface waves are unstable in an ideal medium and correspond to the instability regimes mentioned earlier. The instability interval starting at point 'one'
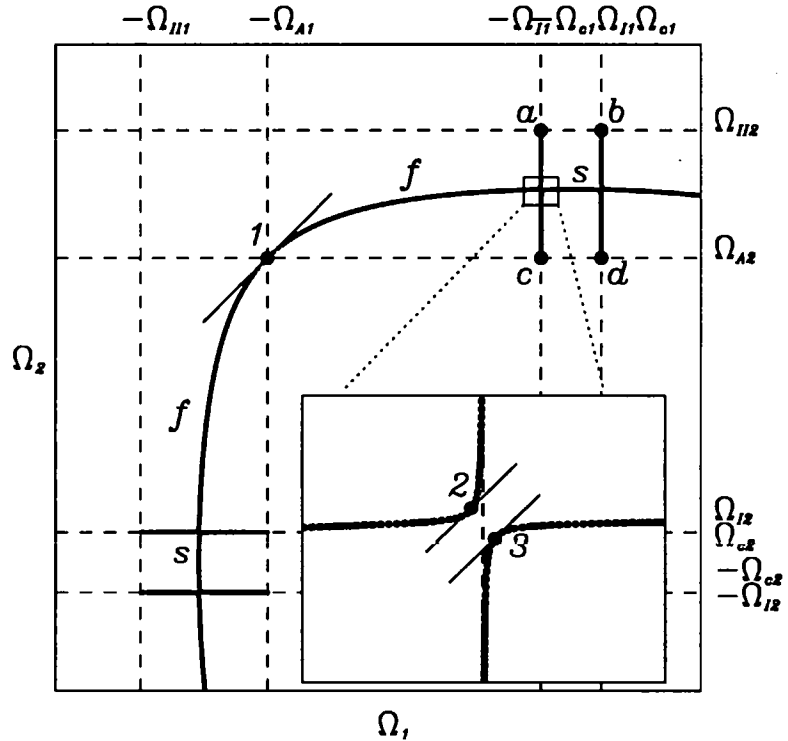
Figure 5.6: Plot of $\Re(\overline{\omega})$, which is the solution of $F_I(\overline{\omega}) = 0$, in a Ω_1-Ω_2 diagram with $\beta = 10^{-2}$, $\alpha = \phi_1 = \phi_2 = 45$ degrees and $\eta = 1.0$. The quantities in the plot have been normalised by a factor kV_A. The numbers denote positions where the line L: $\Omega_2/kV_{A,2} = \Omega_1/kV_{A,2} + 2M\cos\alpha$ is tangent to the solution curve, corresponding to points of marginal stability. The letters 'a' to 'd' denote positions where the line L intersects the asymptotic surface wave branches, where they turn from spurious to non-spurious, or vice versa.

corresponds to the lower limit of the K-H instability in a cold plasma. The critical value of ξ at that point is given by the lower limit of Expression (5.70).

The instability interval between the points 'two' and 'three' vanishes in the cold-plasma limit, because both the frequencies Ω_c and Ω_I tend to zero in this limit. We estimate, from Figure 5.6, the critical value of ξ, where this instability interval is approximately situated. It lies at the approximate coordinates $\Omega_1 \approx -\Omega_c = -\epsilon^{1/2}\cos\phi$ and $\Omega_2 \approx 2\xi_c^2$ (using the equation of the line L passing through $\Omega_1 = 0$). The corresponding value of ξ, for which the line L intersects this point, is given as: $\xi = \xi_c + \epsilon^{1/2}\cos\phi/2$. Later on in this chapter, we shall calculate this expression more rigorously.

The points 'a' and 'b' represent the points where the fast asymptotic branch solutions turn from non-spurious to spurious solutions, with increasing value of M. The points 'c' and 'd' represent the points where the slow asymptotic branch solutions turn from spurious to non-spurious solutions, with increasing value of M. The critical values of ξ (and hence M) for these points are easily calculated from looking at Figure 5.6:

$$
\begin{cases}
\text{a}: & \Omega_1 = -\Omega_{I,1} & , & \xi = \frac{2}{kV_A}(\Omega_{I,1} + \Omega_{II,2}) & \approx \frac{1}{2}\left(1 + \epsilon^{1/2}\cos\phi\right) \\
\text{b}: & \Omega_1 = \Omega_{I,1} & , & \xi = \frac{2}{kV_A}(-\Omega_{I,1} + \Omega_{II,2}) & \approx \frac{1}{2}\left(1 - \epsilon^{1/2}\cos\phi\right) \\
\text{c}: & \Omega_1 = -\Omega_{c,1} & , & \xi = \frac{2}{kV_A}(\Omega_{c,1} + \Omega_{A,2}) & \approx \frac{1}{2}\left(\cos\phi + \epsilon^{1/2}\cos\phi\right) \\
\text{d}: & \Omega_1 = \Omega_{c,1} & , & \xi = \frac{2}{kV_A}(-\Omega_{c,1} + \Omega_{A,2}) & \approx \frac{1}{2}\left(\cos\phi - \epsilon^{1/2}\cos\phi\right)
\end{cases}
$$

$$(5.73)$$

The asymptotic surface wave branches at $\Omega \approx -\Omega_c$ and $\Omega \approx -\Omega_I$ are situated in the second quadrant of the Ω_1-Ω_2 diagram and therefore always contain backward propagating waves.

Because the difference between the surface wave solutions in a plasma of low but finite plasma β, and a cold plasma, is mainly in the appearance of slow surface waves and a second K-H instability interval, we shall discuss the behaviour of the surface wave solutions in that part of the Ω_1-Ω_2 diagram, as a function of ϵ. Figure 5.7, shows the part of the solution branches in a Ω_1-Ω_2 diagram, which contains the instability region in question, for several values of ϵ. The plot for $\epsilon = 10^{-5}$ is used to represent the cold-plasma case.

The line L_2 corresponds to a value of M equal to M_c. In the cold-plasma limit, L_2 intersects the solution branch in one point, where the solution $Y = 0$ is a root of multiplicity three. With increasing ϵ, the asymptotic fast branches split up, as Ω_c becomes finite and the slow wave branches appear in between. At $\epsilon = 10^{-2}$, L_2 has three separate intersections. The triple root has split up, leaving the first root at $Y = 0$, the second on the asymptotic

slow surface wave branch near $\Omega_1 = -\Omega_c$ and the third on the asymptotic fast surface wave branch near $\Omega_1 = \Omega_f$. At $\epsilon = 10^{-1}$ the two latter roots intersect the asymptotic branches at a position lower and higher than point 'c' and point 'b' respectively. Therefore, these solutions are spurious. The left plot of Figure 5.8 confirms this behaviour. It shows the behaviour of the solutions $Y + \xi^2$ of Equation (5.54) as a function of ϵ, for $M = M_c$. No solutions with $Y + \xi^2 < 0$ or $\Im(Y) \neq 0$ are present. The process of splitting-up of the triple root is clearly visible. It is not of interest to calculate this behaviour analytically because no unstable behaviour occurs.

The line L_3 corresponds to a value of M below M_c. In the cold-plasma limit, L_3 intersects the fast surface wave branch and the merged asymptotic slow surface wave branches. The latter double root is spurious, though. At $\epsilon = 10^{-2}$, L_3 intersects the fast surface wave branch and the two, now separated, asymptotic slow surface wave branches. The root on the asymptotic slow surface wave branch near $\Omega_1 = \Omega_c$ is non-spurious and the root on the other branch is still spurious. At $\epsilon = 10^{-1}$, the intersections of L_2 with the asymptotic fast and slow surface wave branches are near to each other, but do not meet. The third intersection is a spurious root. The right plot of Figure 5.8 confirms the behaviour of the solutions for this case. No solutions with $Y + \xi^2 < 0$ or $\Im(Y) \neq 0$ are present. Therefore we shall not investigate this case analytically. We conclude from the previous case and this case, that unstable behaviour only occurs for values of M above M_c, for which backward
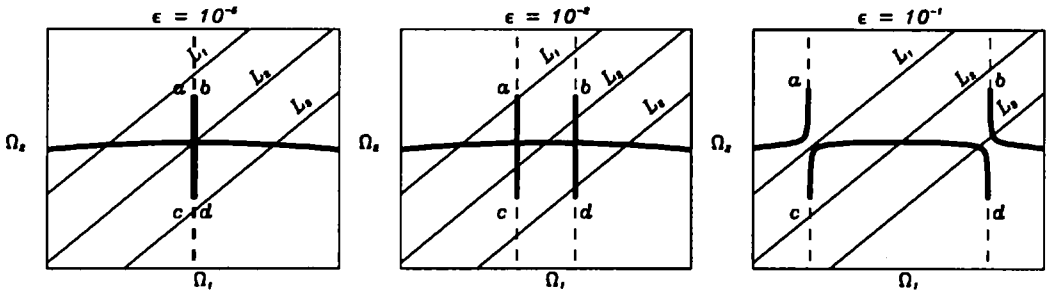
Figure 5.7: Ω_1-Ω_2 diagrams, showing the stable surface wave branches in the parts of the first and second quadrants near $\Omega_1 = 0$ for $\phi = \alpha = \pi/4$, for three values of the parameter ϵ. The dashed lines represent spurious solutions of Equation (5.54). The lines L_1, L_2 and L_3 are defined as $\Omega_2/kV_A = \Omega_1/kV_A + 2M \cos \alpha$ with M equal to $M_c + 0.14$, M_c and $M_c - 0.14$ respectively. The solution branches have been calculated numerically.
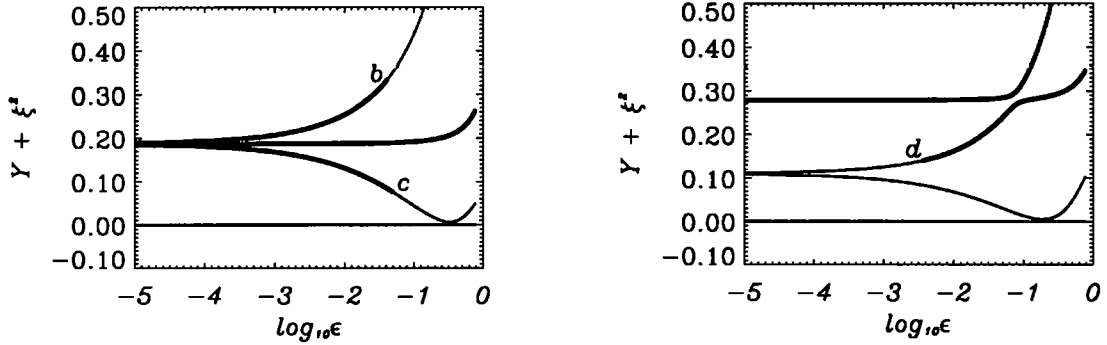
Figure 5.8: Plot of solutions $Y + \xi^2$ of the dispersion relation (5.54) as a function of ϵ for $\phi = \alpha = \pi/4$. The non-spurious roots are represented by thick lines. The range of the y-axis has been chosen to show the non-spurious roots clearly. Therefore the plot does not show all the roots. The solution branches have been calculated numerically. Left: $M = M_c$. Right: $M = M_c$ - 0.14.

propagating waves exist. This is, of course, what was suspected previously.

The line L_1 corresponds to a flow speed above the speed M_c. In the cold-plasma limit, L_1 intersects the fast surface wave branch and the merged asymptotic fast surface wave branches. The latter double root is spurious, though. At $\epsilon = 10^{-2}$, L_1 intersects the fast surface wave branch and the two, now separated, asymptotic fast surface wave branches. The root on the asymptotic fast surface wave branch near $\Omega_1 = -\Omega_I$ is non-spurious and the root on the other branch is still spurious. At $\epsilon = 10^{-1}$, L_3 only intersects the spurious part of the asymptotic fast surface wave branch near $\Omega_1 = \Omega_I$. The left plot of Figure 5.9 shows that, with increasing value of ϵ, the two fast wave solutions Y come together to form a double root (corresponding to point 'two' in Figures 5.6 and 5.9). During a small interval in ϵ, the solution Y consists of a pair of complex conjugate solutions (Fejer, 1964; Duhau & Gratton, 1973; González & Gratton, 1994a). This is shown in the right plot of Figure 5.9. Because the real part of the solution cannot be eliminated by a change of frame of reference, the solution with a positive complex part, represents an overstable wave. The width of the interval is of the same order as the difference Ω_I - Ω_c, which is of order $\epsilon^{3/2}$. The end of the overstability interval is marked by another double root (corresponding to point 'three' in Figures 5.6 and 5.9). As ϵ increases further, two slow wave solutions exist.

5.4.4 Expansion procedure

Equation (5.62) can, in principle, be solved analytically but would result in large and impractical expressions, making the procedure of having to substitute the non-spurious roots $\overline{Y}$ into Expression (5.47), to obtain an approximate solution for the dissipative dispersion relation, undesirable. Instead we shall investigate Equation (5.62) for media which have a low plasma β. Therefore the parameter ϵ is much smaller than unity. In coronal conditions, $\epsilon \sim 10^{-2}$. The dissipative terms are ordered as $f_\nu \sim \mathrm{Re}^{-1} \sim \epsilon^2$ and $f_\chi \sim \mathrm{Re}^{-1}\, \mathrm{Pr}^{-1}\, \epsilon \sim \epsilon^2$.

We use perturbation theory (Nayfeh, 1985) to obtain approximate values of the roots, and compare them with those obtained by numerical solution, which uses the non-spurious roots of the full, ideal dispersion relation to calculate the dissipative contribution via Expression (5.47).

The functions f_I, f_ν and f_χ, and the quantity Y are expanded in series in small ϵ:

$$
\begin{aligned}
f_I(Y) &= \pm 4\xi\sqrt{Y+\xi^2}\left(P_0(Y)+\epsilon P_1(Y)+\epsilon^2 P_2(Y)+\ldots\right), \\
f_\nu(Y) &= \epsilon^2 f_{\nu,0}(Y)+\epsilon^3 f_{\nu,1}(Y)+\ldots,
\end{aligned}
$$
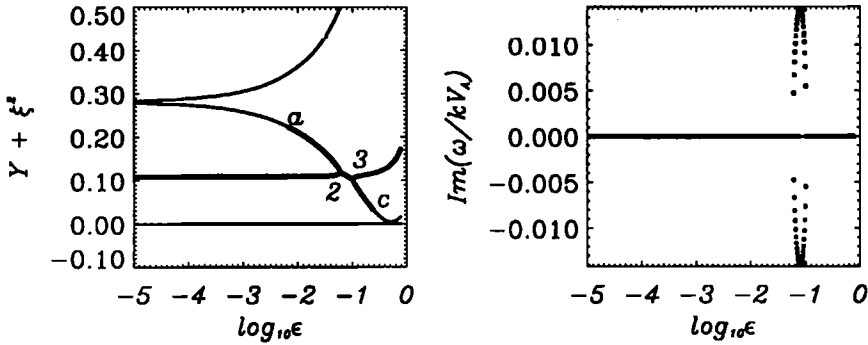
Figure 5.9: Left: Plot of solutions $Y+\xi^2$ of the dispersion relation (5.54) as a function of ϵ for $M = M_c$ - 0.14 and $\phi = \alpha = \pi/4$. The non-spurious roots are represented by thick lines. The range of the y-axis has been chosen to show the non-spurious roots clearly. Therefore the plot does not show all the roots. The solution branches have been calculated numerically. Right: Plot of $\Im(\omega/kV_A)$ as a function of ϵ. Non-spurious roots are represented by thick lines.

$$f_\chi(Y) = \epsilon^2 f_{\chi,0}(Y) + \epsilon^3 f_{\chi,1}(Y) + \dots ,$$

$$Y = Y_0 + \epsilon^{n_1} Y_1 + \epsilon^{n_2} Y_2 + \dots , \tag{5.74}$$

where Y_0 is a root of the reduced equation $f_{I,0}(Y_0) = 0$, which corresponds to the squared ideal dispersion relation in the cold-plasma limit. The numbers n_i are a series of monotonically increasing numbers. The value of these numbers is determined by the multiplicity of the lower-order solution. If the solution, at all orders, always remains a root of multiplicity one, then the numbers n_i are simply the positive integers. We keep Expansion (5.74) general because we shall encounter the necessity of a non-straightforward expansion procedure. The expansion of the function $P(Y)$ in Equation (5.63) entails an expansion of the parameters a, b, c, d and e. From this, we see that the polynomial P_0 is of order four in Y and the higher order polynomials P_1, P_2, ... are of order three in Y.

When we assume that the root Y_0 is a single root, the derivative $f'_{I,0}(Y_0)$ is non-zero. The lowest order dissipative correction, call it $\pm i Y_d$, is of order ϵ^2 and is calculated from Expression (5.53), using Expansions (5.74):

$$Y_d = Y_\nu + Y_\chi \quad , \quad Y_\nu = \frac{f_{\nu,0}(Y_0)}{4\xi\sqrt{Y_0 + \xi^2}\, P'_0(Y_0)} \quad , \quad Y_\chi = \frac{f_{\chi,0}(Y_0)}{4\xi\sqrt{Y_0 + \xi^2}\, P'_0(Y_0)} . \tag{5.75}$$

The frequency ω calculated from Expression (5.75) corresponds to the leading order term of Expression (5.47), with respect to β. Notice that only the cold-plasma solution Y_0 is needed to calculate the dissipative correction. The corrections for viscosity and thermal conduction are also calculated separately from each other. The viscous correction Y_ν corresponds to the dissipative contribution in a model with cold plasmas. Therefore, this correction is unaffected by the parameter β and is also correct when $\beta_1 \neq \beta_2$. The thermal conduction contribution Y_χ is of the same order as the viscous contribution Y_ν, but is not present in a cold-plasma description. It contains the function $f_{\chi,0}(Y_0)$, which is the part of function f_χ, of order β, evaluated at Y_0. The case of $\beta_1 \neq \beta_2$ can be incorporated into this function by replacing, for example, the coefficient χ_2 by $\chi_2 \beta_2/\beta_1$. Therefore it is justified, for studying the lowest-order dissipative correction, to take a model with the parameter β equal in each medium, but with the transport coefficients free to differ.

From the solution Y we calculate, from Definition (5.60), the frequency ω:

$$\omega = \frac{1}{2}\vec{k}.(\vec{v}_{0,1} + \vec{v}_{0,2}) \pm kV_A\sqrt{Y \pm iY_d + \xi^2} , \tag{5.76}$$

where $\overline{Y}$ and Y_d are the ideal and dissipative parts of the solution Y respectively. Consider first ideal media. There are two possible cases for K-H instability:

1) When $\overline{Y} + \xi^2 < 0$, Expression (5.76) is, in the frame of reference which moves with the centre of mass ($\rho_{0,1}v_{0,2} + \rho_{0,2}v_{0,1} = 0$) of the interface (Hollweg *et al.*, 1990; Goossens *et al.*, 1992) equal to:

$$\omega = \pm i \sqrt{\left| k^2 V_A^2 \overline{Y} + \left(\vec{k}.\vec{v}_{0,1} \right) \right|}.$$ (5.77)

Equation (5.77) shows that this type of K-H instability is a monotonic instability and that the interface supports a pair of surface waves with purely imaginary, complex conjugated frequencies. The K-H instability in the cold-plasma limit is clearly of this type.

2) When $\overline{Y}$ is complex, Expression (5.76) cannot, generally, be transformed to a frame of reference in which the frequency is purely complex. Therefore, this type of K-H instability is an overstability.

A dissipative instability is an overstability. The dissipative growth-rate is, using Expression (5.76), approximately equal to:

$$\omega_d = k V_A \frac{Y_d}{2\sqrt{\overline{Y} + \xi^2}}.$$ (5.78)

In principle, surface waves can be dissipatively unstable as well as K-H unstable, although this is not relevant since the assumption of weak dissipation limits the growth-rate of the dissipative instability to be much less than the growth-rate of an ideal instability. Ruderman and Goossens (1995) studied the dispersion relation in the incompressible limit. In this limit, only a monotonic K-H instability exists (Chandrasekhar, 1961), corresponding to the upper instability interval in Figure 5.4. They found that in the domain of parameter space where the interface is K-H unstable, the dissipative contribution Y_d is always negative, *i.e.* the surface waves are damped. Therefore, there is no overlap between the domains of instability in this limit. We shall show that in the case of a finite plasma β, the dissipative contribution due to thermal conduction, Y_χ, can be positive in the domain of parameter space where the interface is K-H instability. This does not occur in the incompressible limit because the contribution due to thermal conduction vanishes.

5.4.5 Ideal corrections to the cold-plasma surface wave solution

Because ideal corrections to the cold-plasma wave solutions are larger than the lowest-order dissipative corrections we shall investigate the effect of a small, but finite plasma β, on

the stability of the surface wave solutions, before discussing the possibility of dissipative instabilities. We shall address two problems: corrections to the cold-plasma instability criterion (5.70) and the appearance of a new interval of K-H instability at flow speeds below the threshold (5.72).

Corrections to the cold-plasma instability criterion

We are interested in corrections to the cold-plasma K-H instability criterion (5.70). Therefore we consider the root (5.68) in a domain of the parameter ξ^2 close to the lower threshold of K-H instability in a cold plasma, $i.e.$ $\xi^2 \approx \cos^2 \phi$. Around these values the solution (5.68) is clearly of multiplicity one. Using the expansions (5.74) with $n_1 = 1$ and retaining terms in Equation (5.53) of order ϵ we have:

$$Y_1 P_0'(Y_0) + P_1(Y_0) = 0 \; , \tag{5.79}$$

where the functions P_0' and P_1 are evaluated at (5.68). The function $P_1(Y_0)$ is, knowing that Y_0 is a root of Equation (5.67), rewritten as:

$$P_1(Y_0) = -2\sin^2 \phi \left(8\xi^2 + (1 + \sin^2 \phi)^2\right) (Y_0 + \xi^2) - 2\sin^2 \phi(1 + \sin^2 \phi)^2 \left(\xi^2 - \cos^2 \phi\right) \; . \tag{5.80}$$

The derivative $P_0'(Y_0)$ is equal to:

$$P_0'(Y_0) = -2\sqrt{4\xi^2 + \sin^4 \phi} \left(1 - \sqrt{4\xi^2 + \sin^4 \phi}\right)^2 \; . \tag{5.81}$$

This function is negative for all values of ξ and ϕ. From Expressions (5.79) and (5.80), we calculate the first-order correction Y_1:

$$Y_1 = -\frac{\sin^2 \phi \left(8\xi^2 + (1 + \sin^2 \phi)^2\right) (Y_0 + \xi^2) + \sin^2 \phi(1 + \sin^2 \phi)^2 \left(\xi^2 - \cos^2 \phi\right)}{\sqrt{4\xi^2 + \sin^4 \phi} \left(1 - \sqrt{4\xi^2 + \sin^4 \phi}\right)^2} \; . \tag{5.82}$$

To investigate if this correction alters the K-H instability criterion (5.70), we consider the expression

$$Y_0 + \epsilon^2 Y_1 + \xi^2 = (Y_0 + \xi^2) \left[1 + \epsilon \frac{\sin^2 \phi \left(8\xi^2 + (1 + \sin^2 \phi)^2\right)}{P_0'(Y_0)}\right]$$
$$+ \epsilon \frac{\sin^2 \phi(1 + \sin^2 \phi)^2 \left(\xi^2 - \cos^2 \phi\right)}{P_0'(Y_0)} \; . \tag{5.83}$$

181

We consider first the case when the cold-plasma solution is marginally stable, *i.e.* $Y_0 + \xi^2$ $= 0$ and $\xi^2 = \cos^2 \phi$. Expression (5.83) is, in this case, also equal to zero. We conclude that the correction does not change the condition of marginal stability and thus also does not change the K-H instability criterion (5.70).

Secondly we consider the case in which the cold-plasma solution is stable ,*i.e.* $Y_0 + \xi^2$ > 0 and $\xi^2 < \cos^2 \phi$. The second term of Expression (5.83) is, in this case, always positive. Therefore Expression (5.83) can only be negative if condition

$$-P_0'(Y_0) < \epsilon \sin^2 \phi \left(8\xi^2 + (2 - \cos^2 \phi)^2 \right) , \qquad (5.84)$$

is satisfied. Because the derivative $P_0'(Y_0)$ is always negative for the considered root, Condition (5.84) implies that the derivative is at least of order ϵ, which occurs for ξ near the value ξ_c. But this makes the correction Y_1 of the same order, or larger, than Y_0 and hence the expansion procedure breaks down. A different ordering of the terms as a function of ϵ is needed to study the case of ξ near ξ_c.

We conclude that the K-H instability criterion, in a cold-plasma, is also valid for plasmas with a low but finite plasma β. In the next section we shall investigate the case of ξ near ξ_c.

Second interval of K-H instability

In this section we investigate the appearance of a second interval of K-H instability, for flow speeds below the cold-plasma threshold speed and for ξ near ξ_c. This interval is clearly visible in the inset of Figure 5.6, as the interval located near $\Omega_1 = -\Omega_c$ or $\Omega_2 = \Omega_c$. For the former case, the relevant interval is between the points 'two' and 'three' where double roots exist.

In the cold-plasma limit, this interval merges into the triple root $Y_0 = 0$. Therefore the corrections to Y_0 are calculated at that point. The quantity ξ^2 is written as:

$$\xi^2 = \xi_c^2 + \epsilon^{1/2} \delta \xi^2 . \qquad (5.85)$$

The value of $\delta \xi^2$ is determined from the conditions that the solution is either marginally stable, or unstable. We have chosen to expand ξ^2 in powers of $\epsilon^{1/2}$ because the interval of instability lies close to $\Omega = \Omega_c$ and this frequency is proportional to $\epsilon^{1/2}$. We also choose $n_1 = 1/2$ and $n_2 = 3/4$ in the Expansion (5.74) of the quantity Y. This choice of powers

is determined from looking at the ordering of the terms in Equation (5.53) for the specific case under consideration here.

The following quantities are calculated from Expressions (5.63) and (5.67):

$$P_0' = 0 \quad , \quad P_0''(0) = -8\epsilon^{1/2}\,\delta\xi^2 \quad , \quad P_0'''(0) = -12 \quad , \quad P_0''''(0) = 24 \,,$$

$$P_1(0) = 16\cos^2\phi\,\left(\epsilon^{1/2}\,\xi_c^2\,\delta\xi^2 + \epsilon\delta\xi^4\right) \quad , \quad P_1'(0) = 8\cos^2\phi\,\left(\xi_c^2 + 2\epsilon^{1/2}\delta\xi^2\right) \,,$$

$$P_1''(0) = -4\left(2\xi_c^2 + \cos^2\phi\right) \quad , \quad P_2(0) = -\cos^8\phi\sin^2\phi \,. \quad (5.86)$$

The lowest-order correction terms in Equation (5.53) are of order $\epsilon^{3/2}$ and, using Expression (5.86), are equal to:

$$Y_1^3 + 2\delta\xi^2\,Y_1^2 - 4\xi_c^2\,\cos^2\phi\,Y_1 - 8\xi_c^2\,\delta\xi^2\,\cos^2\phi = 0$$

$$\Leftrightarrow \quad (Y_1^2 - 4\xi_c^2\,\cos^2\phi)\,(Y_1 + 2\delta\xi^2) = 0 \,, \quad (5.87)$$

which contains the three roots $Y_1 = 2\mid\xi_c\,\cos\phi\mid$, $-2\mid\xi_c\mid\mid\cos\phi\mid$, $-2\delta\xi^2$. The two latter roots are equal, thus forming a double root, if $\delta\xi^2 = \mid\xi_c\mid\mid\cos\phi\mid$. This corresponds to a value of ξ^2 of:

$$\xi^2 = \xi_c^2 + \epsilon^{1/2}\mid\xi_c\,\cos\phi\mid \,, \quad (5.88)$$

which for the case $\phi = \alpha$ corresponds to

$$M^2 = M_c\left(M_c + \epsilon^{1/2}\right) \,. \quad (5.89)$$

This double root corresponds to point 'two' in Figure 5.6 and we estimated this expression previously when discussing the dispersion relation graphically. In the interval of M between the maximum and minimum value of Expression (5.89) with respect to the angle α, there can always be found an angle of propagation, for which a wave solution is overstable. Expression (5.89) is minimal when $\alpha = 0$ and is maximal when $\alpha = \pi/2$. At those angles the width of the interval of instability is equal to zero. The instability criterion,

$$\frac{1}{2}\left(1 + \sqrt{\frac{\beta}{1+\beta}}\right) < M < \frac{\sqrt{2}}{2}\left(1 + \sqrt{\frac{\beta}{2(1+\beta)}}\right) \,, \quad (5.90)$$

or

$$V_A + V_c < \mid v_{0,1} - v_{0,2}\mid < \sqrt{2}V_A + V_c \,, \quad (5.91)$$

was found by Duhau & Gratton (1973) by expanding the ideal dispersion relation (5.54) in the angle α, around the values 0 and $\pi/2$, and evaluating when a double root occurs.

183

The lower limit of Expression (5.90) defines the threshold speed of the K-H instability in a compressible plasma.

The next order terms in Equation (5.53) are of order $\epsilon^{7/4}$ and using Expressions (5.86), give an expression of the form:

$$Y_2 \left(-8\delta\xi^2 Y_1 - 6 Y_1^2 + 8\xi_c^2 \cos^2 \phi \right) = 0 , \qquad (5.92)$$

which, for $Y_1 = -2\xi_c \mid \cos \phi \mid$, is trivially satisfied when $\delta\xi^2$ is given by Expression (5.88). The expansion procedure can, in principle, be carried on to investigate the width and growth-rate of the instability interval. The next order terms are of order ϵ^2 and Equation (5.53) then contains terms which are proportional to Y_2^2. This creates the possibility that the correction Y_2 has a pair of complex conjugate solutions and hence the solution Y has an overstable solution. We shall not investigate these higher-order terms because we already have enough information to compare with the dissipative instabilities we investigate in the next section. With the knowledge that this instability interval lies between the frequencies Ω_c and Ω_I, we estimate that, for small ϵ, the minimum width of the instability interval is of order $\epsilon^{3/2}$. The growth-rate of the K-H instability in this interval is of order $\epsilon^{3/4}$, which is, by assumption, always larger than any dissipative growth-rate.

5.4.6 Dissipative instability

In this section we investigate the dissipative correction, Y_d, to the surface wave solution, given by Expression (5.75). This term is of order ϵ^2 and consists of contributions arising from viscosity and thermal conduction, each of which can be calculated separately.

Instability due to viscosity

The first term in Expression (5.75) is the viscous contribution, Y_ν. It coincides with the viscous contribution in a cold plasma and has been considered by RVEG. It is defined as:

$$Y_\nu = -\frac{f_{\nu,0}(Y_0)}{4\xi\sqrt{Y_0 + \xi^2}\, P_0'(Y_0)} , \qquad (5.93)$$

where the function $f_{\nu,0}$ is equal to

$$\begin{aligned}
f_{\nu,0} &= V_A^{-11} - \frac{1}{3}A_1 A_2 \Omega_1^2 \Omega_2^2 \left(A_2 \Omega_1 \nu_1 - A_1 \Omega_2 \nu_2 \right) k^{-10} V_A^{-12} \\
&= -\frac{1}{3}A_1 A_2 Y_0^2 \left[\pm\sqrt{Y_0 + \xi^2} \left(Y_0 - \cos^2 \phi \right) \left(\nu_1 - \nu_2 \right) \right.
\end{aligned}$$
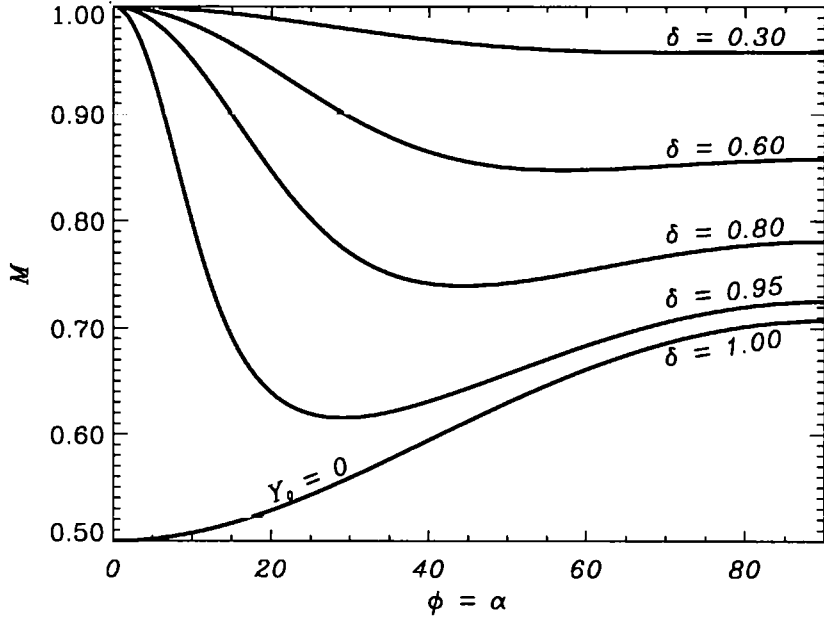
Figure 5.10: Plot of the critical value of M for the existence of an instability due to viscosity, as a function of the angle $\phi = \alpha$ for different values of the parameter δ.

$$- \xi^2 \left(Y_0 + \cos^2 \phi \right) \left(\nu_1 + \nu_2 \right) \right] k^{-3} V_A^{-5} \; . \tag{5.94}$$

Because $f_{\nu,0}$ is proportional to Y_0^2, the viscous correction Y_ν to the cold-plasma solution Y_0 = 0, is equal to zero. We consider the cold-plasma solution (5.68). In the previous section it was shown that for this root, $P_0'(Y_0)$ is always negative and the derivative $P_0'(Y_0)$, for the considered root, is given by Expression (5.81), and is always negative. For a surface wave, which is stable in an ideal plasma, the conditions $A_1 A_2 < 0$, $Y_0^2 > 0$ and $Y_0 + \xi^2 > 0$ are fulfilled. Therefore, Expression (5.93) is positive if

$$\pm \xi \sqrt{Y_0 + \xi^2} \left(Y_0 - \cos^2 \phi \right) \delta > \xi^2 \left(Y_0 + \cos^2 \phi \right) \; , \tag{5.95}$$

where the parameter δ is defined in Table 5.2 as

$$\delta = \left| \frac{\nu_1 - \nu_2}{\nu_1 + \nu_2} \right| \; . \tag{5.96}$$

For the condition that the surface wave is stable in an ideal plasma, the right-hand side of Inequality (5.95) is always positive. Therefore only one of the two surface wave solutions can fulfill Inequality (5.95).

185

The value $\delta = 0$ corresponds to equal values of the viscosity coefficients in the two media ($\nu_1 = \nu_2$). For that case, the right-hand-side term of the Inequality (5.95) is less than zero if $\xi^2 > \cos^2 \phi$. But under this condition, the surface wave is Kelvin-Helmholtz unstable. Therefore we conclude that there is no dissipative instability due to viscosity for flow speeds below the K-H threshold when the viscosity coefficients on both sides of the interface are equal. There are only damped solutions.

The value $\delta = 1$ corresponds to an interface with a viscous and a non-viscous medium ($\nu_1 \nu_2 = 0$). Inequality (5.95) is, by squaring, transformed into:

$$Y_0 \left[\left(Y_0^2 + \cos^4 \phi \right) - 2 \left(Y_0 + 2\xi^2 \right) \cos^2 \phi \right] > 0 . \tag{5.97}$$

We consider the case $Y_0 < 0$. Inequality (5.97) is, by squaring, transformed into:

$$\xi^2 \left(\xi^2 - \cos^2 \phi \right) < 0 , \tag{5.98}$$

where we have assumed that $\phi \neq 0$. Condition (5.98) is satisfied in conjunction with condition $Y_0 < 0$ if

$$\xi_c^2 < \xi^2 < \cos^2 \phi , \tag{5.99}$$

or for the case $\alpha = \phi$, Condition (5.99) is equivalent to

$$M_c^2 < M^2 < 1 . \tag{5.100}$$

For $Y_0 > 0$, Condition (5.97) can never be satisfied. For all angles ϕ, except maybe $\phi = 0$, there exists an interval in the flow speed, which is below the K-H threshold speed, for which a surface wave is stable in an ideal medium, but unstable in a viscous medium. This interval corresponds exactly to the interval where one of the two surface wave solutions is a backward propagating wave. From Condition (5.100), we see that a surface wave which propagates quasi-parallel to the equilibrium magnetic field becomes unstable when approximately $M > 1/2$. This corresponds to the minimum flow speed for which the interface becomes dissipatively unstable in this case.

We now consider the case of an arbitrary value of δ. Figure 5.10 shows the threshold value of M for the existence of an instability due to viscosity, as a function of the angle ϕ for the case $\phi = \alpha$. The value $M = 1$ corresponds to the threshold for the existence of K-H unstable wave solutions. The curves for $\delta < 1$ lie above the curve for $\delta = 1$. Figure 5.11 shows the minimum value, with respect to the angle ϕ, of the threshold value of M as
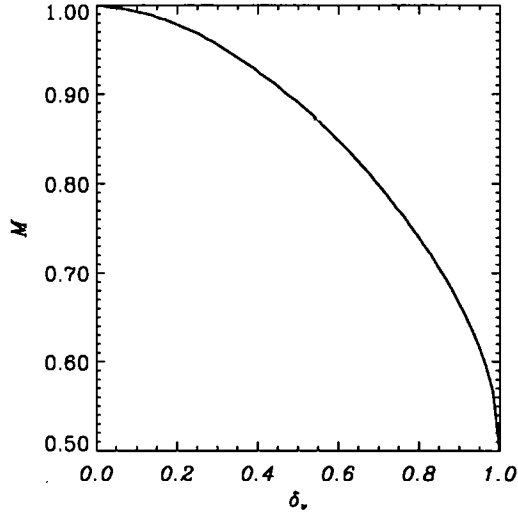
Figure 5.11: Plot of the minimum, with respect to the angle ϕ, in the threshold speed M for the existence of an instability due to viscosity, as a function of the parameter δ for $\phi = \alpha$.

a function of the parameter δ. It shows that the threshold speed is lower, the larger is the difference in the viscosity coefficients. Surface waves are most prone to instability due to viscosity if the plasma is ideal on one side of the interface but viscous on the other side.

When $\phi = \alpha = 0$, Inequality (5.95) becomes equivalent to $\delta > 1$, which is obviously not satisfied. Therefore we conclude that waves which propagate exactly parallel to the equilibrium magnetic field do not become unstable due to viscosity. Condition (5.71) shows that, in a cold plasma, they do not become K-H unstable either. This result can only agree with the result found for $\delta = 1$ when the curve of the threshold speed is discontinuous at $\phi = 0$.

Instability due to thermal conduction

The second term in Expression (5.75) is the thermal conduction contribution, Y_χ, given as:

$$Y_\chi = -\frac{f_{\chi,0}(Y_0)}{4\xi\sqrt{Y_0 + \xi^2}\, P_0'(Y_0)} \,, \qquad (5.101)$$

where the function $f_{\chi,0}$ is equal to

$$f_{\chi,0} = -\frac{(\gamma - 1)}{2} A_1 A_2 \Omega_1 \Omega_2 \left(\vec{k}.\vec{b}_0\right)^2 (A_2 \Omega_2 \chi_1 - A_1 \Omega_1 \chi_2)\ k^{-11} V_A^{-11}$$

187

$$= -\frac{(\gamma - 1)}{2} A_1 A_2 \cos^2 \phi \, Y_0 \left[\pm \sqrt{Y_0 + \xi^2} \left(Y_0 + 4\xi^2 - \cos^2 \phi \right) (\chi_1 - \chi_2) \right.$$
$$\left. - \xi^2 \left(3Y_0 + 4\xi^2 - \cos^2 \phi \right) (\chi_1 + \chi_2) \right] k^{-3} V_A^{-5} \,. \tag{5.102}$$

Because function f_χ is proportional to Y_0, the correction Y_χ, to the cold-plasma solution Y_0 = 0, is equal to zero. We consider the cold-plasma solution (5.68). We have shown that, for this root, $P_0'(Y_0)$ is always negative. For a surface wave which is stable in an ideal medium, we have $A_1 A_2 < 0$, $Y_0^2 > 0$, $Y_0 + \xi^2 > 0$. Expression (5.101) is positive if

$$\pm Y_0 \xi \sqrt{Y_0 + \xi^2} \left(Y_0 + 4\xi^2 - \cos^2 \phi \right) \delta > \xi^2 Y_0 \left(3Y_0 + 4\xi^2 - \cos^2 \phi \right) \,, \tag{5.103}$$

where the parameter δ is defined in Table 5.2 as

$$\delta = \left| \frac{\chi_1 - \chi_2}{\chi_1 + \chi_2} \right| \,. \tag{5.104}$$

There is the possibility that Inequality (5.103) can be fulfilled by both surface wave solutions.

The value $\delta = 1$ corresponds to an interface with a thermally conducting and a non-thermally conducting medium ($\chi_1 \chi_2 = 0$). We consider the case $Y_0 < 0$. Inequality (5.103) is, by squaring, transformed into:

$$Y_0 < 1 - \left(1 + 2\sin^2 \phi \right) \xi^2 < 0 \,, \tag{5.105}$$

where we have assumed that $\phi \neq 0$. Inequality (5.105) is, by squaring, transformed into a second-order inequality in ξ^2:

$$\left(1 + 2\sin^2 \phi \right)^2 \xi^4 - 4\xi^2 - \sin^4 \phi < 0$$
$$\Leftrightarrow \quad \frac{2 - \sqrt{4\sin^4 \phi + 4\sin^2 \phi + 5}}{\left(1 + 2\sin^2 \phi \right)^2} < \xi^2 < \frac{2 + \sqrt{4\sin^4 \phi + 4\sin^2 \phi + 5}}{\left(1 + 2\sin^2 \phi \right)^2} \,. \tag{5.106}$$

Note that the lower boundary is less than zero and the upper boundary is larger than $\cos^2 \phi$ for all angles ϕ. Therefore, Condition (5.106) is fulfilled, in conjunction with the condition that $Y_0 < 0$, if

$$\xi_c^2 < \xi^2 < \cos^2 \phi < \frac{2 + \sqrt{4\sin^4 \phi + 4\sin^2 \phi + 5}}{\left(1 + 2\sin^2 \phi \right)^2} \,. \tag{5.107}$$

When we consider the case $Y_0 > 0$, the inequality in Expression (5.105) reverses. This condition cannot be fulfilled for any value of ξ in the interval where ideally stable surface

waves exist. We conclude from Condition (5.107) that for all angles ϕ, except maybe $\phi = 0$, there exists an interval in the flow speed, which is below the K-H threshold speed, for which a surface wave is stable in an ideal medium, but unstable in a thermally conducting medium. This interval coincides with the interval of viscous instability when $\delta = 1$, so that the same conclusions can be made as for the viscous case.

The value $\delta = 0$ corresponds to equal values of the thermal conduction coefficients in the two media ($\chi_1 = \chi_2$). For this case, the right-hand side of Condition (5.103) is negative when

$$Y_0 \left(3Y_0 + 4\xi^2 - \cos^2 \phi\right) < 0 . \tag{5.108}$$
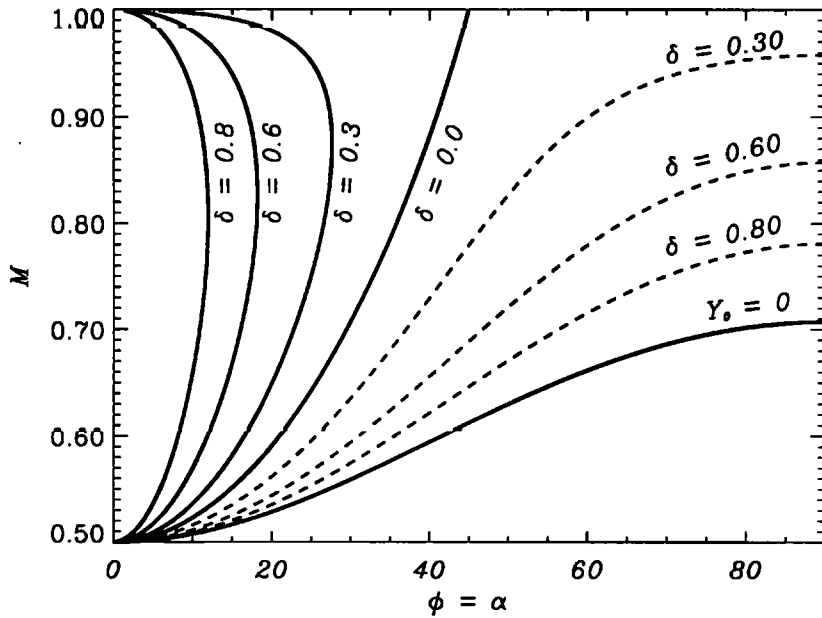
Figure 5.12: Plot of the critical value of M for the existence of an instability due to thermal conduction, as a function of the angle $\phi = \alpha$ for different values of the parameter δ. The minimum threshold for M is, for all values of δ, given by the line $Y_0 = 0$. The solid lines in the left of the plot give, for different values of δ, the minimum angle ϕ for instability. Therefore, the unstable region lies to the right of this critical curve and above the critical curve $Y_0 = 0$. The dashed lines give, for each δ the maximum value of M for the existence of two unstable solutions.

Again we consider the case $Y_0 < 0$ first. The second term of Inequality (5.108) is positive if

$$\xi^2 < \frac{3}{4} - \frac{1}{2}\cos^2\phi \quad \text{or} \quad \xi^2 > \cos^2\phi , \qquad (5.109)$$

which is fulfilled in conjunction with the condition that $-\xi^2 < Y_0 < 0$ if

$$\xi_c^2 < \xi^2 < \frac{3}{4} - \frac{1}{2}\cos^2\phi \quad \text{or} \quad \xi^2 > \cos^2\phi , \qquad (5.110)$$

For the case $Y_0 > 0$, Inequality (5.108) is fulfilled if ξ^2 lies outside the domain given by Condition (5.109), which cannot be satisfied for any value of ξ. We conclude that there exists a domain of instability due to thermal conduction for flow speeds below the K-H threshold in a cold plasma when the thermal conduction coefficients on both sides of the interface are equal. When $\phi = \alpha$, this domain is equal to:

$$M_c^2 < M^2 < \frac{3}{4\cos^2\phi} - \frac{1}{2} . \qquad (5.111)$$

Furthermore, instability due to thermal conduction exists for flow speeds above the K-H threshold in a cold plasma. This is, though, not relevant because the instability growth-rate of the K-H instability is much larger than the dissipative growth-rate.

We consider the case of an arbitrary value of δ. Figure 5.12 shows the curves of the threshold values of M for which the surface waves are unstable due to thermal conduction, as a function of the angle $\phi = \alpha$, for several values of the parameter δ. The solid curve is the threshold speed for the the surface wave solution Y_0, with the plus sign in Expression (5.76). The solid curves on the left show, for different values of δ, the minimum angle ϕ for which unstable solutions exist. Therefore, the region of instability lies to the right of this curve and above the threshold curve. The dashed curve is the threshold speed for the the surface wave solution Y_0, with the minus sign in Expression (5.76). The latter domain of instability is contained within the domain of instability of the other wave solution. Therefore below the dashed curve both surface waves are unstable. When $\delta = 0$, the threshold curves for both wave solutions coincide.

When $\phi = 0$, Inequality (5.103) becomes

$$Y_0 \left(\pm\delta - 1\right) \left(|\xi| - 1\right) \left(|\xi| - \frac{1}{2}\right) > 0 , \qquad (5.112)$$

which shows that for the case $Y_0 < 0$, the lower and upper boundaries for the interval of instability coincide at $\xi = 1$, for all values of δ. The minimum threshold value of M ($\phi = \alpha$)
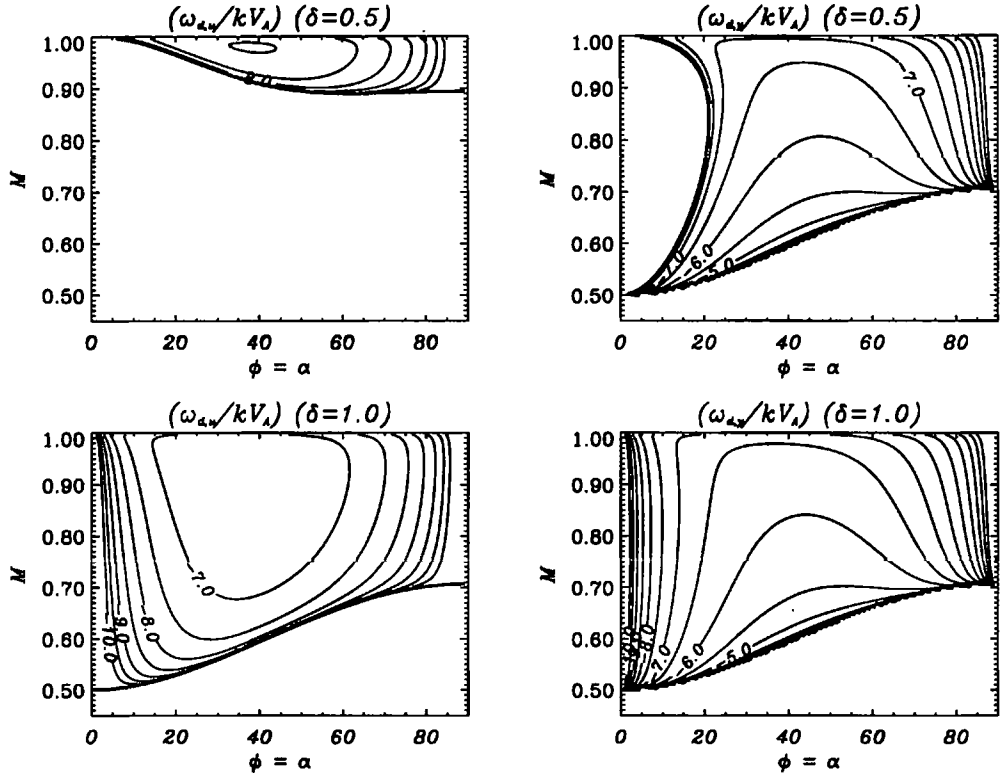
Figure 5.13: Contourplots of the positive values of the analytically derived dissipative growth-rate due to viscosity, $\omega_{d,\nu}$ and due to thermal conduction, $\omega_{d,\chi}$, as a function of angle $\phi = \alpha$ and M, for $\beta = 10^{-1}$, $\delta = 0.5, 1.0$, Re $= 10^4$ and Pr $= 10^{-2}$. The contours are scaled logarithmically. The thick line represents marginal stability.

is the upper limit of $\phi \to 0$, and is equal to $1/2$. It is the minimum threshold for each value of δ. Therefore the difference in the thermal conduction coefficients in each medium does not affect the global stability of the wave solutions.

Dissipative instability

We shall compare the results of studying the corrections due to viscosity and thermal conduction, Y_ν and Y_χ respectively. Expressions (5.93) and (5.101) are substituted into Expression (5.78). Figure 5.13 shows the dissipative growth-rate from both types of dissipation, for two values of the parameter δ, from which it appears that both types of dissipation are the most destabilising to surface waves which propagate at oblique angles with respect to

the direction of the equilibrium magnetic field and its perpendicular direction. Also, when dissipation is present on only one side of the interface, the dissipative instability covers the whole domain where backward propagating waves exist.

From Figures 5.10, 5.12 and 5.13, we see that the domain of instability due to viscosity is contained in the domain of instability due to thermal conduction. Also, the dissipative growth-rate at lower values of M is dominated by thermal conduction. Therefore we conclude that thermal conduction is more destabilizing than viscosity.

The instability due to thermal conduction has its largest growth-rate in the domain near $M = M_c$ and it actually becomes infinite when $M = M_c$. This is because the derivative $P_0'(Y_0)$ becomes small in that domain. This makes Approximation (5.75) invalid and the growth-rate in that domain is therefore incorrect. To calculate the correct growth-rate for this domain, the expansion procedure and ordering of terms has to be reinvestigated, using results of the investigation of the second K-H instability interval. This is a tedious affair and because we expect the surface waves to be K-H unstable in that domain anyway, we do not attempt this here.

When dissipation is only present in one medium ($\delta = 1$), the interface is at its most unstable. The whole domain (M_c,1) is both viscously and thermal conductively unstable. This domain coincides with the domain where the considered pair of surface wave solutions (5.68) consists of both a normal and a backward propagating wave. Only one of the two waves can be viscously overstable but either one or both of the waves can be thermal conductively overstable. It is clear from our investigation that the presence of a backward propagating wave is necessary for dissipative overstability to occur.

5.5   Discussion and comparison with numerical results

In this section, we shall compare the analytical results with numerical results. The roots of (5.54), the tenth-order polynomial $f_I(\omega) = 0$, are found using the NAG routine CO2AFF. This routine uses a variant of Laguerre's method to determine the roots of a polynomial. The non-spurious roots satisfy, besides being solutions of dispersion relation (5.42), the conditions $\Re(\Gamma_{0,1}) > 0$, $\Re(\Gamma_{0,2}) > 0$ and (5.40). Expression (5.47) is used to evaluate the dissipative contribution to the solution frequency.
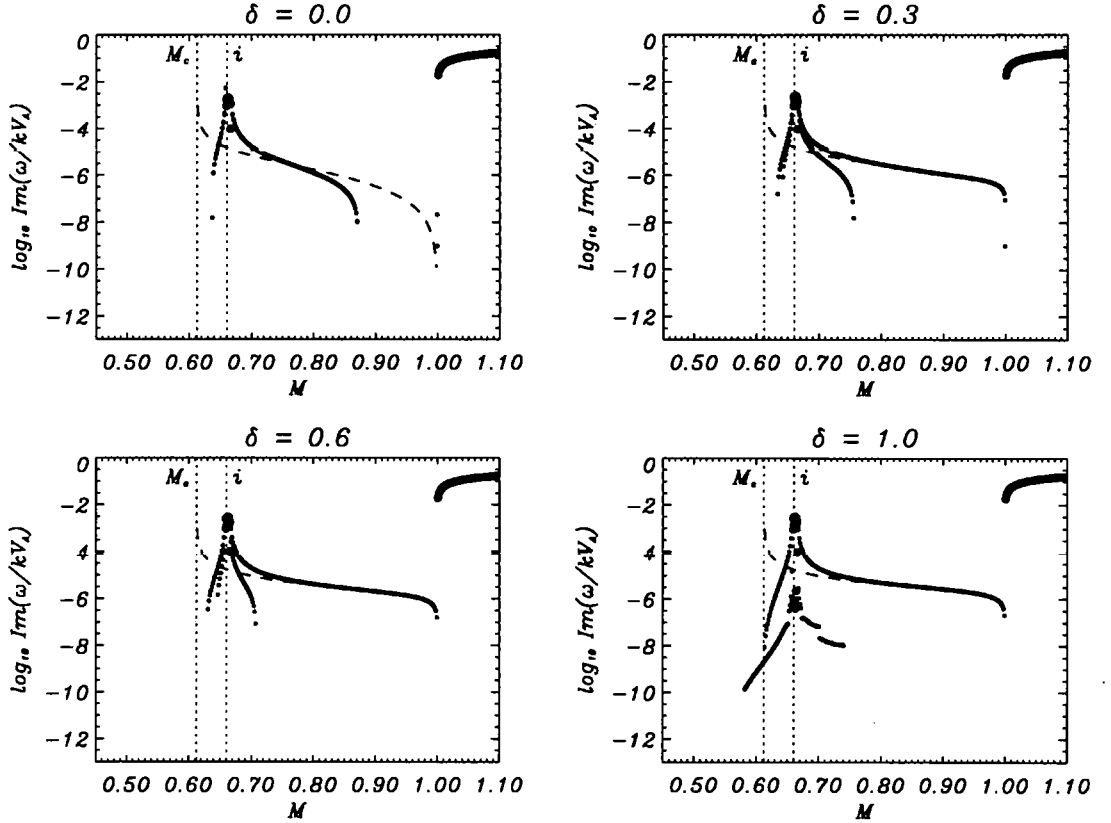
Figure 5.14: Plot of positive values of $Im(\omega/kV_A)$ as a function of the parameter M on a logarithmic scale, for four values of the parameter δ, and with $\phi = \alpha = \pi/4$, $\beta_1 = \beta_2 = 10^{-2}$, $\eta = 1$, $Re = 10^4$ and $Pr = 10^{-2}$. Large dots: K-H instability. Small dots: dissipative instability. Dashed line: leading-order analytical solution (5.78).

5.5.1 Discussion of dissipative growth-rate and dependency on δ

First of all we investigate the dependency of the positive growth-rate $\Im(\omega/kV_A)$ on the parameter δ for $\beta = 10^{-2}$ and $\phi = \alpha = \pi/4$. The two regions of K-H instability are present, shown with thick dots in Figure 5.14. The upper interval corresponds to the monotonic K-H instability discussed in the cold-plasma limit. The lower interval of K-H overstability is narrow and is positioned at the value of M predicted by Expression (5.89) (dotted line denoted with 'i' in Figure 5.14). The small dots represent wave solutions which are dissipatively overstable. For a fixed value of M, it is possible for two overstable solutions to exist. We call the solution branches with the larger growth-rate the 'primary

193

dissipative branch' and the other solution branches the 'secondary dissipative branches'. The primary dissipative branches are the dissipative correction to the cold-plasma solution (5.68), which are of leading order ϵ^2. The dashed line is the analytically derived growth-rate, calculated by substituting Expressions (5.93) and (5.101) into Expression (5.78). The analytical result matches the primary dissipative branch well for values of M larger than 0.75. The difference between the analytical and numerical results, for lower values in M, shows that in this regime the difference between the cold-plasma solutions and solutions for a finite plasma β is more pronounced. The primary dissipative branch has its lower limit at $M = M_c$ as predicted, where the surface wave is of the slow type. The growth-rate of the primary dissipative branch does not become large at $M=M_c$ but does so near the K-H overstability interval. This is because the position where the derivative $P'(Y)$ vanishes, shifts up in M when β is finite, as compared with the cold-plasma limit. Because Expression (5.47) is used to calculate the dissipative growth-rate, the dissipative solution is not valid near the K-H overstability, where it becomes of the same order as the ideal solution, and hence invalid. But because the K-H overstability is expected, by assumption, to have a larger growth-rate than the dissipative instability, we consider only the K-H overstability in this interval. The dissipative branches above and below the K-H instability are from fast and slow surface waves respectively. The numerical results can be improved by not using regular perturbation theory to find the dissipative growth-rate but either by solving the full dispersion relation directly, or by searching for the root of the full dispersion relation in a small circle in the complex plane, around the ideal root.

The other, secondary dissipative branches are the correction to the asymptotic wave branch solutions, which have no contribution at order ϵ^2. The secondary dissipative branch solutions coincide with the primary ones for $\delta = 0$, but differ with increasing value of δ. The asymptotic slow surface wave branch is non-spurious, for values of M larger than the threshold value (5.73), which is thus the lower limit for the secondary dissipative branch (dotted line denoted with a 'c' in Figure 5.14). This value of M is actually below M_c when $\delta = 1$. Therefore in this case, the absolute stability of the interface is governed by the secondary dissipative branch. The secondary dissipative branch does not reach this minimum value, but this could be due to loss of numerical accuracy.

The plot in Figure 5.14 for $\delta = 0$ shows that the dissipative overstability interval has an upper limit, below $M = 1$. This is contrary to what Figure 5.12 predicts for this value
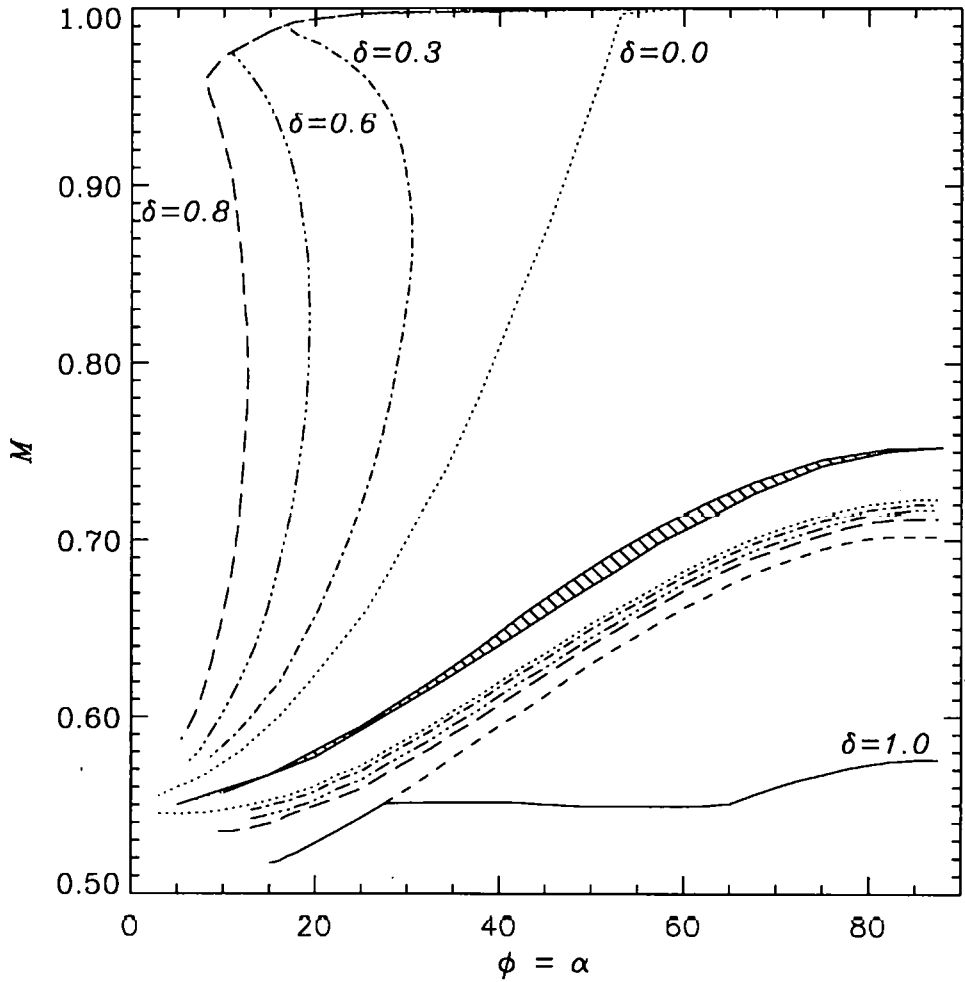
Figure 5.15: Contourplot of the critical value of M for the existence of dissipatively overstable solutions as a function of $\phi = \alpha$, for different values of δ (denoted by different line styles) and with $\beta = 10^{-2}$. The unstable region lies to the right and above the critical curves. The shaded region denotes the K-H overstability interval. The solid line represents the line of marginal stability for $\delta = 1$ when the second dissipative branch is included and the dashed line shows the line of marginal stability when only the primary dissipative branch is included.

of angle ϕ. But Figure 5.12 also shows that the upper limit of the dissipative instability is very sensitive to a small decrease in ϕ from its value of $\pi/4$.

Figure 5.15 shows the domains of dissipative overstability in a M-ϕ diagram. This figure compares well with Figure 5.12, with the modifications we have mentioned earlier.

195

The solid line represents the minimum threshold in M for all values of δ for the existence of dissipatively overstable wave solutions. However, this critical curve is determined by the secondary dissipative branch, which has a much lower growth-rate compared with the primary branch and is therefore of lesser importance. The minimum threshold in M is more realistically described by the dotted line, which is $M = M_c$. The minimum threshold value in M, for all values of δ and ϕ, is $M = 0.5$.

5.5.2 Dependency of dissipative growth-rate on β

Figure 5.16 shows how the dependency on M of the positive growth-rate $\Im(\omega/kV_A)$ of the surface wave solutions varies with the parameter β. The K-H overstability interval is located at $M = M_c + \epsilon^{1/2}/2$ (dotted line with caption 'i' in Figure 5.16), as given by Expression (5.89). The width of the instability domain becomes narrower and the growth-rate decreases, with decreasing values of β. In the plots of $\beta = 10^{-3}$ and 10^{-7}, the width of this instability interval falls below the resolution of the plot. The monotonic K-H instability interval remains virtually unchanged because the lowest-order term in the growth-rate is independent of β and corresponds to the cold-plasma instability connected to the solution (5.68).

The primary dissipative branch solution is situated in the interval $(M_c, 1)$ for all values of β in Figure 5.16. Because the growth-rate of the primary dissipative branch is calculated, to leading order, from the cold-plasma solution, the order of the growth-rate does not depend strongly on the parameter β. The dashed line is the analytically derived growth-rate, c alculated by substituting Expressions (5.93) and (5.101) into Expression (5.78). It is not surprising that the analytical result agrees better with the numerical result, for decreasing values of β. For the case $\beta = 10^{-7}$ the analytical and numerical results are in perfect agreement. This shows that the calculation of the dissipative growth-rate due to viscosity (5.93) has been derived correctly from dispersion relation (5.43).

We see from Expression (5.32), that for $\beta < 10^{-2}$, the dissipative growth-rate due to viscosity is more important than that due to thermal conduction. For $\beta = 10^{-7}$, which represents the cold-plasma limit, the dissipative growth-rate is fully determined by viscosity. For $\beta > 10^{-2}$, the roles are reversed and the dissipative growth-rate due to thermal conduction is more important than that due to viscosity. For $\beta = 10^{-2}$, we have shown that thermal conduction is more important than viscosity.

Figure 5.16: Plots of positive values of $\Im(\omega/kV_A)$ as functions of the parameter M on a logarithmic scale, for four values of the parameter $\beta = \beta_1 = \beta_2$, and with $\phi = \alpha = \pi/4$, $\eta = 1$, $\delta = 1$, Re $= 10^4$ and Pr $= 10^{-2}$. Large dots: K-H instability. Small dots: dissipative instability. Dashed line: leading-order analytical solution (5.78).

The secondary dissipative branch depends strongly on the parameter β. The growth-rate of these solutions is proportional to a power of β and is positioned around the K-H overstability, in the interval defined by the value of M at the points 'a' (5.73) and 'c' (5.73). In the plots for $\beta = 10^{-3}$, 10^{-7}, the secondary dissipative branches do not reach the boundaries of this interval. We believe that this a numerical error because of loss of

197
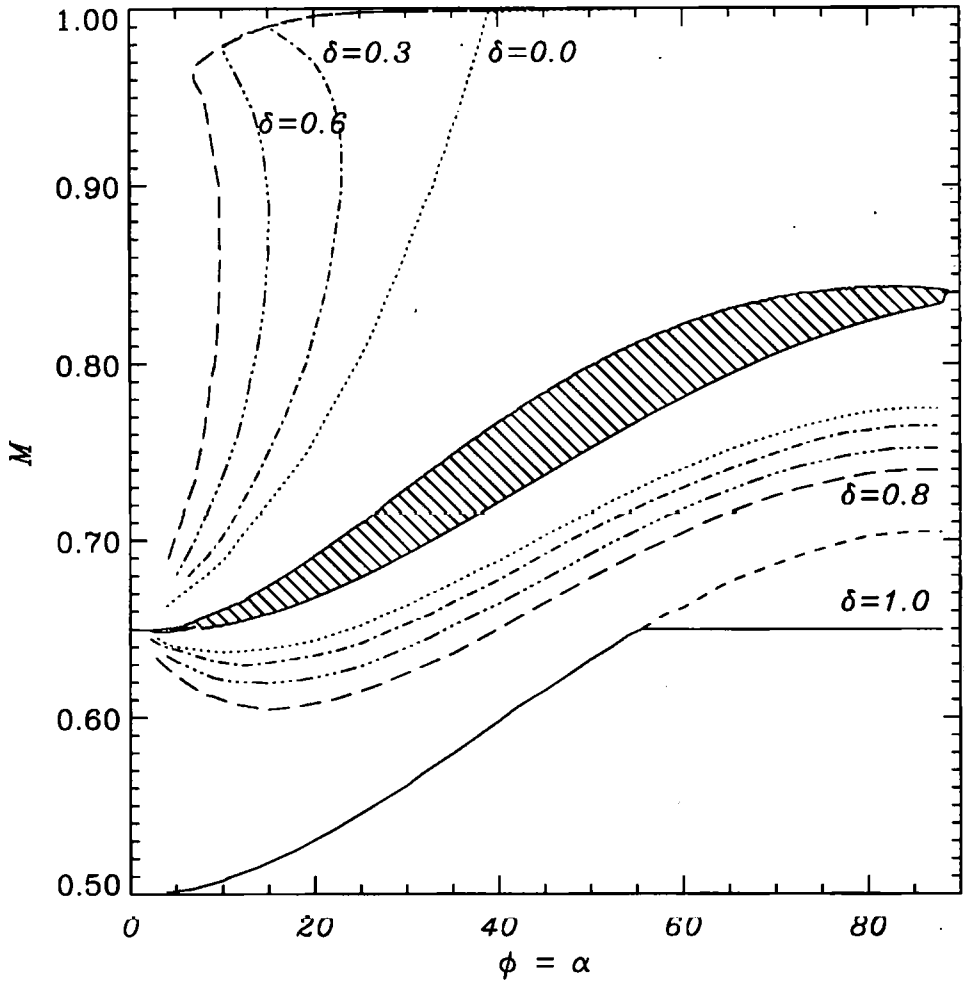
Figure 5.17: Contourplot of the critical value of M for the existence of dissipatively overstable solutions as a function of $\phi = \alpha$, for different values of δ (denoted by different line styles) and with $\beta = 10^{-1}$. The unstable region lies to the right and above the critical curves. The shaded region denotes the K-H overstability interval. The solid line represents the line of marginal stability for $\delta = 1$ when the second dissipative branch is included and the dashed line shows the line of marginal stability when only the primary dissipative branch is included.

accuracy at such low values of growth-rate.

Figure 5.17 shows the domains of dissipative overstability in an M-ϕ diagram for $\beta = 10^{-1}$. The domain of K-H overstability has become wider and is, as expected, positioned at higher values in M, compared with the case of $\beta = 10^{-2}$. With respect to the dissi-

198

pative instability domains, Figure 5.17 resembles Figure 5.15, with the exception that the domain, where the second dissipative branch solution is the only contributor to the dissipative growth-rate, has shrunk. Also in this case, the value of $M = M_c$ determines the lower threshold for dissipative instability, which is clearly lower than the K-H instability threshold.

5.5.3 Dependency of dissipative growth-rate on density ratio

From Table 5.1 is becomes clear that an active region is denser, by at least an order of magnitude, compared with a coronal hole $(\rho_{0,1}/\rho_{0,2} \sim 10)$. A jump in density has not been taken into account in our model. It is expected that a density jump has an influence on the stability criteria (Yang & Hollweg, 1991; Ruderman & Fahr, 1993,1995; González &
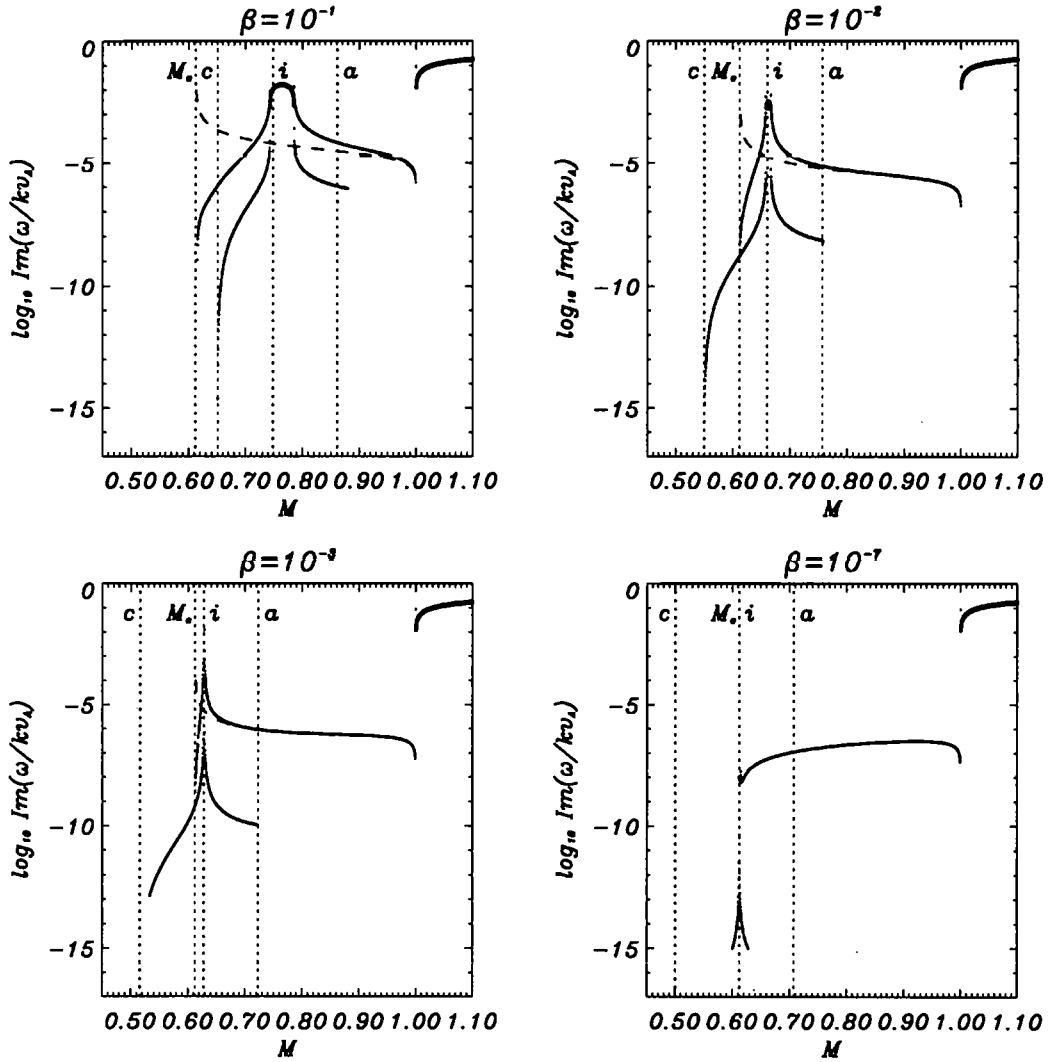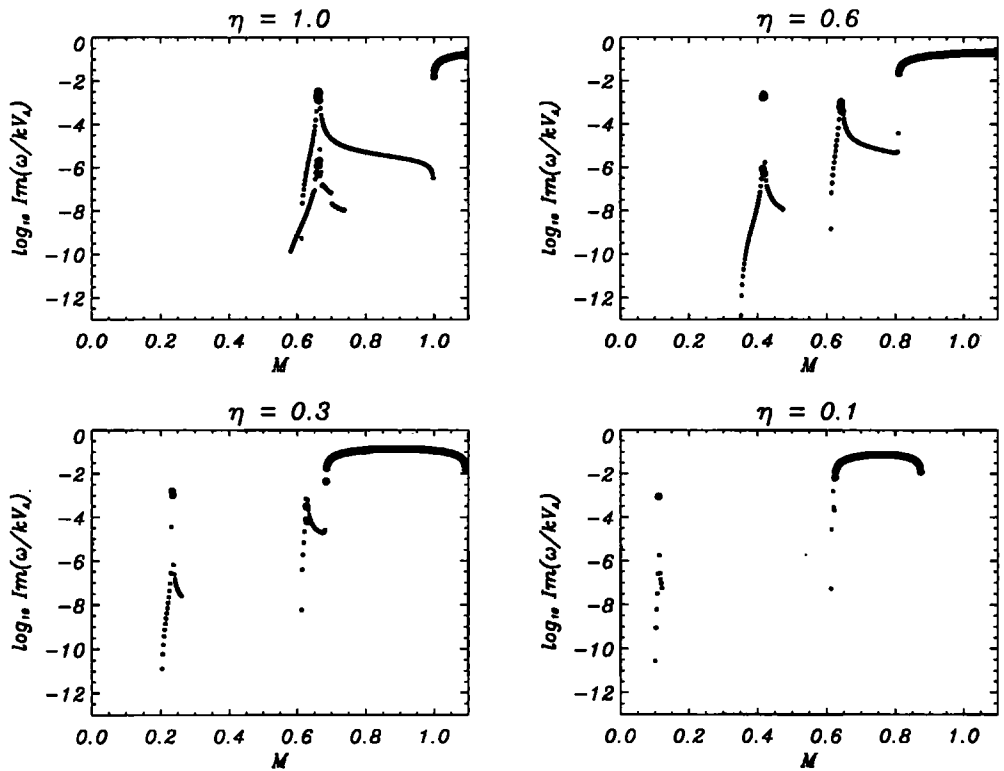

Figure 5.18: Plots of positive values of $\Im(\omega/kV_A)$ as functions of the parameter M on a logarithmic scale, for four values of the parameter η, and with $\phi = \alpha = \pi/4$, $\beta_1 = \beta_2 = 10^{-2}$ and $\delta = 1$. Large dots: K-H instability. Small dots: dissipative instability.

Gratton, 1994b). González & Gratton (1994b) showed that for $\phi = \alpha$ and $\beta = \beta_1 = \beta_2$, the global criterion for K-H instability, is given by

$$M > \frac{1}{2}\left(\eta + \sqrt{\frac{\beta}{1+\beta}}\right) , \qquad (5.113)$$

where η is, from looking at Expression (5.49), equal to $(\rho_{0,1}/\rho_{0,2})^{-1/2}$. A density ratio of 10 corresponds to a value of $\eta \approx 0.32$. Expression (5.113) coincides with the lower limit of Expression (5.90) when $\eta = 1$. The K-H threshold is lowered when the density ratio is increased. Because we have shown that both the K-H and dissipative instabilities are connected with the existence of a backward propagating wave, it is reasonable to assume that the threshold speed for the existence of dissipatively overstable solutions is lowered as well, with an increase in density ratio. Figure 5.18 shows the positive values of $\Im(\omega/kV_A)$ for several values of η. When $\eta \neq 1$, the main K-H instability interval is lowered. The unstable wave solutions are no longer monotonically unstable (González & Gratton, 1994b). The two intervals of K-H overstability do not coincide. One interval remains at its original value in M and the position in M of the other interval is lowered. The two branches of dissipative instability split up as well. The lower limit of the primary dissipative branch remains fixed but its upper limit, which is equal to the lower limit of the main K-H instability, decreases with decreasing values of η. Therefore with decreasing η, the interval of the primary dissipative branch is shortened. At $\eta = 0.1$ (corresponding to $\rho_{0,1}/\rho_{0,2} = 100$), this instability interval has all but disappeared. The secondary dissipative branch also decreases, together with one of the K-H overstability intervals.

We conclude that although an increasing density ratio lowers the threshold speed for the K-H and dissipative instabilities, in practice the threshold speed for the relevant interval of dissipative instability does not change. The width of the dissipative instability intervals decreases. Therefore, the introduction of a density jump stabilises the interface against the dissipative instability. Tirry *et al.* (1998) calculated the threshold speed for which negative energy wave solutions exist for surface waves propagating on a single interface in the cold-plasma limit and in the presence of a density jump. Their threshold speed is in agreement with the threshold speed for backward propagating surface waves, and hence for dissipative instability, as we found in this chapter. It is not clear why the whole domain, where backward propagating waves exist, does not become dissipatively unstable when $\delta = 1$. More research is clearly needed to resolve this question.

5.5.4 Conclusions

In this chapter we investigated a model for a coronal hole boundary by considering the dissipative stability of a tangential discontinuity in the presence of an equilibrium flow to model a coronal hole boundary. We showed that the presence of dissipation can destabilise the tangential discontinuity. We demonstrated that in the solar corona, thermal conduction and viscosity are of equal importance for our model. The strongly magnetised nature of the corona makes the thermal and viscous diffusion mechanisms highly anisotropic so that the momentum flux across magnetic flux surfaces is negligible. Therefore is it possible to consistently consider a tangential discontinuity in a dissipative plasma. Gravity is neglected and the plasma quantities on each side of the discontinuity are uniform. These assumptions limit the length-scale of a disturbance to be much less than the coronal scale-height. A dispersion relation for MHD surface waves, in the weakly dissipative regime, is derived.

The cold-plasma limit is often used to model the corona, but in this limit it is not possible to consider thermal conduction consistently. Therefore, we investigate the stability of surface waves for a small but finite plasma β. The dispersion relation is solved analytically, for a specific choice of the free parameters, in an expansion procedure for small values of the parameter ϵ, which is proportional to the square of the ratio of cusp to Alfvén speed. In the cold-plasma limit, only fast surface waves exist, which become unstable for an equilibrium flow speed given by the lower limit of Expression (5.70). When the flow is parallel to the equilibrium magnetic field, this threshold is equal to twice the Alfvén speed. In a plasma with a small but finite plasma β, slow and fast surface waves exist. Fejer (1964) and Duhau & Gratton (1973) noticed that, when increasing the equilibrium flow speed, the transition from a slow to a fast surface wave is marked by K-H instability. The growth-rate of the solutions in this K-H instability interval is proportional to the plasma β and therefore vanishes in the cold-plasma limit. The threshold speed of this instability interval lies below the cold-plasma K-H instability interval and is approximately given by Expression (5.88).

The dissipative terms in the dispersion relation are considered small compared with the ideal terms. This implies that the influence of viscosity and thermal conduction can be considered separately. They are incorporated into the expansion procedure by noticing that the magnitude of the lowest-order viscous and thermal conduction terms are of order ϵ^2 in the corona. As a consequence the lowest-order thermal conduction contribution to the growth-rate of a surface wave is calculated consistently from the ideal, cold-plasma

solution. We use a diagram, introduced by Chandrasekhar (1961), to investigate graphically the behaviour of the surface waves with real frequencies in ideal plasmas, and to determine the condition for which backward propagating surface waves exist. We investigated the instability domains and growth-rates of both types of dissipative instabilities and established that instability only occurs when a backward propagating wave is present. Dissipation is most destabilizing when the difference between the transport coefficients on each side of the interface, represented by the parameter δ, is large. The viscous instability depends strongly on β and actually vanishes when the viscosity coefficients are equal on both sides of the interface ($\delta = 0$). When viscosity is present in only one of the two media ($\delta = 1$), the whole domain where backward propagating waves exist, is unstable. The instability due to thermal conduction does not depend strongly on the parameter δ. The minimum threshold speed for instability is, for all values of δ, equal to the minimum equilibrium speed at which a fast surface wave in the cold-plasma limit is a backward propagating wave, given by Expression (5.69), which is below the threshold speed for K-H instability. Also, this speed does not depend on β. Surface waves become unstable due to viscosity at that speed, only when $\delta = 1$. We used this fact as one of the reasons to argue that thermal conduction is more destabilizing that viscosity. The difference between the threshold speed for K-H and dissipative instability is of order β and is therefore small in the corona. Therefore, the statement that dissipative instability significantly lowers the threshold speed for instability with respect to the Kelvin-Helmholtz instability (Tirry et al., 1998) is not correct for the corona. The second K-H instability interval is, though, narrow. The dissipative instability destabilizes surface waves in a much larger domain in parameter space for flow speed below the cold-plasma K-H threshold speed.

We compared the results of the analytical expansion procedure with the results of solving the ideal dispersion relation numerically. The numerical analysis showed two unstable solution branches. The branch with the largest growth-rate has a contribution in the cold-plasma limit and corresponds to the analytically derived result. We call this solution the primary dissipative branch. There is a good agreement between the analytical and numerical results. The second branch of dissipatively unstable solutions is the dissipative correction to a surface wave solution which is proportional to a power of β (hence not described in the cold-plasma limit). We call this solution the secondary dissipative branch. The growth-rates of these solutions are much smaller than those of the solutions of the primary

branch. Therefore these solutions are not of great importance, with the one exception that the threshold equilibrium speed for instability of these solutions can be lower than that of the primary dissipative branch solutions, but never lower than the global threshold of the primary solutions in our specific model.

The analytical and numerical results differ for values of the flow speed near to the second K-H instability interval. The analytical result is calculated from the cold-plasma solution and therefore does not describe this second K-H instability. We did not expect any agreement because regular perturbation theory breaks down in this regime. Therefore the numerical result is not valid near the second K-H interval. It is necessary to refine the calculation of the dissipative correction to the ideal solution for this case.

We consider the magnitude of the dissipative instability growth-rate. We assume that the surface wave has a period of 10 s and its wave-length is approximately given by $L \sim V_A P \sim 2 \times 10^4$ km, where the value of the Alfvén speed in Table 5.1 is used. The value of the wave-length is in good agreement with the value of L chosen to estimate the magnitude of the dimensionless parameters in Table 5.1. From Figures 5.13 and 5.14, we estimate that the instability growth-rate due to dissipation is equal to $\omega_d/kV_A \sim 10^{-5}$. From the value of the Alfvén speed given in Table 5.1 and the given wave-length, the time, t_d, for the wave amplitude to increase by a factor e is approximately 16 days. This is very long. If we estimate this time for a surface wave with a period of 1 s, we find a wave-length of 2×10^3 km. The values of the Reynolds numbers and Péclet number are smaller on this length-scale, than those given in Table 5.1, namely Re = 400 and Pe = 8. The time t_d is equal to 1.1 hours. In this time the surface wave has travelled a distance of the order of the solar radius. We conclude that surface waves with wave periods of the order of 1 s or less are necessary to have an effect on a coronal scale. A similar conclusion has been made by *e.g.* Gordon & Hollweg (1983) and Ruderman (1991) for the damping rate of surface waves in the corona. Oscillations in this frequency range have extensively been observed (see Aschwanden *et al*, 1999). The wave period in this range is also less than the ion collision time and the validity of collisional theory in this regime is therefore questionable. The secondary K-H instability has a growth-rate of order $\omega/kV_A \sim 5 \times 10^{-3}$. For a surface wave with a period of 10 s and 1 s, the time t_d is approximately equal to 42 and 4 minutes respectively. It is clear that the K-H instability evolves much faster than the dissipative instability.

The global threshold equilibrium speed for the onset of a dissipative instability is, from

Expression (5.69) given as:

$$| v_{0,1} - v_{0,2} | = \left| \frac{\cos\phi}{\cos\alpha} \right| V_A \ . \tag{5.114}$$

If we consider the equilibrium flow parallel to the equilibrium magnetic field, surface waves become unstable only if the flow speed is super-Alfvénic. The threshold speed is lowered when the direction of the equilibrium flow is oblique with respect to the direction of the equilibrium magnetic field. We need $| \phi - \alpha | > 84$ degrees, for the threshold speed to be subsonic. Therefore, we need the magnetic field to be quasi-perpendicular to the equilibrium flow. This is unlikely to be the case in a coronal hole, which has open magnetic field-lines directed radially from the sun.

The threshold speed is also expected to be lowered if there is a jump in density between the plasmas on both sides of the interface, because the minimum speed for which backward propagating waves exist is lowered. For a coronal hole boundary, we expect density in the coronal hole to be one order in magnitude less dense than an active region. We find that although the threshold speed for dissipative instability (and K-H instability) is lowered to $0.2\ V_A$, the relevant dissipative instability interval remains fixed and its width is decreased. Therefore we conclude that a density jump stabilises the interface against the dissipative instability. This case shows that it is necessary to calculate the growth-rate of the dissipative instability explicitly, to make realistic statements on the stability of the interface.

We conclude from investigating the instability growth-rate and the threshold flow speed for instability, that it is unlikely that the coronal hole boundary can become dissipatively unstable (Joarder *et al.*, 1997). Even if high enough flow speeds could be reached, it is the K-H instability which destabilizes the coronal hole boundary on a much faster time-scale than the dissipative instability.

Chapter 6

Conclusions

In this thesis we considered two topics: (i) the weakly nonlinear evolution of two oppositely directed waves (bounded (standing) waves and two pulses), where we used the concept of the ponderomotive force, and (ii) the dissipative instability of the tangential discontinuity.

A mechanical analogue of bounded, nonlinear Alfvén waves

We investigated, in the weakly nonlinear regime, the motion of frictionless beads along an oscillating, stretched string, of constant tension, and the motion of a fluid in an oscillating elastic tube, as analogues for the behaviour of bounded, nonlinear Alfvén waves. the magnetic tension of the tension force of a In these models, the tension force is the restoring force. In the analogue of the string, we identified the ponderomotive force as the longitudinal component of the tension force, which is proportional to the spatial gradient and the acceleration of the string. It is a basic nonlinear force, which does not depend on the tension of the string. For the case of Alfvén waves, we showed that the ponderomotive force is of this form. The leading-order term of the ponderomotive force has the form of a magnetic wave pressure force.

We considered a string oscillating in one of its normal modes (bounded wave). We described the motion of discrete particles (beads) along the string by the equation of an anharmonic oscillator. The beads oscillate around the positions of the anti-nodes of the string's wave-field. When we considered a continuous spread of beads, at a finite time, the beads concentrated at the anti-nodes and the linear density of the beads became infinite, on a time-scale proportional to a^{-1}. This occurs because the 'compressibility' of the beads

has not been taken into account.

We considered the mechanical analogue of a 'tube' of infinitely small width, filled with a 'fluid' and derived the governing equations for the tube's transverse motions and the fluid's dynamics. Again we considered the tube to be oscillating in one its normal modes. The second-order ponderomotive force of the tube, excites bounded sound waves in the fluid. The linear density of the fluid enhances at the position of the anti-nodes of the tube's wave-field. The maximum density is proportional to a^2/β. Therefore, waves with large amplitudes, or when the kinetic pressure of the fluid is much less than the tension of the tube-fluid system ($\beta \ll 1$) produce large density enhancements. When $\beta = 0$, the linear density of the fluid grows quadratically in time. We calculated the cubically nonlinear moderation of the tube's oscillation by the sound wave. We see the generation of the third spatial harmonic. For $\beta \ll 1$, the moderation is strong. For $\beta = 0$, we showed that the amplitude moderation of the original wave mode is, to leading order, proportional to $a^3 t^3$ and the frequency-shift is proportional to $a^2 t^2$. These results match identically with the case of bounded Alfvén waves (Rankin *et al.*, 1994).

We conclude that the models we have investigated, even though we considered a constant tension, are good mechanical analogues for the weakly nonlinear dynamics of bounded Alfvén waves, especially when $\beta \ll 1$, which is the equivalent of plasmas with a low plasma β, for which large perturbations of density are possible. The results found are in good agreement with the results of Rankin *et al.* (1994) and those of Chapter 3.

The nonlinear evolution of fast magneto-acoustic waves in a two-dimensional cavity

We investigated the weakly nonlinear evolution of bounded, fast magneto-acoustic waves in a two-dimensional cavity and in the cold-plasma limit. We compared analytical results to numerical simulations, using a fully nonlinear Lagrangian code. In the cold-plasma limit, slow magneto-acoustic waves are absent. Because the fast magneto-acoustic wave is driven by pressure and tension forces, the ponderomotive force of fast magneto-acoustic waves is more complicated than in the case of Alfvén waves. The leading-order terms of the ponderomotive force of fast magneto-acoustic waves have the form of a product of a wave quantity and a spatial gradient of a wave quantity. The second-order ponderomotive force has two effects: quadratically nonlinear moderation of the fast waves and excitation of

206

plasma flows along the equilibrium magnetic field. We showed that, because of the selection rules imposed by the boundary conditions, the quadratically nonlinear moderation is non-resonant. This implies that, at this order, there is no generation of a second harmonic and there is not the possibility of three-wave interaction. The component of the second-order ponderomotive force parallel to the equilibrium magnetic field excites, secularly, a plasma flow towards the positions of the anti-nodes of the fast wave velocity field, where the density grows quadratically in time. We found that this behaviour is in accordance with that noted by Allan *et al.* (1991). Furthermore we calculated the cubically nonlinear moderation of the fast magneto-acoustic waves and find that the original wave mode has an amplitude moderation proportional to $a^3 t^3$, and a frequency-shift proportional to $a^2 t^2$. We also see the generation of third spatial harmonics The frequency-shift differs from the case of the moderation of bounded Alfvén waves only by a geometric factor (Rankin *et al.* 1994). We described a multiple-scales approach to calculate the frequency-shift in a more natural way. We recognise that the expansion procedure fails on a time-scale proportional to a^{-1}, at which the component of the velocity parallel to the equilibrium magnetic field forms, at a finite time, a stationary discontinuity. We estimated an upper limit for this time, using the methods of characteristics. At the velocity discontinuity, the density becomes, locally, infinite. This is an unphysical situation, which is a result of the failure of the assumption of a cold plasma. We estimated from the cold-plasma solutions that the kinetic pressure force becomes, locally, important on a time-scale proportional to $\beta^{1/2}$. The maximum density perturbation is proportional to a^2/β. We conclude that it is necessary to consider a plasma with a finite plasma β. The condition for the weakly nonlinear assumption to remain valid is given by the condition $a < 2(2\beta)^{1/2}$, which has previously been noted by Rankin *et al.* (1994). For large wave amplitudes, the numerical simulation showed the formation of a shock travelling in the direction transverse to the magnetic field. We modelled the initial evolution as the superposition of the first-order and second-order fast wave modes.

As it stands, a vital and physical realistic extension to this chapter is to take into account the compressibility of the plasma, *i.e.* a finite finite plasma β, to remove the unphysical manifestation of infinite densities. This complicates the analysis because the fast and slow magneto-acoustic waves are coupled. Also, the assumption of an isolated medium can be adjusted to make the model more physical by considering an external medium. The boundaries in the transverse direction to the magnetic field are replaced by

interfaces (Murawski, 1994). This enables the investigation of the nonlinear response of higly structured coronal features to large amplitude transients. The recent work of Nakariakov *et al.* (1999), Ofman *et al.* (1999) suggest that, the investigation of the dissipation of slow magneto-acoustic waves which are excited by the ponderomotive force of an Alfvén wave, in a plasma with a low plasma β, is worthwhile.

The nonlinear evolution of an Alfvén pulse

We considered the weakly nonlinear interaction of two linearly polarized Alfvén pulses in both cold plasmas and in plasmas with a finite plasma β. We showed that there is an excellent agreement between the analytical results and the results of a numerical simulation, using a fully nonlinear Lagrangian code.

   We investigated the nonlinear evolution of an initially excited, Gaussian-shaped pulse in the transverse velocity. Two Alfvén pulses are created which propagate in opposite directions. We showed that the second-order ponderomotive force associated with the two pulses has three contributions: the first two contributions are the ponderomotive forces of each Alfvén pulse separately, which has the form of a magnetic wave pressure force, and the third contribution contains a combination of the magnetic perturbations of both pulses. We called the latter term the cross-ponderomotive force, which decreases rapidly to zero as the two pulses separate. The cross-ponderomotive force generates a plasma flow towards the original position of the pulses. In a cold plasma there is no force to counteract this acceleration. Therefore the plasma continues to flow, at a constant speed, towards the central position. We showed that at a finite time, which is proportional to a^{-2}, the nonlinear inertia of the plasma produces a stationary velocity discontinuity, where the density had become infinite. We applied the method of characteristics, both analytically and numerically, to model this. We have a unphysical situation arising similar to those in Chapters 2 and 3. There is no force to balance the inertia of the plasma. It is clear that the kinetic pressure force cannot be neglected for all times. We therefore investigated the nonlinear evolution of two Alfvén pulses in a plasma with a finite plasma β. Then the central perturbation splits up into two slow pulses (for $\beta < 1$), of amplitude a^2, which propagate in opposite direction. We found that the ratio between the pressure force and the nonlinear inertial force is proportional to $0.1a^{-4}\beta$. We considered two cases: (i) The nonlinear inertia of the plasma is not important during the time the slow pulses have not

fully split up. The slow pulses are not substantially moderated nonlinearly during this time and are therefore well-described by the second-order solution. The maximum density perturbation is proportional to $a^2\beta^{1/2}$. (ii) The nonlinear inertia of the plasma is important during the time the slow pulses have not fully split up. The behaviour of the slow pulses during this time is similar to the cold-plasma case, until the time that the pressure force becomes of the same order as the nonlinear inertia. The maximum density perturbation is proportional to $a^4\beta^{-1}$. We also showed that the nonlinear evolution of the separate, travelling pulses is governed by quasi-linear differential equations. The evolution of the Alfvén waves is given by the scalar Cohen-Kulsrud equation. We showed that on a time-scale proportional to $a^2(1-\beta)^{-1}$, a shock is formed on the preceding side of the pulse. The evolution of the slow pulses is governed by the quasi-linear differential equation for sound waves and we showed that a shock is formed on the preceding side of the pulse, on a time-scale proportional to a^2. The Alfvén and slow shocks convert the wave energy effectively into heat (*e.g.* Cohen & Kulsrud, 1974).

In this chapter we looked at an initial pulse in the transverse velocity component v_z. The case of two oppositely travelling Alfvén pulses crossing each other is qualitatively the same. An Alfvén pulse can, of course, also be excited in the transverse displacement component ξ_z or in the transverse magnetic field component B_z. It can be seen that the former case is very similar to the case we considered, because the second-order ponderomotive force is the same as Expression (4.11), but with the shape of the pulse now a spatial derivative of the pulse shape, mass accumulation at $x/\Delta x=0$ is still observed. The latter case, though, is different, because the second-order ponderomotive force is different from Expression (4.11) by a change of sign for the cross-ponderomotive force. The quadratically nonlinear solution to this problem in the cold-plasma limit, is Expression (4.17) with opposite signs for the last term. Consequently, mass is now pushed out from the region around $x/\Delta x = 0$. Also Expression (4.36) only differs by sign. Therefore Expression (4.42) becomes

$$\frac{V_A t_{sc}}{\Delta x} = \min\left\{ \frac{-1}{\sqrt{2\pi}a^2\frac{\partial}{\partial x}\left(x e^{-2x^2/\Delta x^2}\right)} \right\} = \frac{1}{2e^{-3/2}\sqrt{2\pi}\,a^2} \,. \tag{6.1}$$

A surface discontinuity appears at the positions $x/\Delta x = \pm\sqrt{3}/2$. For the case of a finite plasma β, the quadratically nonlinear solution to this problem differs from Expression (4.66)

because the velocity term $v_{x,2c}$ now has the opposite sign:

$$
\begin{aligned}
\frac{v_{x,2}}{V_A} &= -\frac{a^2}{2(1-\beta)} \left[e^{-(X+T)^2} - e^{-(X-T)^2} \right] \\
&\quad + \frac{a^2}{\sqrt{\beta}(1-\beta^2)} \left[e^{-(X+\sqrt{\beta}T)^2} - e^{-(X-\sqrt{\beta}T)^2} \right] \\
&\quad - \mathcal{A}_+(T,X)\, e^{-\frac{(X+\sqrt{\beta}T)^2}{1+\beta}} - \mathcal{A}_-(T,X)\, e^{-\frac{(X-\sqrt{\beta}T)^2}{1+\beta}} \,.
\end{aligned} \tag{6.2}
$$

This problem corresponds to the perfect reflection of an Alfvén pulse at a boundary. This can be seen as the nonlinear interaction between two pulses in the transverse velocity which travel in opposite directions and have opposite signs.

The model we presented is, of course, not only applicable to Gaussian-shaped pulses, as functions of the form $1/(1+s^2)$ or $\mathrm{sech}^2 s$ produce qualitatively the same results.

The results we have shown in this chapter represent basic characteristics of nonlinear Alfvén wave interactions. They are important for the interpretation of more sophisticated numerical simulations of initial-value nonlinear MHD problems, *e.g.* Nakariakov *et al.* (1997, 1998); Oliver *et al.* (1998). This work can be extended by considering more spatial dimensions (to include the nonlinear excitation of fast magneto-acoustic waves), inhomogeneities in the direction of propagation (*e.g.* an atmosphere), transverse structuring (*e.g.* slab geometry) with the effects of dispersion. A possible application under consideration is the interaction of the planet Jupiter with its moon Io by inductively generated travelling Alfvén disturbances along the Jovian magnetic field from Io to the Jupiter ionosphere.

The dissipative instability of the tangential discontinuity

We considered the dissipative instability of a tangential discontinuity, in the presence of flow, as a model of a coronal hole boundary. We found a dissipative instability for flow speeds below the threshold speed of Kelvin-Helmholtz instability in a cold plasma. We related the onset of instability with the existence of backward propagating waves. We showed that in the corona, viscosity and thermal conduction, for our model, are of equal importance. We assumed weak dissipation. We derived a general dispersion relation for surface waves, which has earlier been derived by Ruderman *et al.* (1996). We extended their work by considering a plasma with a finite plasma β, so that thermal conduction is included in the analysis. The dissipative growth-rate is calculated using regular perturbation theory. The effect of vicosity and thermal conduction can be calculated separately from each other.

We investigated a specific model for a plasma with a low but finite plasma β, which assumed no jump in density. The roots of the dispersion relation are calculated, from the cold-plasma limit, analytically in an expansion procedure. In this way, the leading-order effect of thermal conduction is included. We discussed the Kelvin-Helmholtz instability criteria. In the cold-plasma limit, the Kelvin-Helmholtz instability occurs at a threshold flow speed, $v_0 = 2V_A$. In a plasma with a low but finite plasma β, there is the appearance of a small, second Kelvin-Helmholtz instability interval with a threshold speed, $v_0 = V_A + V_c$, which is below the first Kelvin-Helmholtz instability interval. This second interval separates the slow and fast surface wave solutions. We investigated the appearance of this instability interval both graphically and mathematically.

We calculated the dissipative growth-rate due to viscosity and thermal conduction. We showed that the minimum flow speed for dissipative instability is the Alfvén speed and that dissipation is most destabilising when dissipation is only present in one of the two media. For that case, the domain of instability coincides with the domain of backward propagating waves. The threshold speed for the dissipative instability due to viscosity increases as the difference between the viscosity coefficients decreases. When the viscosity coefficients are equal, we found that there is no dissipative instability due to viscosity. The threshold speed due to thermal conduction is, for all values of the difference in thermal conduction coefficients, equal to the threshold flow speed for the appearance of backward propagating waves. The domain of instability due to thermal conduction encompasses the domain of instability due to viscosity. We therefore concluded that thermal conduction is more destabilising than viscosity. We discussed the dependency of the dissipative growth-rate on the plasma β and a jump in density. We showed that for all values of the plasma β smaller than unity, the threshold flow speed for dissipative instability is below the Kelvin-Helmholtz threshold flow speed. In the corona ($\beta \sim 10^{-2}$), the difference is expected to be small, though. We also concluded that a density jump stabilises the interface, although the threshold flow speed for dissipative instability is lowered.

We discussed the relevance of the dissipative instability to coronal holes. We estimated that waves of periods of a second or less, may grow significantly unstable in the corona. Waves with periods larger than a second grow unstable too slowly. We also concluded that the equilibrium magnetic field needs to be quasi-perpendicular to the flow in order for the the threshold flow speed to be below the expected flow speed of the solar wind in

211

a coronal hole. This is not expected to occur in a coronal hole. We therefore concluded that the dissipative instability (and Kelvin-Helmholtz) instability may not be important for coronal hole boundaries. There is the possibility that the dissipative and K-H instability are important in the solar wind (Joarder *et al.*, 1997) and the heliopause. This is, though, for future consideration.

We explained the need for improving the calculation of the dissipative growth-rate, because regular perturbation theory fails near the lower Kelvin-Helmholtz instability domain. The work of this chapter can be extended and improved in many ways . We have only considered a specific case of the dispersion relation. The effect of different magnetic fields on each side of the interface and the existence of a density jump , for example, have not been explored in full. We also did not investigate the dissipation of surface waves. This model could also be extended to incorporate a smooth density transition between the two media, which introduces the possibility of resonant absorption. For this, it is necessary to include the shear viscosity coefficient η_1 (Mok, 1987; Ofman *et al.*, 1994). Also, Nakariakov *et al.* (1999) claim to observe that shear viscosity is more important than the classical value that Braginskii (1965) gives. This suggests that shear viscosity has to be included in viscous models.

concluding remarks

In this thesis, we investigated the properties of the ponderomotive force of magnetohydrodynamical waves and dissipative effects for simple models, which are important for interpreting more sophisticated nonlinear numerical MHD simulations and to help, for example, explain the wealth of recent, high-quality, solar observations of wave and transient behaviour from the SOHO and TRACE space crafts.

References

Abramowitz, M. & Stegun, I.A.: 1965 Handbook of mathematical functions with formulas, graphs and mathematical tables, *Dover publ.*, New-York.

Allan, W., Manuel J. & Poulter E. 1990 Does the ponderomotive force move mass in the magnetosphere, *Geophys. Res. Lett.* **17**, 917-920.

Allan, W., Manuel J. & Poulter, E. 1991 Magnetospheric cavity modes: some nonlinear effects, *J. Geophys. R.* **96**, 11461-11473.

Allan, W.: 1992 Ponderomotive mass transport in the magnetosphere, *J. Gephys. R.* **97**, 8483-8493.

Allan, W. & Poulter, E.M. 1992 ULF waves - their relationship to the structure of the Earth's magnetosphere, *Rep. Prog. Phys.* **55**, 533-598.

Allan, W. & Manuel, J. 1996 Ponderomotive effects in magnetospheric hydromagnetic waves, *Annales Geophysicae* **14**, 893-905.

Arber T.D., Longbottom A.W. & Van Der Linden, R.A.M. 1999 Unstable coronal loops: numerical simulations with predicted observational signatures, *Astrophys. J.* **517**, 990-1001.

Arons, A. & Peppard, M. 1965 Einstein's proposoal of the photon concept - a translation of the Annalen der Physik paper of 1905, *American J. of Phys.* **33**, 367-374.

Aschwanden, M.J., Fletcher, L., Schrijver, C.J. & Alexander,D.: 1999 Coronal loop oscillations observed with the transition region and coronal explorer, *Astrophys. J.* **520**, 880-894.

Baranov, V.B.: 1990 Gasdynamics of the solar wind interaction with the interstellar medium, *Space Sci. Rev.* **52**, 89-120.

Baranov, V.B., Fahr, H.J., Ruderman, M.S.: 1992 Investigation of macroscopic instabilities at the heliopause boundary surface, *Astron. Astrophys.* **261**, 341-347.

Benz, A.O. 1993 Plasma astrophysics, *Kluwer Academic Publishers*, Dordrecht.

Bittencourt, J.A.: 1986 Fundamentals of plasma physics, *Pergamon Press*, Oxford.

Braginskii, S.I.: 1965 Transport processes in plasma, *Rev. Plasma Phys.* **1**, 205-309.

Boynton, G.C. & Torkelsson, U. 1996 Dissipation of non-linear Alfvén waves, *Astron. Astrophys.* **308**, 299-308.

Cairns, R.A.: 1979 The role of negative energy waves in some instabilities of parallel flows, *J. Fluid. Mech.* **92**(1), 1-14.

Cally, P.S.: 1986 Leaky and non-leaky oscillations in magnetic flux tubes, *Solar Phys.* **103**, 277-298.

Cargill, P.J., Spicer, D.S. & Zalesak, S.T. 1997 Magnetohydrodynamic simulations of Alfvénic pulse propagation in solar magnetic flux tubes: two dimensional slab geometries, *Ap.J.* **488**, 854-866.

Chandrasekhar, S.: 1961 Hydrodynamic and hydromagnetic stability, *Clarendon Press*, Oxford.

Cohen, R.H. & Kulsrud, R.M. 1974 Nonlinear evolution of parallel-propagating hydromagnetic waves, *Phys. Fluids* **17**, 2215-2225.

Cowling,T.G.: 1957 Magnetohydrodynamics, *Interscience*, New-York.

Craik, A.D.D. & Adam, J.A.: 1979 Explosive resonant wave interactions in a three-layer fluid flow, *J. Fluid Mech.* **92**, 15-33.

Craik, A.D.D.: 1985 Wave interactions and fluid flows, *Cambridge University Press*, Cambridge.

Davila, J.M.: 1987 Heating of the solar corona by the resonant absorption of Alfvén waves, *Astrophys. J.* **317**, 514-521.

Dendy, R.O.: 1990 Plasma dynamics, *Clarendon Press*, Oxford.

Dendy, R.O. (ed.): 1993 Plasma Physics, An introductory course, *Cambridge University Press*, Cambridge.

Duhau, S. & Gratton, J.: 1973 Effect of compressibility on the stability of a vortex sheet in an ideal magnetofluid, *J. Plasma Physics* **13**, 451.

Dym, H. & McKean, H.P.: 1972 Fourier series and integrals, *Academic Press*, New York.

Edwin, P.M.: 1992 Wave propagation in inhomogeneous space plasmas from the solar atmosphere viewpoint, *Ann. Geophysicae* **10**, 631-643.

Elliot, J.A. 1993 Plasma physics: chapter 2, *Cambridge University Press*, Cambridge.

Ershkovich, A.I. & Dolan, J.F.: 1985 Pulsar magnetospheres in binary systems, *Astrophys. J.* **293**, 25-30.

Fejer, J.A.: 1964 Hydromagnetic stability at a fluid velocity discontinuity between compressible fluids, *Phys. Fluids* **7**(4), 499-503.

Fiedler, R. & Jones, T.W.: 1984 MHD Kelvin-Helmholtz instability in extended radio jets *Astropys. J.***283**, 532-539.

Geddie, W.: 1952 Chamber's twentieth century dictionary, *W. & R. Chambers Ltd.*, Edinburgh.

Gerwin, R.A. 1967 Stability of the interface between two fluids in relative motion, *Rev. Mod. Phys.* **40**, 652-658.

Glassmeier, K.-H. & Scholer, M: 1991 Plasmaphysic im Sonnensystem, *Wissenshaftsverlag*, Mannheim.

Goedbloed, J.P.: 1979 Lecture notes on ideal magnetohydrodynamics, *Rijnhuizen report* **83-145**, Rijnhuizen.

Goldstein,H.: 1950 Classical mechanics, *Addison-Wesley*, Reading.

González, A.G. & Gratton, J.: 1990 Compressibility effects on the gravitational instability of a plasma-vacuum interface, *Plasma Phys. Contr. Fussion* **32**, 3-19.

González, A.G. & Gratton, J.: The Kelvin-Helmholtz instability in a compressible plasma: the role of the orientation of the magnetic field with respect to the flow, *J. Plasma Phys.* **51**(1), 43-60, 1994a.

González, A.G. & Gratton, J.: The role of a density jump in the Kelvin-Helmholtz instability of a compressible plasma, *J. Plasma Phys.* **51(2)**, 223-244, 1994b.

Goossens, M., Hollweg, J.V. & Sakurai T.: 1992 Resonant behaviour of MHD waves on magnetic flux tubes. III. Effect of equilibrium flow, *Solar Phys.* **138**, 233-255.

Goossens,M: 1995 Magnetohydrodynamica, Physics honours course, Leuven.

Gordon, B.E. & Hollweg, J.V.: 1983 Collisional damping of surface waves in the solar corona, *Astrophys. J.* **266**, 373-382.

Guglielmi, A.V.: 1997 Comment on the ponderomotive self-action of Alfvén waves, *J. Geophys. R.* **102**, 209-210.

Hasegawa, A. & Uberoi, C.: 1982 The Alfvén wave, *US Departement of Energy*, Washington.

Heyvaerts, J. & Priest, E.: 1983 Coronal heating by phase-mixed shear Alfvén waves, *Astron. Astrophys.* **117**, 220-234.

Hollweg, J.V. 1971 Density fluctuations driven by Alfvén waves, *J.Geoph.Res.* **76**, 5155-5161.

Hollweg, J.V.: 1978 Some physical processes in the solar wind, *Rev. Geophys. Space Sci.* **16**, 689-720.

Hollweg, J.V., Jackson, S. & Galloway, D. 1982 Alfvén waves in the solar atmosphere, *Solar Phys.* **75**, 35-61.

Hollweg, J.V.: 1985 Viscosity in magnetized plasma: physical interpretation, *J.Geophys.Res.***90**, 7620-7622.

Hollweg, J.V.: 1986 Viscosity and the Chew-Goldberger-Low equations in the solar corona, *Astrophys, J.* **306**, 730-739.

Hollweg, J.V.: 1987a Resonance absorption of MHD surface waves: physical discussion, *Astrophys. J.*, **312**, 880-885.

Hollweg, J.V.: 1987b Resonance absorption of magnetohydrodynamic surface waves: viscous effects, *Astrophys. J., 320*, 875-883.

Hollweg, J.V., Yang, G., Cadez, V.M., Gakovic, B.: 1990 Surface waves in an incompressible fluid: resonant instability due to velocity shear, *Astrophys. J.* **349**, 335-344.

Hollweg, J.V. 1992 Alfvénically driven slow shocks in the solar chromosphere and corona, *Ap.J.* **389**, 731-738.

Ionson, J.: 1978 Resonant absorption of Alfvénic surface waves and the heating of solar coronal loops, *Astrophys. J.* **226**, 650-673.

Jain, R. & Roberts, B.: 1991 Magnetoacoustic surface waves at a single interface, *Solar Phys* **133**, 263-280.

Joarder, P.S. & Roberts, B. 1992 The modes of oscillation of a prominence: I. The slab with longitudinal magnetic field, *Astron. Astrophys.* **256**, 264-272.

Joarder, P.S., Nakariakov, V.M., Roberts, B.: 1997 A manifestation of negative energy waves in the solar atmosphere, *Solar Phys.* **176**, 285-297.

Kadomtsev, B.B. & Pogutse, O.P.: 1974 Nonlinear helical perturbations of a plasma in the tokamak, *Sov.Phys.-JETP* **38**, 281-290.

Kadomtsev, B.B.: 1975 Disruptive instability in tokamaks, *Sov.Phys.Plasma Phys.* **1**, 389-391.

Laing, G.B. : 1996 Dissipation of magnetohydrodynamic waves in the upper solar atmosphere, *PhD thesis*, The Open University.

Landau, L.D. & Lifshitz, E.M. 1959 Fluid Mechanics, *Pergamon Press*, Oxford.

Landshoff,R.K.M.: 1957 Magnetohydrodynamics, *Stanford University Press*, Stanford.

Lee, L.C. & Olson, J.V.: 1980 Kelvin-Helmholtz instability and the variation of geomagnetic pulsation activity, *Geophys. Res. Let.* **7**, 777-780.

Lee, M.A. & Roberts, B.: 1986 On the behaviour of hydromagnetic surface waves, *Astrophys. J.* **301**, 403-439.

Lighthill, M. 1960 Studies on magneto-hydrodynamic waves and other anisotropic wave motions, *Phil. Trans. Roy. Soc.* **252**, 397-426.

Longbottom, A.W., Rickard, G.J., Craig,I.J.D. & Sneyd, A.D.: 1999 Magnetic flux braiding: force-free equilibria and current sheets, *Astrophys.J.* **500**, 471-

Mann, G. 1995 Simple magnetohydrodynamic waves, *J. Plasma Phys.* **53**, 109-125.

Martin, C., Heyvaerts, J. & Priest, E. 1997 Alfvén wave support of a dwarf molecular cloud. I. An isothermal model, *Astron. Astrophys.* **326**, 1176-1186.

Manheimer, W.M., Lashmore-Davies, C.N.: 1989 MHD and microinstabilities in confined plasmas, *Adam Hilger*, Bristol.

Miles, A.J. & Roberts, B.: 1989 On the properties of magnetoacoustic surface waves, *Solar Phys.* **119**, 257-278.

Mio, K., Ogino, T., Minami, K. & Takeda, S. 1976 Modified nonlinear Schrödinger equation for Alfvén waves propagating along the magnetic field in cold plasmas, *J. Phys. Soc. Jpn.* **41**, 265-271.

Mok, Y.: 1987 Viscous damping of Alfvén normal modes in non-uniform plasmas, *Astron. Astrophys.* **172**, 327-331.

Morse, P.M. & Feshbach, H.: 1953 Methods of theoretical physics, *McGraw-Hill Book Co. Inc.*, New-York.

Mundie, C.A. : 1998 MHD wave propagation in solar atmospheric structures, *PhD Thesis*, University of St Andrews.

Murawski, K.: 1994 Impulsively generated MHD waves in a coronal plasma, *Acta Astron.* **44**, 99-113.

Nakariakov, V.M. & Oraevsky, V.N. : 1995 REsonant interactions of modes in coronal magnetic fluxtubes, *Solar phys.* **160**, 289-302.

Nakariakov, V.M. & Roberts, B. : 1996 Nonlinearly selected frequencies in coronal loops, *Solar Phys* **168**, 273-277.

218

Nakariakov V.M., Roberts B. & Murawski K. 1997 Alfvén wave phase mixing as a source of fast magnetosonic waves, *Solar Phys.* **175**, 93-105.

Nakariakov V.M., Roberts B. & Murawski K. 1998 Nonlinear coupling of MHD waves in inhomogeneous steady flows, *Astron. Astrophys.* **332**, 795-804.

Nakariakov, V.M., Ofman, L., DeLuca, E.E., Roberts, B. & Davila, J.M.: 1999 TRACE observation of damped coronal loop oscillations: implications for coronal heating, *Science* **285**, 862-865.

Nayfeh, A.H.: 1985 Problems in Perturbations, *Wiley-Interscience*, New-York.

Neukirch, T.: 1997 private communication.

Nishikawa, M. & Wakatami: 1990 Plasma physics with fusion applications, *Springer Verlag*, Berlin.

Ofman, L., Davila, J.M. & Steinolfson, R.S.: 1994 Coronal heating by the resonant absorption of Alfvén waves: the effect of viscous stress tensor, *Astrophys. J.* **421**, 360-371.

Ofman, L., Nakariakov, V.M. & DeForest, C.E.: 1999 Slow magnetosonic waves in coronal plumes, *Astrophys. J.* **514**, 441-447.

Ofman, L., Nakariakov, V.M. & Seghal, N.: 1999 Dissipation of slow magnetosonic waves in coronal plumes, *Astrphys. J.*, submitted.

Ong, S.B. & Roderick, N.: 1972 On the Kelvin-Helmholtz instability of the earth's magnetopause, *Planet. Space Sci.* **20**, 1-10.

Oliver, R., Murawski, K. & Ballester, J.L. 1998 Numerical simulations of impulsively generated MHD waves in a potential coronal arcade, *Astron. Astrophys.* **330**, 726-738.

Ostrovskii, L.A., Rybak, S.A., Tsimring, L.Sh.: 1986 Negative energy waves in hydrodynamics, *Soviet Phys. Usp.* **29**, 1040-1052.

Parker, E.N.: 1979 Cosmical magnetic fields, *Clarendon Press*, Oxford.

Pippards, A.B.: 1978 The physics of vibration, *Cambridge University Press*, Cambridge.

Priest, E.R.: 1982 Solar Magnetohydrodynamics, *D. Reidel Publ. Co.*, Dordrecht.

Pu, Z.Y. & Kivelson, M.G.: 1983 Kelvin-Helmholtz instability at the magnetopause: solution for compressible plasmas, *J. Geophys. Res.* **88**, 841-852.

Rae, I. & Roberts, B.: 1982 On MHD wave propagation in inhomogeneous plasmas and the mechanism of resonant absorption, *Mon. Not. R. Astr. Soc.* **201**, 1171-1182.

Rankin, R., Harrold, G., Samson, J. & Frycz, P. 1993 The nonlinear evolution of field line resonances in the earth's magnetosphere, *J. Geophys. R.*, **98**, 5839-5853.

Rankin, R., Frycz, P., Tikhonchuk, V.T. & Samson, J. 1994 Nonlinear standing shear Alfvén waves in the Earth's magnetosphere, *J. Geophys. R.* **99**, 21291-21301.

Roberts, B. & Webb, A.R.: 1978 Vertical motions in an intense magnetic fluxtube, *Solar Phys.* **56**, 5-35.

Roberts,B.: 1981 Wave propagation in a magnetically structured atmosphere. I. Surface waves at a magnetic interface, *Solar Phys.* **69**, 27-38.

Roberts,B. & Mangeney, A.: 1982, Solitons in magnetic flux tubes, *Solar Phys.*, 198, P7-P11.

Roberts,B.: 1991, Advances in solar system magnetohydrodynamics (ed. Priest, E.R. & Hood, A.W.). *Cambridge Univ. Press*, 105-136.

Roberts,P.H.: 1967, An introduction to magnetohydrodynamics, *Longmans*, London.

Rosenbluth, M.N., Dagazian, R.Y. & Rutherford, P.H.: 1973 Nonlinear properties of the internal $m = 1$ kink instability in the cylindrical tokamak, *Phys. Fluids* **16**, 1894-1902.

Ruderman, M.S.: 1991, Viscous damping of surface magnetohydrodynamic waves on magnetic interface in cold plasmas, *Solar Phys.* **131**, 11-24.

Ruderman, M.S.: 1992, Nonlinear dissipation of surface Alfvén waves in the solar corona, *Astrophys. J.* **399**, 724-732.

Ruderman, M.S. & Fahr, H.J.: 1993 The effect of magnetic fields on the macroscopic instability of the heliopause. I. Parallel interstellar magnetic fields, *Astron. Astrophys.* **275**, 635-644.

Ruderman, M.S. & Fahr, H.J.: 1995 The effect of magnetic fields on the macroscopic instability of the heliopause. II. Inclusion of solar wind magnetic fields, *Astron. Astrophys.* **299**, 258-266.

Ruderman, M.S. & Goossens, M.: 1995 Surface Alfvén waves of negative energy, *J. Plasma Phys.* **54**, 149-155.

Ruderman, M.S., Verwichte, E., Erdélyi & Goossens, M.: 1996 Dissipative instability of MHD tangential discontinuity in magnetized plasmas with anisotropic viscosity and thermal conductivity, *J. Plasma Phys.* **56**, 285-306.

Rutherford, P.H.: 1973 Nonlinear growth of the tearing mode, *Phys. Fluids* **16**, 1903-1908.

Ryutova, M.P.: 1988 Negative energy waves in a plasma with structured magnetic fields, *Sov. Phys. J.E.T.P.* **43**, 491-504.

Sen, A.K.: 1963 Stability of hydromagnetic Kelvin-Helmholtz discontinuity, *Phys. Fluids* **6**(8), 1154-1163.

Sen, A.K.: 1964 Effect of compressibility on Kelvin-Helmholtz instability in a plasma, *Phys. Fluids* **7**(8), 1293-1298.

Shercliff, J.A.: 1965 A textbook on magnetohydrodynamics, *Pergamon Press*, Oxford.

Shu, F.H.: 1992 The physics of astrophysics, II. Gas dynamics, *University Science Books*, Mill Valley, California.

Somasundaram, K. & Uberoi, C.: 1982, Compressibility effects on hydromagnetic surface waves, *Solar Phys.* **81**, 19-24.

Somasundaram, K. & Satya Narayanan, A.: 1987, Characteristics of Alfvén surface waves along moving cylindrical plasma columns, *Plasma Phys. Contr. Fusion* **29**(4), 497-504.

Soward, A.M.: 1983 Stellar and planetary magnetism, *Gordon and Breach Science Publ.*, New York.

Spitzer, L.Jr.: 1962 Physics of fully ionized gases, *Interscience Publishers*, New York.

Stark,B.A., Musielak, Z.E. & Suess, S.T.: 1995 Alfvén wave resonances and induced flow due to nonlinear Alfvén waves in a stratisfied atmosphere, *Solar Wind 8*, 66.

Steinolfson, R.S., Priest, E.R., Poedts, S., Nocera, L. & Goossens, M.: 1986, Viscous normal modes on coronal inhomogeneities and their role as a heating mechanism, *Astrophys. J.* **304**, 526-531.

Stix, T.H. 1962 Waves in plasmas *McGraw-Hill Book Co. Inc.*, New-York.

Syrovatskii, S.I.: 1971 Formation of current sheets in a plasma with a frozen-in strong magnetic field, *Sov.Phys.-JETP* **33**, 933-940.

Taniuti, T. & Yajima, N.: 1969 Perturbation method for a nonlinear wave modulation *J. Math. Phys.* **10**, 1369-1372.

Taylor, J.B.: 1974 Relaxation of toroidal plasma and generation of reverse magnetic field, *Phys. Rev. Lett.* **33**, 1139-1141.

Tirry, W.J., Cadez, V.M., Erdélyi, R. & Goossens, M.: 1998 Resonant flow instability of MHD surface waves, *Astron. Astrophys.* **332**,786-794.

Torkelsson, U. & Boynton, G.C. 1998 Non-linear spherical Alfvén waves, *Mon. Not. R. Astron. Soc.* **295**, 55-65.

Tikhonchuk, V.T., Rankin, R., Frycz, P. and Samson, J.C. 1995 Nonlinear dynamics of standing shear Alfvén waves, *Phys. Plasmas* **2**, 501-515.

Turland, B.D. & Scheuer, P.A.G.: 1976 Instabilities of Kelvin-Helmholtz type for relativistic streaming *Mon. Not. R. Astr. Soc.* **176**, 421-441.

Uberoi,C. & Somasundaram, K.: 1982 Two-mode structure of Alfvén surface waves, : *Phys. Rev. Lett.* **49**(1), 39-42.

Uberoi,C. : 1982 A note on the existence of Alfvén surface waves, *Solar Phys.* **78**, 351-354.

Van der Linden, R.A.M. & Goossens, M.: 1991 Thermal instability in slab geometry in the presence of anisotropic thermal conduction, *Solar Phys.* **131**, 79-105.